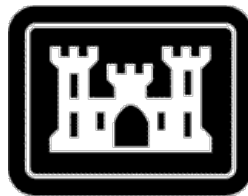# CEDAR LAKE AQUATIC ECOSYSTEM RESTORATION FEASIBILITY STUDY

CEDAR LAKE, INDIANA

APPENDIX A
HYDROLOGY & HYDRAULICS

U.S. Army Corps of Engineers
Chicago District

July 2016

CEDAR LAKE, INDIANA
CEDAR LAKE AQUATIC ECOSYSTEM RESTORATION
FEASIBILITY STUDY

APPENDIX A – HYDROLOGY & HYDRAULICS

July 2016

Executive Summary

The hydrology and hydraulics (H&H) appendix documents detailed hydrodynamic, sediment transport and water quality modeling that was done by Sandia National Laboratory using environmental fluid dynamics code (EFDC). Supporting information used to construct the model including field collection analyses of sediment erosion characteristics and tributary boundary condition hydrograph and loading analyses is also attached.

List of Attachments

Attachment 1: Sandia EFDC Model Report – October 2007
Attachment 2: Tributary Synthetic Hydrographs Memorandum – March 2006
Attachment 3: Tributary Loading Memorandum – February 2006
Attachment 4: Sandia Field Collection Report – September 2005

Attachment 1:

Development of a Hydrodynamic, Sediment Transport, and Water Quality Model for Evaluation of Ecosystem Restoration Measures at Cedar Lake, Indiana

October 2007

Development of a Hydrodynamic, Sediment Transport, and Water Quality Model for Evaluation of Ecosystem Restoration Measures at Cedar Lake, Indiana

Scott C. James, Ph.D., Sandia National Laboratories
Michael Ahlmann, Sandia National Laboratories Craig
C. Jones, Ph.D., Sea Engineering, Inc.
David F. Bucaro, P.E., U.S. Army Corps of Engineers, Chicago District Jesse
D. Roberts, Sandia National Laboratories

October 2007

Abstract

The U.S. Army Corps of Engineers (USACE), under Section 206 of the Water Resources Development Act of 1996, has commissioned a study to evaluate the feasibility of implementing several aquatic ecosystem restoration measures to help alleviate eutrophication problems in Cedar Lake, Indiana. The lake suffers from a highly phosphorous-laden sediment bed leading to high diffusive flux rates and frequent algal blooms. In conjunction with this study, the USACE is funding development of a combined hydrodynamic, sediment transport, and water quality model for the lake based on the U.S. Environmental Protection Agency sponsored Environmental Fluid Dynamics Code (EFDC). Sandia National Laboratories (SNL) has been commissioned to perform the study and has made several updates to the code which is now called SNL-EFDC. The newly incorporated SEDZLJ sediment transport algorithm, which allows direct incorporation of site-specific erosion data from the Sediment Erosion with Depth flume (SEDflume), facilitates accurate prediction of sediment behavior. The model was developed and calibrated based on field data collected in 2005 and calibration results suggest the model is able to sufficiently reproduce water quality trends. The primary calibration parameter was the diffusion coefficient in pore water. Several proposed ecosystem restoration measures were modeled over a 9-month period from March through November. To significantly reduce eutrophication and increase ecosystem output, the model suggests remediating or removing phosphorous-laden bottom sediments is critical for success; however, unless the future influx of phosphorous is significantly decreased by reducing nutrient loadings from tributaries that drain to Cedar Lake, the benefits will be temporary.

1

TABLE OF CONTENTS

LIST OF FIGURES

LIST OF TABLES

Introduction

The U.S. Army Corps of Engineers (USACE), Chicago District is performing a feasibility study authorized under Section 206 of the Water Resources Development Act of 1996 that will evaluate the practicability of various aquatic ecosystem restoration measures within Cedar Lake located in northwest Indiana. This glacial lake experiences periodic resuspension of bottom sediments due to bed shear stresses created by wind and boat induced waves. Diffusive flux of phosphorus from the sediment bed, periodic sediment resuspension, and tributary nutrient loadings are the main contributors to water quality and ecosystem degradation in Cedar Lake (Harza Environmental Services 1999, see also Figure 5 in this report). As part of this feasibility study, the Chicago District supported the development of a hydrodynamic, sediment transport, and water quality model to estimate the effectiveness of potential ecosystem restoration measures and to evaluate relative differences among them.

Sandia National Laboratories (SNL) developed a hydrodynamic, sediment transport, and water quality model of Cedar Lake using a modified version of the U.S. Environmental Protection Agency supported Environmental Fluid Dynamics Code (EFDC). SNL was contracted by the U.S. Army Corps of Engineers (USACE) to perform multiple tasks associated with the Cedar Lake modeling study:

1) Collect field measurements within and around Cedar Lake to determine sediment erosion and bulk property characteristics;
2) Develop and calibrate a combined hydrodynamic, sediment transport and water quality model;
3) Evaluate various ecosystem restoration measures and alternatives specified by the USACE using the model.

This document details the development, calibration, and implementation of the Cedar Lake model as well as a discussion of the improvements made to the EFDC model by SNL. Various restoration measures are compared to help identify the efficacy of each.

Environmental conditions that were used in the development of the model including wind, air temperature, rainfall, and solar radiation were taken from data collected in 2005. Tributary loadings were modeled by USACE using the Long-Term Hydrologic Impact Assessment and Non-Point Source Pollutant (L-THIA/NPS) model (Engle and Harbor 2005). The L-THIA/NPS modeling results provided boundary condition influxes of water, nutrient (phosphorous, nitrogen, etc.), and sediment loadings. The model was calibrated against measured water quality and suspended sediment concentration data collected in the summer of 2005.

The newly incorporated SEDZLJ sediment transport subroutines facilitate direct use of measured erosion-rate data collected with the Sediment Erosion with Depth flume (SEDflume). Erosion rates are included as functions of both depth within the sediment bed and applied shear stresses. This in-situ method reduces problems associated with empirical erosion formulas, which are typically based on disaggregated particle size and underestimate cohesive effects.

The water quality model for Cedar Lake tracks algae, oxygen, temperature, carbon, phosphorous, and nitrogen kinetics, as well as sediment bed diagenesis. Organic phosphorous and nitrogen exist in three states within the system: labile particulate, refractory particulate, and dissolved. The only mineral form of phosphorous considered is phosphate, which also exists in three states: algal phosphate, phosphate sorbed to sediment particles, and dissolved phosphate. There are two inorganic forms of nitrogen modeled: nitrate and ammonia.

The calibrated model was used to simulate a nine month period from March to November and results suggest that the model simulates sediment transport and associated water quality correctly. Several

restoration measures were considered, including physical substrate restoration, chemical substrate restoration using flocculants, tributary restoration, creation of habitat islands, restoration of littoral macrophytes, institutional controls, fish community management, and reduction of nutrient loadings from tributaries. In addition, an analysis of several restoration alternatives that comprise multiple restoration measures was conducted.

Model Description

The fully implemented model, EFDC (Hamrick 1996), incorporates hydrodynamics, temperature, multiple size classes of cohesive and non-cohesive sediments, and water-quality state variable transport. It is a three-dimensional model that may use a curvilinear-orthogonal grid in the horizontal (a Cartesian grid was used for the Cedar Lake model), but is based on a sigma transformation in the vertical. It uses a finite volume-finite difference formulation and ensures conservation of mass. Water column transport is based on the same high-order advection-diffusion scheme used for salinity and temperature. A number of options are included for the specification of settling velocities and sediment deposition (James et al. 2006).

EFDC has been modified with improved sediment dynamics using the SEDZLJ formulations (Jones and Lick, 2001a,b) and the new code is called SNL-EFDC. The SEDZLJ formulations are important upgrades to EFDC because they allow the direct inclusion of site-specific data into the model. Data collected using either SEDflume or the Adjustable Shear Stress Erosion and Transport (ASSET) flume can be used (McNeil et al. 1996; Roberts et al. 2003). These data are critical for quantitative understanding and prediction of the transport and fate of sediments and water-quality parameters for a wide range of conditions, but especially during large floods on rivers and major storms on lakes and oceans, which is when most sediment and nutrient transport occurs. Consequently, it is necessary to accurately determine the erosion rates of sediments at different locations in the system. Erosion rates are needed at high shear stresses and as functions of depth in the sediment bed (often down to a meter or more).

The Cedar Lake hydrodynamics, sediment transport, and water quality model is built within the SNL-EFDC framework. An orthogonal grid with 498 80×80-m^2 cells describes the shape and extent of Cedar Lake. The model internally calculates wind-driven currents and wind-driven waves that are used to estimate combined wave/current bottom shear stresses within a model cell (Christoffersen and Jonsson 1985). These shear stresses resuspend sediments, which are transported throughout the lake according to advection and turbulent dispersion. A combination of diffusive flux from the sediment bed, tributary loadings, and sediment resuspension controls water quality constituents in the water column.

Hydrodynamic Model

The hydrodynamic portion of the model solves the hydrostatic, free surface, Reynolds-averaged Navier-Stokes equations with turbulence closure similarly to the model of Johnson et al. (1993). The numerical solution techniques are the same as those of Blumberg and Mellor (Blumberg and Mellor) except for the solution of the free surface, which is done using a preconditioned conjugate gradient (direct) solver (explicit scheme) rather than an alternating-direction-implicit method (Hamrick 1996). EFDC's hydrodynamic component uses a semi-implicit, conservative finite-volume solution scheme for the hydrostatic primitive equations with either two- or three-level time stepping (two-time-level option used for the Cedar Lake model). Temperature transport is dynamically coupled through one of several high-accuracy advection schemes available in the code. Anti-diffusion corrections can be made and flux limiters may be applied, although they were not used in the Cedar Lake model runs. The EFDC model is described in detail by Hamrick (1992; Hamrick 1996).

Sediment Transport Model

Sediment erosion and transport are implemented with the SEDZLJ formulations (Jones and Lick 2001a; b). Considering the flow of water over a sediment bed, as the rate of flow is increased starting from rest, there is a range of velocities (or shear stresses) for which the movement of the easiest-to-move particles (generally among the smallest) is first noticeable to an observer. These eroded particles remain in transport for a short while until the shear stress drops below the critical value for suspension resulting in deposition to the sediment bed. This initial motion tends to occur only at a few isolated spots. As the flow velocity and shear stress increase further, more particles participate in this process of erosion, transport, and deposition, and movement of the sediments across the bed is sustained (Bagnold 1966; 1973; Dyer 1986).

A typical application of SEDflume yields erosion rates, E usually specified in units of cm/s, as a function of depth with shear stress, $\square$ Erosion rates are generally highest at the surface and often decrease with depth; they also increase with applied shear stress. In general, information of this type for sediments throughout a riverine or lacustrine system is necessary for accurate predictions of sediment transport and these data can be directly incorporated into the SNL-EFDC framework.

Sediment may be transported as both bedload and suspended load depending on the flow conditions; however the combination of extremely small sediment particle sizes and lack of consistent currents observed in lakes are not sufficient for bedload transport and thus this mode was not considered within the model of Cedar Lake. Initiation of both modes of transport begins with erosion or resuspension of sediment in a model cell whose characteristics are defined by SEDflume data. This occurs when the bed stress exceeds the critical shear stress, $\square_{cr}$ (as measured by SEDflume). The critical shear stress depends upon the sediment particle size, density, mineralogy, and other site-specific factors (van Rijn 1984a; b; c).

A number of approaches have been used to distinguish whether a particular sediment size is transported as bedload or suspended load under some specific local flow condition. The approach proposed by van Rijn (1984c) is adopted in SNL-EFDC. When the bed velocity is less than the critical shear velocity (see Garcia 1999, Chapter 6), no erosion or resuspension takes place and there is no bedload transport. Sediment in suspension under this condition will deposit to the bed. When velocity-induced shear on the sediment bed (bed shear velocity) exceeds the critical shear velocity, but remains less than the settling velocity, which was calculated as described by Cheng (1997), sediment will be eroded and transported as bedload. Sediment in suspension under this condition will also deposit to the bed. When the bed shear velocity exceeds both the critical shear velocity and the settling velocity, bedload transport ceases and the eroded or resuspended sediment will be transported as suspended load.

Because of the often significant (potentially exponential) increase in sediment erosion as the shear stress increases, it is difficult to precisely define the critical velocity or critical shear stress when sediment erosion begins. More quantitatively, a critical shear stress for erosion can be defined as the shear stress at which a small but accurately measurable rate of erosion occurs. In most studies, this rate is defined to be 10^{-4} cm/s; this represents 1 mm of erosion after approximately 15 minutes. Sixteen sediment cores within Cedar Lake were collected and analyzed in July 2005 by SNL, and all critical shear stress measurements were typically on the order of about 1 dyne/cm^2 (0.1 Pa). While collection of more erosion cores would facilitate higher resolution modeling, time and budget constraints precluded these efforts. A flowchart for the SEDZLJ algorithm is included as Figure 1.
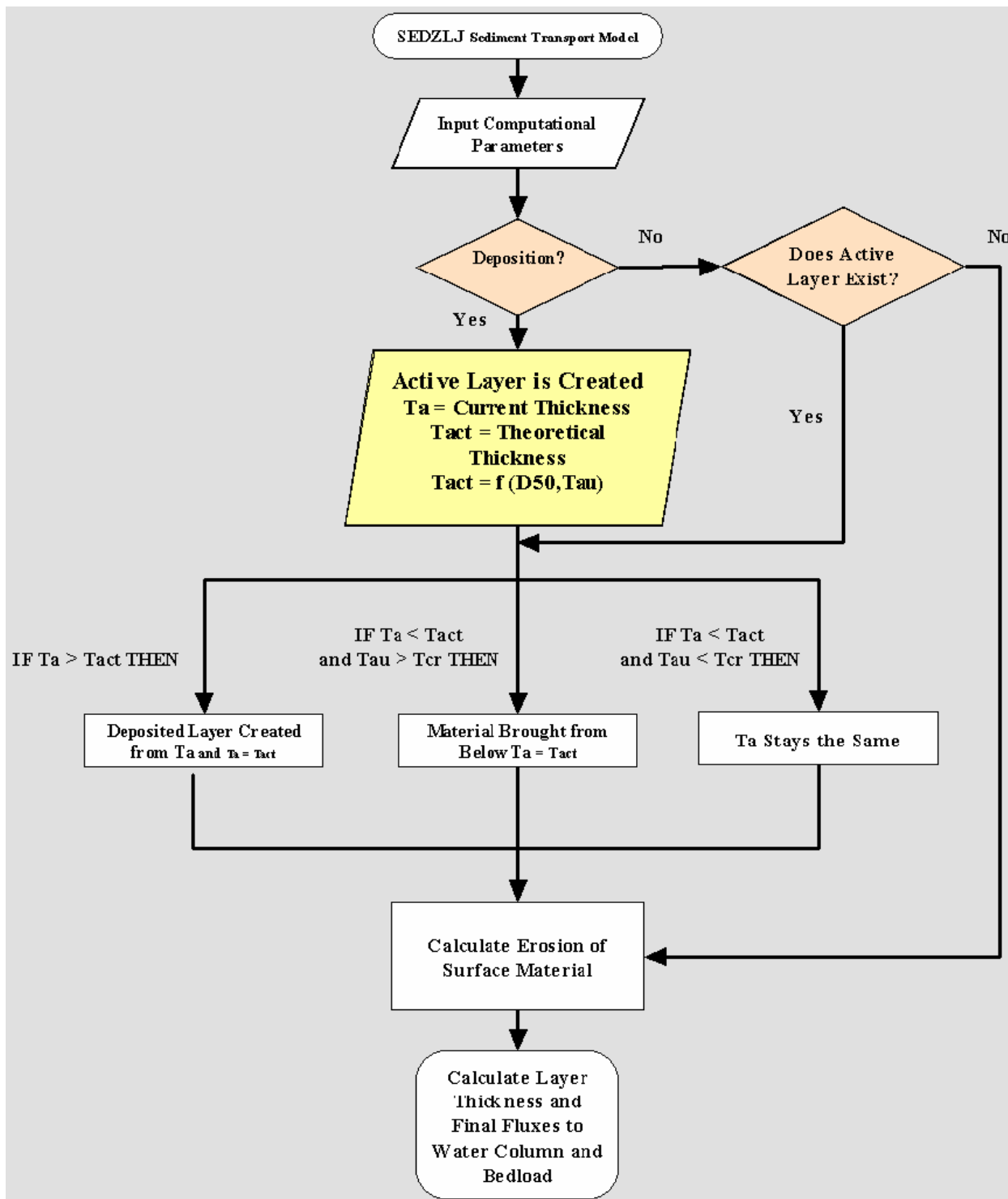
Figure 1. SEDZLJ flow chart.

Water Quality Model

A water quality model was developed for Cedar Lake using the EFDC formulation of the USACE CE-QUAL model (Cerco and Cole 1995) and includes:

- Green algal growth kinetics,
- Carbon, phosphorus, and nitrogen kinetics,
- Dissolved oxygen kinetics,
- Temperature kinetics,
- Sediment bed diagenesis.

More specifically, a water quality model with the above-mentioned state variables was developed and integrated with SNL-EFDC to form a three-dimensional water-quality model for Cedar Lake. The water quality model, upon receiving the hydrodynamic and sediment transport information for advective and dispersive transport, simulates the spatial and temporal distributions of water-quality parameters which may include, among other available options, dissolved oxygen, suspended algae, and various components of carbon, nitrogen, and phosphorus. A sediment diagenesis model was also developed. The sediment process model, upon receiving the particulate organic matter deposited from the overlying water column, simulates sediment bed diagenesis and the resulting fluxes of organic and inorganic substances (carbon, ammonium, nitrate, and phosphate) and sediment oxygen demand back to the water column. The coupling of the sediment process model with the water-quality model enables the simulation of long-term changes in water-quality conditions in response to changes in nutrient loading and defined ecosystem restoration measures.

Site Characterization

A detailed site analysis was performed to ensure models were developed accurately. Important data used in the development of the Cedar Lake model include bathymetry, physical and chemical properties of bed sediments, sediment erosion characteristics, water quality information, and boundary conditions that include flow, sediment, and nutrient loadings from tributaries and atmospheric conditions.

Bathymetry

The Cedar Lake model was constructed based on a bathymetric survey conducted by the USACE in June 2005 using a single-beam fathometer and GPS tracking unit as shown in Figure 2. Cedar Lake has a surface area of approximately 316 ha (781 acres) with an average depth of 2.4 m (7.9 ft) and a maximum depth of 4.2 m (13.9 ft) in the center lobe. Modeled volume is $3.2{\times}10^7$ m^3. The bathymetric data facilitated the development of a GIS surface and corresponding model grid. Bathymetric data were used to define the depth of each model cell. Because the Cedar Lake model was constructed on a standard grid, spatial averaging of survey data was done to construct the model bathymetry. Figure 3 shows the model-approximated bathymetry for Cedar Lake. Because EFDC is based on a sigma coordinate system in the vertical direction, a bottom slope was defined for each grid cell. Cedar Lake was represented by 498 orthogonal $80{\times}80$-m^2 grid cells.
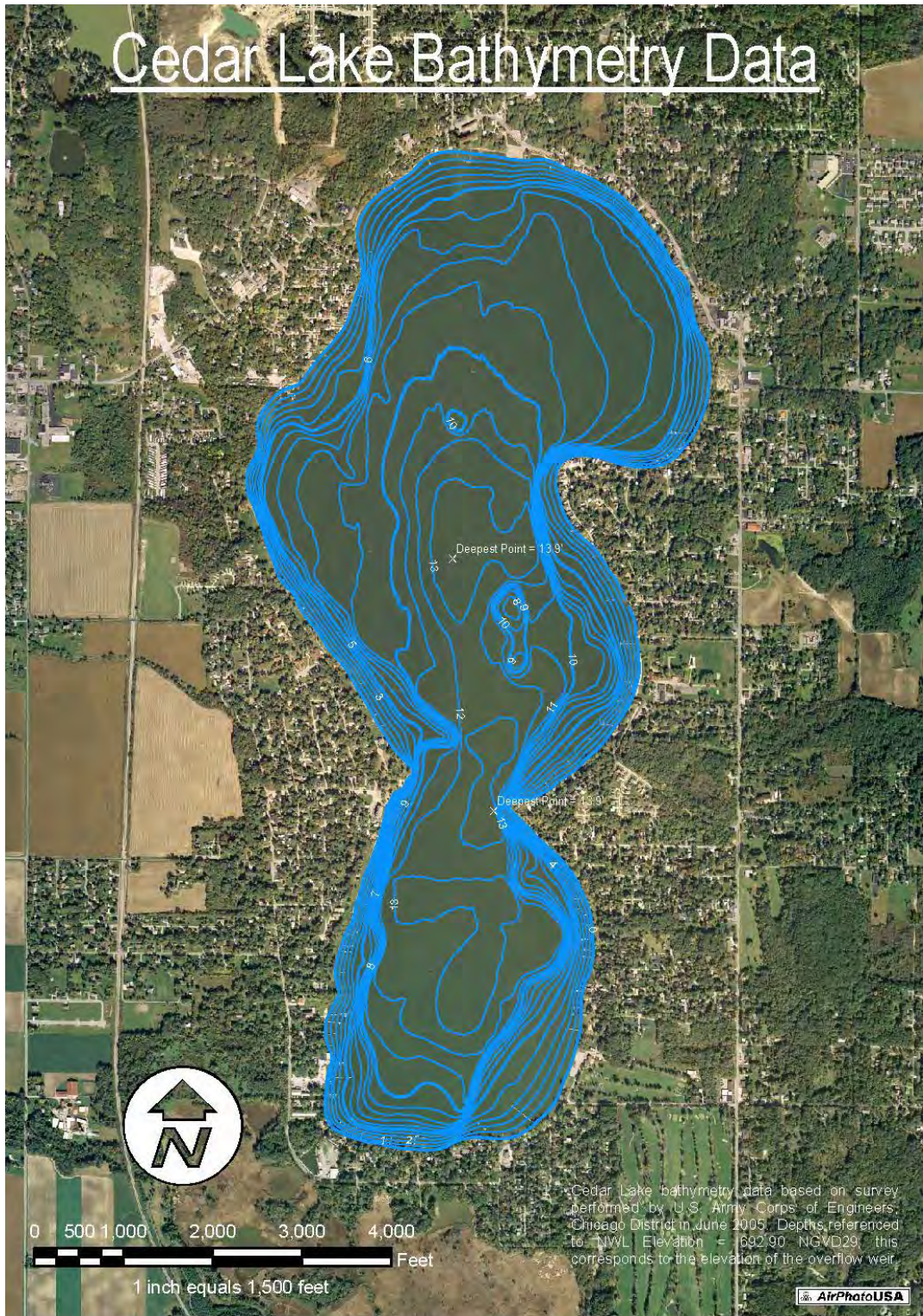
Figure 2. Bathymetric contour map of Cedar Lake surveyed in 2005.
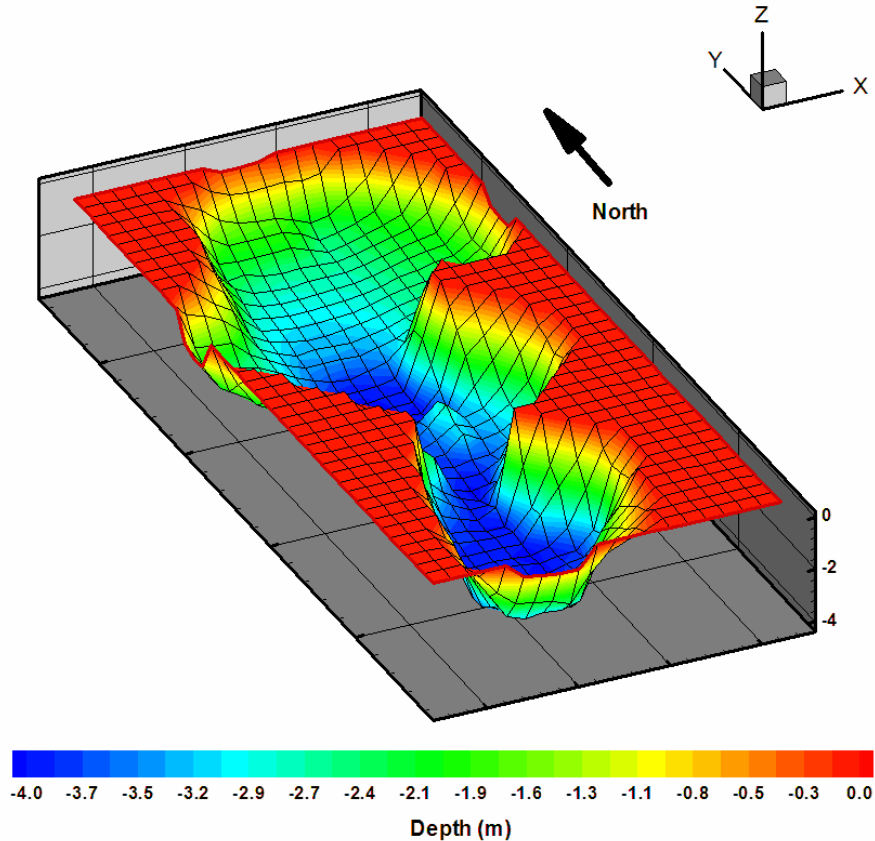
Figure 3. Hydrodynamic model grid based on 2005 bathymetric survey of Cedar Lake.

Water Quality

Phosphorus was determined to be the limiting nutrient in Cedar Lake and is responsible for frequent algal blooms in the summer when the release of phosphorus from sediments is the greatest (Harza Environmental Services 2001). Because phosphorus is the primary contributor to the eutrophication of Cedar Lake, accurate modeling of phosphorus kinetics is of specific interest. The initial phosphorus, nitrogen, and carbon concentrations in the sediment bed were derived from sediment sampling and analysis data from twenty-two sediment cores collected in 1998 (Harza Environmental Services 1998). Initial total phosphorus, nitrogen and carbon concentrations were assigned for each model cell by distributing the measured core data across the entire model grid using kriging interpolation and extrapolation techniques. To extrapolate phosphorus concentrations between areas near the shore where sands dominate and no core samples were taken, a background phosphorus concentration of 50 mg/kg was assumed because this is a reasonable concentration for non-cohesive sediments (the minimum phosphorus concentration measured for cohesive sediments was 73 mg/kg). The average total phosphorus concentration across the sediment bed was determined to be 494 mg/kg. Figure 5 shows the initial distribution of total organic phosphorus concentrations that range from 50 to 1,200 mg/kg in the sediment bed that was assigned to the top layer of each sediment grid cell in the Cedar Lake model.

12

The water quality model incorporated into SNL-EFDC was developed by Cerco and Cole (1995). Organic phosphorus was considered in three states: dissolved, labile particulate, and refractory particulate. A single mineral form, total phosphate, was considered and it exists in three states within the model: dissolved phosphate, phosphate sorbed to inorganic solids, and phosphate incorporated in algal cells. Equilibrium partition coefficients were used to distribute the total among the three states. The phosphate sorbed to inorganic solids to dissolved phosphate partitioning coefficient is 0.04, but the algal phosphate is dependent on a variable carbon to phosphorous ratio calculated at every time step within the model. Algae ingest dissolved phosphate during their growth cycle and release dissolved phosphate and organic phosphorus through mortality. The fate of algal phosphorus released by metabolism and predation is also represented by distribution coefficients. Total inorganic phosphorus is the sum of total phosphate (comprising dissolved phosphate, phosphate sorbed onto inorganic solids, and phosphate incorporated in algal cells) and the three states of organic phosphorus (dissolved, labile particulate, and refractory particulate). All of the coefficients used in the current effort are based on the values specified in the work of Cerco and Cole (1995) and have been determined to provide an accurate water quality baseline in other systems (Jin et al. 1998; Jin et al. 2001).

Monthly water quality samples were taken between June 2005 and May 2006 at three locations corresponding to the three lobes within Cedar Lake as shown in Figure 4. A total of twenty-one water quality samples were taken and analyzed for several parameters. These data were used to set the initial conditions of the model and to calibrate and validate the baseline model results. Table 1 shows the results of the monthly water quality sampling at Cedar Lake.

Figure 4. Tributary locations and water quality sample collection sites.

Figure 5. Initial sediment phosphorus concentrations based on cores sampled in 1998.

Table 1. Monthly water quality data sampled at Cedar Lake.

Sample Locations (NAD83 SPCS-IN-W meters)

North Basin	41.37828 N	87.42908 W
Main Basin	41.36935 N	87.43165 W
South Basin	41.35912 N	87.43322 W

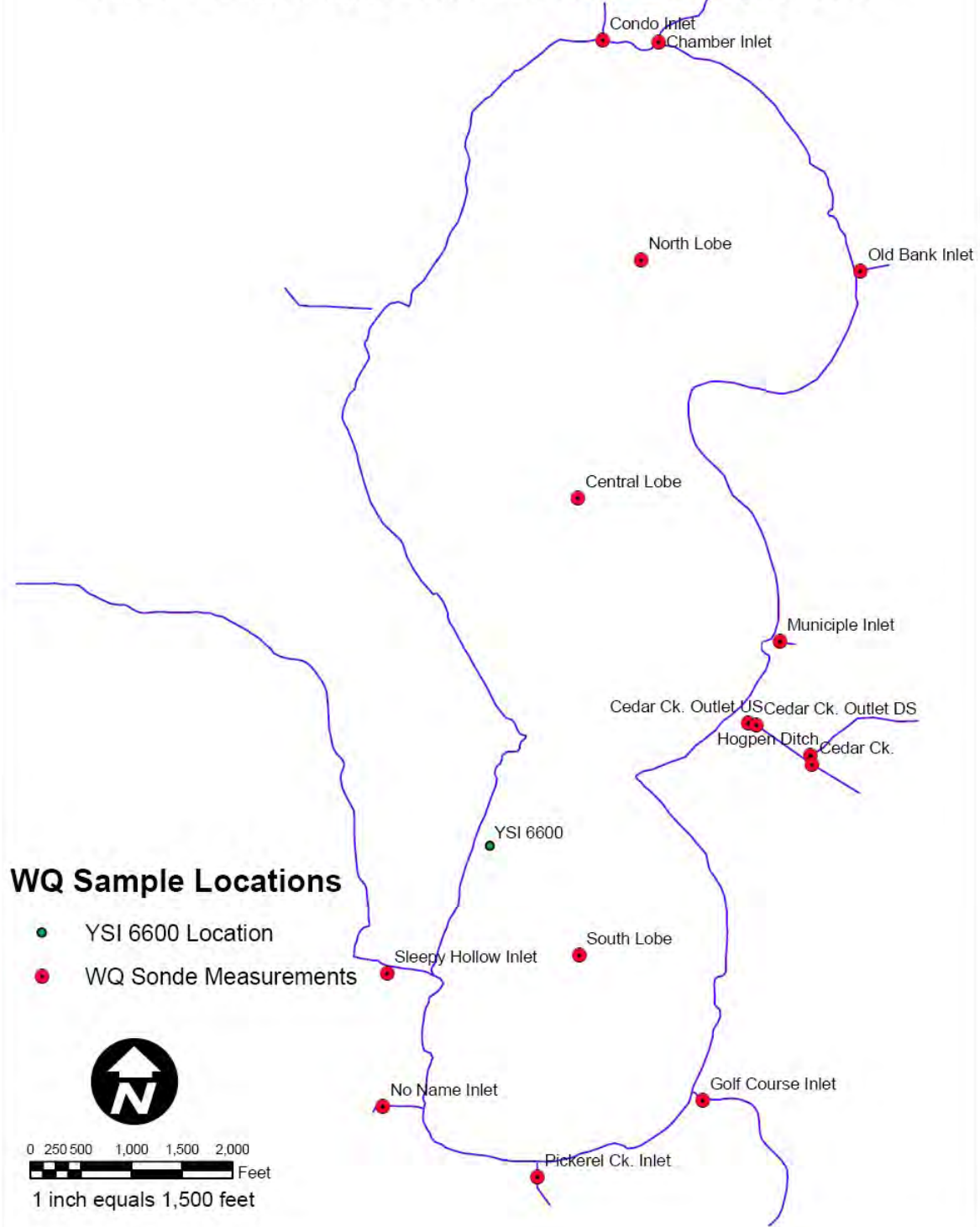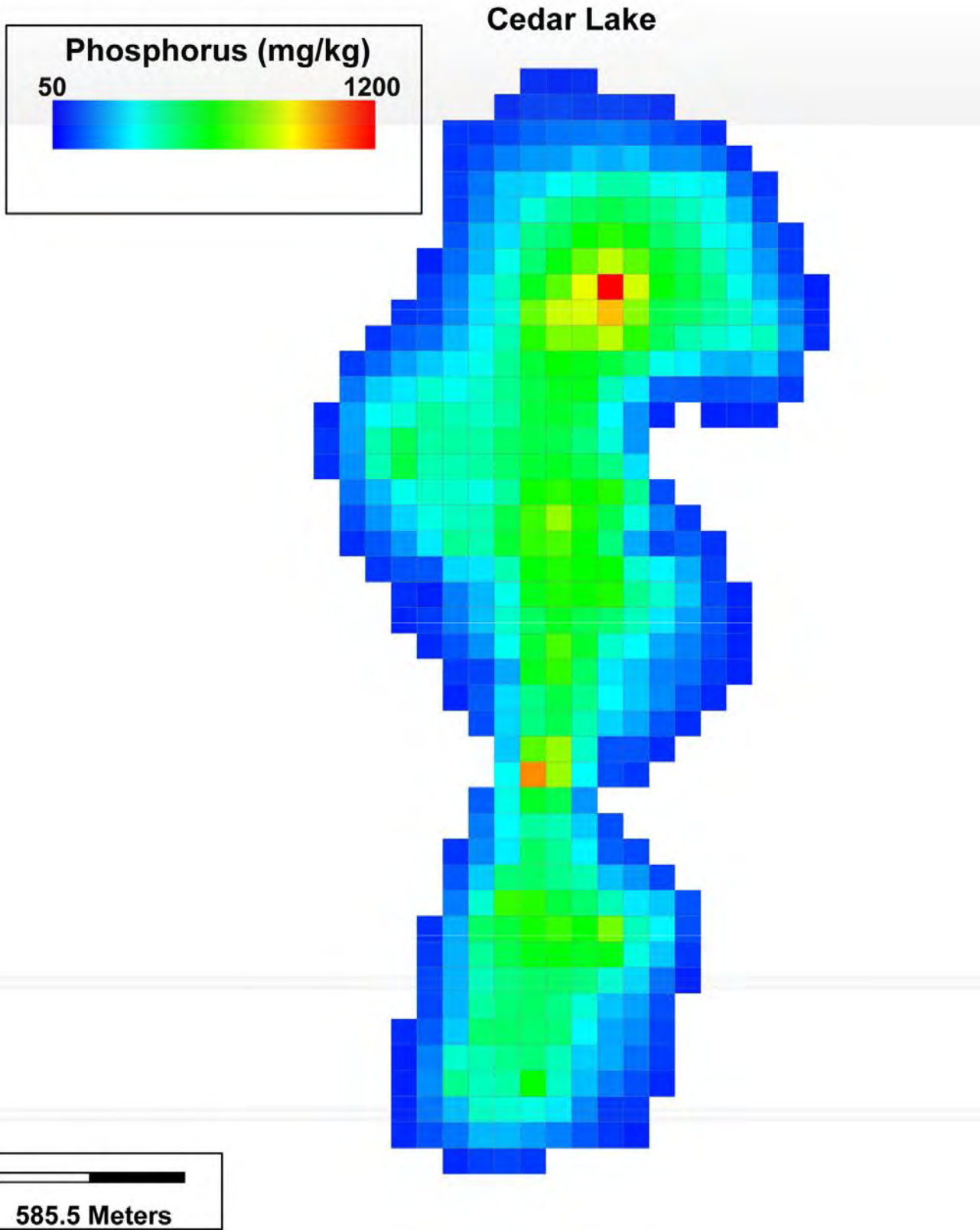| Month		June 2005			July 2005			August 2005			September 2005			November 2005			March 2006			May 2006		
Sample Designation		CL2005-JUN-NB	CL2005-JUN-MB	CL2005-JUN-SB	CL2005-JUL-NB	CL2005-JUL-MB	CL2005-JUL-SB	CL2005-AUG-NB	CL2005-AUG-MB	CL2005-AUG-SB	CL2005-SEP-NB	CL2005-SEP-MB	CL2005-SEP-SB	CL2005-NOV-NB	CL2005-NOV-MB	CL2005-NOV-SB	CL2006-MAR-NB	CL2006-MAR-MB	CL2006-MAR-SB	CL2006-MAR-NB	CL2006-MAR-MB	CL2006-MAR-SB
Date Sampled		09-Jun-05	09-Jun-05	09-Jun-05	14-Jul-05	14-Jul-05	14-Jul-05	11-Aug-05	11-Aug-05	11-Aug-05	22-Sep-05	22-Sep-05	22-Sep-05	22-Nov-05	22-Nov-05	22-Nov-05	20-Mar-06	20-Mar-06	20-Mar-06	23-May-06	23-May-06	23-May-06
Parameter	**Unit**																					
Water Depth	feet																					
Sample Depth	feet bws	10	13	14	8	11	13	11	13	ND	10	11	14	ND	ND	ND	11	13	13.5	10	12	13.5
Temperature	°C	3	4	4	3	4	4	3	4	ND	3	3	4	3	3	3	3	4	4	3	4	4
pH	std. Unit	25.3	24.9	24.1	27.7	28.5	27.8	27.5	27.4	27.7	23.0	22.8	22.4	4.6	4.6	4.7	5.8	5.7	6.1	16.7	16.7	17.7
Dissolved Oxygen	(mg/L)	8.99	9.13	9.08	8.57	8.74	8.78	8.75	8.87	8.95	9.20	9.21	8.90	8.26	8.32	8.31	8.42	8.42	8.51	8.92	9.00	9.02
		8.92	10.75	10.63	7.72	7.90	7.95	7.23	7.44	7.91	11.45	10.17	7.66	17.42	16.58	16.12	12.31	12.90	11.93	13.82	11.70	12.29
Ammonia-Nitrogen	(mg/L)	0.26	0.37	0.29	0.36	0.25	0.19	< 0.20	< 0.20	< 0.20	0.15 (1)	< 0.20	0.21	0.3	0.38	0.36	0.77	0.73	0.64	0.39	0.35	0.35
Nitrate (NO₃-N)	(mg/L)	< 0.1	< 0.1	0.031 (1)	< 0.1	< 0.1	< 0.1	< 0.1	< 0.1	< 0.1	0.026 (1)	< 0.10	0.03 (1)	< 0.10	< 0.10	< 0.10	0.62	0.6	0.74	0.37	0.37	0.4
Nitrite (NO₂-N)	(mg/L)	0.018 (1)	0.02 (1)	0.019 (1)	< 0.02	0.018 (1)	0.018 (1)	0.011 (1)	0.012 (1)	0.01 (1)	< 0.02	< 0.02	< 0.02	0.01 (1)	< 0.02	< 0.02	0.014 (1)	0.013 (1)	0.013 (1)	0.028	0.027	0.028
Total Kjeldahl Nitrogen (TKN)	(mg/L)	2	2.1	2.2	2.5	2.5	2.5	1.7	1.5	1.6	1.8	1.5	1.8	1.4	1.4	1.3	1.9	2	1.8	2.3	2.4	2.4
Total Phosphorous	(mg/L)	0.11	0.15	0.16	0.068	0.066	0.077	0.055	0.074	0.054	0.13	0.068	0.074	0.045 (1)	0.044 (1)	0.046 (1)	0.049 (1)	0.053	0.043 (1)	0.15	0.17	0.096
Ortho-Phosphorous (reactive)	(mg/L)	< 0.05	0.009 (1)	0.008 (1)	0.018 (1)	0.023 (1)	0.024 (1)	0.016 (1)	0.013 (1)	0.015 (1)	0.009 (1)	0.011 (1)	0.012 (1)	0.009 (1)	0.011 (1)	0.006 (1)	< 0.05	< 0.05	< 0.05	0.056	0.084	0.035 (1)
Total Dissolved Solids	(mg/L)	250	240	260	260	230	430	260	250	240	240	300	240	260	240	260	260	260	260	280	300	260
Total Suspended Solids	(mg/L)	48	38	44	57	46	47	36	28	31	42	42	28	18	16	18	23	22	24	51	56	55

(1) Analyte was detected in the sample below the reporting limit, but above the method detection limit   ND = not determined

Weather notes:

June 2005   Overcast and 80 F. Calm on lake, low to no winds, and few too no boats. Weather in past 24 hrs - showers and   overcast.

July 2005   Clear/Sunny, warm and windy on lake. Few to no boats. Weather in past 24 hours - overcast.

August 2005   Showers - rain during sampling, just after storm. Warm. Lake calm. Weather in past 24 hours - storm.   September 2005
Clear/Sunny, warm (70 F). Few to no boats. Weather in past 24 hours - storm.

November 2005   Overcast and cold. Very windy on lake. No boats.

March 2006   Cold and overcast.

May 2006   Clear and Sunny 60F. Calm on lake, low to no winds, and few to no boats. Weather in past 24 hours,   clear.

Tributary Loading and Boundary Conditions

Table 2 lists the nine tributary inlets that contribute flow, sediment, and nutrients to Cedar Lake. Loadings were simulated using the Long-Term Hydrologic Impact Assessment and Non Point Source Pollutant Model (L-THIA/NPS), which was developed at Purdue University (Engle and Harbor 2005). Flow, sediment, and nutrient loadings were computed for runoff events using L-THIA/NPS based on measured precipitation records collected for nine months (276 days) between March 1st and November 31st, 2005, or day 60 to 334 of the year (USACE Chicago District 2006). In-situ measurements were taken at the confluence of each tributary to assess the water quality during baseflow conditions. Figure 4 shows the locations where baseflow water quality was measured. The computed hydrographs and associated sediment loadings indicate that during this period there were eight storm events that contributed runoff, sediment and nutrient flux into Cedar Lake. Outside of these eight storm events, nutrient and sediment influxes were considered negligible and not included in the model; however, baseflow was included corresponding to an influx of 0.0993 m^3/day (0.0182 gpm, calculated by David Bucaro of the USACE, September 7th, 2006).

Table 2. Tributary inlets to Cedar Lake and their location.

Tributary Inlet	Easting[a] (I-cell)	Northing[a] (J-cell)
North Point Marina	870163.9 (13)	680489.9 (45)
Condo	870824.9 (15)	681308.6 (44)
Chamber	870993.8 (22)	681301.5 (36)
Old Bank Building	871602.0 (16)	680610.3 (6)
Founders Creek[b]	*871451.1*	*679144.9*
Sleepy Hollow Ditch	870314.7 (4)	678482.3 (34)
No Name	870286.5 (10)	678076.6 (3)
Pickerel Creek	870627.7 (6)	677918.8 (5)
Golf Course	871103.0 (7)	678113.9 (10)

[a]Note: Coordinates referenced to SPCS, Indiana West – 1302 (meters).

[b]Note: Founders Creek data were only used for restoration Measure C.1 and subsequent restoration alternatives because it currently does not flow into Cedar Lake.

Figure 6 presents the total flow rate summed over all inlets as a function of time. Sediment loads were generally positively correlated to flow rate. Tributary loading data were also computed using L-THIA/NPS for phosphorus, dissolved phosphorus, chemical oxygen demand (COD), nitrogen, Kjeldahl nitrogen, and nitrate. These data were used in SNL-EFDC loading input files. Without site-specific data available on the distributions of nutrient forms, the specified distributions were based on those listed by Cerco and Cole (1995). Specifically, inlet COD was divided into 10% refractory particulate organic carbon, 35% labile particulate organic carbon, and 55% dissolved organic carbon. Inlet dissolved phosphorus was distributed into 10% refractory particulate organic phosphorous, 80% labile particulate organic phosphorous, and 10% dissolved organic phosphorus. Inlet nitrogen was specified as Kjeldahl nitrogen, and because typically 60% of Kjeldahl nitrogen is in the form of nitrate, for which there are actual measurements, the remaining 40% of Kjeldahl nitrogen was divided into 14% labile particulate organic nitrogen, 12% ammonia nitrogen, 10% dissolved organic nitrogen, and 4% refractory particulate organic nitrogen. A preliminary sensitivity analysis showed that the model is not sensitive to reasonable variations in the partitioning of the different forms of phosphorus and nitrogen. Dissolved oxygen and algae concentrations were assigned as 8.9 mg/L and 0.01 mg/L respectively.
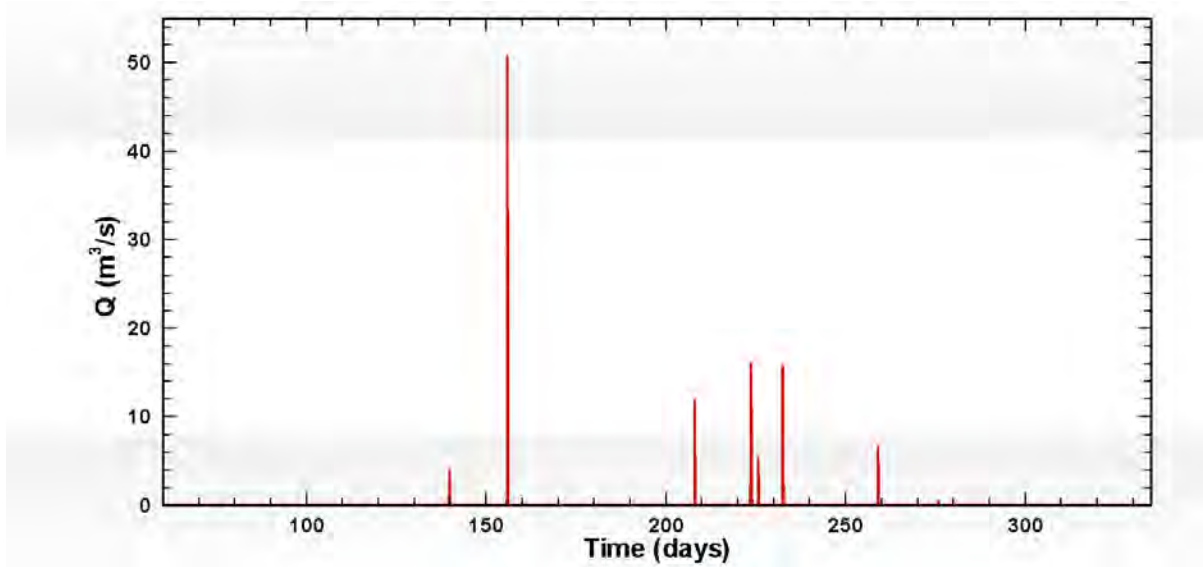
Figure 6. Total tributary flow rates during eight storm events in 2005.

There are several sources of phosphorus loading to Cedar Lake, namely: atmospheric deposition, tributary inlet loading, and sediment bed flux. The sediment bed accounts for the majority of phosphorus loading into Cedar Lake, and Figure 7 shows a breakdown of estimated phosphorus loading by source over nine months in 2005.

□ P from wet atmospheric deposition, 137 kg (0.72%)

□ P from tributaries (9 months), 1729 kg (9.04%)

□ P from dry atmospheric deposition, 85 kg (0.44%)

□ P in bed, 17186 kg (89.8%)
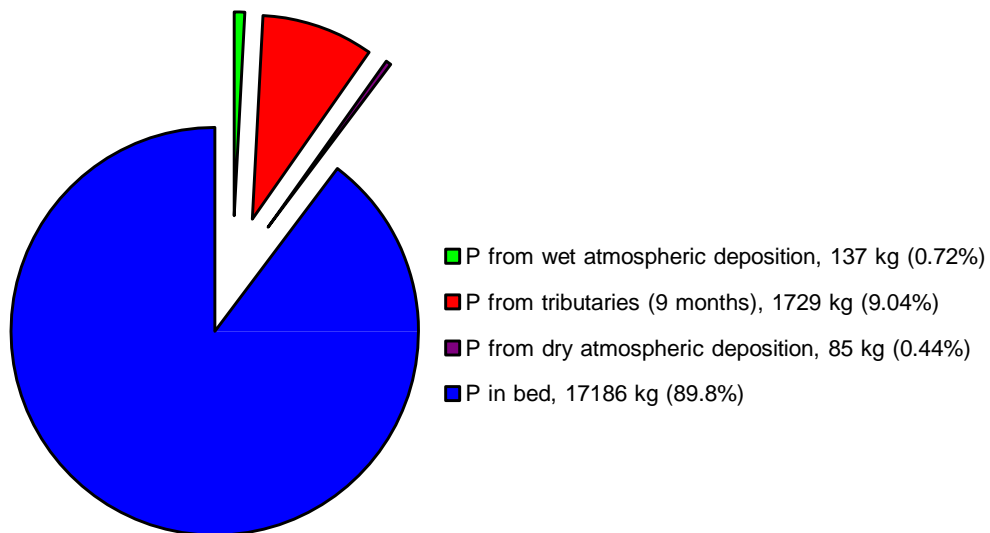
Figure 7. Estimated phosphorus loading by source for Cedar Lake. Listed values are estimates and are intended to show relative magnitudes of different sources.

Outlet Boundary Condition

Flow out of Cedar Lake is controlled by a broad-crested weir located midway along the eastern shore of the lake as shown in Figure 4. The weir is at an elevation of 211.86 meters above sea-level (masl) and when water in the lake rises above this level, outflow follows the rating curve shown in Figure 8, which is derived from the flow equation for a broad-crested weir (Franzini and Finnemore 1997, Chapter 10). It should be noted that the lake must rise 4 cm before any water flows out (zero water level is set 4 cm below the weir). The width of the weir is approximately 10 m.
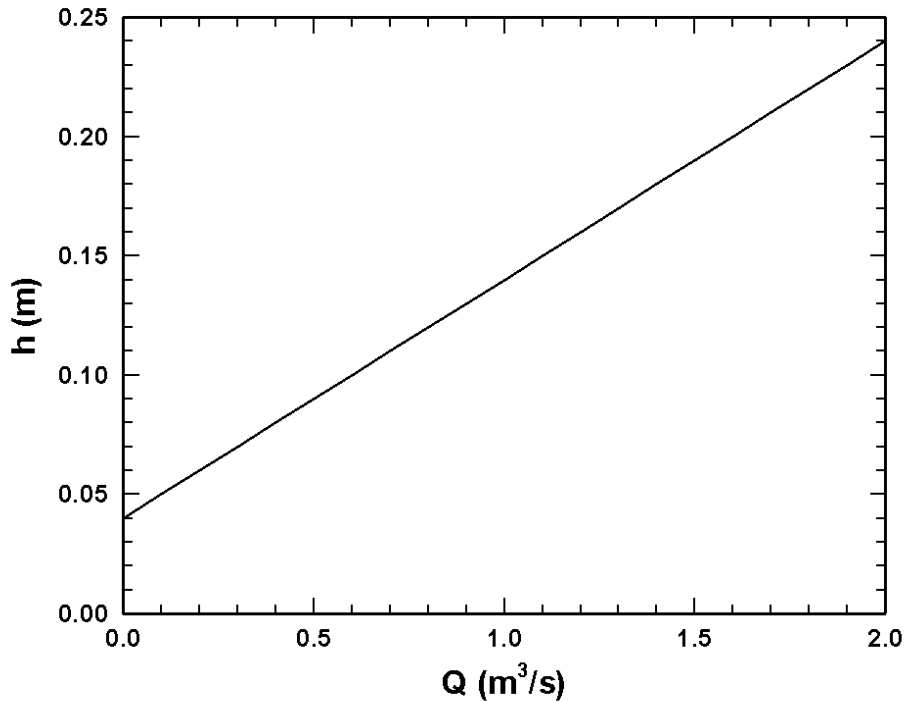
Figure 8. Broad-crested weir rating curve for Cedar Lake outlet.

Atmospheric Forcing

Atmospheric conditions (e.g., rain, wind circulation, and wind-driven waves) are the primary driving forces for hydrodynamic transport throughout Cedar Lake. For the 2005 calendar year, hourly data collected at the Porter County Municipal Airport in Valparaiso, Indiana located at latitude 41°27'N and longitude 87°01'W were incorporated into the model. Valparaiso Airport is located about 35 km east-northeast from Cedar Lake. The wind direction and magnitude are direct inputs for the model. Figure 9 is provided as a representation of the entire year of data where stick lengths correspond to wind speed, angle corresponds to direction and color indicates air temperature. A corresponding windrose is shown in Figure 10 representing average wind speed and directions over the same time period.
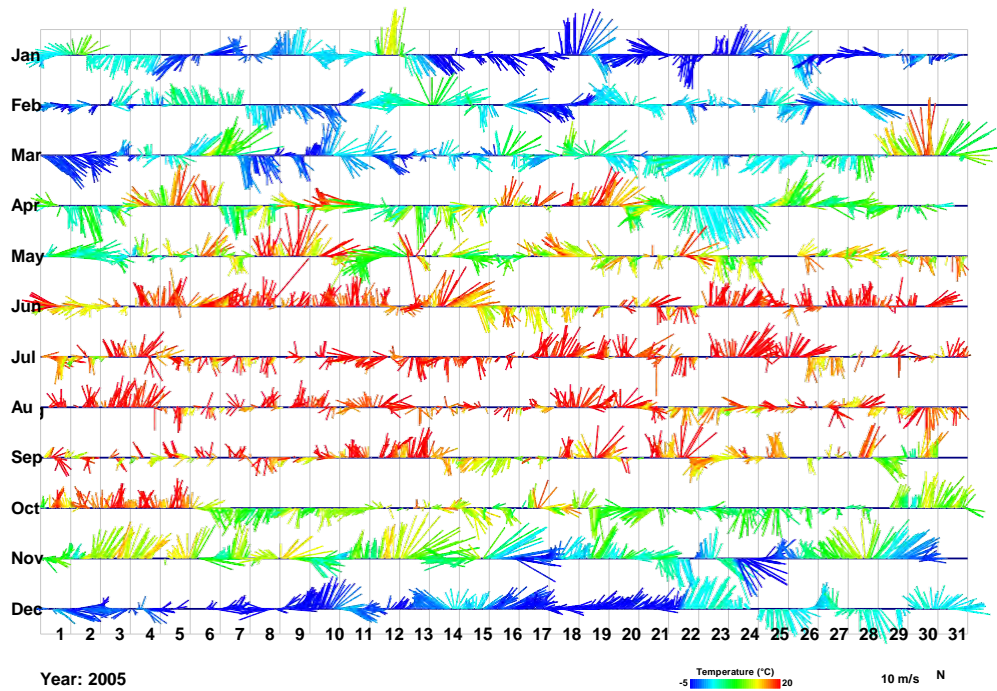
Figure 9. Wind direction and magnitude measured at Valparaiso Airport in 2005.
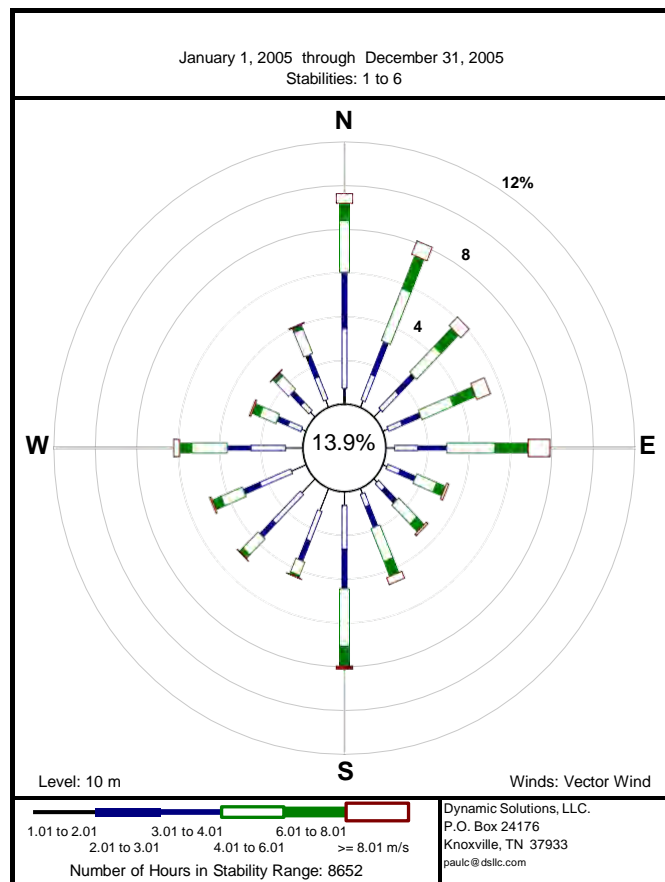
Figure 10. Windrose of measurements taken at Valparaiso Airport in 2005.

Temperature

Seasonal water temperature data at three different depths were collected by the USACE in 2005 at each of the three lobes within Cedar Lake as shown in Figure 4. Temperature profiles measured within the lake reveal only a small temperature gradient with depth, which indicates that Cedar Lake is well mixed. Due to the shallow depth and the long wind fetch length of Cedar Lake, waves tend to fully mix the water column. The water temperature of tributary inflows were assumed to roughly equal the temperature in the lake, therefore water temperature was averaged across depths and sample locations and used as tributary inflow temperatures. Table 3 lists the average water temperature and the corresponding day of the year for 2005 as applied to tributary inflows.

Table 3. Water temperature measured in 2005 and applied to tributary inflows.

Day of year	Temperature (°C)
0	3.0
62	2.7
97	4.7
132	19.7
146	13.9
160	22.1
174	23.2
188	20.9
202	23.1
216	21.8
229	20.6
244	23.5
258	19.9
293	11.6
366	3.0

Sediment Properties

As part of this modeling study, a field effort was conducted in July 2005 by SNL to determine the transport properties of Cedar Lake sediments. Sediment cores were collected from 16 locations around Cedar Lake to measure erosion rates and critical shear stresses. The data were measured as a function of depth in the sediment core and shear stress for each core using the SEDflume (McNeil et al. 1996). Particle size distributions and bulk densities were also measured as a function of depth for each erosion core. In addition, particle size distributions for 42 surface sediment samples (34 collected with a Ponar sediment sampler and 8 sediment samples collected by hand while wading in shallow water) were measured. The location of the SNL erosion core samples, Ponar samples, and grab samples indicating their respective median surficial particle sizes (in microns) are shown in Figure 11.
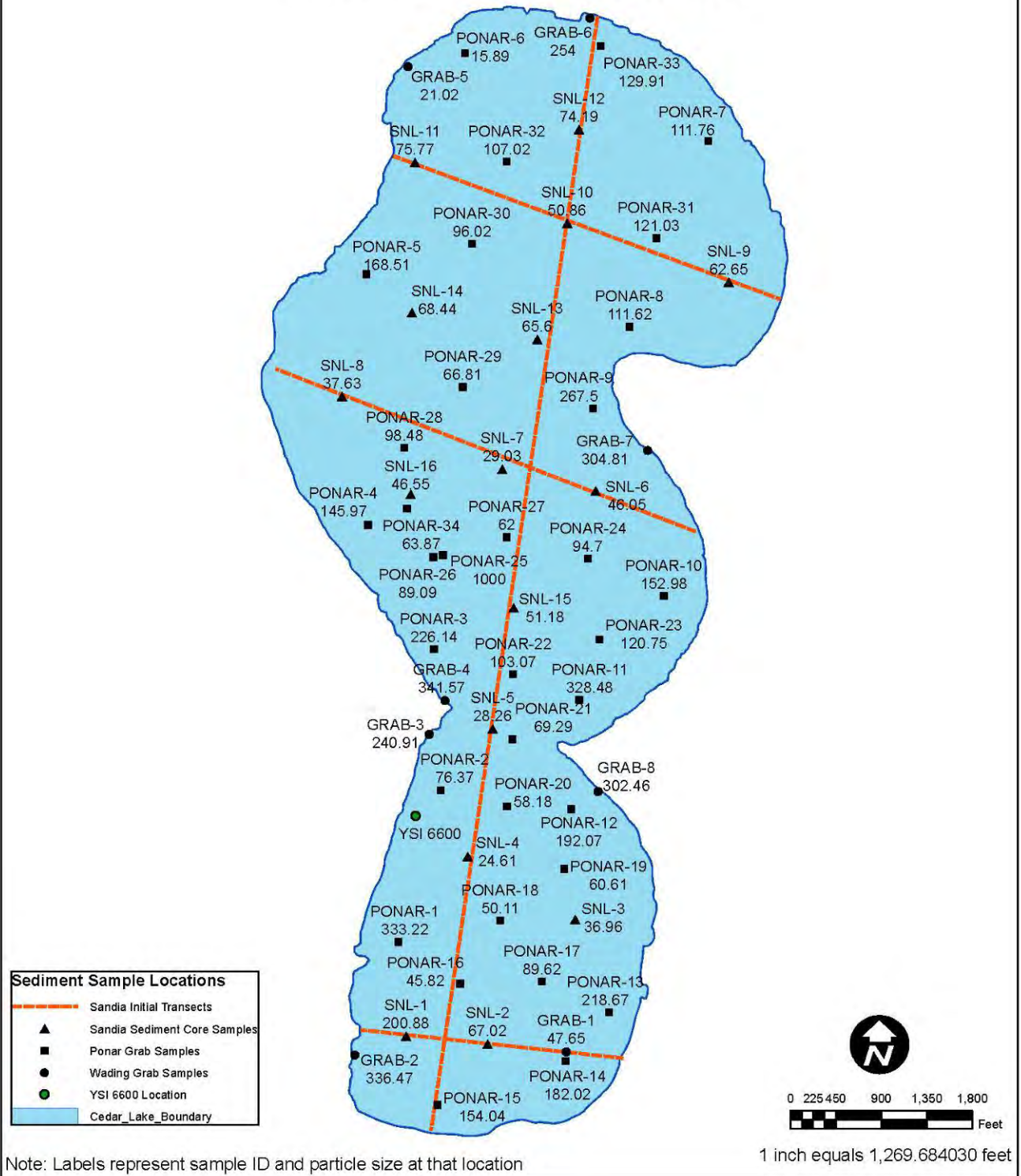
Figure 11. Sediment samples collected in Cedar Lake in July 2005 with associated particle sizes (microns).

At each sample site, triplicate particle size distributions were measured with a Malvern Mastersizer at various depths within each core. The Malvern distributes mass fractions across 64 particle-size ranges described by an exponentially increasing median bin size ranging from 0.06−880 □m. Particle-size measurements with corresponding sample numbers, locations (including local water depths), and depth within the core are presented in Table 4. A complete breakdown of sediment properties including erosion rates for the cores is documented in the report *Cedar Lake Sediment Erosion Study: Field Activities* (Roberts et al. 2005).

Table 4. SNL sediment core data collected in July 2005.

| Sample	Easting[a]	Northing[a]	Water depth (m)	Bulk properties measurement depths (cm)
SNL1	870455.6	678207.1	−2.6	2,7,11,16
SNL2	870702.0	678183.0	−3.3	6,12,16
SNL3	870966.7	678558.4	−3.7	1,3,5,8,13,18
SNL4	870642.0	678748.7	−3.9	5,10,15,22
SNL5	870717.7	679133.6	−3.5	4,8,13
SNL6	871028.8	679850.7	−3.8	3,8,14,15
SNL7	870746.5	679916.6	−4.1	4,8,13,20
SNL8	870262.2	680135.9	−2.6	4,9,15
SNL9	871430.7	680480.5	−2.0	3,8,13,17
SNL10	870942.8	680658.5	−2.8	3,9,14
SNL11	870483.0	680841.7	−2.3	3,8,12,16
SNL12	870978.2	680940.8	−2.5	3,7,11
SNL13	870852.8	680307.9	−3.4	4,8,12
SNL14	870474.2	680388.8	−2.8	3,7,12,16,20,25
SNL15	870780.8	679498.5	−3.7	5,10,15,25
SNL16	870469.7	679841.1	−2.7	4,22,26

[a]Note: coordinates referenced to SPCS, Indiana West – 1302 (meters)

Particle Size Classes

To model sediment transport, sediment distributions must be described with discrete particle size classes for each cell in the model grid. Previous work suggests that model accuracy and computational efficiency are maximized when an odd number of size classes are selected (James et al. 2006). Computational efficiency also dictates selection of fewer effective size classes. To effectively describe the sediment distribution in Cedar Lake, five size classes were used.

A two-part procedure was used to define the five size classes such that the variable sediment bed through Cedar Lake was adequately characterized at each grid cell. The smallest three size classes were calculated from the ensemble of erosion core particle-size data by dividing each particle size distribution into three "bins" with Malvern-Mastersizer-measured size ranges between: 0.1−12.2 (fine silt/clay), 14.2−56.2 (silt), and 65.5−878.7 □m (sand). This selection of ranges ensured that the mass-fraction averages across all samples were close to ⅓ in each bin (0.33, 0.34, and 0.33, respectively). The mass-fraction-weighted effective particle sizes of each bin are 5.4, 32.8, and 132.0 □m, respectively, and these values define the median size of the smallest three size classes. Various mass fractions of these three size classes were used to define all cohesive sediment cores (Roberts et al. 2005).

Nearshore sediments were often sandy and nearshore grab samples were used to define the size class distribution in shallow-water cells. The two largest size classes were calculated from grab sample data at

six of eight collection sites shown in Table 5. These data were collected near shore and therefore better represent the non-cohesive sediments typical of that region where SNL erosion cores were *not* collected. The non-cohesive samples were divided into two bins with effective sizes of 206.6 and 459.7 ☐m, respectively, based on the average of the six grab samples used. This division yielded an average mass fraction of 0.57 for the smaller size class and 0.43 for the larger size class. These non-cohesive sediment properties were assigned to a representative near-shore core designated as SNL17. Using the five size classes selected, a variable three-dimensional, three-layer sediment bed was defined in the model. Grain size distributions for each layer in each cell were defined using core-specific mass fractions as shown in Table 6 and Figure 12.

Table 5. Grab sample data collected by the US Army Corps of Engineers, Chicago District.

Sample	Easting[a]	Northing[a]	Mean particle size (μm)	
GRAB-1[2]	*678159.8*	*870940.3*	*47.7*	
GRAB-2	679117.2	870526.1	336.5	
GRAB-3	679218.9	870573.7	240.9	
GRAB-4	681130.9	870462.0	341.6	
GRAB-5[b]	*681277.2*	*871011.9*	*21.0*	
GRAB-6	679973.5	871186.0	254.0	
GRAB-7	678945.2	871036.4	304.8	
GRAB-8	678150.4	870301.4	302.5	

[a]Note: coordinates referenced to SPCS, Indiana West – 1302 (meters) [b]Note: Grab-1 and Grab-5 samples were excluded from the particle size analysis because they were hardpan clay and represent cohesive samples

Table 6. Size fractions of each sediment size class for each SNL sediment core. Note that in SNL-EFDC layers 1 and 2 are established after the initiation of erosion (i.e., they contain no sediment at the start of the model).

Core	SNL1	SNL2	SNL3	SNL4	SNL5	SNL6	SNL7	SNL8	SNL9	SNL10	SNL11	SNL12	SNL13	SNL14	SNL15	SNL16	SNL17[a]
Size class (μm)	LAYER 3 Size Fractions (%)																
5.4	6.0	30.1	43.4	47.5	42.6	25.9	39.8	33.0	22.5	25.2	19.5	19.6	23.4	19.1	24.3	29.8	0
32.8	5.1	29.1	35.7	41.7	41.7	36.1	46.2	42.1	36.5	39.7	34.3	33.2	36.2	32.7	42.2	38.8	0
132.0	88.9	40.8	21.0	10.8	15.7	38.0	14.0	24.9	41.0	35.1	46.2	47.2	40.5	48.2	33.5	31.4	0
206.6	0.0	0.0	0.0	0.0	0.0	0.0	0.0	0.0	0.0	0.0	0.0	0.0	0.0	0.0	0.0	0.0	56.6
459.7	0.0	0.0	0.0	0.0	0.0	0.0	0.0	0.0	0.0	0.0	0.0	0.0	0.0	0.0	0.0	0.0	43.4
Size class (μm)	LAYER 4 Size Fractions (%)																
5.4	6.4	39.2	34.7	39.0	49.3	26.6	46.3	22.4	31.0	27.2	25.9	20.4	40.1	52.4	35.1	40.7	0
32.8	7.2	30.4	35.4	39.5	37.6	36.7	43.2	31.4	31.4	36.1	30.8	36.0	38.5	26.7	42.0	36.5	0
132.0	86.4	27.8	29.9	21.5	13.2	36.7	10.5	46.2	37.6	36.7	43.3	43.6	21.3	20.9	22.9	22.8	0
206.6	0.0	0.0	0.0	0.0	0.0	0.0	0.0	0.0	0.0	0.0	0.0	0.0	0.0	0.0	0.0	0.0	56.6
459.7	0.0	0.0	0.0	0.0	0.0	0.0	0.0	0.0	0.0	0.0	0.0	0.0	0.0	0.0	0.0	0.0	43.4
Size class (μm)	LAYER 5 Size Fractions (%)																
5.4	6.3	33.1	32.6	58.7	49.3	26.1	44.6	22.4	38.4	27.2	27.0	20.4	40.1	49.7	48.4	38.4	0
32.8	7.7	32.8	35.1	35.2	37.6	36.2	43.9	31.4	31.0	36.1	33.7	36.0	38.5	29.1	40.5	36.5	0
132.0	86.1	34.0	32.3	6.1	13.2	37.7	11.5	46.2	30.6	36.7	39.3	43.6	21.3	21.3	11.1	25.1	0
206.6	0.0	0.0	0.0	0.0	0.0	0.0	0.0	0.0	0.0	0.0	0.0	0.0	0.0	0.0	0.0	0.0	56.6
459.7	0.0	0.0	0.0	0.0	0.0	0.0	0.0	0.0	0.0	0.0	0.0	0.0	0.0	0.0	0.0	0.0	43.4

[a]Artificial sediment core used to represent non-cohesive sediments near shore.

Table 7. Sediment densities with depth. Note that in SNL-EFDC layers 1 and 2 are established after the initiation of erosion.

Layer	SNL1	SNL2	SNL3	SNL4	SNL5	SNL6	SNL7	SNL8	SNL9	SNL10	SNL11	SNL12	SNL13	SNL14	SNL15	SNL16	SNL17[a]
	Density (g/cm^3)																
3	1.81	1.16	1.14	1.08	1.12	1.11	1.07	1.11	1.12	1.10	1.34	1.11	1.10	1.08	1.07	1.09	1.90
4	1.58	1.14	1.11	1.13	1.17	1.09	1.12	1.16	1.20	1.13	1.42	1.18	1.17	1.17	1.13	1.14	1.90
5	1.52	1.10	1.09	1.15	1.17	1.09	1.13	1.16	1.21	1.13	1.32	1.18	1.17	1.17	1.14	1.17	1.90

[a]Artificial sediment core used to represent non-cohesive sediments near shore.

Vertical Distribution of Sediment Density and Particle Size

Based on the number of erosion and density measurements taken for each core, the sediment bed was discretized into three 10-cm increments of 0−10, 10−20, and 20−30 cm. While numerous sediment layers are preferred to better capture the heterogeneity of the sediment bed, the amount of available data did not warrant more than three sediment layers in the model. Sediment bulk density was measured with depth in each core and assigned as listed in Table 7. Average measured density was 1.17 g/cm^3 (SNL17 was not included in this average because it was a hypothetical noncohesive core) and densities were not used to modify erosion rates. Where multiple density and mass-fraction measurements existed within a 10-cm depth interval, their values were averaged (e.g., for SNL14, the 3- and 7-cm, 12- and 16-cm, and 20- and 25-cm measurements were averaged). If only a single measurement existed, its value was used (e.g., SNL2 where the 6-cm measurement was used for the 0−10 cm interval). When no measurement was taken within an interval, the measurement from the nearest depth was used (e.g., SNL13 where the 12-cm measurement was used for the 20−30-cm interval). Overall, data collected by Roberts et al. (2005) were used to specify spatially variable (both horizontally and vertically) densities and mass fractions The density of SNL17 was set equal to 1.9 g/cm^3, a common density for non-cohesive sands (Roberts et al. 1998). The interested reader should refer to the Roberts et al. (2005) report *Cedar Lake Sediment Erosion Study: Field Activities*, which carefully outlines the data collection activities, analyses, and results.

Horizontal Distribution of Sediment Data

Median particle size was assumed to be a strong indicator of sediment characteristics and erosion behaviors and was thus used to specify horizontally distributed sediment properties throughout the model domain. Recall that median erosion rate variance within grouped cores was generally an order of magnitude less that erosion rate variance across all cores (see Roberts et al. 2005 for these data). Particle-size data consist of median particle size for multiple surface samples collected at Cedar Lake including SNL cores, Ponar, and grab sediment samples. These data were spatially distributed smoothly over the model domain using kriging interpolation to yield median particle sizes for each model-cell center coordinate. These interpolated surficial particle sizes were used to determine which sediment erosion core and corresponding erosion rates were assigned to each grid cell.

A category system was developed from the surface particle-size data collected with the SNL erosion core samples. The eight categories with particle size ranges of 0–30, 30–40, 40–50, 50−60, 60–70, 70−100, 100–200, and >200 ☐m are listed in Table 8. The median erosion rate variances within grouped cores were generally an order of magnitude less that erosion rate variance across all cores (see Roberts et al. 2005 for these data). Six of the eight categories include multiple SNL erosion cores because their surficial particle sizes are similar and fall within the same specified range. The eighth category represents large particle sizes, found mostly near the shoreline, that are outside of the range of sizes captured in SNL erosion samples. The hypothetical erosion core designated by SNL17 (Category 8) represents non-cohesive, large-grained sediments with erosion properties derived from previous erosion measurements on narrowly graded quartz sand with SEDflume (Roberts et al. 1998). The weighted-average median particle size for the non-cohesive Ponar samples was 315.4 ☐m and this was assigned to SNL17.

The contoured (kriged) particle size representative of each grid cell is associated with the particle size category into which it falls. Once all model cells are partitioned into these categories, the specific core with which to associate the model cell must be selected (i.e., contoured surficial particle size was used to specify the erosion core used to simulate erosion within a model cell). Because categories 1–6 comprised multiple SNL erosion samples, the sample core physically closest to the grid cell in question was assigned to that model cell. Roberts et al. (2005) graphically display all erosion rates and correlations are easily observed between grouped sediment cores. A statistical analysis comparing erosion rates within grouped cores to erosion rates across all cores consistently (with only a few exceptions) showed significantly smaller variance (typically an order of magnitude) within grouped cores than across all cores indicating that grouped cored generally eroded similarly. Overall, while variances generally increased as applied shear stresses increased, inter-group variance was usually less than variance across all cores.

Table 8. Surficial median particle size and corresponding sediment core.

Category ID	Sample ID	Surface Particle Size (μm)	Range of Critical Shear Stresses (Pa)	Category Particle Size Range (μm)
1	SNL4	24.6	0.05–0.61	0–30
	SNL5	28.3	0.06–0.30	
	SNL7	29.0	0.06–2.00	
2	SNL3	37.0	0.05–0.65	30–40
	SNL8	37.6	0.06–0.53	
3	SNL6	46.1	0.07–1.50	40–50
	SNL16	46.6	0.13–0.56	
4	SNL10	50.9	0.06–0.48	50–60
	SNL15	51.2	0.05–0.28	
5	SNL9	62.7	0.07–0.48	60–70
	SNL13	65.6	0.07–0.33	
	SNL2	67.0	0.06–0.27	
	SNL14	68.4	0.13–2.90	
6	SNL12	74.2	0.05–0.28	70–100
	SNL11	75.8	0.14–1.90	
7	SNL1	200.9	0.24–0.60	100–200
8[a]	SNL17	315.4	NA	>200

[a]Note: Category 8 represents a hypothetical non-cohesive sediment core.

As a two-step process, erosion characteristics are first assigned to the erosion core category with the nearest particle size. For categories containing multiple erosion cores, the nearest neighbor as measured by minimum physical distance within the category is selected. In certain instances, the core number assigned to a nearshore model cell was manually adjusted to ensure that erosion was not excessive. For example, it is unlikely to find an easily eroded core near most shoreline areas where high shear stresses are prevalent (the northwest coast is an exception). When such an instance was detected (by the model indicating erosion greater than the 30-cm core length), the core number was changed to SNL17, which corresponds to non-cohesive sandy sediments. Figure 12 shows the distribution of cores used to model Cedar Lake (based on contoured surficial particle sizes).
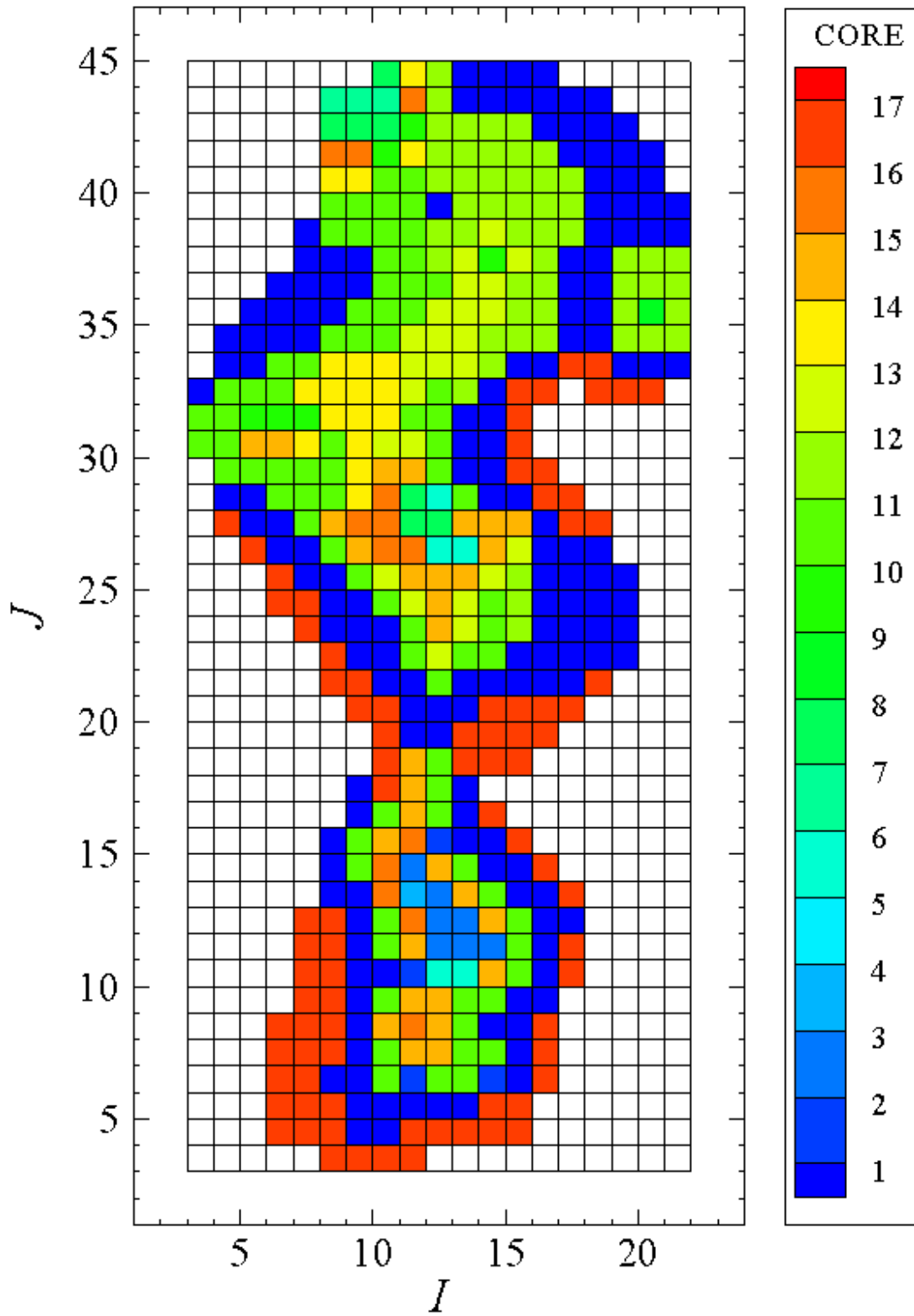
Figure 12. Distribution of sediment cores in the Cedar Lake model.

Transport of eroded sediment

As discussed above, five individual size classes are used to approximate the distribution of sediments in the Cedar Lake model. Both critical shear for erosion (minimum shear yielding some erosion) and critical shear for suspension (minimum shear yielding suspension) must be specified for each effective particle size to describe the particle size class' transport characteristics. Based on the classic Shields curve (van Rijn 1993) for cohesive sediments (smallest three size classes) and the Roberts et al. (1998) data[1] for non-cohesive sediment (largest two size classes), critical shear stresses for erosion are 0.50, 0.60, 1.10, 2.26, and 3.03 dynes/cm^2 for the 5.4-, 32.8-, 132.0-, 206.6-, and 459.7-μm particles, respectively. Critical shear for suspension of these particles are 0.50, 0.60, 1.10, 3.00, and 4.30 dynes/cm^2, respectively (van Rijn 1993). The reader is referred to the Cedar Lake sediment analysis report of Roberts et al. (2005) for a thorough description of sediment characteristics at the site.

Erosion rate of *newly deposited* sediments

Newly deposited sediments are defined as those that have undergone erosion (and perhaps suspension) and have come to rest again on the bed. Subsequent re-erosion of these sediments is described by the SEDflume data collected within the top 5 cm of each sediment core. That is, only surficial erosion rate data collected with SEDflume are used to describe *newly deposited* sediment erosion rates. To this end, five sediment size interpolants were selected: 5.4, 32.8, 132.0, 422.0, and 1,020.0^2 □m. Erosion rates of these *newly deposited* sediment layers are based on SEDflume data from Cedar Lake (Roberts et al. 2005) where erosion data from only the top 5 cm (2 in) were used[3]. The derivation of the erosion rates for each of the five interpolants (5.4, 32.8, 132, 422, and 1,020 □m) at each of the five SEDflume shear stresses is discussed below and presented in Table 9.

Table 9. Interpolation table used to calculate the erosion rates (cm/s) of newly deposited sediments in Cedar Lake based on the d50 within a grid cell.

d_{50} (μm)	Shear stress (dynes/cm^2)					
	1.0	2.5	5.0	10.0	20.0	40.0
5.4	8.44×10^{-4}	7.89×10^{-3}	1.95×10^{-2}	4.67×10^{-2}	0.1	0.1
32.8	1.09×10^{-3}	5.22×10^{-3}	8.08×10^{-3}	1.05×10^{-2}	1.24×10^{-2}	1.24×10^{-2}
132.0	2.58×10^{-4}	1.21×10^{-3}	6.10×10^{-3}	1.40×10^{-2}	1.76×10^{-2}	5.71×10^{-2}
422.0	10^{-9}	3.65×10^{-4}	3.82×10^{-3}	2.25×10^{-3}	1.33×10^{-1}	7.82×10^{-1}
1,020.0	10^{-9}	2.01×10^{-4}	2.00×10^{-3}	1.14×10^{-3}	6.49×10^{-2}	3.70×10^{-1}

---

[1]Although the Roberts et al. (1998) data were collected with quartz particles, for the individual size-class properties (not bed properties) at Cedar Lake, it is not possible to measure the critical shear stresses for erosion or suspension without a prohibitively detailed site-specific investigation. Therefore, the Roberts data are used as an initial specification for recently deposited sediment only. These data are consistent with the specifications predicted for individual size classes by van Rijn (1993).

[2]The 422- and 1,020-□m size classes were selected because erosion data specific to these size classes were reported by Roberts et al. (1998).

[3]Without incorporation of a consolidation model or development of consolidation erosion data, it is assumed the surface material is most representative of *newly deposited* sediment with regard to its erosion properties.

Because the minimum size for sediment in the model is 5.4 μm, this is the smallest d_{50} size in the interpolation table. To estimate critical shear stress for the 5.4-μm interpolant particle size (0.8 dynes/cm^2), all critical shear stress measurements (in the top 5 cm) for cores with median surficial particle size less than 30 μm (Category 1 in Table 8) were averaged. The surface critical erosion rate variance within this core group is 0.001, while the surface erosion rate variance across all cores is 0.013 indicating that this is an appropriate approximation. Equating critical shear to an erosion rate of 10^{-4} cm/s and using log-linear interpolation produces an erosion rate of 8.44×10^{-4} cm/s at 1.0 dynes/cm^2 for this size class. Next, erosion rates at higher shear stresses were taken directly from core measurements as the averages across Category 1 resulting in erosion rates of 7.89×10^{-3}, 1.95×10^{-2}, and 4.67×10^{-2} cm/s at shear stresses of 2.5, 5.0 and 10.0 dynes/cm^2, respectively. There were no erosion measurements at higher shear stresses because none of these cores withstood such shear stresses, hence the maximum 0.1-cm/s erosion rate specified for this particle size at high shear stresses. In addition, the deeper depositional portions of Cedar Lake never experience these high shear stresses; nevertheless, the data are included for generality here.

The newly deposited 32.8-μm interpolant size was specified to erode as the average of the top 5 cm of the SNL sediment cores with mean surficial sizes between 30.0 and 50.0 μm (Categories 2 and 3) yielding erosion rates of 1.09×10^{-3}, 5.22×10^{-3}, 8.08×10^{-3}, 1.05×10^{-2}, 1.24×10^{-2}, and 1.24×10^{-2} cm/s for shear stresses of 1.0, 2.5, 5.0, 10.0, 20.0, and 40.0 dynes/cm^2, respectively.

Erosion rates for the newly deposited 132.0-μm interpolant size are calculated as the average erosion rates of the top 5 cm of the cores with mean surficial particle size greater than 50 μm (Categories 5 through 7) yielding erosion rates (within the top 5 cm) of 2.58×10^{-4}, 1.21×10^{-3}, 6.10×10^{-3}, 1.40×10^{-2}, 1.76×10^{-2}, and 5.71×10^{-2} cm/s for shear stresses of 1.0, 2.5, 5.0, 10.0, 20.0, and 40.0 dynes/cm^2, respectively.

The two largest interpolant sizes (422 and 1,020 μm) for newly deposited sediments are specified to erode equivalent to the erosion rate data collected by Roberts et al. (1998). If no erosion occurs, erosion rates are set equal to 10^{-9} cm/s. The equivalency is based on the common assumption that larger quartz sands erode similarly. It is important to note that these large particle sizes are used only to interpolate an erosion rate of newly-deposited sediments for grid cells where d_{50} is larger than 132.0 μm (i.e., site data were used for the three smallest size classes and the Roberts et al. (1998) data were used for the largest two size classes). Critical shear stresses for the sandy sediments were determined using the van Rijn (1993) technique. The methodology is again based on the common assumption that larger quartz sands erode similarly.

It is important to note that the erosion of these sediments is based on the model-calculated d_{50} (median particle size) of the *newly deposited* sediment layer. Using the five different sediment sizes and corresponding erosion rates, the model log-linearly interpolates to find the corresponding erosion rate at the calculated d_{50}. For example, consider a newly deposited sediment layer having a d_{50} of 100 μm. If the model calculates a shear stress of 2.0 dynes/cm^2 (0.2 Pa), the erosion rate (1.44×10^{-3} cm/s) must fall somewhere within the four adjacent entries in Table 9 (1.09×10^{-3}, 5.22×10^{-3}, 2.58×10^{-4}, and 1.21×10^{-3} cm/s). Although erosion rates of newly deposited sediments were correlated to surficial particle sizes (see Table 9), their strength was not explicitly measured and is beyond the scope of this study. Nevertheless, this method is an appropriate approximation, especially considering that fine-grained sediments deposited near the center of the lake are not significantly re-eroded given the low shear stresses there (re-erosion primarily occurs in sandy sediments near the shore

where non-cohesive particle size dictates erosion rates).

Boat Waves

Cedar Lake is heavily used for recreation and significant boat activity leads to wave action and sediment resuspension, particularly in the near-shore environment. There currently is a 61-m (200-ft) no-wake zone along the perimeter, which corresponds approximately to depths less than 0.8 m (2.6 ft). In addition, there are no restrictions on the size or horsepower of boat allowed on Cedar Lake. Boat waves were simulated in the SNL-EFDC model through an increase in wave heights that leads to an increase in bed shear stresses. These wave heights are calculated using the following equation (Bhowmik et al. 1991):

$$\left(\frac{H_m}{d}\right)^2 = 0.139 V^{1.374} \left(\frac{x}{L}\right)^{-0.915},$$

where H_m is the wave height in meters, d is the boat draft (depth of the hull below the water surface), V is boat velocity, L is boat length, and x is the distance between the boat and the wave location. Based on observations of boating activity within Cedar Lake during the summer of 2005, a representative boat size was selected to simulate boat-induced waves in the model. It was assumed that the typical boat is a 7-m (23-ft)-long V-hull traveling at 15.6 m/s (35 mph or 51.3 ft/s) with a draft of 1 m (3.3 ft). A median distance for wave travel, which corresponds to the average distance between the boat and the shore, of 400 m (1,222 ft) yields a maximum wave height of about 40 cm (1.3 ft). The corresponding wave period was approximated to be 2 seconds (USACE Rock Island District 1997; 2001). Because boats on Cedar Lake are not present all the time, boat waves were implemented in the model between May 1st and September 30th, only when wind velocities are low and the weather is warm. These criteria are meant to simulate boating activity only during warm and relatively calm daylight hours. Although it is recognized that this is a major assumption, wave heights are implemented in the model as a direct function of normalized solar radiation only when wind speeds are below 10 knots (5.1 m/s). When boat waves are greater than wind driven waves, the boat-induced waves are used and assigned a 2-second period.

Baseline Simulation

The model was run for the nine-month period from March 1st through November 30th, 2005 to establish baseline sediment transport and water quality information. This nine month period is used to represent a normal open-water season at Cedar Lake. Ice cover conditions that normally occur in the winter between December and February were not simulated. SNL-EFDC tracks several hydrodynamic, sediment transport and water quality parameters, however only certain parameters are needed to indicate levels of eutrophication and ecosystem degradation. Baseline results are presented as averaged sediment concentrations, phosphorus concentrations, and algae concentrations. The goal of this section is to outline model calibration and validation, and to establish confidence that the baseline model will produce sufficient results when analyzing the various ecosystem restoration measures and alternatives.

Initial Water Column Conditions

The initial conditions listed in Table 10 were specified to correspond with various data measured in 2005. For constituents with multiple forms (such as labile, refractory, and dissolved nitrogen) the concentrations were assumed to be evenly distributed unless additional measured data were available.

The nutrient cycle within the model assumes dissolved phosphorus is metabolized by algae during growth and released as phosphate and organic phosphorus through respiration and predation. A portion of the particulate organic phosphorus hydrolyzes to dissolved organic phosphorus. The remainder settles to the sediments. Dissolved organic phosphorus is mineralized to phosphate. A portion of the phosphate sorbs to inorganic solids and settles to the sediments. Within the sediments, particulate phosphorus is mineralized and recycled to the water column as dissolved phosphate. Additional information on nutrient cycling in the water column and sediment bed diagenesis is available in the work of Cerco and Cole (1995).

Table 10. Initial water column concentrations.

Parameter	mg/L
Cyanobacteria	0
Diatoms	0
Green algae	1
Refractory POC	0.05
Labile POC	0.05
Dissolved organic carbon	0.045
Refractory particulate organic phosphorous	0.003
Labile particulate organic phosphorous	0.003
Dissolved organic phosphorous	0.003
Total phosphate	0.001
Refractory particulate organic nitrogen	0.5
Labile particulate organic nitrogen	0.5
Dissolved organic nitrogen	0.5
Ammonia nitrogen	0.3
Nitrate nitrogen	0.1
Particle biogenic silica	0.1
Dissolved available silica	1.2
Chemical oxygen demand	1
Dissolved oxygen	10
Total active metal	0
Fecal coliform	0
Suspended sediment class 1	12[a]
Suspended sediment class 2	12[a]
Suspended sediment class 3	12[a]
Suspended sediment class 4	0
Suspended sediment class 5	0

[a]Average sediment concentration simply divided into the three classes because there are no data to specify this distribution any differently.

Model Calibration

The nine-month baseline model runs were calibrated against phosphorus concentrations in the water column collected between June and November, 2005. Three samples were collected each month at fixed depths in the water column from each of the three lobes of the lake. Because the samples at each location in the lake were generally quite consistent, they were averaged and compared to lake-wide-

averaged model outputs, which were also similarly consistent indicated well-mixed conditions. Table 11 lists the averaged measured total phosphorus, total phosphate, and total suspended solids (TSS) concentrations. The full data set of measured variables was presented in Table 1. Because no reliable data were available for algae, this parameter was not examined during calibration other than to ensure that it remained below the TSS levels measured in Cedar Lake.

Table 11. Averaged measured concentrations in the water column (also, see Table 1).

Sample	Total phosphorus (mg/L)	Total phosphate (mg/L)	TSS (mg/L)
June	0.14	0.02	43.3
July	0.07	0.07	50.0
August	0.06	0.01	31.7
September	0.09	0.01	37.3
November	0.05	0.05	17.3

Limited data are available on suspended sediment concentrations; only TSS concentrations were available and they include algae, sediments, and other large solid material suspended in the water column. The model runs showed that sediment concentrations remained below TSS measurements during most of the simulation period, although storm events can yield localized sediment concentration up to an order of magnitude higher. Sediment concentrations were largely controlled by wave activity in the near shore region. The wave-generated shear stresses are dependent on the specified bed roughness. A site-wide bed roughness of 10^{-4} m was used throughout the lake based on the surficial particle size in the lake and exploratory model calibration runs (recall that most of the lake bottom was less than 75 $\square$m, see Table 8). Although surface roughness largely controlled suspended sediment concentrations, the roughness parameter was not specifically calibrated, because water quality modeling (phosphorus and algae concentrations) was the focus of this work. Efforts were spent calibrating the phosphorus diffusion coefficient from the sediment bed rather than bed roughness, which controlled the sediment concentrations.

Based on the magnitude of phosphorus loads from: (1) tributaries; (2) diffusion from the sediment bed; (3) desorption from suspended sediments; and (4) atmospheric deposition, diffusive flux of phosphorus from the sediment bed was consistently shown to be the primary contributor to water column phosphorus concentrations as shown in Figure 7. Diffusive fluxes from the bed are largely controlled by the model-specified diffusion rates. For calibration, sediment bed diffusion coefficients were varied until water column total phosphorus concentrations approximated measured phosphorus concentrations with results shown in Figure 13. Sediment bed diffusion coefficients were the only parameters adjusted during calibration because they are largely site specific. The calibrated diffusion coefficient in pore water was determined to be 9.4×10^{-6} m^2/s while the calibrated diffusion coefficient for particle mixing (bed diffusion, including increases due to bioturbation, etc.) was determined to be 8×10^{-5} m^2/s. The diffusion coefficient in pore water proved to be the most sensitive parameter in controlling overall phosphorous concentrations. The baseline simulation underestimates phosphorous concentrations against measured data toward the beginning of the year, but with such sparse data, it is difficult to establish if the measured datum is an outlier or if this discrepancy is due to some other external forcing condition (e.g., significant phosphorus source due to fertilizer use in the spring). It should be noted that in the context of model calibration on Cedar Lake (where there are extremely limited data), the phosphorus diffusion coefficient from the bed is an effective parameter that represents multiple processes including sediment resuspension and phosphorus/sediment partition coefficient.

The model was calibrated to the measured phosphorus data in Table 11. In a preliminary sensitivity analysis, a strong correlation was observed between phosphorous and algae

33

concentrations. If the phosphorous concentration is greater than 0.2 mg/L, further increases yield minimal effect on algal growth; but if the phosphorous concentration is less than 0.2 mg/L decreases in phosphorous result in significant decreases in algal growth. This suggests the model correctly represents phosphorous as the limiting reagent. Recall that the phosphorous concentration within Cedar Lake (both modeled and observed) remains well below 0.2 mg/L. Also, when algae concentrations are high and phosphorous low, algae die off rapidly due to nutrient deficiency. Variations of other factors such as nitrate and ammonia concentrations had negligible effects on algal concentration.
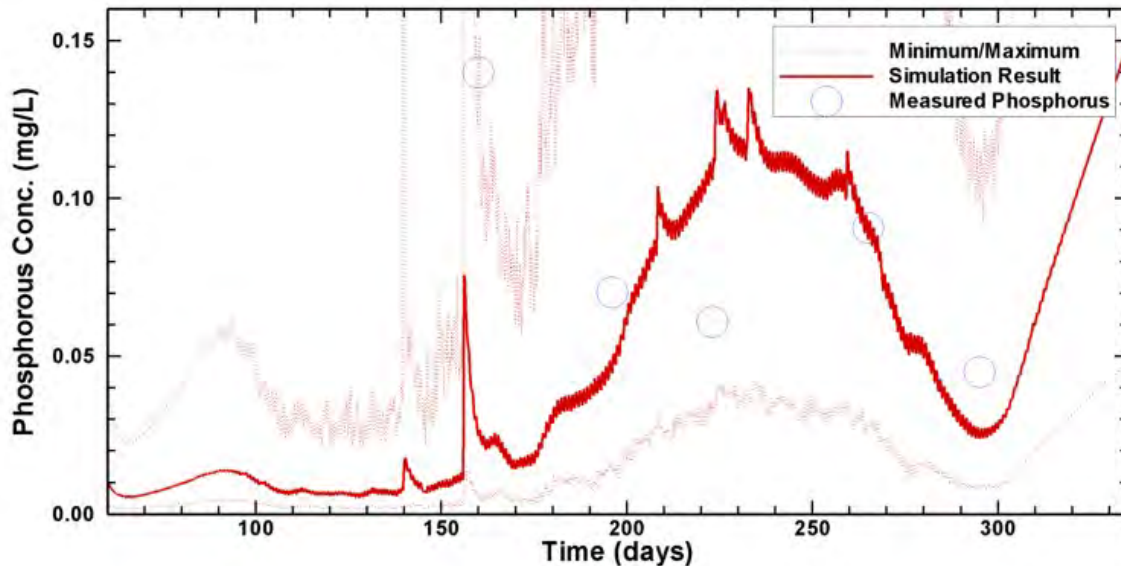
Figure 13. Simulated versus measured lake-averaged phosphorus concentrations. The maximum/minimum throughout the lake is also presented.

Baseline Model

In any system, bottom shear stresses drive sediment resuspension. In Cedar Lake, peaks in sediment concentration as shown in Figure 14 correspond to peaks in shear stress, which are shown in Figure 15. Some shear events have a greater effect than others because wind direction dictates the fetch length and determines which shore receives increased shear due to wind-induced wave action. For example, because of the relatively fine sediments located along the northern shore of the lake, high concentrations of suspended sediment are observed when wind comes from the south. Note from Figure 10 that southern winds are prominent. Afterward, the sediments settle quickly and show only minimal increases in water column concentrations in ensuing days. Tributary loading raises sediment concentrations for short periods and the effects of boat waves on lake-averaged stress are evident when examining days 120 to 274 in Figure 15. Boat activity significantly increases shear stresses and sediment resuspension in summer months.

34
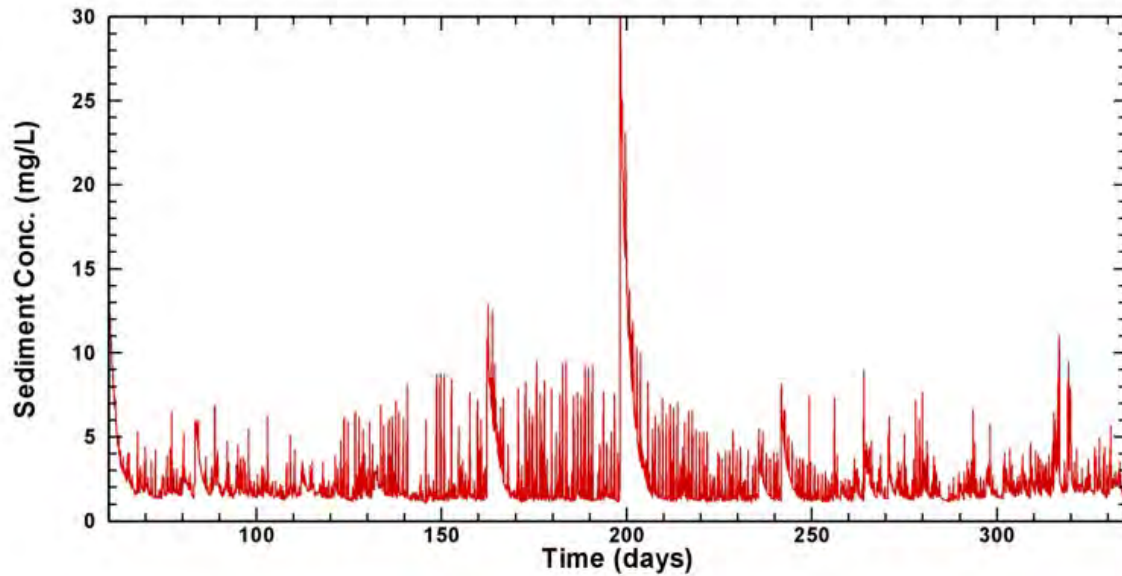
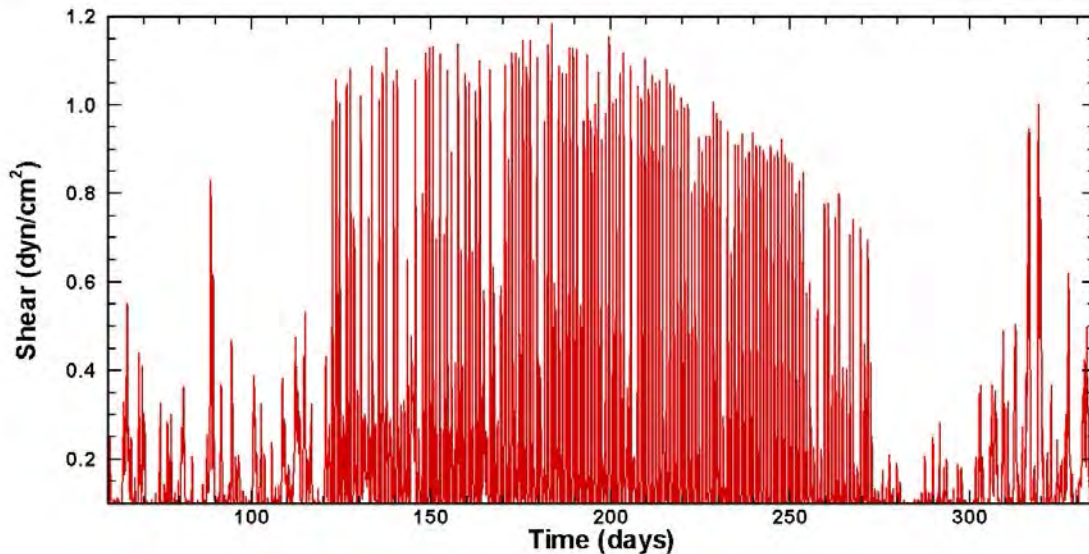Figure 14. Simulated baseline average suspended sediment concentration within Cedar Lake.

Figure 15. Simulated bottom shear stresses within Cedar Lake with boating activity between May 1st and September 30th (or day 120 to 274).

Measured and model averaged phosphorous concentrations for the nine-month baseline simulation are shown in Figure 13. The reasonably sharp increase that begins around day 180 is correlated to an increase in overall air temperature. The corresponding water temperature increase facilitates an increased diffusive flux of phosphorus from the sediment bed. Although the model does not exactly reproduce observed concentrations, the overall model average is within the scatter of the measured data. Note the diurnal variation in phosphorus concentrations due to temperature and incident sunlight changes, which impact algal concentrations. Because phosphorus in algae is not counted in the aqueous phosphorus concentrations, when algae die off they evolve phosphorus yielding the significant increase

35

that begins around day 295. Figure 16 illustrates the roughly constant rate of algal die-off starting at day 295 and continuing toward the end of the modeling period. If the simulation time were extended, the rate of algal die-off would decrease as there would be little or no algae left thus stopping the evolution of phosphorous from dead algae and stabilizing the phosphorous concentration. Because low temperatures inhibit diffusive fluxes and a frozen surface virtually eliminates lake mixing, labile and refractory phosphorous eventually settle to the sediment bed yielding a low water column phosphorous concentration (as specified in the beginning of the model).

Model results show a correlation between increases in dissolved phosphorus concentrations and increases in sediment concentrations because phosphorus desorbs from suspended sediments according to the equilibrium partition coefficient of 0.001 L/kg (Haggard and Moore 2005; Wodka et al. 1983). The model shows that after times of increased suspended sediment concentrations, peaks are observed in phosphorous concentrations. Tributary influx can also increase phosphorous concentrations which is particularly apparent around day 156, the largest influx event. Despite the obvious contributions from sediment desorption and tributary loading, diffusive flux from the sediment bed is the primary contributor to phosphorous concentrations within the lake.

Green algae growth is governed by a multiplicative relationship between the availability of nutrients, light intensity, and ambient temperature (Cerco and Cole 1995). During the summer months, sunlight and high water and air temperatures yield significant algal growth limited only by the availability of nutrients – most notably phosphorous. When water temperatures climb above about 20°C algae growth is stimulated and when temperatures fall below about 15°C, algae die off. Lack of sunlight during late fall causes algae die-off and the availability of nutrients is less important during these cooler months. Figure 16 shows the relationship between water temperature and algae concentrations in Cedar Lake.
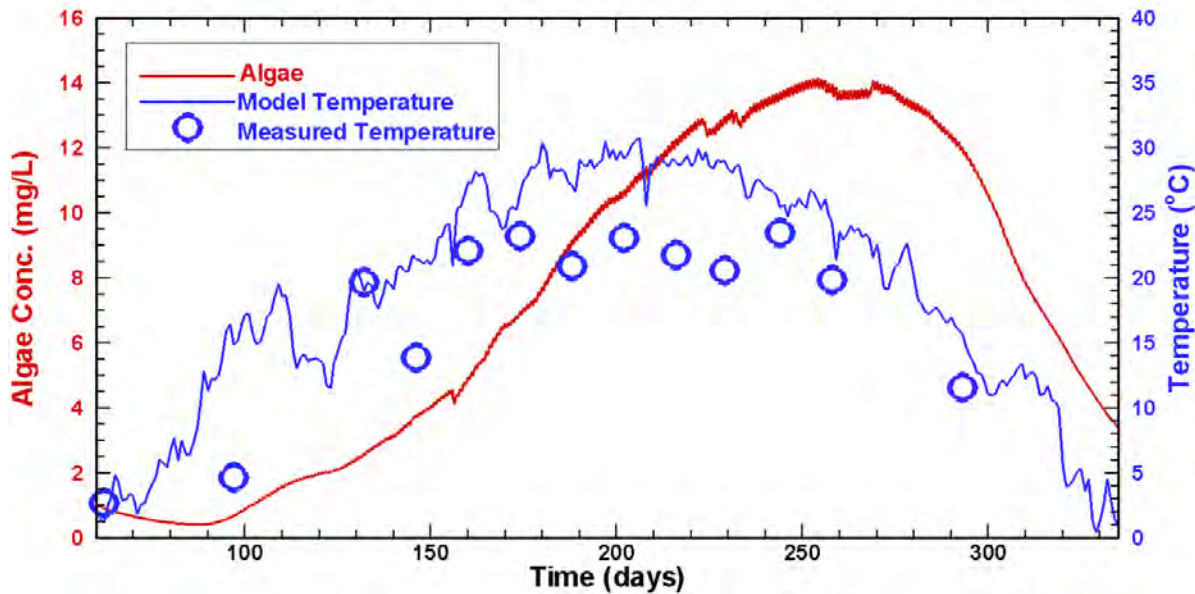

Figure 16. Simulated baseline average algae concentration and water temperature in Cedar Lake.

Because phosphorous concentrations are always less than 0.2 mg/L, phosphorous is the limiting factor in algal growth. Algal concentrations increase with increasing phosphorous concentrations and rising temperatures. The rate of increase of algae concentration begins to decrease around day 280. The maximum algae concentration is observed between days 250 and 280, while the drop in temperature at approximately day 280 causes algal die-off. Note the corresponding increase in total phosphorus levels evolved from dead algae.

The net mass of total (refractory plus labile plus dissolved) phosphorus evolved from the sediment bed is calculated as the product of the net phosphorus flux, grid cell area, and time as shown in Figure 17. Note that at first, phosphorus mass from the bed is negative indicating that phosphorus was deposited onto the bed due to the initial water column concentration. Also, decreases are noticed after storm events when phosphorus is deposited onto the sediment bed after tributary loading increases concentrations across the lake. Contributions over the 9-month model run from atmospheric deposition were 159 kg and tributary flux added an additional 1,729 kg. From Figure 17, the sediment bed is the main source of phosphorus for the system.
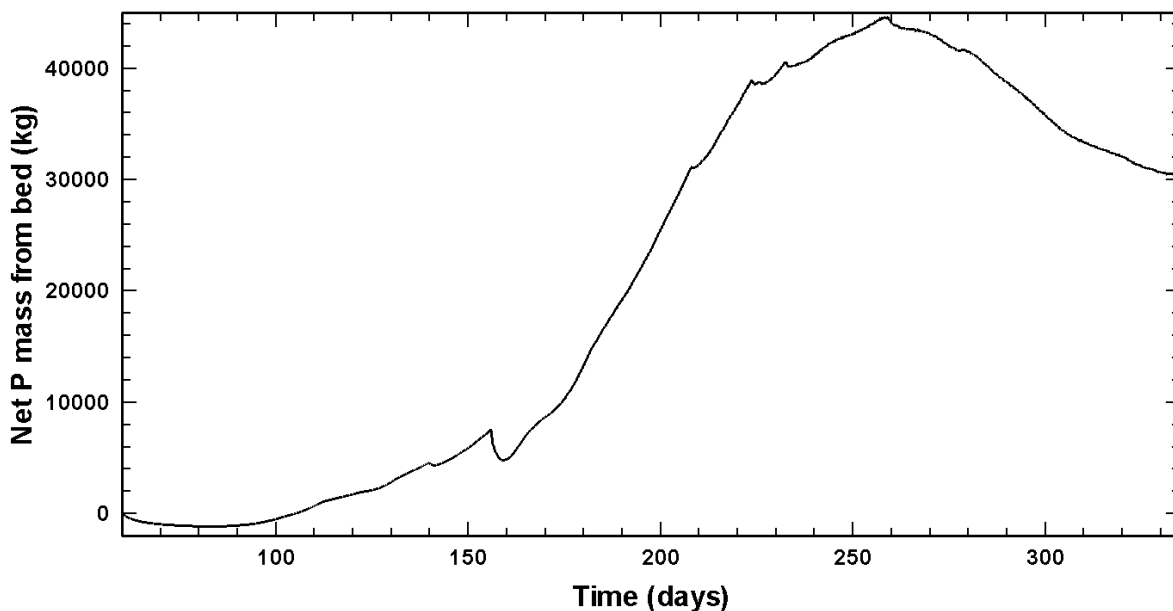
Figure 17. Simulated baseline mass transfer of phosphorus from sediment bed to water column.

Evaluating Ecosystem Restoration Measures

Several potential ecosystem restoration measures have been proposed to decrease phosphorous concentrations, prevent future eutrophication, and restore aquatic habitats in Cedar Lake. Addressing phosphorus laden sediments within Cedar Lake is necessary to reduce water column concentrations and level of eutrophication. Physical substrate restoration through dredging and chemical substrate restoration through aluminum sulfate treatments are being considered to address the existing flux of nutrients from bottom sediments. Tributary restoration by rerouting Founders Creek which naturally drained to Cedar Lake is also being considered. Reducing wave induced bottom shear stresses that contribute to resuspension of sediments is being investigated by the creation of habitat islands to reduce wind fetch length and implementing institutional controls on boat activity. The restoration of aquatic plants is being considered for structural habitat and nutrient uptake capabilities. A restoration of natural fish communities through management is also being investigated to replace non-native benthic feeders that intake and excrete phosphorus laden sediments. Because tributary loadings were historically the source of nutrient

rich sediments deposited in the lake, a reduction in future tributary inputs is advisable or benefits from implemented ecosystem restoration measures in the lake may be short lived. A list of proposed ecosystem restoration measures that were simulated are shown in Table 12.

Table 12. Description of proposed ecosystem restoration measures for Cedar Lake.

Measure	Description
A.1	180 ha (444 acres) dredged to 0.30 m (1 ft) depth
A.2	34 ha (83 acres) dredged to 1.65 m (5.4 ft) depth
A.3	34 ha (83 acres) dredged to 0.82 m (2.7 ft) depth
A.4	91 ha (224 acres) dredged to 0.30 m (1 ft) depth
A.5	25 ha (61 acres) dredged to 0.82 m (2.7 ft) depth
B.1	Apply aluminum sulfate treatment to 91-ha (224-acre) area (see A4)
B.2	Apply aluminum sulfate treatment to 34-ha (83-acre) area (see A2 and A3)
C.1	Reroute and clean Founders Creek
D.1	Insert a break water in the throat to the southern lobe
D.2	Insert floating wave break in same area as D1
D.3	Create 4 islands within the lake
D.4	Create 2 islands within the lake
E.1	Plant native aquatic vegetation within the littoral zone
F.1	Increase no wake zone from 61 (200) to 122 m (400 ft) from shoreline
F.2	Restrict motorboats to engines having less than 7.5 kW (10 HP)
G.1	Decrease fish community phosphorous excretion by 75%
H.1	Decrease nutrient loading from Sleepy Hollow and Pickerel Creek by 50%
H.2	Decrease nutrient loading from all tributaries by 25%
H.3	Decrease nutrient loading from Pickerel Creek by 75%

The "overall health" of a lake is commonly characterized by determining the trophic status. Trophic state is defined as the total weight of living biological material (biomass) in a water body at a specific location and time and provides a measurement of biological response to forcing factors such as nutrient additions. Nutrients promote growth of microscopic plant cells (phytoplankton) that are fed upon by microscopic animals (zooplankton). Higher nutrient concentrations yield increases in microscopic plant and animal development thus making the water "cloudy." This relationship, called eutrophication, is a natural aging process of lakes, but it can be unnaturally accelerated by the addition of too many nutrients as is the case in Cedar Lake. To quantify the degree at which eutrophication occurs, the Carlson trophic state index (TSI) was used for Cedar Lake (Carlson 1977). The TSI quantifies the concept that changes in nutrient levels (measured by total phosphorus) causes changes in algal biomass (measured by chlorophyll a) which in turn causes changes in lake clarity (measured by Secchi disk transparency). The TSI was calculated for each restoration measure according to the following equation:

$$TSI = 14.42\ln(P[\mu g/L]) + 4.15,$$

where *P* is the spatially averaged phosphorus concentration. Normalized and maximum phosphorus concentrations and TSI are tabulated and presented for each restoration measure and alternative at the end of the report.

Physical Substrate Restoration

Measures under this category involve physical removal of bottom sediments to reduce both the internal nutrient loading as well as turbidity caused by resuspension. Five dredging scenarios have been selected according to two distinct dredging approaches (shallow depth/large extent versus a deep depth/hotspot focus). Phosphorus concentrations of daylighted sediments (those exposed after dredging) are assumed to be 400 mg/kg regardless of the dredging depth based upon concentrations measured at various depths in three sediment cores taken within Cedar Lake (Echelberger 1984). Table 13 describes each of the measures and **Figure 18** and **Figure 19** show a layout of each dredging measure.

Table 13. Description of physical substrate restoration measures using dredging.

ID		Area, km^2 (ac)	Depth, m (ft)	Volume, m^3 (cu-yd)	Measure Description
MEASURE	A.1	1.8 (444)	0.30 (1.0)	547,965 (716,712)	Dredge all areas that contain silts and clays. This alternative is meant to show the impact of aerial extent differences.
MEASURE	A.2	0.3 (83)	1.65 (5.4)	547,965 (716,712)	Dredge only areas that contain elevated levels of phosphorus > 700 mg/kg. The volume of dredge material was set equal to Alternative 1 to show the impact of aerial extent differences.
MEASURE	A.3	0.3 (83)	0.82 (2.7)	273,984 (358,357)	Dredge only areas that contain elevated levels of phosphorus > 700 mg/kg. The depth of dredging was cut in half in comparison of Alternative 3 to show the impacts of depth differences.
MEASURE	A.4	0.9 (224)	0.30 (1.0)	276,805 (362,047)	Dredge only areas that contain elevated levels of phosphorus > 500 mg/kg. The volume of dredge material is roughly equal in scale to Alternative 3 to show the impact of aerial extent and depth differences.
MEASURE	A.5	0.2 (61)	0.82 (2.7)	202,472 (264,823)	Dredge only areas in the northern basin that contain elevated levels of phosphorus > 500 mg/kg to a depth equal to Alternative 3. This alternative is meant to show the impact of concentrating dredging efforts on the Northern Basin where preliminary modeling has shows elevated levels of turbidity.
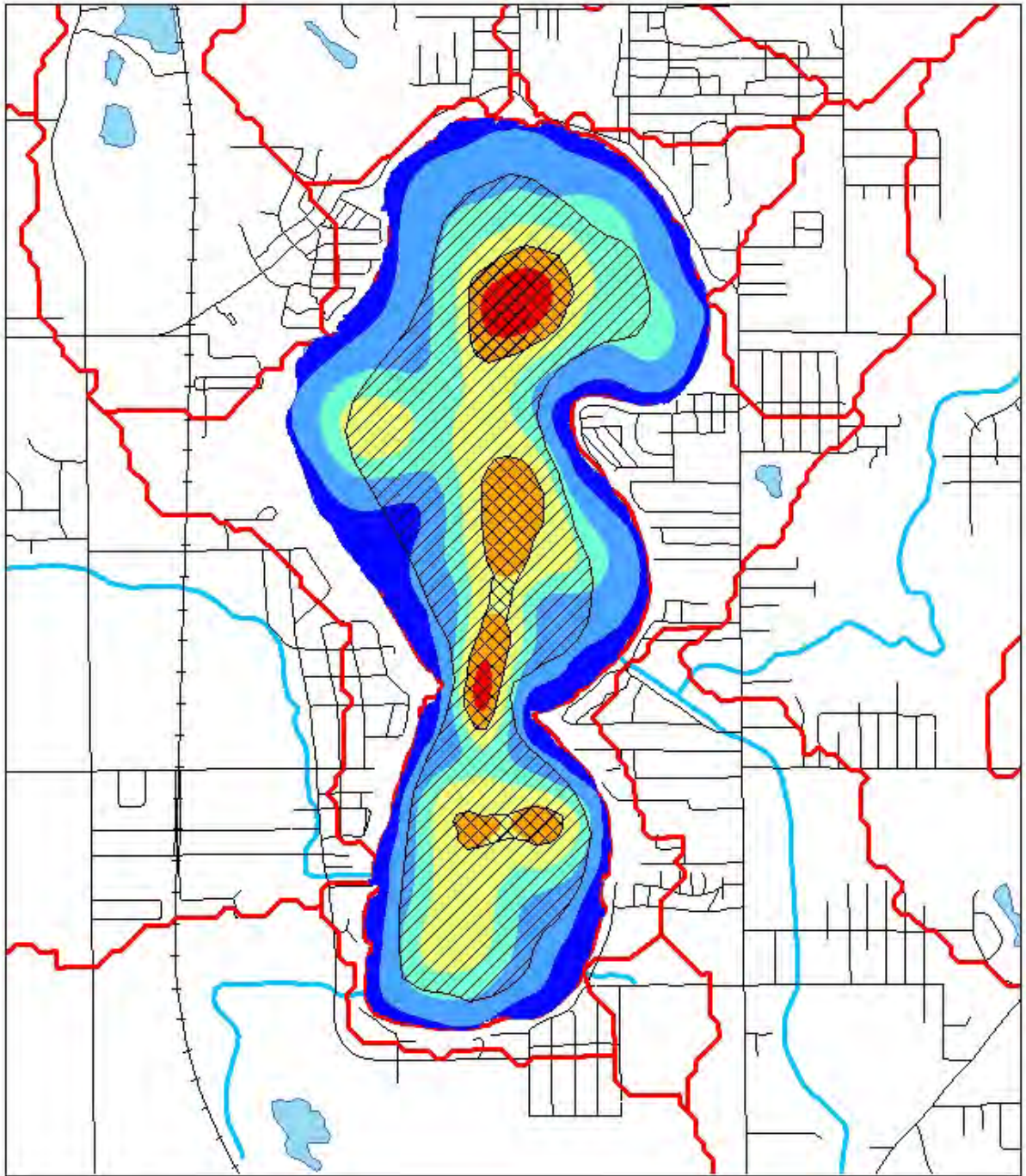
Physical Substrate Restoration - A.2
☒ D = 5.4 ft, A = 83 ac, V = 717,000 cy
Physical Substrate Restoration - A.1
☐ D = 1 ft, A = 444 ac, V = 717,000 cy
Phosphorus - Spline Interpolated [Total Phosphorus (mg/kg)]
■ < 100
■ 100 - 300
■ 300 - 500
■ 500 - 700
■ 700 - 900
■ 900 - 1,100
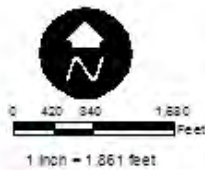
Cedar Lake bathymetry data based on survey performed by U.S. Army Corps of Engineers, Chicago District in May 2005. Elevations computed from lake depth soundings converted by using Normal Water Level = 692.90 NGVD29, this corresponds to the elevation of the overflow weir.

1 inch = 1,861 feet

US Army Corps of Engineers
Chicago District

Cedar Lake Ecosystem Restoration Feasibility Study
Appendix A Hydrology and Hydraulics

Map of Physical Substrate Restoration Measures A.1 and A.2

Chicago District, U.S. Army Corps of Engineers

Figure 18. Physical substrate restoration measures using dredging, A.1 and A.2.
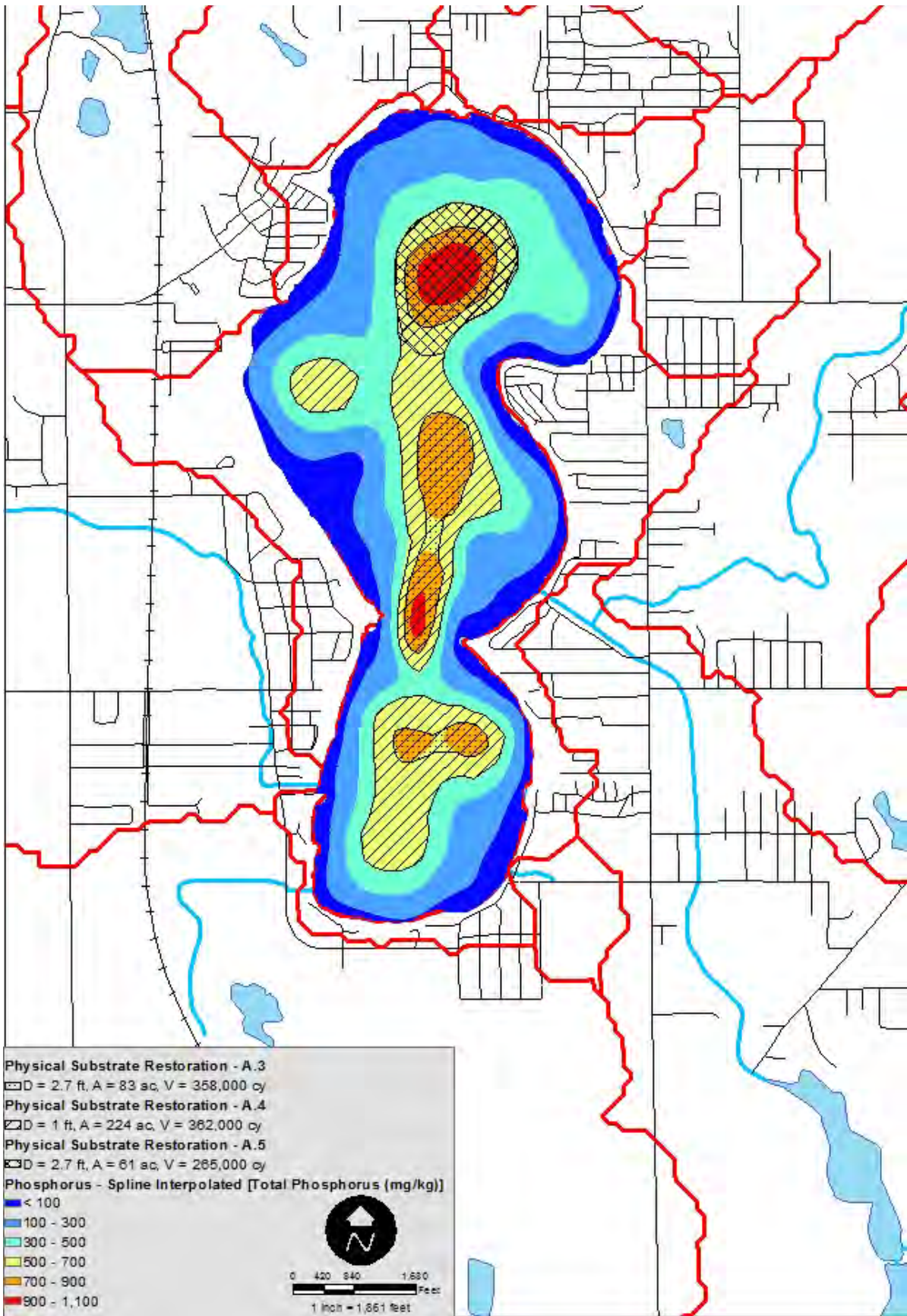
Figure 19. Physical substrate restoration measures using dredging, A.3, A.4 and A.5.

The simulation results for the phosphorus concentration and corresponding TSI over nine months for each of the dredging measures are shown in Figure 20. Phosphorus concentrations in the water column are primarily driven by fluxes from the bed and secondarily by desorption from suspended sediments and tributary loadings. Dredging decreases phosphorus loads from bed flux and from resuspended sediments (sediments resuspended from dredged areas will have less phosphorus sorbed onto them). Between days 180 and 250 diffusive flux from the bed is the primary cause of phosphorous increase within the system. Measure A.1 results in the least phosphorous entering the water column because it has the lowest average sediment bed phosphorous concentration. As shown in Figure 21, Measure A.4 provides the most efficient reduction in phosphorus concentration per volume of sediment removed.
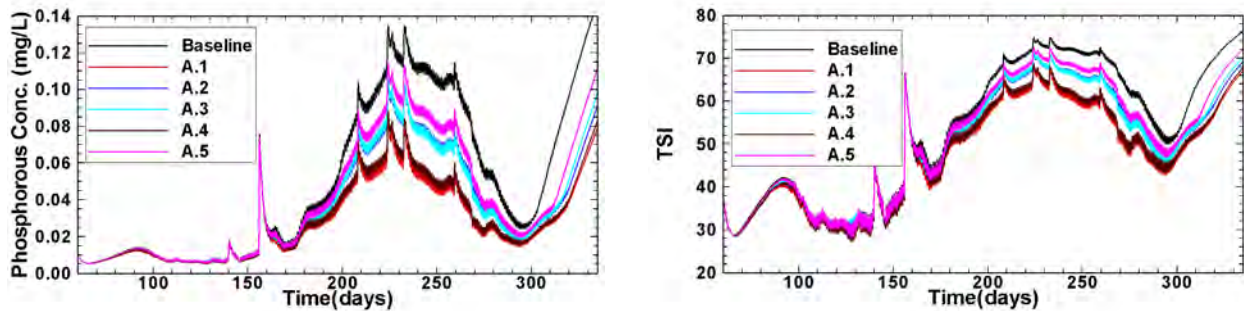
Figure 20. Simulated phosphorous concentrations and TSI for physical substrate restoration measures.
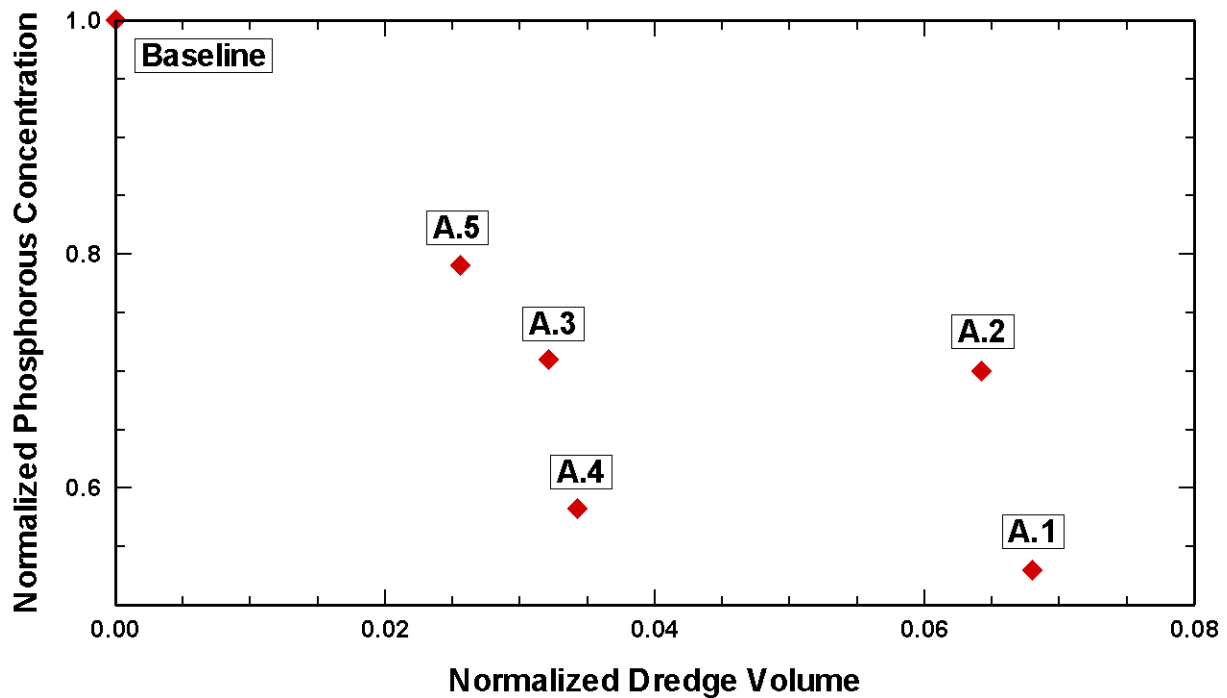
Figure 21. Dredging effectiveness (phosphorus reduction as a function of volume).

Chemical Substrate Restoration

The primary source of phosphorous loading to Cedar Lake is through flux from the sediment bed. Application of flocculants, such as aluminum sulfate (alum) can decrease sediment resuspension through increasing particle size and decreasing flux from the bed by creating a physical barrier to flux. Insufficient data are available to accurately characterize the effect of flocculants on sediment particle size, and thus this is not considered in these model runs. It is important to note that chemical substrate restoration through flocculent application may only be a temporary control to phosphorus diffusion from the sediment bed. Without reapplication, degradation of the flocculent "cap" could yield high diffusive flux of phosphorus from the exposed bed to the water column.

For this study, two different chemical substrate restoration measures were modeled as illustrated in **Figure 22**. Measure B.1 specifies application of aluminum sulfate to a 91-ha (224-acre) area within the lake (equivalent to dredging Measure A.4). Measure B.2 involves applying flocculants to an 34-ha (83-acre) area (equivalent to dredging Measures A.2 and A.3). To implement this scenario, it is assumed that flocculants decrease phosphorous release from bottom sediments by 80%. Because significant upgrades of SNL-EFDC would be needed to directly simulate flocculants or to manipulate phosphorus diffusion rates in individual cells (currently SNL-EFDC can only model a lake-wide diffusion coefficient), sediment bed phosphorous concentrations were decreased to approximate this restoration measure. Specifically, the phosphorous concentration within all affected cells for each of the two measures was lowered by 80%, which implicitly lowers the diffusion rate. Also, the model does not account for the degradation of the flocculants over time. Further study is recommended to determine the long-term effectiveness of alum treatment measures within Cedar Lake.
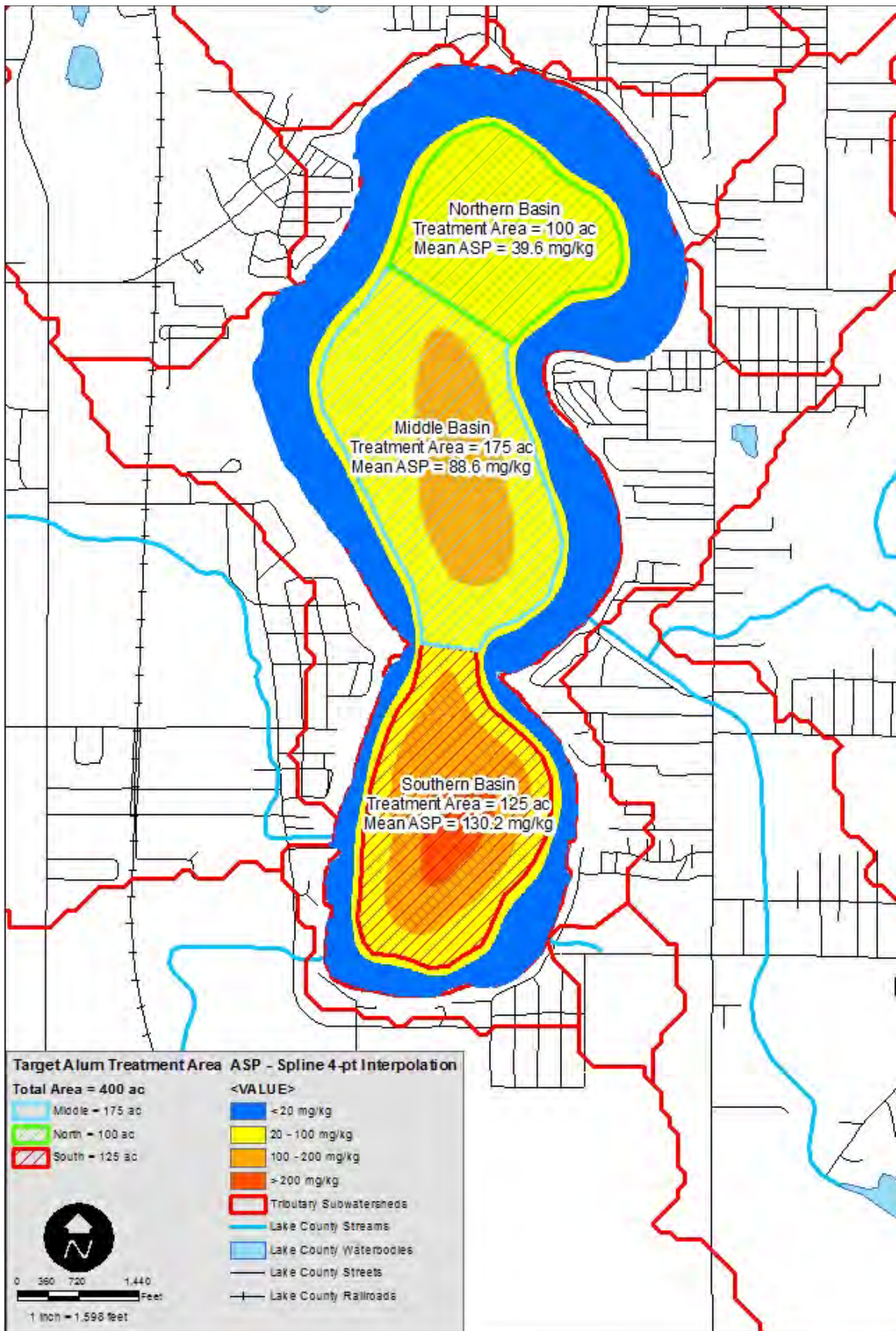
Figure 22. Chemical substrate restoration measures using flocculants, Measures B.1 and B.2.

The simulation results for the flocculation treatments are shown in Figure 23. It takes several weeks for the diffusive bed flux to increase phosphorus concentrations in the water column and it is not until approximately day 180 that notable changes are observed. Measure B.1, corresponding to a treatment area of 91 ha (224 acres), yields a total decrease in the spatio-temporally averaged water-column phosphorous concentration of about 64%. Measure B.2, corresponding to a treatment area of 34 ha (83 acres), yields a total decrease in the spatio-temporally averaged water-column phosphorous concentration of about 42%. Differences across the three simulations are most obvious during the summer months when the temperatures and corresponding phosphorus fluxes are greatest. Model results indicate that flocculent application can be an effective restoration measure for reducing diffusive phosphorus flux from the sediment bed. These results are only applicable for the first year after flocculent application, as the physical cap created during application will degrade over time and may impact performance.
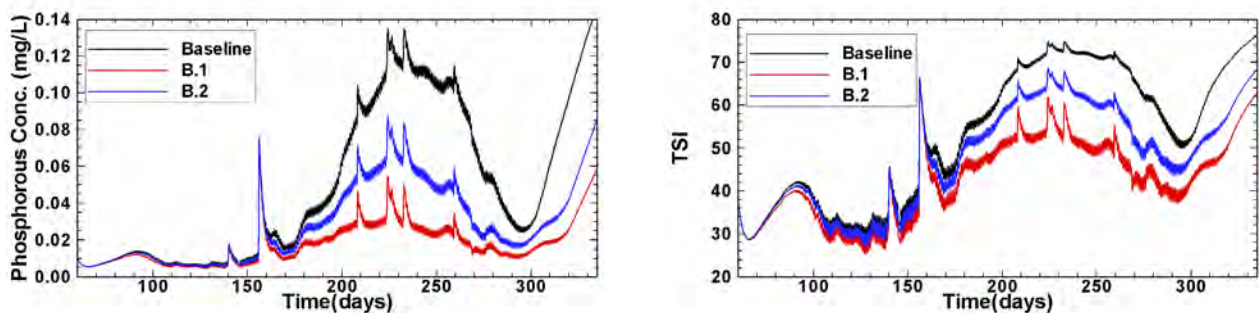
Figure 23. Simulated phosphorous concentrations and TSI for chemical substrate restoration measures.

Tributary Restoration

Cedar Lake has a small watershed size and thus the amount of surface runoff that drains into the lake is limited by drainage area. During most of the year, the lake acts as a source to the underlying aquifer. As shown in Figure 4, Cedar Lake is fed by drainage from seven tributaries plus direct runoff. Due to the small drainage basin size and the loss of water to groundwater, the residence time for Cedar Lake is extremely long in the range of 1.5 to 2 years based on a water budget analysis (Echelberger 1984). The restoration of tributary streams to Cedar Lake could provide dilution to nutrient concentrations in the lake. In addition, flushing of the system with additional volume could provide water quality benefits by physically removing nutrient-rich water out of the lake. Both dilution and flushing measures would require a source for nutrient-low water. Founders Creek, which historically drained into Cedar Lake, currently bypasses the lake and drains directly into Cedar Creek just downstream of the outlet weir. As water quality measurements taken in August 2005 suggest, Founders Creek is a potential source of low-nutrient water during baseflow conditions where groundwater is the source. Rerouting this tributary to feed the lake may improve water quality by decreasing residence time. Unfortunately, if there is a significant nutrient load from Founders Creek, this could decrease Cedar Lake water quality.

Simulation results shown in Figure 24 suggest a 3% decrease in spatially and temporally averaged phosphorous concentrations as a result of rerouting Founders Creek. Because Cedar Lake is a well-mixed system, rerouting Founders Creek improves water quality despite the inlet's proximity to the outlet weir. The benefits to water quality are not significant unless the associated influx of nutrients generated during runoff conditions is decreased. Model results suggest that if significant decreases in phosphorous loadings can be achieved during runoff conditions there are benefits to water quality. When assigning zero nutrient concentrations to flows input to the lake from Founders Creek, the model results indicated a 30% decrease in spatially and temporally averaged phosphorous concentrations. Without implementing measures to reduce existing nutrient loads in the Founders Creek watershed, benefits to Cedar Lake at this scale will not be realized.
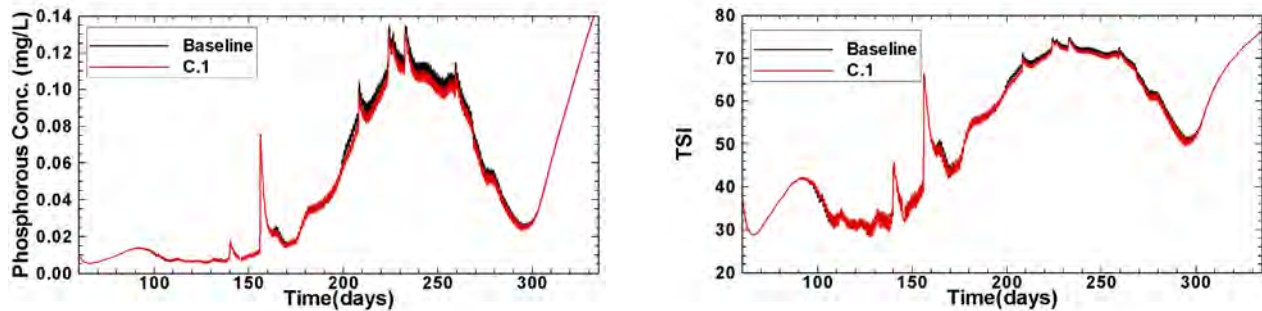
Figure 24. Simulated phosphorous concentrations and TSI for tributary restoration measures.

Creation of Habitat Islands

Cedar Lake has a long fetch length in the north/south direction with winds predominantly from the north and south. There is significant wave action and corresponding sediment resuspension along leeward shorelines. Wind-driven waves can be decreased by building habitat islands. However, impacts to water column phosphorus concentrations may be minimal because wind-driven wave action is largely relegated to shoreline areas where phosphorus concentrations in the sediment bed are lowest.

Table 14 describes the proposed habitat islands for consideration. Three of the four different measures illustrated in Figure 25 were simulated by removing the indicated cells from the model grid and recalculating the fetch lengths for the reconfigured lake. The accuracy of each scenario is limited by grid resolution. For example, one grid cell is 80×80 m^2 (262×262 ft^2); therefore the width of the passageway in Measure D.1 is equal to one grid cell. Similarly, the width of the breakwater itself is also restricted to a minimum of one grid cell or 80 m (262 ft). Grid resolution limits the ability to precisely model these scenarios. Also, it must be noted that the model implements these islands by removing these cells from consideration (i.e., the model does not consider that when an island is created, the lake bed will gradually slope up to the island). However, even with these modeling limitations, the relative effectiveness of these measures can be assessed using the SNL-EFDC model.

Table 14. Description of habitat islands measures.

ID		Area (ac)	Elevation (ft above water)	Volume (cu-yd)	Measure Description
MEASURE	D.1	1.7	1.0	34,000	Create two hard breakwaters across the narrow part of the lake between the central and south lobes allowing 61-m (200-ft) separation for boat passage.
MEASURE	D.2	1.7	1.0	N/A	Create two floating breakwaters in the same configuration as Measure D.1. Only analyze if Measure D.1 shows a water quality improvement.
MEASURE	D.3	31.7	Varies between 3.0 and 4.0	362,000	Dispose of dredged material from Measure A.4 in four in-lake disposal sites located along the shoreline of Cedar Lake in areas currently undeveloped by residential housing. All disposal areas are above water level and these cells are removed from the model.
MEASURE	D.4	12.4	1.0	155,000	Create two islands located near the narrow part of the lake between the central and south lobes with material from Measure A.4. Additional dredged material will be disposed of outside the lake. Islands are above water level and these cells are removed from the model.

Simulation results suggest that breakwaters are not an effective way of lowering phosphorous concentrations in the water column because the change in the average phosphorous is within 1% of the baseline value for all three scenarios. Measure D.1 indicates negligible increases in shear stress and phosphorus concentrations (well within model uncertainty) and thus Measure D.2 (the floating wave break) was not modeled because it would only be a less effective version of Measure D.1 (an earthen wave break). Measures D.3 and D.4 show no statistically significant change in water-column phosphorus concentrations. Measure D.3 was most effective at lowering the shear stress, presumably because the islands are created near shore where the wave action leads to the highest shear stresses. Thus, model output may reflect artificially low shear stresses because the cells next to newly created islands are not modified and are therefore deeper than would otherwise be expected. Because habitat islands primarily serve to change shear stresses in the near-shore region where phosphorus concentrations are already low (see Figure 5), these measures are not effective ways of reducing phosphorus concentrations in Cedar Lake.
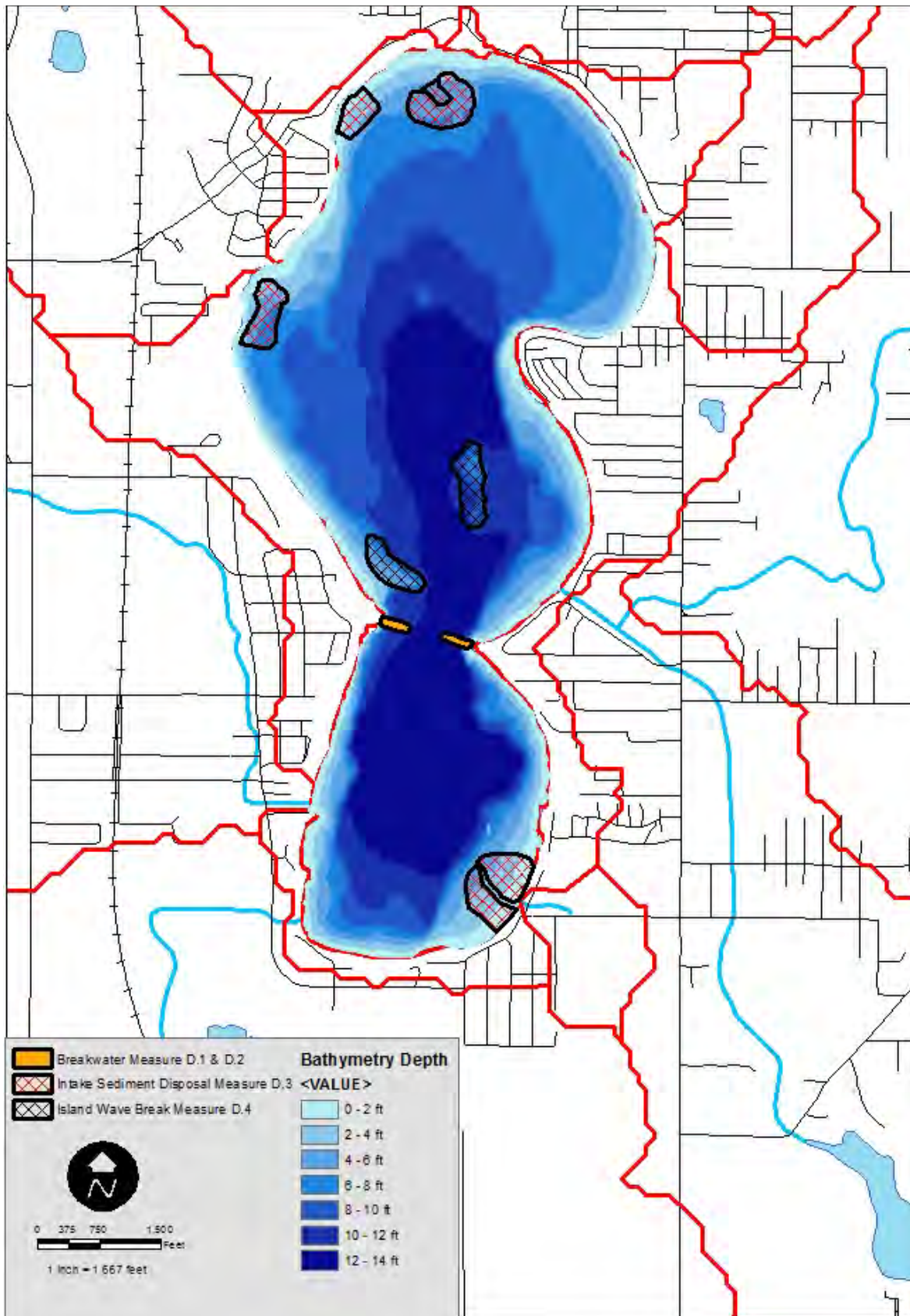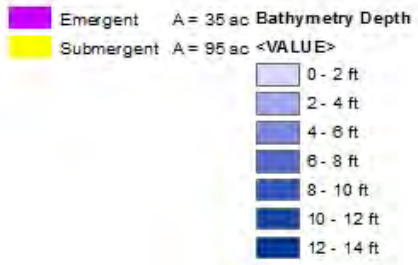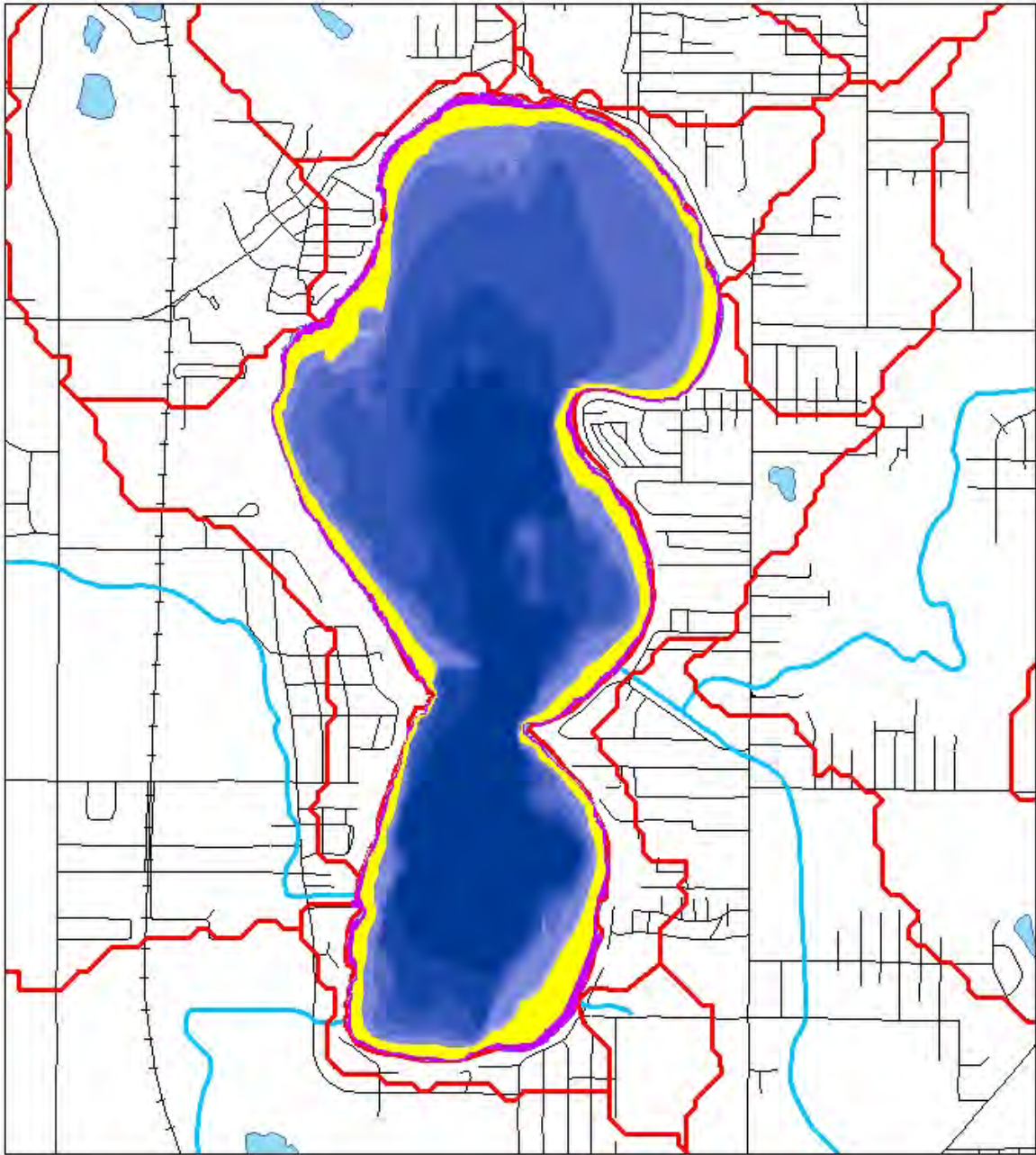
Figure 25. Creation of habitat islands, Measures D.1 through D.4.

Littoral Macrophyte Restoration

In addition to the restoration of natural ecosystem structure for aquatic species, restoring native shoreline aquatic emergent and submergent vegetation has three potential benefits to water quality. Littoral macrophytes (i.e., aquatic vegetation) have the potential to uptake phosphorus from the water column during seasonal growth processes. Emergent vegetation that would be planted in the shallow regions near shore was assumed to have a phosphorous removal rate of up to 160 kg/ac/yr (Boyd 1974); (Pellikaan and Nienhuis 1988). Submergent vegetation that would be planted in areas between 0.30 and 1.22 m (1 and 4 feet respectively) in depth was assumed to have a phosphorus removal rate of 80 kg/ac/yr yr (Boyd 1974); (Pellikaan and Nienhuis 1988). Because most of Cedar Lake is quite shallow, littoral macrophyte restoration could lead to significant decreases in phosphorous because approximately 53 ha (130 acres) are less than 1.22 m (4 ft) deep as shown in Figure 26. Aquatic vegetation also decreases the shear stress on the sediment bed by damping near-bed velocity and stabilizing sediments with root networks. However, because there are no SEDflume studies available to establish erosion potential for sediments stabilized by vegetation, these effects were not included in the model.
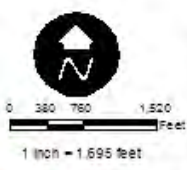
Legend:

Emergent   A = 35 ac
Submergent A = 95 ac

Bathymetry Depth
<VALUE>

- 0 - 2 ft
- 2 - 4 ft
- 4 - 6 ft
- 6 - 8 ft
- 8 - 10 ft
- 10 - 12 ft
- 12 - 14 ft

0   380   760   1,520
                      Feet

1 inch = 1,695 feet

Cedar Lake bathymetry data based on survey performed by U.S. Army Corps of Engineers, Chicago District in May 2005. Elevations computed from lake depth soundings converted by using Normal Water Level = 692.90 NGVD29, this corresponds to the elevation of the overflow weir.

Cedar Lake Ecosystem Restoration Feasibility Study
Appendix A Hydrology and Hydraulics
Layout Map of Littoral Zone Restoration Measure
Chicago District, U.S. Army Corps of Engineers

US Army Corps of Engineers
Chicago District

Figure 26. Restoration of emergent and submergent aquatic vegetation, Measure E.1.

SNL-EFDC would require considerable development to directly model vegetative phosphorous consumption; therefore this measure was approximated by decreasing the sediment bed phosphorous concentrations in cells corresponding to areas of submergent and emergent vegetation restoration. The total phosphorous mass removed by plant life over a year was calculated based on the vegetation type (emergent or submergent). This mass was then removed from cells meeting the depth criteria for submergent and emergent plant life. This procedure does not provide a real-time simulation of phosphorus removal by aquatic vegetation; instead, it estimates the maximum potential benefits after the plants have been in place for one year.

As shown in Figure 27, the effect of adding both emergent and submergent vegetation leads to a decrease in the spatio-temporal averaged phosphorous concentrations of about 12%. The phosphorus reduction is significant although aquatic vegetation is only planted in the shallower areas of the lake, less than 1.22 m (4 ft) deep, where phosphorous concentrations are relatively low. Simulation results suggest that restoration of littoral macrophytes could be used in conjunction with physical substrate restoration or chemical substrate restoration targeted at sediments in deep portions of the lake where the phosphorous concentrations are highest in an attempt to lower the total phosphorous concentrations throughout the lake.
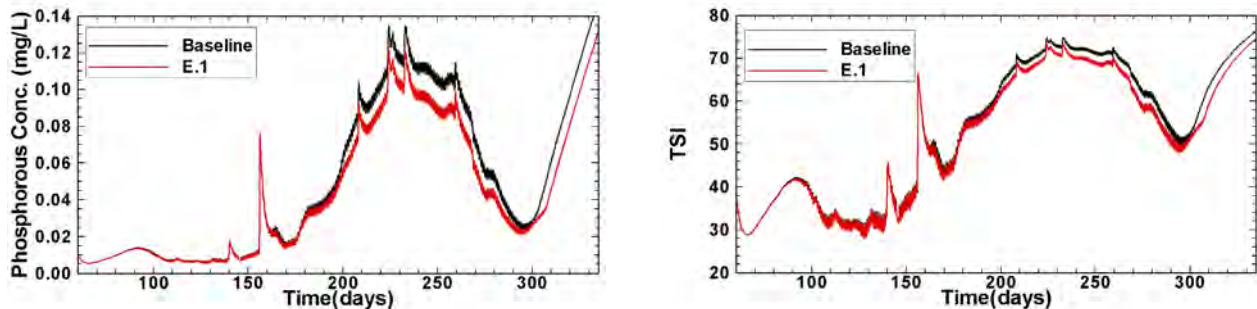
Figure 27. Simulated phosphorous and TSI for littoral macrophyte restoration measure.

Institutional Controls
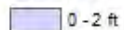
Cedar Lake is a popular recreational destination and significant boat activity leads to wave action and sediment resuspension, particularly in the near-shore environment. Institutional controls aimed at reducing boat-induced waves were considered as a possible water quality restoration measure. Two measures were proposed for decreasing sediment resuspension caused by boat activity. Measure F.1 doubles the width of the existing no-wake zone areas to 122 m (400 ft) as shown in Figure 28. This area roughly corresponds to eliminating boat-induced waves to depths less than 1.22 m. This measure was modeled by turning off boat-induced waves in areas where the lake is less than 1.22 m (4 ft) deep. Measure F.2 restricts all motorboats to engines of less than 10 horsepower, which is implemented by applying a representative 10-hp boat-induced wave to areas outside of the 61 m (200 ft) baseline no-wake region. A maximum boat induced wave height of 15 cm (5.9 in) was calculated using the same equation as outlined above based on a representative boat having a 7-m (23-ft)-long V-hull with a draft of 1 m (3.3 ft) equipped with a 10 horsepower engine. A maximum speed of 4 m/s (8.5 mph or 12.5 ft/s) was assumed.
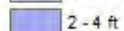
Simulation results show a significant decrease in boat-induced waves, and a measurable impact on the water quality. The spatio-temporally averaged phosphorous concentration decreased by about 4.0% for Measure F.1 and 4.3% for Measure F.2. The associated decreases in shear stresses are 20% and 35% respectively.

Legend:
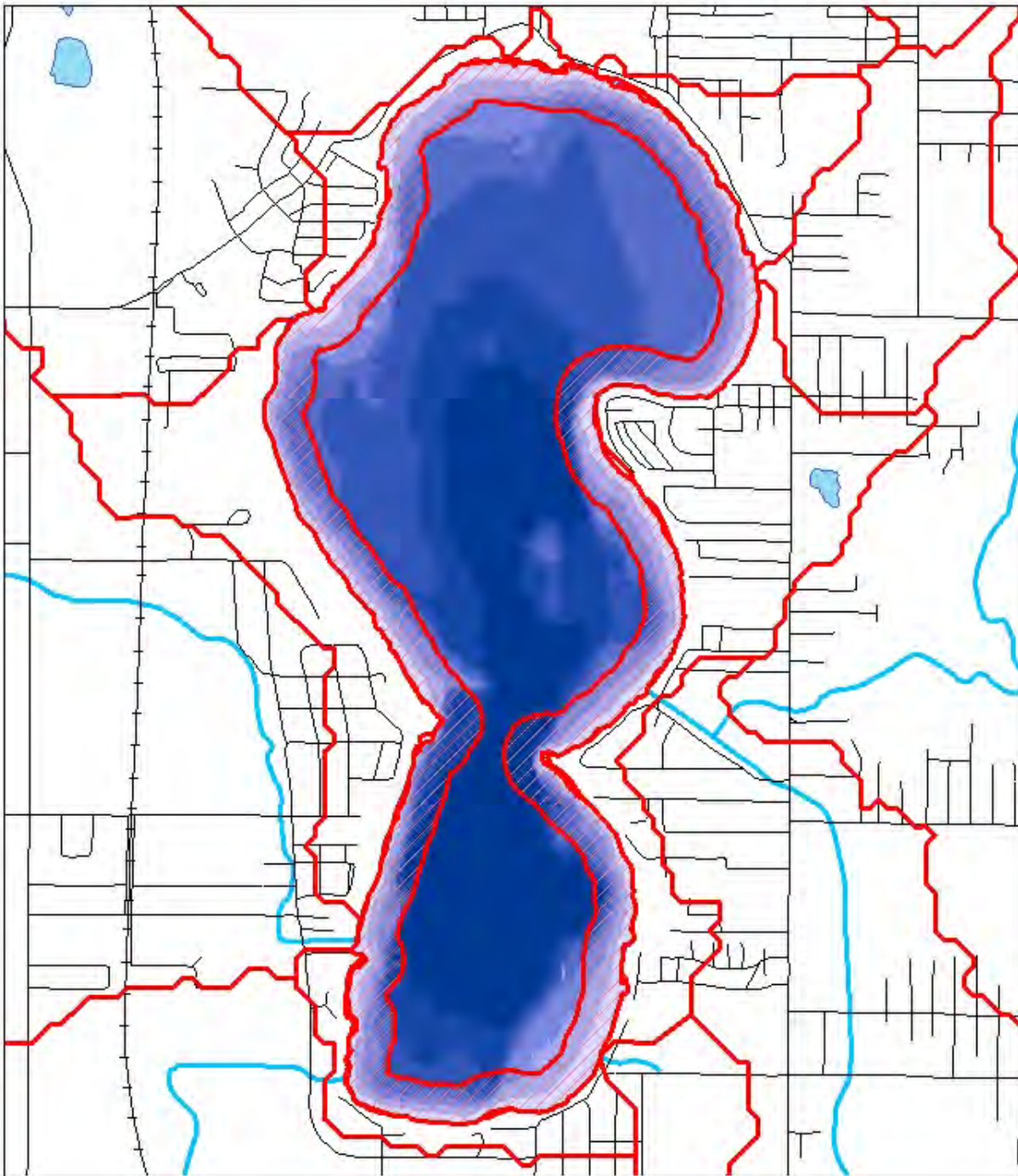
- 400 ft No Wake Zone F.1

Bathymetry Depth
<VALUE>

- 0 - 2 ft
- 2 - 4 ft
- 4 - 6 ft
- 6 - 8 ft
- 8 - 10 ft
- 10 - 12 ft
- 12 - 14 ft

0   360   720   1,440
Feet

1 inch = 1,596 feet

Cedar Lake bathymetry data based on survey performed by U.S. Army Corps of Engineers, Chicago District In May 2005. Elevations computed from lake depth soundings converted by using Normal Water Level = 692.90 NGVD29, this corresponds to the elevation of the overflow weir.

Cedar Lake Ecosystem Restoration
Feasibility Study
Appendix A Hydrology and Hydraulics

Layout Map of Institutional Control Measure

Chicago District, U.S. Army Corps of Engineers

US Army Corps of Engineers ®
Chicago District

Figure 28. Institutional controls by additional no-wake zones and boat limitations Measures F.1 and F.2.

Fish Community Management

Benthic organisms can increase nutrient fluxes from the sediment bed to the water column by bioturbation which is the displacement and mixing of sediment particles. In lakes, bioturbation is typically caused by annelid worms (e.g., polychaetes or oligochaetes), bivalves (e.g. mussels or clams) and gastropods. Non-native, benthivorous fish also cause bioturbation and can be a key contributor to the resuspension of sediments and associated contaminants in shallow, nutrient-rich lakes by burrowing, ingestion and defecation of sediment grains, which displace sediment grains and mix the sediment matrix. The sediment-water interface increases in area as a result of bioturbation, affecting chemical fluxes and thus the exchange of nutrients between the sediment bed and water column. Natural excretion from benthic feeders is a direct source of water-column nutrients including phosphorus, nitrogen and carbon. Unfortunately, the effects of bioturbation are not adequately quantified for direct incorporation into the SNL-EFDC model. Some experiments show that much of the phosphorous release due to fish communities can be linked to excretion while others suggest that bioturbation increases nutrients through increases in sediment resuspension. Conversely, sediment resuspension may actually decrease water-column phosphorus spikes if increased sediment concentration leads to an increased potential for the excretion products to fuse to sediment particles and re-deposit on the sediment bed (Vanni 2002). The current SNL-EFDC model cannot capture the complex nature of mixing bioturbation except through a change in phosphorus diffusion rate from the sediment bed. Unfortunately, it is unclear how much bioturbation quantitatively changes phosphorus flux from the sediment bed and any flux parameters assigned would be somewhat speculative. Thus, the direct effects from bioturbation through mixing were not considered.

However, fish community management can seek to increase water clarity by manipulating the biomass and structure of the fish community. This process has been conducted throughout Europe and North America during the past fifty years, and has often been successful in improving water clarity and/or lowering algal biomass. Proper management of the local fish communities (specifically targeting benthivorous fish species) could lead to a decrease in phosphorous excretion of up to 75% within the littoral zones, which correspond to a depth less than 1.52 m (5 ft). This equates to a release of 0.8 kg/ac/yr (down from 3.2 kg/ac/yr for the baseline condition), which was simulated in the model by a direct removal of 2.4 kg/ac/yr of phosphorous from the sediment bed. Because the bed is divided into three distinct 10-cm sediment layers, 20% of the phosphorous removal from the affected cells was taken from each of the top and bottom layers and the remaining 60% was removed from the middle layer. Littoral areas affected by fish community management Measure G.1 are illustrated in Figure 29.

Simulation results show the amount of phosphorous released into the water column by the fish populations is insignificant in comparison to direct diffusion from deeper portions of the lake where sediment bed phosphorus is highest. Management of fish communities yields a decrease in water column phosphorus concentrations of less than 1% compared to the baseline scenario. The model results suggest that fish community management would not significantly reduce eutrophication within Cedar Lake; however, restoration benefits to the structure and function of the ecosystem may be realized.
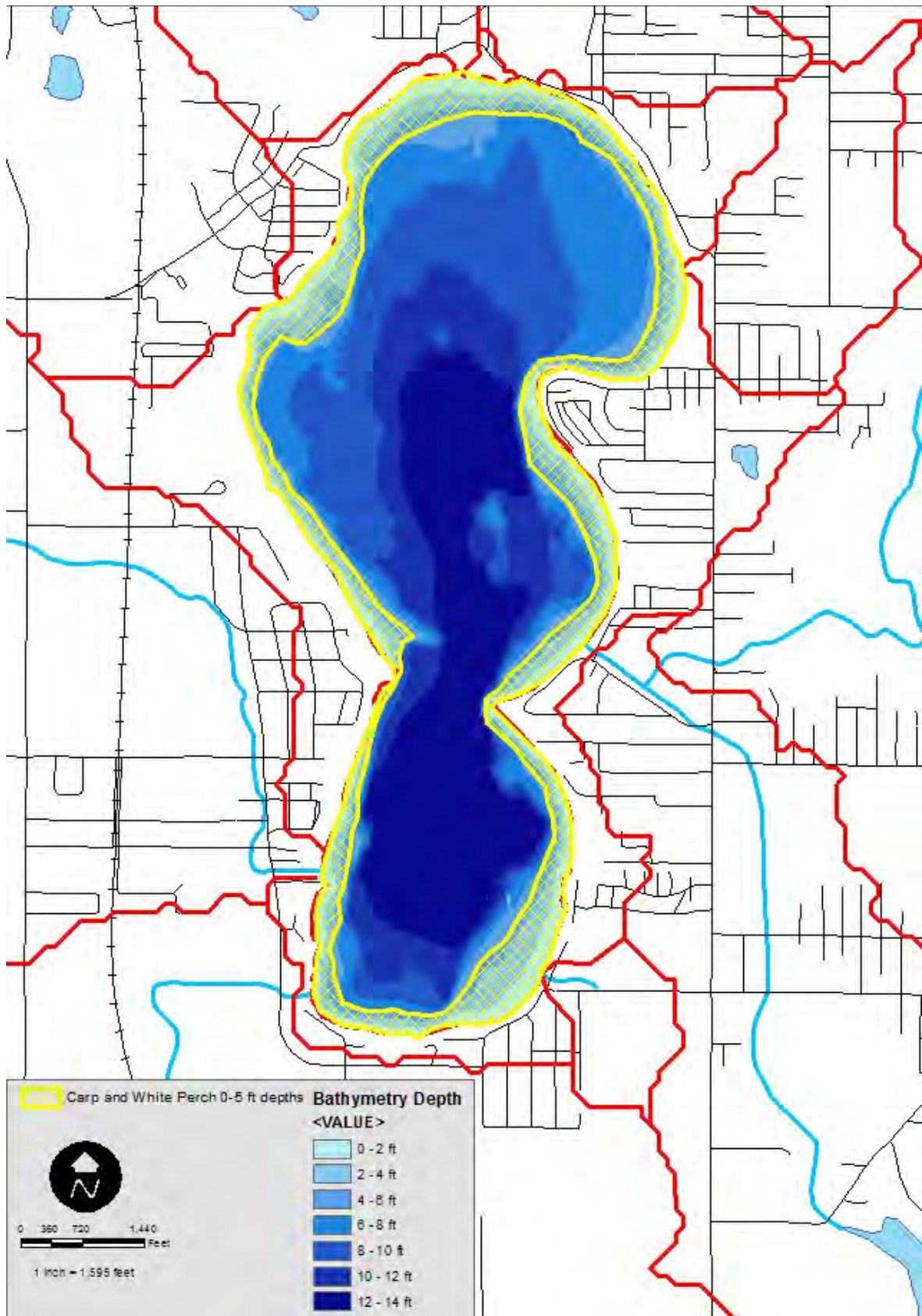
Figure 29. Fish community management littoral areas, Measure G.1.

Reducing Tributary Sediment and Nutrient Loadings

Cedar Lake currently receives drainage of water, sediment and nutrient loads from seven tributaries as well as direct drainage. Cedar Lake is also fed by a rapidly developing predominantly agricultural watershed. Because of the current heavy agricultural use, significant nutrients from fertilizer drain into Cedar Lake during storm events. A map showing the layout of sub-watersheds and tributary locations is shown in Figure 30. The goal for measures that reduce tributary nutrient loads is to decrease the influx of phosphorous, nitrogen, and sediment that enters Cedar Lake. Reduction in loadings can be accomplished by several methods including the following: agricultural best management practices (BMPs), construction BMPs, upland ecosystem restoration, streambank stabilization, sediment traps, filter wetlands, and restrictions on fertilizer use through ordinances. For example, decreased tilling of agricultural lands could reduce the potential for erosion and associated nutrient runoff. Also, encouraging limited fertilizer application has yielded significant improvements in similar watersheds. Using wetlands to filter portions of flow entering Cedar Lake or increasing the filtering capacity of the Cedar Lake Marsh (around the southern portion of the lake) are both options for reducing tributary nutrient loads. Instead of formulating specific designs aimed to reduce sediment and nutrient loads to each tributary, a suite of target percent reductions was selected to determine the effectiveness on reducing the eutrophication of Cedar Lake. As listed in Table 15, three different measures with varying target percent reductions were modeled.

Table 15. Description of tributary sediment and nutrient load reduction measures.

Measure	Description
H.1	Decrease sediment and nutrient loading from Sleepy Hollow Ditch and Pickerel Creek by 50%
H.2	Decrease sediment and nutrient loading from all seven tributaries by 25%
H.3	Decrease sediment and nutrient loading from Pickerel Creek by 75%

Simulation results show that reducing sediment and nutrient loads from tributaries have a small effect on the phosphorous concentrations within Cedar Lake in the first year of simulation. Measures H.1, H.2, and H.3 yield spatio-temporal averaged phosphorous decreases of 7.1%, 5.9%, and 6.8% respectively as shown in Figure 31. The effect of each of these measures on the phosphorous concentration during the largest influx event over a 20-day period is shown in Figure 32. While restoring tributaries with low-nutrient water to Cedar Lake, as laid out in Measure C.1, resulted in improved water quality in Cedar Lake, simply reducing nutrient loads from the tributaries without increasing water influx does not greatly reduce phosphorus levels in the lake because the nutrient flux from the sediment bed is the predominant factor in eutrophication. Nevertheless, over a long-term period encompassing several years, current levels of sediment and nutrients inputs from tributaries will continue to contribute to the eutrophication of Cedar Lake. Without reducing tributary loadings, the long-term effectiveness of other restoration measures such as physical substrate restoration and/or chemical substrate restoration will be significantly diminished.

Tributary Sediment/Nutrient Reduction Measures

Subwatershed Deliniation Based on 30-meter USGS Hydrographic Corrected DEM

condo inlet

chamber inlet

old bank building inlet

direct drainage

direct drainage

hog pen ditch

sleepy hollow ditch

unnamed inlet/pickerel creek
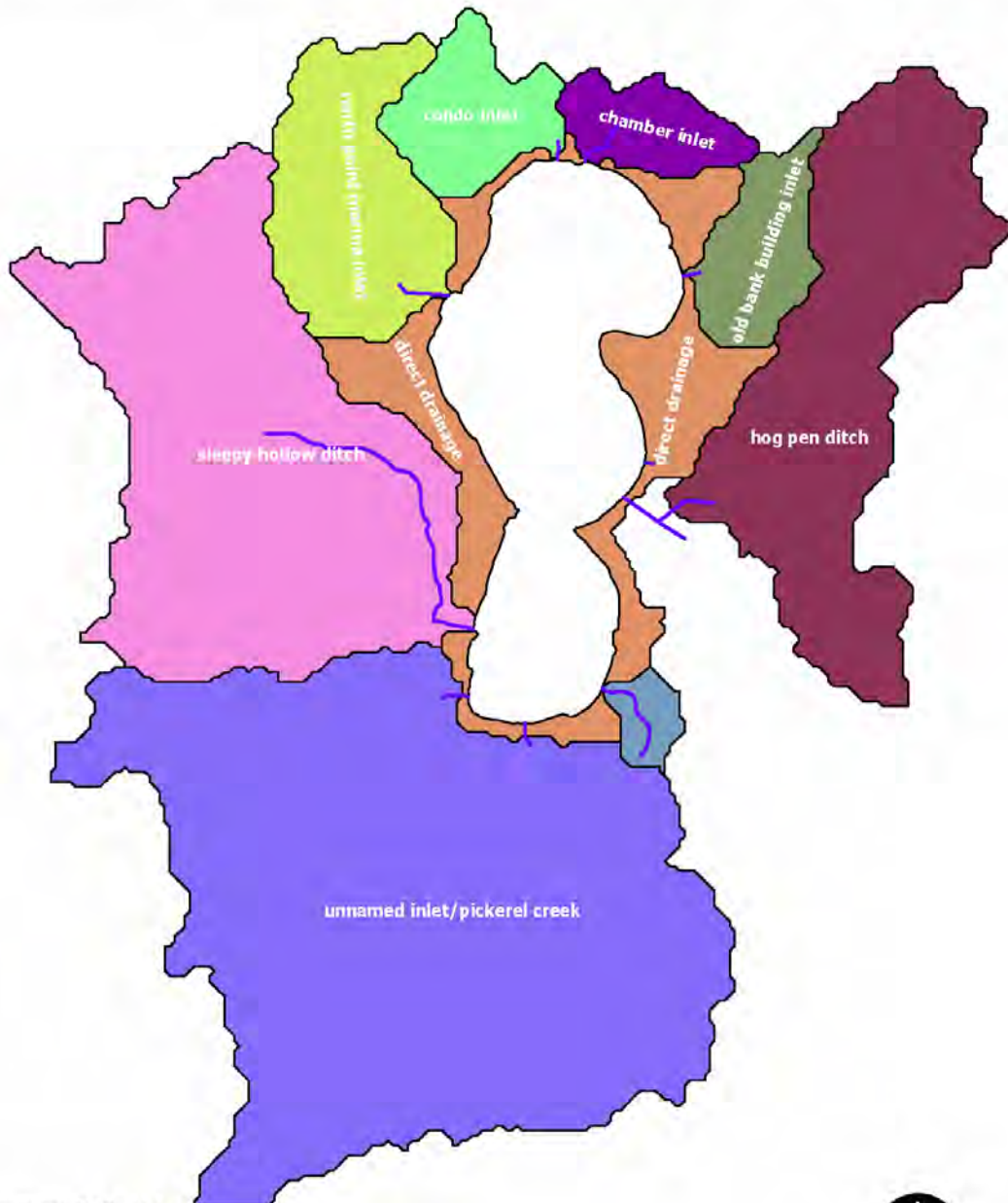
Agricultural BMPs H.1
  Reduce 50% to Sleepy Hollow & Unnamed/Pickerel

Filter Wetlands H.2
  Reduce 25% to all Tributaries except Direct Drainage
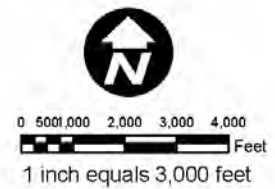
Cedar Lake Marsh H.3
  Reduce 75% to Unnamed/Pickerel

0 500 1,000 2,000 3,000 4,000
Feet
1 inch equals 3,000 feet

Figure 30. Reducing tributary sediment and nutrient loadings, Measures H.1, H.2, and H.3.
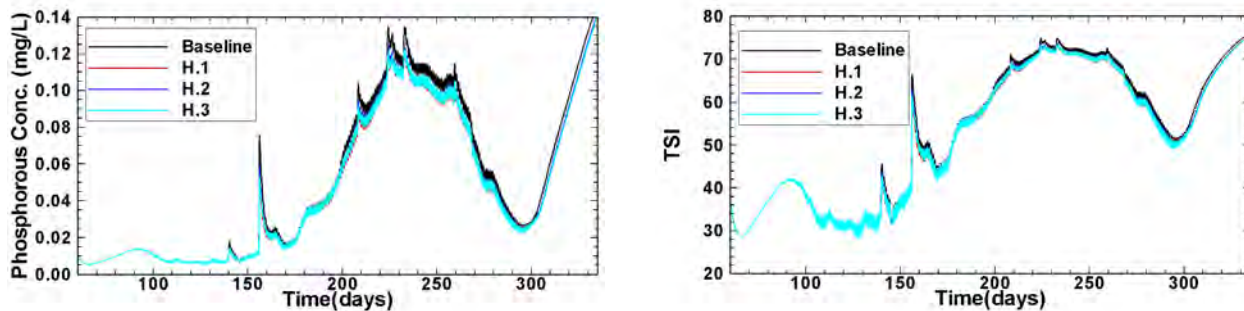
Figure 31. Simulated phosphorous concentrations and TSI for reducing tributary sediment and nutrient loadings measures.
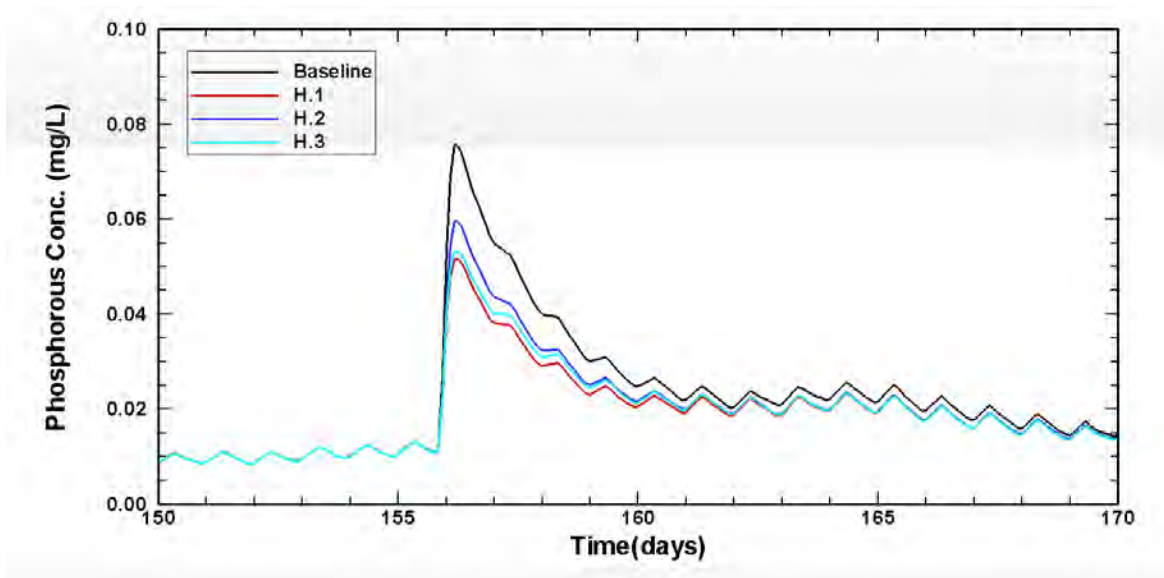
Figure 32. Simulated phosphorous concentration during the largest influx event.

Evaluating Ecosystem Restoration Alternatives

The USACE used the simulation results from each ecosystem restoration measure to formulate six ecosystem restoration alternatives that comprise combinations of the restoration measures. Each alternative was formulated to determine the contribution of and relative benefits from each measure and thereby assist in developing a long-term restoration plan for Cedar Lake. A description of each restoration alternative is summarized in Table 16.

Table 16. Description of proposed ecosystem restoration alternatives for Cedar Lake.

Alternative	Measures Included	Alternative Plan Description
ALT.1	A.3, C.1, H.2	Dredge 34 ha (83 acres) to 0.82 m (2.7 ft), reroute Founders Creek, and reduce loadings from all tributaries by 25%
ALT.2	A.4, C.1, H.1	Dredge 91 ha (224 acres) to 0.30 m (1.0 ft), reroute Founders Creek, and reduce loadings from Sleepy Hollow and Pickerel Creek by 50%
ALT.3	B.2, C.1, H.2	Alum treatment across 34-ha (83-acre) area, reroute Founders Creek, reduce loadings from all tributaries by 25%
ALT.4	B.1, C.1, H.1	Alum treatment for 91-ha (224-acre) area, reroute Founders Creek, and reduce loadings from Sleepy Hollow and Pickerel Creek by 50%
ALT.5	A.3, C.1, E.1, F.1, G.1, H.2	Dredge 34 ha (83 acres) to 0.82 m (2.7 ft), reroute Founders Creek, plant aquatic vegetation, increase no-wake zones by 35%, implement fish community management, and reduce loadings from all tributaries by 25%
ALT.6	B.2, C.1, E.1, F.1, G.1, H.2	Alum treatment for 34-ha (83-acre) area, reroute Founders Creek, plant aquatic vegetation, increase no wake zones by 35%, implement fish community management, reduce loadings from all tributaries by 25%

It is important to note that some of these alternatives are composed of combinations of measures that intersect, and without site-specific information it is difficult to know how to apply those overlaps within a single model cell. For example, when considering alternatives that contain dredging or alum treatment measures in combination with the littoral macrophyte restoration and fish community management measures, one measure must take modeling precedence when an overlap occurs. For modeling purposes, dredging and alum treatment measures were given the highest priority. In addition, the order in which benefits from each measure are realized must be considered. Fish community management and littoral macrophyte restoration measures were modeled by removing phosphorous directly from the sediment bed. More specifically, due to modeling limitations, the amount of phosphorous removed over a period of one year was subtracted from the sediment bed, and thus simulation results estimate benefits the year after they were applied. SNL-EFDC would need significant upgrades to allow for a user-specified gradual removal of phosphorous from the bed. Hence, degradation of the alum treatments during the year fish community management and littoral macrophyte restoration measures were implemented would not be considered.

Simulation results for the ecosystem restoration alternatives are shown in Figure 33. As noted earlier in the evaluation of chemical substrate restoration measures section, modeling results assume no degradation of alum treatment over time and further study is recommended to determine the long-term effectiveness of alum treatment measures within Cedar Lake.
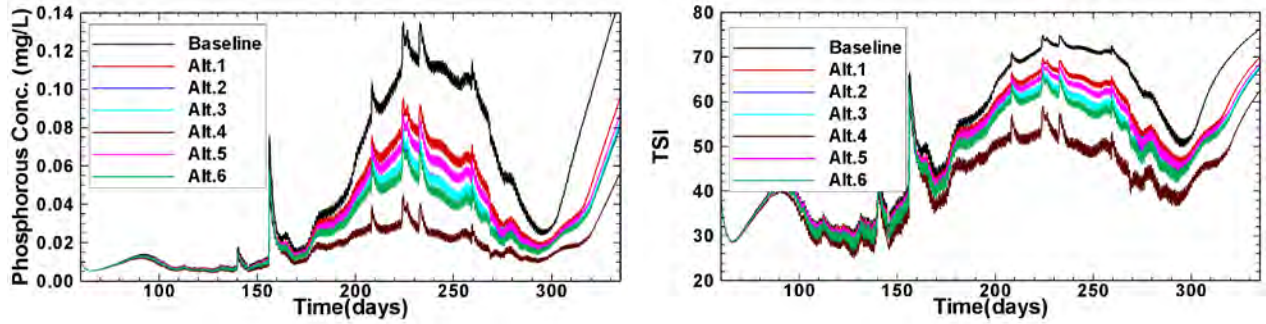
Figure 33. Simulated phosphorous concentrations and TSI for ecosystem restoration alternatives.

Short-Term Impacts during Dredging

Upland disposal of dredged material is costly due to many factors including the treatment of effluent return water to within regulatory water quality standards. Based on sediment and elutriate tests performed by the USACE on Cedar Lake (USACE Chicago District 2006), recommended treatment processes require six steps including breakpoint chlorination, alum treatment, polymer addition, sand filtration, and carbon filtration. Treatment aims at reducing concentrations to 1 mg/L for ammonia, 1 mg/L for phosphorous, and 10 mg/L for TSS, which are considered acceptable regulatory levels.

The impacts to the phosphorus concentration and short term eutrophication during dredging operations were evaluated. Both mechanical dredging and hydraulic dredging are currently under consideration for Cedar Lake. To evaluate the impacts solely from dewatering, the water quality within the lake from the additional influx of flow, sediment, and nutrient loadings were compared to baseline conditions. Based on projected dredging operations provided by USACE, mechanical (AM.1) and hydraulic (AH.1) operations would yield return flow rates of 6,541 m3/day (1,200 gpm) and 1,772 m^3/day (325 gpm), respectively. Treated flow would enter the lake through Pickerel Creek resulting in an increase in baseflow of 50% for mechanical dredging and nearly 300% for the hydraulic case.

Dredging is assumed to occur between April 1st and October 31st for both mechanical and hydraulic operations. Simulation results and impacts to phosphorus concentrations and TSI are shown in Figure 34.
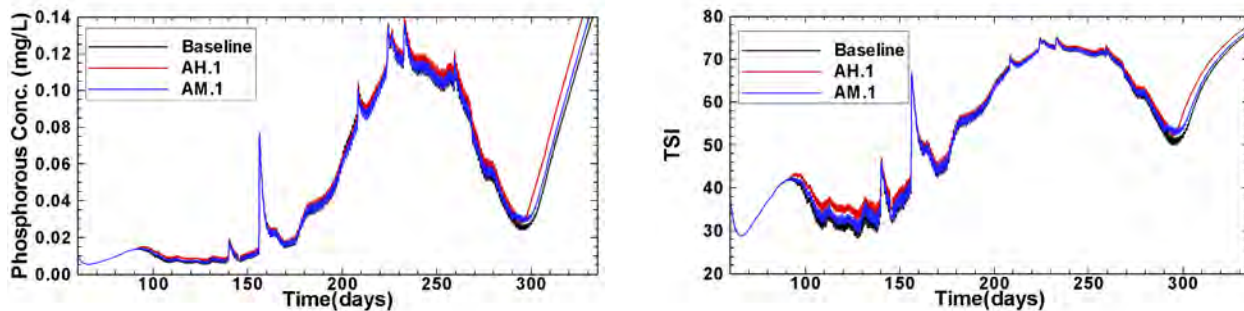
Figure 34. Simulated increases in phosphorous concentrations and TSI from treated return water during dredging.

The increases in average phosphorous concentrations as compared to baseline conditions are 2% and 8% for mechanical and hydraulic dredging respectively. These relative percentages will increase when coupled with each dredging measure because dredging itself removes phosphorus from the bed. For example, a 3% relative increase in average phosphorous for the baseline scenario equates to a 5% relative increase for dredging measure A.4. Simulation results suggest that mechanical dredging has less of an impact to water quality.

Conclusions

The goal of this modeling study was to develop a hydrodynamic, sediment transport and water quality model for Cedar Lake that reproduces observed trends and accurately reflects how boundary-condition perturbations (ecosystem restoration measures and alternatives) impact water quality. While we are less confident in the absolute values of modeled water quality parameters and simulation results, relative differences across restoration measures and alternatives provide sufficient confidence to aid in the selection of an ecosystem restoration plan. As is common in many water quality analyses, the data set available for model calibration and verification was not extensive, but it does provide insight into the trends and magnitudes of the parameters impacting water quality within Cedar Lake. This model illustrates the strong correlation between sediment bed phosphorus concentrations and algal concentrations, which reinforces that phosphorous is the limiting nutrient. During calibration, the pore water diffusion rate was adjusted to match modeled and observed phosphorus concentrations. Based on the reproduction of observed and inferred trends, the model is considered an adequate tool for the comparative evaluation of the ecosystem restoration measures and alternatives.

Once the baseline model was developed and calibrated, it was used to analyze several restoration measures as well as various combinations of restoration measures formulated into restoration alternatives. The simulation results are shown in Figure 35, which illustrates the spatio-temporal averaged normalized phosphorous concentration and maximum TSI for each measure and alternative considered. This figure clearly reflects how maximum TSI mirrors normalized phosphorus concentrations. Table 17 presents the simulated spatio-temporally averaged phosphorus and TSI, as well as the maximum spatially averaged phosphorous and TSI results for all the ecosystem restoration measures and alternatives modeled using the Cedar Lake SNL-EFDC model.

61
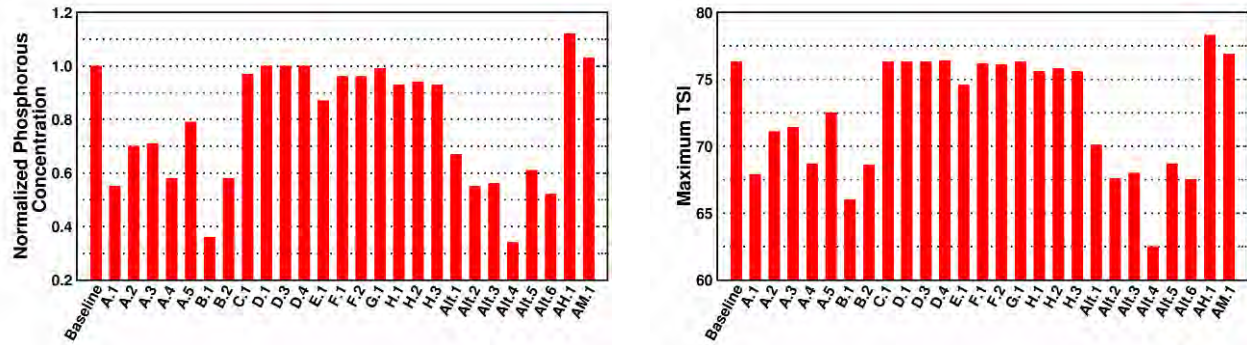
Figure 35. Simulated normalized spatio-temporally averaged phosphorus concentration and maximum TSI for each measure and alternative.

Table 17. Simulated spatio-temporally averaged phosphorus and TSI results for ecosystem restoration measures and alternatives.

Measure / Alternative	Maximum Phosphorous Concentration (mg/L)	Maximum Normalized Phosphorous Concentration	Average TSI	Maximum TSI
Baseline	0.0500	1.00	53.4	76.3
A.1	0.0276	0.55	47.6	67.9
A.2	0.0351	0.70	50.0	71.1
A.3	0.0354	0.71	50.1	71.4
A.4	0.0291	0.58	48.1	68.7
A.5	0.0395	0.79	51.2	72.5
B.1	0.0180	0.36	42.8	66.0
B.2	0.0289	0.58	48.1	68.6
C.1	0.0485	0.97	53.2	76.3
D.1	0.0500	1.00	53.4	76.3
D.3	0.0500	1.00	53.4	76.3
D.4	0.0498	1.00	53.5	76.4
E.1	0.0435	0.87	52.1	74.6
F.1	0.0480	0.96	53.1	76.2
F.2	0.0478	0.96	53.1	76.1
G.1	0.0497	0.99	53.4	76.3
H.1	0.0464	0.93	52.7	75.6
H.2	0.0470	0.94	52.8	75.8
H.3	0.0466	0.93	52.7	75.6
Alt.1	0.0336	0.67	49.6	70.1
Alt.2	0.0274	0.55	47.5	67.6
Alt.3	0.0278	0.56	47.7	68.0
Alt.4	**0.0171**	**0.34**	**42.4**	**62.5**
Alt.5	0.0306	0.61	48.6	68.7
Alt.6	0.0259	0.52	46.9	67.5
AH.1	0.0542	1.12	55.0	78.0
AM.1	0.0511	1.02	54.0	76.9

A total of nineteen ecosystem restoration measures and six ecosystem restoration alternatives were evaluated using the SNL-EFDC model. Measures and alternatives that include dredging or alum treatment show the greatest reductions in phosphorus concentrations and eutrophication because the largest source of phosphorus in the water column is diffusive flux from the sediment bed. While alum treatments are shown to decrease water-column phosphorus levels, these results may be temporary without periodic reapplication. Further study is recommended to determine the long-term effectiveness of alum treatment measures within Cedar Lake. Nevertheless, even a temporary decrease in phosphorus and algae concentrations and subsequent increases in water clarity could help the establishment of emergent and submergent vegetation. Institutional controls on boat activity are shown to yield positive impacts on the phosphorous concentrations through decreases in shear stress within the deeper, phosphorous-laden, portions of the lake. Simulation results suggest that habitat islands and fish community management would not significantly reduce eutrophication levels. Littoral macrophyte restoration appears to have a measurable reduction to phosphorus concentrations by removing nutrients within the shallow portions of the lake, although the near shore phosphorous concentrations are already fairly low. Because most of the phosphorus introduced to Cedar Lake is through tributary runoff, reductions to current loadings are necessary to prevent future accumulation of phosphorus-rich sediments. Finally, in conjunction with reducing sediment and nutrient tributary loadings, rerouting Founders Creek to Cedar Lake is shown to have a notable decrease in water-column phosphorus concentrations.

References

Bagnold, R. A. (1966). "An approach to the sediment transport problem for general physics." U.S Geologic Survey, Washington, D.C.

Bagnold, R. A. (1973). "The nature of saltation and 'bedload' transport in water." *Proceedings of the Royal Society of London: A*, 332, 473-504.

Bhowmik, N. G., Soong, T. W., Reichelt, W. F., and Seddik, N. M. L. (1991). "Waves generated by recreational traffic on the Upper Mississippi River System." U.S. Army Corps of Engineers.

Blumberg, A. F., and Mellor, G. L. (Year). "A description of a three-dimensional coastal ocean circulation model." *Coastal and Estuarine Sciences*, American Geophysical Union, 1-16.

Boyd, C. E. (1974). "Utilization of aquatic plants." In: *Aquatic vegetation and its use and control*, D. S. Mitchell, ed., Unesco, Paris, France.

Carlson, R. E. (1977). "Trophic State Index for Lakes." *Limnology and Oceanography*, 22, 361- 369.

Cerco, C. F., and Cole, T. (1995). "User's Guide to the CE-QUAL-ICM Three-Dimensional Eutrophication Model, Release Version 1.0." U.S. Army Corps of Engineers.

Cheng, N. S. (1997). "Simplified settling velocity formula for sediment particle." *Journal of Hydraulic Engineering-ASCE*, 123(2), 149-152.

Christoffersen, J., and Jonsson, I. (1985). "Bed friction and dissipation in a combined current and wave motion." *Ocean Engineering*, 17(4), 479-494.

Dyer, K. (1986). *Coastal and estuarine sediment dynamics*, Wiley and Sons, New York, New York.

Echelberger, W. F. (1984). "Cedar Lake Restoration Feasibility Study Final Report." Indiana University, Cedar Lake, Indiana.

Engle, B., and Harbor, J. (2005). "L-THIA NPS Version 3.2 GIS Extension Users Manual." Purdue University and the U.S. Environmental Protection Agency, Lafayette, Indiana.

Franzini, J. B., and Finnemore, E. J. (1997). *Fluid Mechanics with Engineering Applications*, 9th Ed., McGraw-Hill, New York, New York.

Garcia, M. H. (1999). "Sedimentation and Erosion Hydraulics." In: *Hydraulic Design Handbook*, L. W. Mays, ed., McGraw-Hill, 1024.

Haggard, B., and Moore, P. (2005). "Phosphorus flux from reservoir bottom sediments in Lake Eucha, Oklahoma." *Journal of Environmental Quality*, 34, 724-728.

Hamrick, J. M. (1992). "A Three-Dimensional Environmental Fluid Dynamics Computer Code: Theoretical and Computational Aspects." The College of William and Mary.

Hamrick, J. M. (1996). "User's Manual for the Environmental Fluid Dynamics Computer Code." Virginia Institute of Marine Sciences, Gloucester Point, Virginia.

Harza Environmental Services, I. (1998). "Draft Cedar Lake Dredging Feasibility Study." Cedar Lake, Indiana.

Harza Environmental Services, I. (1999). "Cedar Lake Engineering Feasibility Study." Cedar Lake Enhancement Association, Inc., Cedar Lake, Indiana.

Harza Environmental Services, I. (2001). "Cedar Lake Diagnostic Feasibility Study." Cedar Lake, Indiana.

James, S. C., Shrestha, P. L., and Roberts, J. D. (2006). "Modeling noncohesive sediment transport using multiple sediment size classes." *J. Coast. Res.*, 22(5), 1125-1132.

Jin, K. R., James, R. T., Lung, W. S., Loucks, D. P., Park, R. A., and Tisdale, T. S. (1998). "Assessing lake Okeechobee eutrophication with water-quality models." *Journal of Water Resource Planning and Management*, 124, 22-30.

Jin, K. R., Zhang, Q. Y., Chan, E. S., and Chou, L. M. (2001). "Three-dimensional ecological eutrophication model for Singapore." *J. Environ. Eng.-ASCE*, 127, 928-937.

Johnson, B., Kim, K., Heath, R., Hsieh, B., and Butler, H. (1993). "Validation of three- dimensional hydrodynamic model of Chesapeake Bay." *Journal of Hydraulic Engineering-ASCE*, 119(1), 2-20.

Jones, C., and Lick, W. (Year). "Contaminant flux due to sediment erosion." *The 7th International Conference: Estuarine and Coastal Modeling*, St. Pete Beach, Florida, 280- 293.

Jones, C., and Lick, W. (Year). "Sediment erosion rates: Their measurement and use in modeling." *The Texas A&M Dredging Seminar*, College Station, Texas, 1-15.

McNeil, J., Taylor, C., and Lick, W. (1996). "Measurement of erosion of undisturbed bottom sediments with depth." *Journal of Hydraulic Engineering-ASCE*, 122(6), 316-324.

Pellikaan, G. C., and Nienhuis, P. H. (1988). "Nutrient uptake and release during growth and decomposition of eelgrass, Zostera marina L., and its effects on the nutrient dynamics of Lake Grevelingen." *Aquatic Botany*, 30, 189-214.

Roberts, J. D., Jepsen, R. A., and James, S. C. (2003). "Measurement of sediment erosion and transport with the Adjustable Shear Stress Erosion and Transport Flume." *Journal of Hydraulic Engineering-ASCE*, 29(11), 862-871.

Roberts, J. D., Jepsen, R. A., and Lick, W. (1998). "Effects of particle size and bulk density on erosion of quartz particles." *Journal of Hydraulic Engineering-ASCE*, 124(12), 1261- 1267.

Roberts, J. D., O'Daniels, D., and Buhalts, R. (2005). "Cedar Lake Sediment Erosion Study: Field Activities." Sandia National Laboratories, Carlsbad, New Mexico.

USACE Chicago District. (2006). "Memorandum for Record, Estimates of Tributary Runoff, Sediment, and Contaminant Loadings Using Purdue Universities L-Thia NPS GIS v2.3 Model for Cedar Lake, Indiana." U.S Army Corps of Engineers, Chicago, Illinois.

USACE Rock Island District. (1997). "Interim Report for the Upper Mississippi River – Illinois Waterway System Navigation Study." U.S. Army Corps of Engineers, Rock Island, Illinois.

USACE Rock Island District. (2001). "Interim Report for the Upper Mississippi River – Illinois Waterway System Navigation Study." U.S. Army Corps of Engineers, Rock Island, Illinois.

van Rijn, L. C. (1984a). "Sediment transport, II: Suspended load transport." *Journal of Hydraulic Engineering-ASCE*, 110(11), 1613-1641.

van Rijn, L. C. (1984b). "Sediment transport, III: Bed forms and alluvial roughness." *Journal of Hydraulic Engineering-ASCE*, 110(12), 1733-1754.

van Rijn, L. C. (1984c). "Sediment transport, Part I: Bed load transport." *Journal of Hydraulic Engineering-ASCE*, 110(11), 1613-1641.

van Rijn, L. C. (1993). *Principles of sediment transport in rivers, estuaries and coastal seas*, Aqua Publications, Amsterdam, the Netherlands.

Vanni, M. J. (2002). "Nutrient cycling by animals in freshwater ecosystems." *Annual Review of Ecological Systems*, 33, 341-370.

Wodka, M. C., Effler, S. W., Driscoll, C. T., Field, S. D., and Devan, S. P. (1983). "Diffusivity- based flux of phosphorus in Onondaga Lake." *J. Environ. Eng.-ASCE*, 109(6), 1403- 1415.

Attachment 2:

Synthetic Hydrographs for Inlets to Cedar

Lake March 2006

MEMORANDUM FOR PM-PL-E (Bucaro)

SUBJECT: Synthetic Hydrographs for Inlets to Cedar Lake

1. <u>Introduction.</u> The purpose of this memorandum is to summarize the procedure used to develop synthetic hydrographs for the inlets to Cedar Lake in northwest Indiana. The methodology was also applied to sediment and nutrient data for the watershed to develop sediment and nutrient loading time-series data. The results of this analysis will be used to investigate how changes in land use, agricultural practices, and best management practices would affect the water quality of Cedar Lake.

2. <u>References.</u>

   a. CELRC-PM-PL-E. 8 Feb 2006. Estimates of Tributary Runoff, Sediment, and Contaminant Loadings Using Purdue Universities L-Thia NPS GIS v2.3 Model for Cedar Lake, Indiana (Memorandum for Record).

   b. Soil Conservation Service. August 1972. Hydrographs. NEH Notice 4-102, National Engineering Handbook, Section 4, Chapter 16.

   c. Chow, V.T.; Maidment, D.R.; and Mays, L.W. 1988. Applied Hydrology. McGraw-Hill, New York, NY.

3. <u>Available Data.</u> The subbasin delineation, area, and average curve numbers were obtained during the analysis described in Reference (a) using online GIS data. Elevation data was available from a 30-m digital elevation map (DEM) of the Chicago District. This was used to compute the longest flow path and average basin slope for each subbasin. The following table summarizes the subbasin characteristics.

Subbasin	Area (acres)	CN	Length (ft)	Slope (%)
Chamber Inlet	123	70.2	3,575	4.77
Condo Inlet	179	71.6	4,234	3.65
Direct Drainage	488	71.6	2,693	3.36
Golf Course Inlet	47	66.0	1,541	2.38
North Point Marina Inlet	371	72.8	8,356	4.00
Old Bank Building Inlet	161	73.7	4,073	3.03
Sleepy Hollow Ditch	1,209	78.1	13,818	1.22
Unnamed Inlet/Pickerel Creek	2,096	68.1	14,323	1.72
Hog Pen Ditch	795	68.2	13,701	2.83

CELRC-TS-DH
SUBJECT: Synthetic Hydrographs for Inlets to Cedar Lake

Precipitation data was taken from the nearest gage, in Crete, Illinois. This gage is approximately 11 miles away from Cedar Lake as shown in Enclosure 1. The period of record was June 2005 through August 2005 (Enclosure 2). The L-THIA model computed runoff depth for a given depth of precipitation. It also computed the mass of non-point source pollution for fifteen different compounds for each rain event modeled.

4. Methodology. Since streamflow records were not available for the subbasins surrounding Cedar Lake, synthetic unit hydrographs were generated for each inlet based on the SCS dimensionless hydrograph (Reference b). Sample calculations can be found in Enclosure 3. An Excel worksheet was created for each subbasin that generated the hydrograph for user-entered values of precipitation and storm duration.

    a. SCS Dimensionless Hydrograph. The amount of runoff for a given precipitation depth was found by fitting 3rd-order polynomials to the L-THIA results. The time between the start of the storm and the beginning of runoff is the time to ponding. This was computed using the SCS method of abstractions, assuming constant rainfall intensity. The time of concentration T_c was calculated for each subbasin using the SCS lag equation (Reference c) and basin characteristics. The SCS dimensionless unit hydrograph can be represented by a curve, or a triangular approximation (Enclosure 4). The two representations have the same time to peak and volume of runoff in the rising limb. The Excel spreadsheet computes both the curvilinear and triangular hydrographs.

    b. Application to Mass Flux. For the purposes of this analysis, it was assumed that the mass flow of pollutants into Cedar Lake follow the SCS dimensionless unit hydrograph as well. This means that the peak mass flux occurs at the same time as the peak flow. The concentration is constant over time and equal to (peak mass flow) / (peak discharge). The L-THIA results in Reference (a) included the total mass of pollutants at each inlet for various storms, and linear relationships were developed for each compound with respect to runoff depth. Enclosure 3 includes the derivation of the equation for peak mass flow rate.

    c. Runoff-Generating Storms. Based on the average curve numbers of the subbasins, runoff will occur near Cedar Lake when the amount of precipitation is greater than one inch. For the period of record, five storms produced enough precipitation to generate runoff. The storm characteristics are summarized below.

Date	Start Time	End Time	Duration (hr)	Precipitation (in)
6/04	16:00	19:00	3.0	3.5
7/26	18:30	21:30	3.0	1.4
8/11	8:30	15:00	6.5	1.9
8/13	8:15	16:00	7.75	1.1
8/20	4:30	10:00	5.5	1.8

The precipitation gage recorded data every 15 minutes, but for this analysis constant rainfall intensity was assumed for each storm.

CELRC-TS-DH
SUBJECT: Synthetic Hydrographs for Inlets to Cedar Lake

5. Results and Discussion. Runoff, sediment, and pollutant flow data were generated for June 2005 – August 2005 for each subbasin adjacent to Cedar Lake. The triangular unit hydrograph was used to create time series data for the entire period of record with a time step of 0.5 hr. The triangular unit hydrograph was used because it was easier to implement a constant time step, despite the different time of concentration and runoff duration experienced in each subbasin. The disadvantage of using a constant time step was that the peak could be missed if it occurred at a time other than a multiple of Δt. In some cases a smaller Δt was used to generate the hydrographs to create a better fit to the curvilinear graph, but the values were reported at 0.5-hr intervals.

6. Point of contact is the undersigned at brigid.j.briskin@usace.army.mil or 312-846-5514.

                                                /Original Signed/
4 Encls: BRIGID J. BRISKIN
1. Rain Gage Location   Hydraulic Engineer
2. Rain Gage Data
3. Sample Calculations
4. SCS Dimensionless Hydrograph
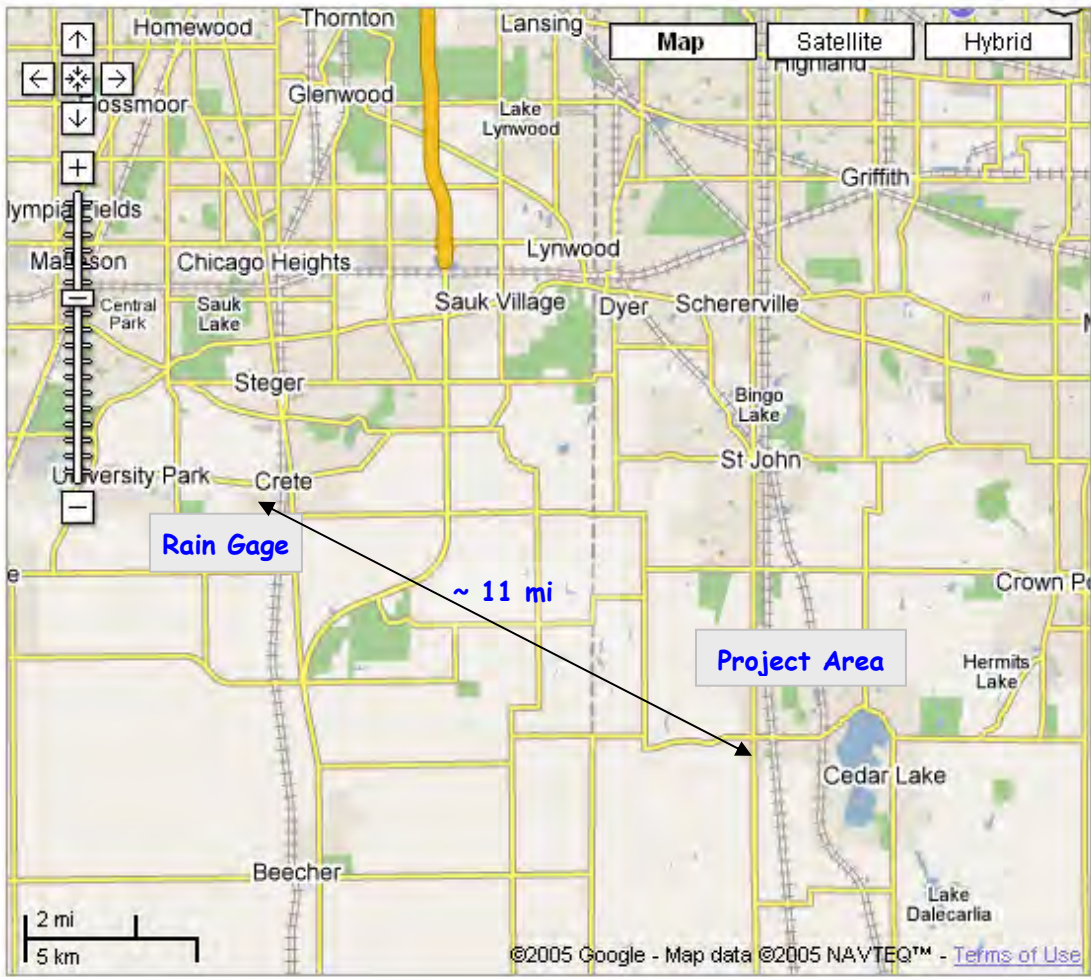
COOPID	STATION NAME	CD	ELEM	UN	YEAR	MO	DA	TIME	VALUE	F
112011	CRETE		2 QPCP	HT	2005	5	1	15	0	g
112011	CRETE		2 QPCP	HT	2005	5	1	2500	0	
112011	CRETE		2 QPCP	HT	2005	5	11	630	20	
112011	CRETE		2 QPCP	HT	2005	5	11	645	10	
112011	CRETE		2 QPCP	HT	2005	5	11	700	10	
112011	CRETE		2 QPCP	HT	2005	5	11	2500	40	
112011	CRETE		2 QPCP	HT	2005	5	12	245	10	
112011	CRETE		2 QPCP	HT	2005	5	12	415	10	
112011	CRETE		2 QPCP	HT	2005	5	12	700	10	
112011	CRETE		2 QPCP	HT	2005	5	12	2500	30	
112011	CRETE		2 QPCP	HT	2005	5	19	200	10	
112011	CRETE		2 QPCP	HT	2005	5	19	430	10	
112011	CRETE		2 QPCP	HT	2005	5	19	445	10	
112011	CRETE		2 QPCP	HT	2005	5	19	500	40	
112011	CRETE		2 QPCP	HT	2005	5	19	515	10	
112011	CRETE		2 QPCP	HT	2005	5	19	545	10	
112011	CRETE		2 QPCP	HT	2005	5	19	600	10	
112011	CRETE		2 QPCP	HT	2005	5	19	1730	10	
112011	CRETE		2 QPCP	HT	2005	5	19	2500	110	
112011	CRETE		2 QPCP	HT	2005	6	1	15	0	g
112011	CRETE		2 QPCP	HT	2005	6	1	2500	0	
112011	CRETE		2 QPCP	HT	2005	6	2	1500	10	
112011	CRETE		2 QPCP	HT	2005	6	2	1645	10	
112011	CRETE		2 QPCP	HT	2005	6	2	1745	10	
112011	CRETE		2 QPCP	HT	2005	6	2	2500	30	
112011	CRETE		2 QPCP	HT	2005	6	4	1600	50	
112011	CRETE		2 QPCP	HT	2005	6	4	1615	70	
112011	CRETE		2 QPCP	HT	2005	6	4	1630	10	
112011	CRETE		2 QPCP	HT	2005	6	4	1645	10	
112011	CRETE		2 QPCP	HT	2005	6	4	1700	60	
112011	CRETE		2 QPCP	HT	2005	6	4	1715	90	
112011	CRETE		2 QPCP	HT	2005	6	4	1730	40	
112011	CRETE		2 QPCP	HT	2005	6	4	1745	10	
112011	CRETE		2 QPCP	HT	2005	6	4	1900	10	
112011	CRETE		2 QPCP	HT	2005	6	4	2500	350	
112011	CRETE		2 QPCP	HT	2005	6	5	830	10	
112011	CRETE		2 QPCP	HT	2005	6	5	2500	10	
112011	CRETE		2 QPCP	HT	2005	6	7	1915	10	
112011	CRETE		2 QPCP	HT	2005	6	7	2500	10	
112011	CRETE		2 QPCP	HT	2005	6	9	1330	10	
112011	CRETE		2 QPCP	HT	2005	6	9	1915	20	
112011	CRETE		2 QPCP	HT	2005	6	9	2500	30	
112011	CRETE		2 QPCP	HT	2005	6	14	300	10	
112011	CRETE		2 QPCP	HT	2005	6	14	330	10	
112011	CRETE		2 QPCP	HT	2005	6	14	400	10	
112011	CRETE		2 QPCP	HT	2005	6	14	2500	30	
112011	CRETE		2 QPCP	HT	2005	6	29	1515	20	
112011	CRETE		2 QPCP	HT	2005	6	29	2500	20	
112011	CRETE		2 QPCP	HT	2005	6	30	630	10	
112011	CRETE		2 QPCP	HT	2005	6	30	1230	10	
112011	CRETE		2 QPCP	HT	2005	6	30	2500	20	
112011	CRETE		2 QPCP	HT	2005	7	1	15	0	g
112011	CRETE		2 QPCP	HT	2005	7	1	2500	0	
112011	CRETE		2 QPCP	HT	2005	7	4	2330	10	
112011	CRETE		2 QPCP	HT	2005	7	4	2500	10	
112011	CRETE		2 QPCP	HT	2005	7	12	1115	10	
112011	CRETE		2 QPCP	HT	2005	7	12	1500	10	
112011	CRETE		2 QPCP	HT	2005	7	12	1530	30	
112011	CRETE		2 QPCP	HT	2005	7	12	1700	10	
112011	CRETE		2 QPCP	HT	2005	7	12	2015	10	
112011	CRETE		2 QPCP	HT	2005	7	12	2500	70	
112011	CRETE		2 QPCP	HT	2005	7	13	1200	10	

112011	CRETE	2 QPCP	HT	2005	7	13	2500	10	
112011	CRETE	2 QPCP	HT	2005	7	18	730	10	
112011	CRETE	2 QPCP	HT	2005	7	18	745	10	
112011	CRETE	2 QPCP	HT	2005	7	18	1300	20	
112011	CRETE	2 QPCP	HT	2005	7	18	2500	40	
112011	CRETE	2 QPCP	HT	2005	7	20	1500	20	
112011	CRETE	2 QPCP	HT	2005	7	20	1515	20	
112011	CRETE	2 QPCP	HT	2005	7	20	1815	10	
112011	CRETE	2 QPCP	HT	2005	7	20	2230	10	
112011	CRETE	2 QPCP	HT	2005	7	20	2315	10	
112011	CRETE	2 QPCP	HT	2005	7	20	2500	70	
112011	CRETE	2 QPCP	HT	2005	7	25	1015	10	
112011	CRETE	2 QPCP	HT	2005	7	25	1030	10	
112011	CRETE	2 QPCP	HT	2005	7	25	1330	10	
112011	CRETE	2 QPCP	HT	2005	7	25	2500	30	
112011	CRETE	2 QPCP	HT	2005	7	26	1830	30	
112011	CRETE	2 QPCP	HT	2005	7	26	1845	50	
112011	CRETE	2 QPCP	HT	2005	7	26	1900	10	
112011	CRETE	2 QPCP	HT	2005	7	26	1930	10	
112011	CRETE	2 QPCP	HT	2005	7	26	2000	10	
112011	CRETE	2 QPCP	HT	2005	7	26	2015	10	
112011	CRETE	2 QPCP	HT	2005	7	26	2100	10	
112011	CRETE	2 QPCP	HT	2005	7	26	2130	10	
112011	CRETE	2 QPCP	HT	2005	7	26	2500	140	
112011	CRETE	2 QPCP	HT	2005	7	27	215	10	
112011	CRETE	2 QPCP	HT	2005	7	27	2500	10	
112011	CRETE	2 QPCP	HT	2005	8	1	15	0	g
112011	CRETE	2 QPCP	HT	2005	8	1	700	99999	[
112011	CRETE	2 QPCP	HT	2005	8	1	1100	99999	]
112011	CRETE	2 QPCP	HT	2005	8	1	2500	0	I
112011	CRETE	2 QPCP	HT	2005	8	4	600	10	
112011	CRETE	2 QPCP	HT	2005	8	4	1100	10	
112011	CRETE	2 QPCP	HT	2005	8	4	2500	20	
112011	CRETE	2 QPCP	HT	2005	8	10	630	10	
112011	CRETE	2 QPCP	HT	2005	8	10	1330	10	
112011	CRETE	2 QPCP	HT	2005	8	10	2500	20	
112011	CRETE	2 QPCP	HT	2005	8	11	830	10	
112011	CRETE	2 QPCP	HT	2005	8	11	900	20	
112011	CRETE	2 QPCP	HT	2005	8	11	915	10	
112011	CRETE	2 QPCP	HT	2005	8	11	930	10	
112011	CRETE	2 QPCP	HT	2005	8	11	1000	50	
112011	CRETE	2 QPCP	HT	2005	8	11	1015	20	
112011	CRETE	2 QPCP	HT	2005	8	11	1030	10	
112011	CRETE	2 QPCP	HT	2005	8	11	1045	20	
112011	CRETE	2 QPCP	HT	2005	8	11	1100	10	
112011	CRETE	2 QPCP	HT	2005	8	11	1130	10	
112011	CRETE	2 QPCP	HT	2005	8	11	1445	10	
112011	CRETE	2 QPCP	HT	2005	8	11	1500	10	
112011	CRETE	2 QPCP	HT	2005	8	11	2500	190	
112011	CRETE	2 QPCP	HT	2005	8	13	815	20	
112011	CRETE	2 QPCP	HT	2005	8	13	830	10	
112011	CRETE	2 QPCP	HT	2005	8	13	900	10	
112011	CRETE	2 QPCP	HT	2005	8	13	1430	10	
112011	CRETE	2 QPCP	HT	2005	8	13	1445	20	
112011	CRETE	2 QPCP	HT	2005	8	13	1500	10	
112011	CRETE	2 QPCP	HT	2005	8	13	1515	10	
112011	CRETE	2 QPCP	HT	2005	8	13	1545	10	
112011	CRETE	2 QPCP	HT	2005	8	13	1600	10	
112011	CRETE	2 QPCP	HT	2005	8	13	2500	110	
112011	CRETE	2 QPCP	HT	2005	8	17	1430	99999	{
112011	CRETE	2 QPCP	HT	2005	8	17	1600	99999	}
112011	CRETE	2 QPCP	HT	2005	8	17	2500	0	P
112011	CRETE	2 QPCP	HT	2005	8	18	1500	10	
112011	CRETE	2 QPCP	HT	2005	8	18	2500	10	

112011 CRETE	2 QPCP	HT	2005	8	20	430	10
112011 CRETE	2 QPCP	HT	2005	8	20	445	50
112011 CRETE	2 QPCP	HT	2005	8	20	500	20
112011 CRETE	2 QPCP	HT	2005	8	20	515	20
112011 CRETE	2 QPCP	HT	2005	8	20	530	40
112011 CRETE	2 QPCP	HT	2005	8	20	545	30
112011 CRETE	2 QPCP	HT	2005	8	20	1000	10
112011 CRETE	2 QPCP	HT	2005	8	20	2500	180
112011 CRETE	2 QPCP	HT	2005	8	30	1015	10
112011 CRETE	2 QPCP	HT	2005	8	30	2500	10
112011 CRETE	2 QPCP	HT	2005	9	1	15	0 g
112011 CRETE	2 QPCP	HT	2005	9	1	2500	0
112011 CRETE	2 QPCP	HT	2005	9	11	915	10
112011 CRETE	2 QPCP	HT	2005	9	11	2500	10
112011 CRETE	2 QPCP	HT	2005	9	15	1945	10
112011 CRETE	2 QPCP	HT	2005	9	15	2030	10
112011 CRETE	2 QPCP	HT	2005	9	15	2115	10
112011 CRETE	2 QPCP	HT	2005	9	15	2130	10
112011 CRETE	2 QPCP	HT	2005	9	15	2145	10
112011 CRETE	2 QPCP	HT	2005	9	15	2230	20
112011 CRETE	2 QPCP	HT	2005	9	15	2245	10
112011 CRETE	2 QPCP	HT	2005	9	15	2300	10
112011 CRETE	2 QPCP	HT	2005	9	15	2315	10
112011 CRETE	2 QPCP	HT	2005	9	15	2400	10
112011 CRETE	2 QPCP	HT	2005	9	15	2500	110
112011 CRETE	2 QPCP	HT	2005	9	16	1415	10
112011 CRETE	2 QPCP	HT	2005	9	16	2500	10
112011 CRETE	2 QPCP	HT	2005	9	19	815	10
112011 CRETE	2 QPCP	HT	2005	9	19	1145	10
112011 CRETE	2 QPCP	HT	2005	9	19	2500	20
112011 CRETE	2 QPCP	HT	2005	9	25	1100	10
112011 CRETE	2 QPCP	HT	2005	9	25	1345	10
112011 CRETE	2 QPCP	HT	2005	9	25	1715	10
112011 CRETE	2 QPCP	HT	2005	9	25	2500	30
112011 CRETE	2 QPCP	HT	2005	9	28	1730	10
112011 CRETE	2 QPCP	HT	2005	9	28	1745	10
112011 CRETE	2 QPCP	HT	2005	9	28	1800	10
112011 CRETE	2 QPCP	HT	2005	9	28	1830	10
112011 CRETE	2 QPCP	HT	2005	9	28	2500	40

	PROJECT TITLE: CEDAR LAKE		COMPUTED BY: BJB	DATE: 3/24/06	SHEET:
US Army Corps of Engineers. Chicago District	COMPUTATION TITLE: Synthetic Hydrograph Sample Calculations		CHECKED BY:	DATE:	1 of 4

SCS Dimensionless Hydrograph Equations

$$q_p = \frac{CA}{T_p}$$

where q_p = peak specific discharge (cfs/in)
C = 483.4 for English units
A = drainage area (mi²)
T_p = time to peak (hr)

$$T_p = \frac{t_r}{2} + t_{pe}$$

where t_r = duration of excess precip
t_{pe} = lag time after excess precip

$$t_{pe} = 0.6\, T_c$$

where T_c = time of concentration

$$T_r = 1.67\, T_p$$

where T_r = time of recession

SCS Lag Equation for Time of Concentration

$$T_c = \frac{100\, L^{0.8}\,[(1000/CN) - 9]^{0.7}}{1900\, S^{0.5}}$$

where L = longest flowpath (ft)
CN = curve number
S = average basin slope (%)

SCS Method for Abstractions for Ponding Time
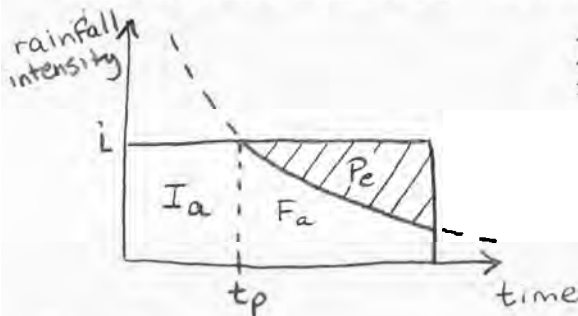
I_a = initial abstractions (in)
F_a = additional infiltration
    = excess precipitation
S = potential maximum retention (in

$$I_a = 0.2\,S$$

$$S = \frac{1000}{CN} - 10$$

For constant intensity i,

$$i\, t_p = I_a$$

$$i\, t_p = 0.2\left(\frac{1000}{CN} - 10\right)$$

$$\boxed{t_p = \frac{0.2}{i}\left(\frac{1000}{CN} - 10\right)}$$

Using SCS Dimensionless Hydrograph
<u>for Sedigraphs and Chemographs</u>
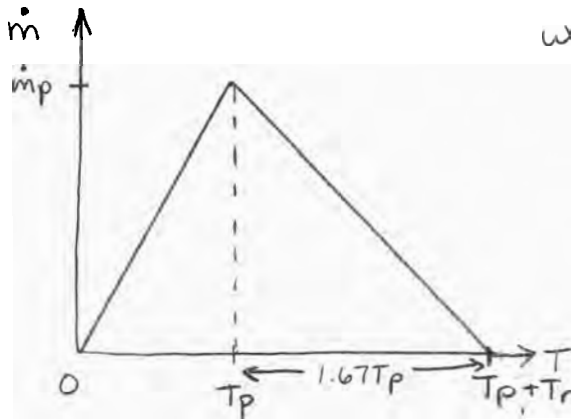
where $\dot{m}$ = mass flux
M = total mass = $\int \dot{m}\,dt$
T_p = time to peak
T_r = recession time

$$A = \frac{1}{2} B h$$

$$M = \frac{1}{2} T_p \dot{m}_p + \frac{1}{2} T_r \dot{m}_p = \frac{\dot{m}_p}{2}(T_p + T_r)$$

$$\dot{m}_p = \frac{2M}{T_p + T_r}$$

Let $K = \dfrac{2}{1 + \frac{T_r}{T_p}}$ $\Rightarrow$ $\dot{m}_p = \dfrac{KM}{T_p}$

but $T_r = 1.67\,T_p$ $\Rightarrow$ $K = 0.75$ and $\boxed{\dot{m}_p = \dfrac{0.75M}{T_p}}$

<u>Sample Calculations for Golf Course Inlet</u>

A = 47 acres   Assume P = 4 in
CN = 66   T = 4 hr
L = 1541 ft
S = 2.38%

Total precip = 4 in. From L-THIA, runoff = 0.19 in.

Ponding time $t_p = (0.2)\left(\frac{hr}{1\,in}\right)\left(\frac{1000}{CN}-10\right)in = 1.03\,hr.$

Time of concentration $T_c = \dfrac{100(1541)^{0.8}\left[(1000/66)-9\right]^{0.7}}{1900\,(2.38)^{0.5}}$

$$T_c = 43.2\ min$$

Lag time $t_{pe} = 0.6(43.2) = 25.9\ min = 0.432\,hr$

Time to peak $T_p = \dfrac{(4-1.03)}{2} + 0.432 = 1.92\ hr$

$q_{fp} = \dfrac{(483.4)}{(1.92)}(47\,ac)\left(\dfrac{43560\,ft^2}{1\,ac}\right)\left(\dfrac{1\,mi}{5280\,ft}\right)^2 = 18.49\ cfs/in$

$Q_p = (0.19\,in)\left(\dfrac{18.49\,cfs}{in}\right) = 3.51\ cfs = 0.099\ m^3/s$

Sample Calculations for Golf Course Inlet (cont.)

Nutrient loading from L-THIA results,
P = 4in → Dissolved Solids = 210.05 kg

$T_p = 1.92$ hr

$$\dot{m}_p = \frac{(0.75)(210.05)}{(1.92)} = 82.1 \frac{kg}{hr} = 2.28 \times 10^{-2} \, kg/s$$

$$\text{Concentration of DS} = \left(\frac{2.28 \times 10^{-2} \, kg}{s}\right)\left(\frac{s}{0.099 \, m^3}\right)$$

$$[DS] = 0.230 \, kg/m^3$$

16.4

Table 16.1 Ratios for dimensionless unit hydrograph and mass curve.

Time Ratios (t/T_p)	Discharge Ratios (q/q_p)	Mass Curve Ratios (Q_a/Q)
0	.000	.000
.1	.030	.001
.2	.100	.006
.3	.190	.017
.4	.310	.035
.5	.470	.065
.6	.660	.107
.7	.820	.163
.8	.930	.228
.9	.990	.300
1.0	1.000	.375
1.1	.990	.450
1.2	.930	.522
1.3	.860	.589
1.4	.780	.650
1.5	.680	.705
1.6	.560	.751
1.7	.460	.790
1.8	.390	.822
1.9	.330	.849
2.0	.280	.871
2.2	.207	.908
2.4	.147	.934
2.6	.107	.953
2.8	.077	.967
3.0	.055	.977
3.2	.040	.984
3.4	.029	.989
3.6	.021	.993
3.8	.015	.995
4.0	.011	.997
4.5	.005	.999
5.0	.000	1.000

Elements of a Unit Hydrograph
The dimensionless curvilinear unit hydrograph (figure 16.1) has 37.5% of the total volume in the rising side, which is represented by one unit of time and one unit of discharge. This dimensionless unit hydrograph also can be represented by an equivalent triangular hydrograph having the same units of time and discharge, thus having the same percent of volume in the rising side of the triangle (figure 16.2).
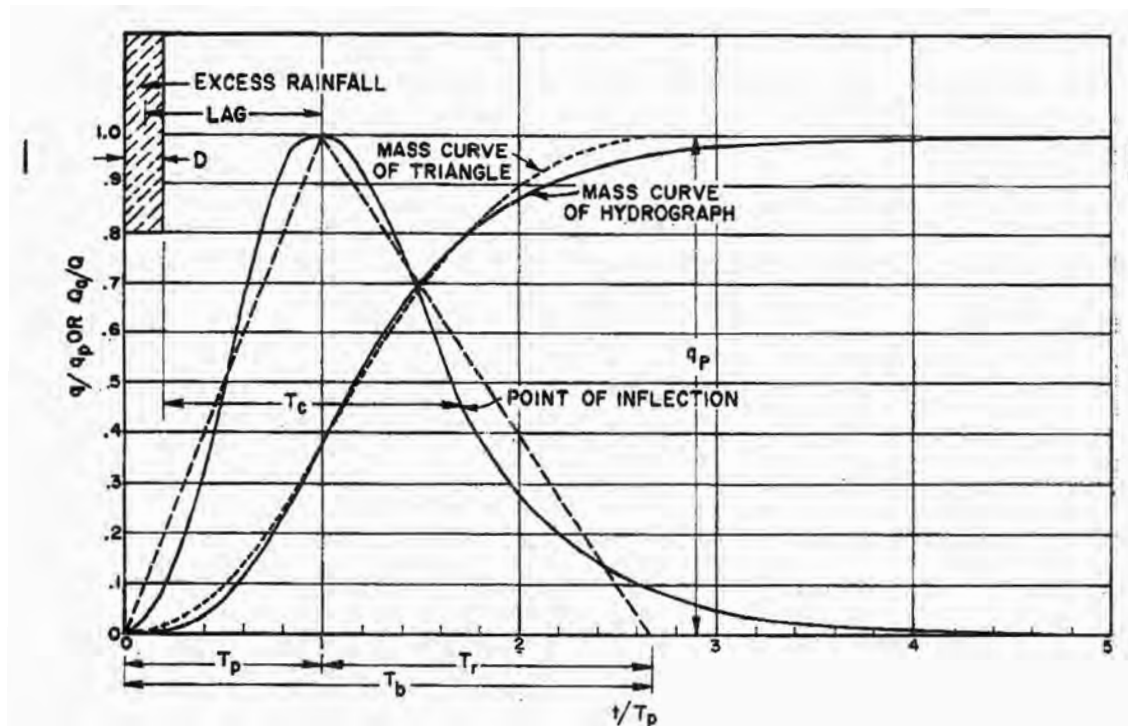
Figure 16.2 Dimensionless curvilinear unit hydrograph and equivalent triangular hydrograph

Attachment 3:

Estimates of Tributary Runoff, Sediment, and Contaminant Loadings Using L-Thia NPS GIS v2.3 Model for Cedar Lake, Indiana

February 2006

MEMORANDUM FOR RECORD

SUBJECT: Estimates of Tributary Runoff, Sediment, and Contaminant Loadings Using Purdue Universities L-Thia NPS GIS v2.3 Model for Cedar Lake, Indiana.

1. <u>References:</u>

    a. Baird, C., and Jennings M., Characterization of Nonpoint Sources and Loadings to the Corpus Christi Bay National Estuary Program Study Area, Texas Natural Resource Conservation Commission. 1996.; and,

    b. Engle, B. and Harbor, J., L-THIA version 3.2 GIS extension Users Manual. Purdue University and U.S. Environmental Protection Agency. 2005. http://www.ecn.purdue.edu/runoff/lthianew/lthia_gis.htm

2. Boundary conditions including runoff, sediment loading, and nutrient loadings are a required input to the Environmental Fluid Dynamics Computer Code (EFDC) lake model being developed for Cedar Lake by Sandia National Lab (SNL) under contract to the Chicago District. In order to determine impacts to water quality as a result to restoration measures located in upland areas of the Cedar Lake, watershed tributary loadings represented as boundary conditions in the lake model must be determined. Changes in landuse, agricultural practices, and best management practices (BMPs) along with other upland measures and their effects on Cedar Lake will be investigated using the EFDC model by varying the boundary conditions.

3. The Long-Term Hydrologic Impact Assessment for Non-Point Source Pollutants Model (L-Thia NPS) developed by Purdue University was utilized for this analysis. L-Thia, originally developed as a spreadsheet-based model, has developed to a simple web-based computation table, a standalone Geographical Information Systems (GIS) extension, or a web-based tool that incorporates GIS data manipulation, online digitizing, and detailed output. The L-Thia model in all forms can be accessed via the following website: http://www.ecn.purdue.edu/runoff/. L-Thia has been developed as a straightforward analysis tool that provides estimates of changes in runoff, recharge, and non-point source pollution resulting from past or proposed land use changes. The L-Thia model is an excellent tool to determine impacts as a result to land use changes. In this analysis, the L-Thia model was used to determine quantified estimates that can be used as inputs to the EFDC model. L-Thia calculates runoff depth and volumes based on the NRCS Curve Number (CN) methodology. For this Cedar Lake analysis, tributary watersheds were delineated via the online hydrologic mapping tools (HYMAPS-OWL) (http://danpatch.ecn.purdue.edu/~watergen/owls/htmls/sele0.html) and GIS data was downloaded for use by the standalone L-Thia v2.3 GIS extension for ArcView v3.x. A summary list of GIS data used in this analysis is shown in Table 1.

MEMORANDUM FOR RECORD

SUBJECT: Estimates of Tributary Runoff, Sediment, and Contaminant Loadings Using Purdue Universities L-Thia NPS GIS v2.3 Model for Cedar Lake, Indiana.

Table 1: GIS data used in L-Thia Analysis

Type	Source	Description	Format
Land Use	USGS	30-m resolution National Land Cover Database (based primarily on Landsat TM 1992 imagery.)	Polygon
Soil Data	NRCS	30-m resolution National SSURGO Database	Polygon
DEM	USGS	30-m resolution National Elevation Data	Grid
Watershed Boundary	Purdue	Using HYMAPS-OWL online digitizing tool (delineated watershed boundaries by selecting outlet locations at tributary confluences)	Polygon

4. A total of seven tributaries were delineated by the online mapping tools and GIS data corresponding to each of catchments was downloaded. In addition, areas of direct drainage to Cedar Lake and Hog Pen Ditch, which originally drained to the lake was delineated data downloaded. A map of the sub-basins is shown in Plate 1 attached. Basin delineations and drainage areas were determined from the national seamless 30-meter hydrologically corrected digital elevation model (DEM). Landuse category data and hydrologic soil group (HSG) data was used to compute curve number data. The hydrologic soil group for the entire Cedar Lake watershed HSG Group C, which are soils that are sandy clay loam and have low infiltration rates. The relationship between landuse, hydrologic soil group C, and curve number is shown in Table 2. Table 3 is a summary list of tributaries data. A map showing curve number and landuse by sub-basin in Plate 2 is attached.

Table 2: Curve Number Relationship

Landuse Type	HSG Group	CN
Commercial	C	94
Industrial	C	91
HD Residential	C	90
LD Residential	C	80
Agricultural	C	82
Grass / Pasture	C	74
Forest	C	70
Water	C	0

MEMORANDUM FOR RECORD

SUBJECT: Estimates of Tributary Runoff, Sediment, and Contaminant Loadings Using Purdue
Universities L-Thia NPS GIS v2.3 Model for Cedar Lake, Indiana.

Table 3: Cedar Lake Tributary Data

Tributary / Watershed	Area (acres)	Average CN
Chamber Inlet	123	76.9
Condo Inlet	179	72.0
Golf Course Inlet	47	71.0
North Point Marina Inlet	371	69.6
Old Bank Building Inlet	161	77.8
Sleepy Hollow Ditch	1209	79.3
Unnamed Inlet / Pickerel Creek	2096	74.7
Direct Drainage	488	68.3
Hog Pen Ditch (bypasses Cedar Lake)	795	69.9

5. The L-Thia GIS extension has the ability to model long-term average annual precipitation
event based on local rain gage data and user defined single storm events based on rainfall
depth. A long-term rainfall data for the entire country was compiled by Purdue
University based weather station data on a thirty-year period of record and broken out by
state and county. Single storm rainfall depths for the Cedar Lake area were determined
using the National Weather Service Bulletin 71: Rainfall Frequency Atlas of the
Midwest. (http://www.sws.uiuc.edu/pubdoc/B/ISWSB-71.pdf) A listing of sectional
mean frequency distributions for storm periods of 5 minutes to 10 days and recurrence
intervals of 2 months to 100 years for Northwest Indiana is shown in Plate 3 attached. A
range of rainfall depths (0.5", 1", 2", 3", 4", 5", 6", 8", 10" rainfalls) covering all the
storm frequencies were ran using L-Thia.

6. L-Thia utilizes the NRCS Curve Number methodology to compute runoff depth for each
grid cell in a given watershed. The standard antecedent moisture condition AMCII was
utilized as the starting hydrologic condition for the single storm events. A map showing
rainfall depth by sub-basin for the long-term annual event is shown in Plate 4 attached.
Runoff volume is determined by multiplying the runoff depth multiplied by cell area.
Event Mean Concentration (EMC) data are used to predict non-point source (NPS)
pollutant masses by multiplying the runoff volume of a grid cell by the EMC value and
converting units. The Event Mean Concentration (EMC) data used was compiled by the
Texas Natural Resource Conservation Commission (Baird and Jennings, 1996).
Numerous literature and existing water quality data were reviewed with respect to eight
categories of land use and several parameters. Land use categories defined were: (1)
industrial; (2) transportation; (3) commercial; (4) residential; (5) agricultural cropland

MEMORANDUM FOR RECORD

SUBJECT: Estimates of Tributary Runoff, Sediment, and Contaminant Loadings Using Purdue Universities L-Thia NPS GIS v2.3 Model for Cedar Lake, Indiana.

(dry land and irrigated); (6) range land; (7) undeveloped/open; and (8) marinas. The total pollutant load for various NPS pollutants divided by runoff volume during a runoff event yielded the Event Mean Concentration. However, some pollutant concentrations vary with time for rainfall events, so flow-averaged sample values were used as Event Mean Concentrations in these cases, therefore, EMCs should be reliable for determining average concentrations and calculating constituent loads. A listing of the EMCs used in the L-Thia model is listed in Table 4 below. For this analysis, point loadings at the confluence of each tributary with Cedar Lake are needed for input to the EFDC model. In order to aggregate runoff volumes and NPS masses at each tributary location, ArcGIS ver. 9.1 was used to aggregate by sub-watershed each of the grid loadings. A summary of results for each tributary is attached in Plate 5.

Table 4: Event Mean Concentrations (Baird and Jennings, 1996)

NPS Pollutant	Land use classification						
	Resid - ential	Com - mercial	Indu - stry	Transi - tion	Mixed	Agric - ultural	Range
Total Nitrogen (mg/L)	1.82	1.34	1.26	1.86	1.57	4.4	0.7
Total Kjeldahl Nitrogen (mg/L as N)	1.5	1.1	1.0	1.5	1.25	1.7	0.2
Nitrate+Nitrite (mg/L)	0.23	0.26	0.3	0.56	0.34	1.6	0.4
Total Phosphorus (mg/L)	0.57	0.32	0.28	0.22	0.35	1.3	0.01
Dissolved Phosphorus (mg/L)	0.48	0.11	0.22	0.1	0.23	---	---
Suspended Solids (mg/L)	41	55.5	60.5	73.5	57.9	107	1
Dissolved Solids (mg/L)	134	185	116	194	157	1225	245
Total Lead (µg/L)	9	13	15	11	12	1.5	5.0
Total Copper (µg/L)	15	14.5	15	11	13.9	1.5	10
Total Zinc (µg/L)	80	180	245	60	141	16	6
Total Cadmium (µg/L)	0.75	0.96	2	1	1.05	1	1
Total Chromium (µg/L)	2.1	10	7	3	5.5	10	7.5
Total Nickel (µg/L)	10	11.8	8.3	4	7.3	---	---
BOD (mg/L)	25.5	23	14	6.4	17.2	4.0	0.5
COD (mg/L)	49.5	116	45.5	59	67.5	---	---
Oil and Grease (mg/L)	1.7	9	3	0.4	3.5	---	---

7. The L-Thia model utilizes the NRCS curve number rainfall/runoff process for generating runoff volumes. There are limitations to this methodology in that snowmelt and ice cover

MEMORANDUM FOR RECORD

SUBJECT: Estimates of Tributary Runoff, Sediment, and Contaminant Loadings Using Purdue Universities L-Thia NPS GIS v2.3 Model for Cedar Lake, Indiana.

conditions are not modeled.   The results from the L-Thia model should be used as input to the EFDC lake model while understanding the limitations. It is suggested that the NPS pollutant results of the L-Thia model should be analyzed for consistency by water quality expert prior to utilizing the data in the EFDC lake model.

8. Point of contact for this memorandum for record is Mr. David Bucaro, PM-PL-E at (312) 846-5583 or david.f.bucaro@usace.army.mil.

/ORIGINAL SIGNED/
David F. Bucaro, P.E.
Hydraulic Engineer

Cedar Lake, Indiana

Subwatershed Deliniation Based on 30-meter USGS Hydrographic Corrected DEM
Water Quality Sample Locations Collected: 22 August 2005

condo inlet

chamber inlet

north point marina inlet

Condo Inlet

Chamber Inlet

old bank building inlet

North Lobe

Old Bank Inlet

direct drainage

Central Lobe

direct drainage

hog pen ditch

sleepy hollow ditch

Municiple Inlet

Hogpen Ditch Cedar Ck.

South Lobe

Sleepy Hollow Inlet

No Name Inlet

Golf Course Inlet

Pickerel Ck. Inlet

unnamed inlet/pickerel creek

Legend

● WQ Sonde Measurements

0 500 1,000   2,000   3,000   4,000
Feet

1 inch equals 3,000 feet

N

PLATE 1

Cedar Lake, Indiana

Subwatershed Deliniation Based on 30-meter USGS Hydrographic Corrected DEM
NRCS Curve Numbers created based on Landuse and Soil Classification Data
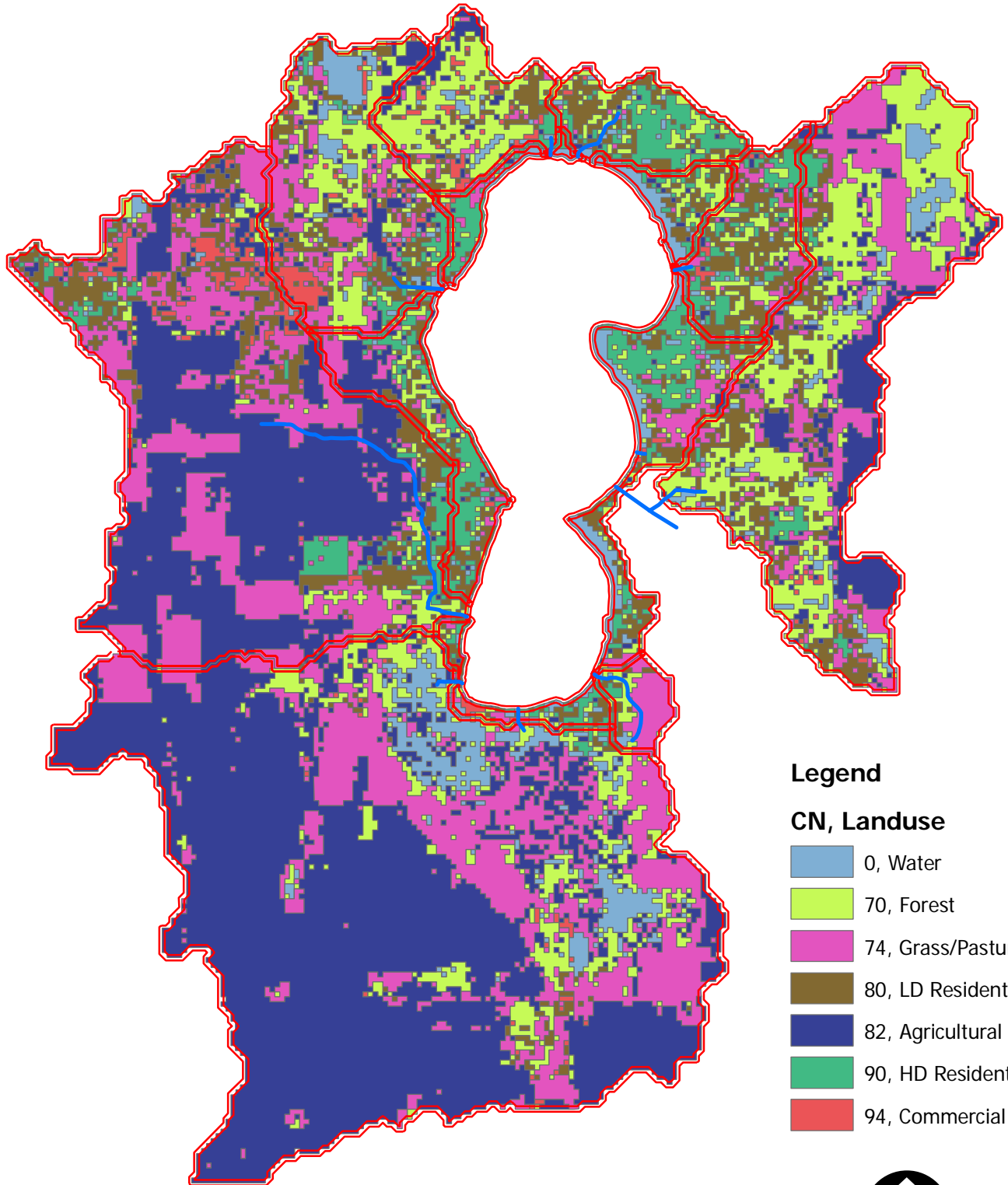
Legend

CN, Landuse

- 0, Water
- 70, Forest
- 74, Grass/Pasture
- 80, LD Residential
- 82, Agricultural
- 90, HD Residential
- 94, Commercial

0 500 1,000 2,000 3,000 4,000
Feet
1 inch equals 3,000 feet

PLATE 2

Part2, Table 2. Sectional Mean Frequency Distributions for Storm Periods of 5 Minutes to 10 Days and Recurrence Intervals of 2 Months to 100 Years in Indiana

Sectional code (see figure 1 below)
Rainfall (inches) for given recurrence interval

Section	Duration	2-month	3-month	4-month	6-month	9-month	1-year	2-year	5-year	10-year	25-year	50-year	100-year
01	10-day	2.07	2.50	2.88	3.38	3.89	4.23	4.84	5.79	6.67	8.03	9.23	10.58
01	5-day	1.68	2.01	2.27	2.63	3.03	3.29	3.84	4.70	5.50	6.81	7.99	9.37
01	72-hr	1.53	1.80	2.04	2.36	2.71	2.95	3.46	4.24	4.97	6.10	7.17	8.38
01	48-hr	1.40	1.64	1.83	2.12	2.44	2.65	3.12	3.87	4.56	5.58	6.52	7.58
01	24-hr	1.33	1.55	1.69	1.96	2.23	2.42	2.89	3.61	4.22	5.22	6.10	7.12
01	18-hr	1.25	1.45	1.59	1.84	2.09	2.27	2.72	3.39	3.97	4.91	5.73	6.69
01	12-hr	1.16	1.35	1.48	1.71	1.94	2.11	2.51	3.14	3.67	4.54	5.31	6.19
01	6-hr	1.00	1.16	1.27	1.47	1.67	1.82	2.17	2.71	3.16	3.91	4.57	5.34
01	3-hr	0.85	0.99	1.08	1.26	1.43	1.55	1.85	2.31	2.70	3.34	3.90	4.56
01	2-hr	0.77	0.90	0.98	1.13	1.29	1.40	1.68	2.09	2.45	3.03	3.54	4.13
01	1-hr	0.63	0.73	0.80	0.92	1.05	1.14	1.36	1.70	1.98	2.45	2.87	3.35
01	30-min	0.50	0.58	0.63	0.73	0.83	0.90	1.07	1.34	1.56	1.93	2.26	2.63
01	15-min	0.36	0.42	0.45	0.53	0.60	0.65	0.78	0.97	1.14	1.41	1.65	1.92
01	10-min	0.28	0.33	0.36	0.41	0.47	0.51	0.61	0.76	0.89	1.10	1.28	1.50
01	5-min	0.16	0.19	0.20	0.23	0.27	0.29	0.35	0.43	0.51	0.63	0.73	0.85
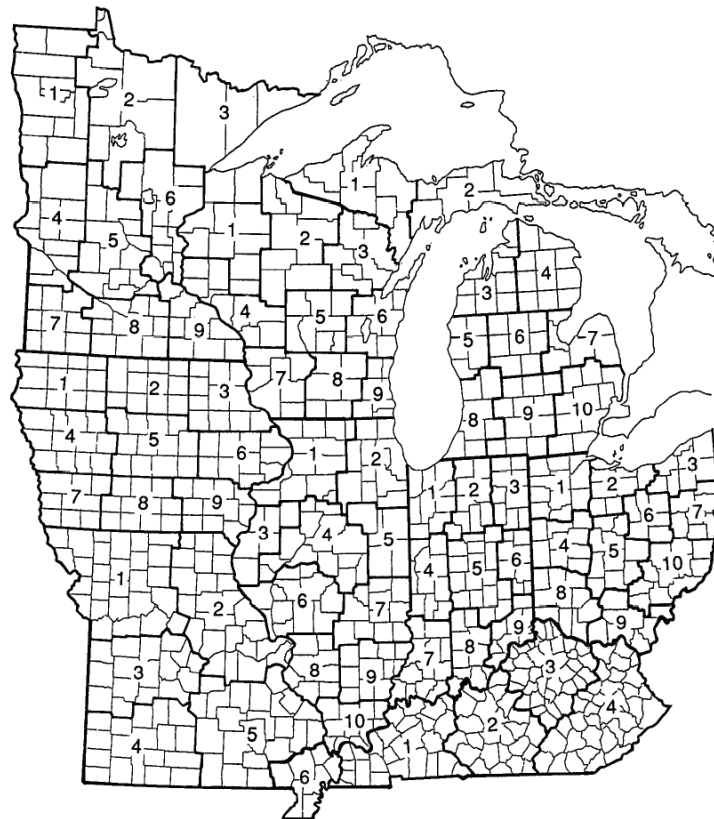
Figure 1. Climatic sections for the Midwest

PLATE 3

Cedar Lake, Indiana

Subwatershed Deliniation Based on 30-meter USGS Hydrographic Corrected DEM
Annual Runoff (cm) Generated by L-Thia v.2.3 ArcView Extension
Frequency Analysis From Daily Rain Gage Data for Lake County, Indiana from 1966-97
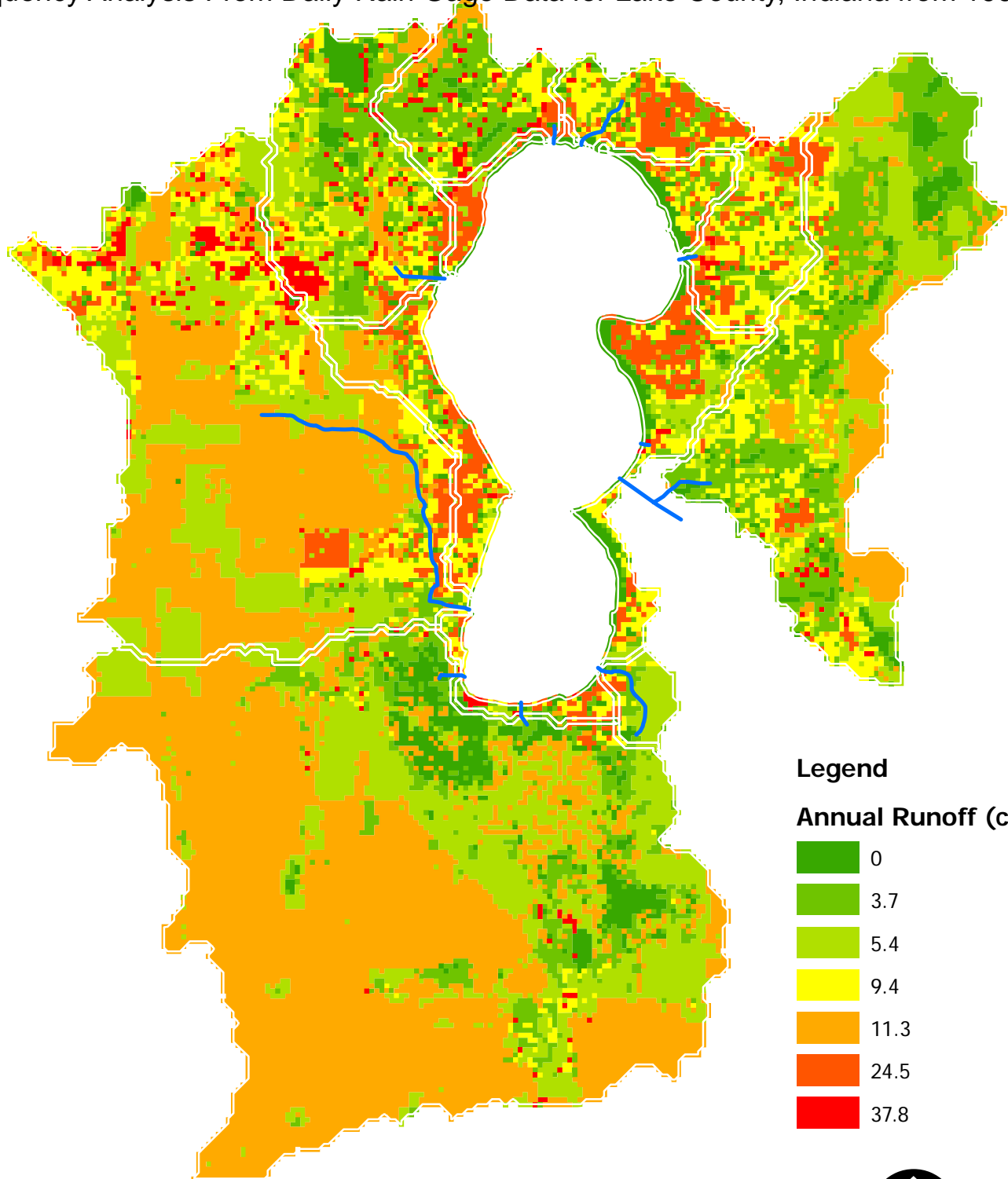
Legend

Annual Runoff (cm)

- 0
- 3.7
- 5.4
- 9.4
- 11.3
- 24.5
- 37.8

0 500 1,000 2,000 3,000 4,000
Feet
1 inch equals 3,000 feet

PLATE 4

DFB

PLATE 5.A

Watershed	Precipitation (inches)	Runoff Depth (cm)	Runoff Volume (m^3)	Suspended Solids (kg)	Dissolved Solids (kg)	BOD (kg)	COD (kg)	Phosphorus (kg)	Dissolved Phosphorus (kg)	Nitrogen (kg)	Kjeldahl Nitrogen (kg)	Nitrate Nitrate (kgasN)	Cadmium (kg)	Chromium (kg)	Copper (kg)	Lead (kg)	Nickel (kg)	Zinc (kg)
Chamber Inlet	0.5	0.1	279	12	38	7.1	14.5	0.16	0.13	0.50	0.41	0.06	0.00	0.00	0.00	0.00	0.00	0.02
Chamber Inlet	1	0.4	1,933	81	289	48.2	96.2	1.10	0.89	3.54	2.86	0.48	0.00	0.00	0.03	0.02	0.02	0.16
Chamber Inlet	2	1.7	8,373	323	1,360	190.9	376.7	4.41	3.54	14.66	11.53	2.24	0.01	0.02	0.12	0.07	0.07	0.61
Chamber Inlet	3	3.4	16,931	624	2,841	368.1	723.6	8.53	6.83	28.90	22.41	4.68	0.01	0.05	0.24	0.14	0.14	1.19
Chamber Inlet	4	5.3	26,550	953	4,534	561.1	1,100.5	13.03	10.40	44.63	34.32	7.45	0.02	0.08	0.37	0.22	0.22	1.81
Chamber Inlet	5	7.4	36,788	1,297	6,354	762.5	1,493.6	17.74	14.13	61.21	46.79	10.44	0.03	0.12	0.51	0.30	0.30	2.46
Chamber Inlet	6	9.5	47,423	1,650	8,254	969.2	1,896.6	22.56	17.96	78.30	59.61	13.55	0.04	0.16	0.66	0.39	0.38	3.13
Chamber Inlet	8	13.9	69,425	2,372	12,208	1,391.5	2,719.8	32.43	25.78	113.44	85.87	20.03	0.06	0.24	0.95	0.56	0.54	4.49
Chamber Inlet	10	18.5	92,011	3,106	16,285	1,820.8	3,556.1	42.47	33.73	149.32	112.60	26.70	0.07	0.32	1.26	0.74	0.71	5.88
Chamber Inlet	annual	13.5	67,007	2,634	10,570	1,566.7	3,114.5	35.89	28.99	118.40	94.02	17.52	0.05	0.18	0.97	0.58	0.62	5.07

Watershed	Precipitation (inches)	Runoff Depth (cm)	Runoff Volume (m^3)	Suspended Solids (kg)	Dissolved Solids (kg)	BOD (kg)	COD (kg)	Phosphorus (kg)	Dissolved Phosphorus (kg)	Nitrogen (kg)	Kjeldahl Nitrogen (kg)	Nitrate Nitrate (kgasN)	Cadmium (kg)	Chromium (kg)	Copper (kg)	Lead (kg)	Nickel (kg)	Zinc (kg)
Condo Inlet	0.5	0.0	284	15	54	6.6	30.4	0.10	0.04	0.41	0.33	0.08	0.00	0.00	0.00	0.00	0.00	0.05
Condo Inlet	1	0.2	1,628	93	522	32.7	126.6	0.83	0.30	3.05	2.04	0.73	0.00	0.01	0.02	0.02	0.01	0.20
Condo Inlet	2	1.2	8,588	374	2,983	121.6	403.3	3.80	1.35	14.96	8.85	4.27	0.01	0.06	0.10	0.07	0.05	0.67
Condo Inlet	3	2.6	19,104	733	6,622	232.5	725.4	7.72	2.73	31.63	17.92	9.58	0.02	0.14	0.21	0.14	0.10	1.23
Condo Inlet	4	4.4	31,586	1,129	10,889	353.9	1,067.6	12.09	4.26	50.75	28.12	15.84	0.03	0.22	0.34	0.22	0.15	1.83
Condo Inlet	5	6.3	45,282	1,545	15,535	481.1	1,420.8	16.72	5.88	71.32	38.96	22.68	0.04	0.32	0.49	0.31	0.20	2.46
Condo Inlet	6	8.3	59,783	1,974	20,429	612.1	1,780.6	21.50	7.56	92.83	50.22	29.89	0.06	0.42	0.64	0.40	0.25	3.11
Condo Inlet	8	12.5	90,322	2,854	30,680	880.4	2,511.8	31.34	11.01	137.57	73.49	45.05	0.08	0.63	0.96	0.60	0.35	4.42
Condo Inlet	10	16.9	122,120	3,751	41,308	1,153.9	3,251.9	41.40	14.54	183.70	97.35	60.78	0.11	0.85	1.30	0.80	0.46	5.76
Condo Inlet	annual	9.3	67,485	3,132	21,914	1,075.3	3,921.4	29.66	10.74	115.79	72.22	31.24	0.06	0.51	0.80	0.59	0.48	6.37

Watershed	Precipitation (inches)	Runoff Depth (cm)	Runoff Volume (m^3)	Suspended Solids (kg)	Dissolved Solids (kg)	BOD (kg)	COD (kg)	Phosphorus (kg)	Dissolved Phosphorus (kg)	Nitrogen (kg)	Kjeldahl Nitrogen (kg)	Nitrate Nitrate (kgasN)	Cadmium (kg)	Chromium (kg)	Copper (kg)	Lead (kg)	Nickel (kg)	Zinc (kg)
Direct Drainage	0.5	0.0	894	38	130	22.5	50.0	0.49	0.39	1.60	1.31	0.22	0.00	0.00	0.01	0.01	0.01	0.08
Direct Drainage	1	0.3	6,400	286	1,306	150.1	312.1	3.75	2.69	12.28	9.33	2.03	0.00	0.02	0.09	0.06	0.06	0.51
Direct Drainage	2	1.5	28,708	1,185	6,650	591.3	1,193.5	15.64	10.63	53.22	38.33	10.20	0.02	0.10	0.38	0.23	0.23	1.98
Direct Drainage	3	3.0	58,672	2,322	14,061	1,139.0	2,276.7	30.68	20.50	106.40	75.04	21.54	0.05	0.23	0.77	0.46	0.44	3.80
Direct Drainage	4	4.7	92,493	3,568	22,520	1,735.0	3,450.6	47.17	31.22	165.46	115.34	34.48	0.08	0.37	1.20	0.71	0.67	5.79
Direct Drainage	5	6.5	128,563	4,875	31,591	2,357.3	4,673.5	64.46	42.42	227.83	157.63	48.36	0.11	0.52	1.65	0.98	0.91	7.86
Direct Drainage	6	8.4	166,069	6,218	41,052	2,995.6	5,926.1	82.23	53.90	292.27	201.14	62.84	0.14	0.69	2.12	1.26	1.16	9.99
Direct Drainage	8	12.3	243,727	8,968	60,691	4,300.1	8,483.3	118.63	77.36	424.84	290.31	92.91	0.20	1.02	3.09	1.83	1.66	14.34
Direct Drainage	10	16.4	323,494	11,768	80,899	5,626.1	11,079.9	155.67	101.20	560.31	381.15	123.86	0.27	1.37	4.09	2.41	2.17	18.77
Direct Drainage	annual	11.5	226,739	9,513	49,519	4,875.4	10,031.6	124.93	87.26	420.80	309.79	76.53	0.18	0.79	3.08	1.88	1.91	16.51

Watershed	Precipitation (inches)	Runoff Depth (cm)	Runoff Volume (m^3)	Suspended Solids (kg)	Dissolved Solids (kg)	BOD (kg)	COD (kg)	Phosphorus (kg)	Dissolved Phosphorus (kg)	Nitrogen (kg)	Kjeldahl Nitrogen (kg)	Nitrate Nitrate (kgasN)	Cadmium (kg)	Chromium (kg)	Copper (kg)	Lead (kg)	Nickel (kg)	Zinc (kg)
Golf Course Inlet	0.5	0.0	17	1	2	0.4	0.8	0.01	0.01	0.03	0.02	0.00	0.00	0.00	0.00	0.00	0.00	0.00
Golf Course Inlet	1	0.1	208	6	39	3.5	6.7	0.08	0.06	0.31	0.22	0.06	0.00	0.00	0.01	0.00	0.00	0.01
Golf Course Inlet	2	1.0	1,835	27	398	15.8	29.5	0.37	0.29	2.01	1.16	0.65	0.00	0.01	0.02	0.01	0.01	0.06
Golf Course Inlet	3	2.4	4,486	55	998	32.1	58.9	0.75	0.57	4.59	2.49	1.63	0.00	0.03	0.05	0.03	0.01	0.12
Golf Course Inlet	4	4.0	7,706	87	1,732	50.2	91.5	1.18	0.89	7.65	4.02	2.83	0.01	0.05	0.09	0.05	0.02	0.18
Golf Course Inlet	5	5.9	11,276	120	2,549	69.4	125.8	1.63	1.22	11.00	5.66	4.16	0.01	0.07	0.12	0.07	0.03	0.26
Golf Course Inlet	6	7.9	15,076	155	3,422	89.2	161.1	2.09	1.56	14.54	7.38	5.59	0.01	0.10	0.17	0.09	0.03	0.33
Golf Course Inlet	8	12.1	23,116	226	5,270	130.1	233.8	3.05	2.27	21.97	10.96	8.60	0.02	0.15	0.25	0.13	0.05	0.49
Golf Course Inlet	10	16.5	31,513	299	7,204	171.9	307.9	4.03	2.99	29.68	14.65	11.76	0.03	0.20	0.34	0.18	0.06	0.65
Golf Course Inlet	annual	6.4	12,241	209	2,583	122.6	230.0	2.86	2.23	14.15	8.64	4.23	0.01	0.07	0.14	0.08	0.05	0.42

Watershed	Precipitation (inches)	Runoff Depth (cm)	Runoff Volume (m^3)	Suspended Solids (kg)	Dissolved Solids (kg)	BOD (kg)	COD (kg)	Phosphorus (kg)	Dissolved Phosphorus (kg)	Nitrogen (kg)	Kjeldahl Nitrogen (kg)	Nitrate Nitrate (kgasN)	Cadmium (kg)	Chromium (kg)	Copper (kg)	Lead (kg)	Nickel (kg)	Zinc (kg)
North Point Marina Inlet	0.5	0.0	535	28	100	12.5	52.8	0.21	0.11	0.80	0.64	0.14	0.00	0.00	0.01	0.00	0.01	0.08
North Point Marina Inlet	1	0.2	3,471	186	1,094	68.7	234.5	1.83	0.78	6.60	4.41	1.54	0.00	0.02	0.04	0.03	0.03	0.38
North Point Marina Inlet	2	1.2	18,245	781	6,231	266.1	781.7	8.48	3.43	32.53	19.53	8.97	0.02	0.12	0.21	0.14	0.11	1.31
North Point Marina Inlet	3	2.7	39,897	1,546	13,673	515.0	1,431.0	17.24	6.90	68.29	39.57	19.84	0.04	0.26	0.44	0.29	0.21	2.44
North Point Marina Inlet	4	4.4	65,249	2,392	22,319	788.2	2,126.4	27.01	10.75	109.05	62.03	32.52	0.06	0.43	0.72	0.45	0.32	3.67
North Point Marina Inlet	5	6.2	92,845	3,283	31,681	1,075.1	2,846.9	37.34	14.81	152.70	85.86	46.29	0.09	0.61	1.01	0.63	0.43	4.95
North Point Marina Inlet	6	8.1	121,908	4,201	41,504	1,370.3	3,582.7	48.03	19.01	198.20	110.57	60.75	0.11	0.80	1.33	0.82	0.54	6.27
North Point Marina Inlet	8	12.2	182,795	6,087	62,006	1,975.8	5,081.3	70.01	27.65	292.58	161.54	90.99	0.17	1.20	1.98	1.21	0.78	8.95
North Point Marina Inlet	10	16.4	245,923	8,010	83,194	2,592.8	6,600.4	92.47	36.47	389.64	213.75	122.28	0.23	1.62	2.65	1.61	1.02	11.69
North Point Marina Inlet	annual	9.4	140,766	6,382	45,241	2,280.6	7,358.1	65.38	27.14	248.53	156.25	64.99	0.13	0.96	1.68	1.17	0.98	12.06

Watershed	Precipitation (inches)	Runoff Depth (cm)	Runoff Volume (m^3)	Suspended Solids (kg)	Dissolved Solids (kg)	BOD (kg)	COD (kg)	Phosphorus (kg)	Dissolved Phosphorus (kg)	Nitrogen (kg)	Kjeldahl Nitrogen (kg)	Nitrate Nitrate (kgasN)	Cadmium (kg)	Chromium (kg)	Copper (kg)	Lead (kg)	Nickel (kg)	Zinc (kg)
Old Bank Building Inlet	0.5	0.0	257	11	38	6.4	15.7	0.14	0.11	0.45	0.37	0.06	0.00	0.00	0.00	0.00	0.00	0.03
Old Bank Building Inlet	1	0.3	2,027	87	357	48.3	105.2	1.13	0.85	3.70	2.91	0.57	0.00	0.01	0.03	0.02	0.02	0.17
Old Bank Building Inlet	2	1.5	9,942	380	1,915	207.9	432.3	4.99	3.72	17.17	12.89	3.05	0.01	0.04	0.14	0.08	0.08	0.71
Old Bank Building Inlet	3	3.2	20,936	757	4,141	413.2	847.8	10.02	7.43	35.15	25.94	6.59	0.02	0.08	0.28	0.17	0.16	1.40
Old Bank Building Inlet	4	5.2	33,514	1,175	6,715	640.2	1,304.6	15.58	11.53	55.36	40.45	10.69	0.03	0.13	0.45	0.27	0.25	2.16
Old Bank Building Inlet	5	7.2	47,025	1,616	9,496	879.1	1,784.2	21.45	15.85	76.83	55.78	15.12	0.04	0.18	0.63	0.37	0.34	2.97
Old Bank Building Inlet	6	9.4	61,135	2,070	12,410	1,125.4	2,277.7	27.50	20.31	99.11	71.63	19.77	0.05	0.24	0.81	0.48	0.44	3.80
Old Bank Building Inlet	8	13.9	90,464	3,002	18,486	1,631.1	3,289.7	39.94	29.45	145.11	104.23	29.45	0.08	0.36	1.19	0.70	0.64	5.49
Old Bank Building Inlet	10	18.6	120,681	3,953	24,761	2,146.8	4,320.6	52.62	38.78	192.25	137.54	39.45	0.10	0.49	1.58	0.93	0.84	7.23
Old Bank Building Inlet	annual	11.7	76,047	2,996	14,162	1,649.1	3,525.2	38.92	29.17	132.44	100.94	22.58	0.06	0.27	1.06	0.65	0.65	5.75

Watershed	Precipitation (inches)	Runoff Depth (cm)	Runoff Volume (m^3)	Suspended Solids (kg)	Dissolved Solids (kg)	BOD (kg)	COD (kg)	Phosphorus (kg)	Dissolved Phosphorus (kg)	Nitrogen (kg)	Kjeldahl Nitrogen (kg)	Nitrate Nitrate (kgasN)	Cadmium (kg)	Chromium (kg)	Copper (kg)	Lead (kg)	Nickel (kg)	Zinc (kg)
Sleepy Hollow Ditch	0.5	0.0	1,019	57	272	22.4	87.8	0.49	0.21	1.80	1.29	0.38	0.00	0.00	0.01	0.01	0.01	0.14
Sleepy Hollow Ditch	1	0.3	12,667	950	9,044	155.0	414.9	10.93	1.67	37.84	18.25	12.09	0.01	0.10	0.10	0.07	0.06	0.76
Sleepy Hollow Ditch	2	1.5	71,705	4,929	51,999	666.7	1,451.2	58.60	7.54	207.69	94.36	69.93	0.07	0.57	0.50	0.34	0.22	2.97
Sleepy Hollow Ditch	3	3.2	155,566	10,286	111,584	1,330.2	2,706.1	123.17	15.25	440.76	197.37	150.47	0.15	1.23	1.08	0.70	0.42	5.77
Sleepy Hollow Ditch	4	5.2	252,098	16,303	179,325	2,066.1	4,061.3	195.82	23.84	704.64	313.40	242.20	0.24	2.00	1.75	1.13	0.64	8.86
Sleepy Hollow Ditch	5	7.3	356,018	22,685	251,685	2,842.5	5,471.8	272.98	32.92	985.89	436.74	340.29	0.34	2.81	2.47	1.58	0.87	12.09
Sleepy Hollow Ditch	6	9.5	464,633	29,293	326,918	3,643.7	6,915.9	352.91	42.30	1,277.92	564.60	442.34	0.44	3.67	3.23	2.05	1.11	15.42
Sleepy Hollow Ditch	8	14.1	690,467	42,907	482,536	5,290.7	9,863.8	517.65	61.61	1,881.24	828.38	653.56	0.66	5.45	4.81	3.03	1.60	22.26
Sleepy Hollow Ditch	10	18.9	923,107	56,826	642,156	6,972.0	12,857.4	686.16	81.33	2,499.50	1,098.38	870.34	0.88	7.28	6.44	4.04	2.10	29.24
Sleepy Hollow Ditch	annual	10.5	515,605	35,590	360,602	5,362.9	13,239.2	415.58	58.77	1,469.14	686.62	484.91	0.49	4.10	3.83	2.66	1.88	25.48

Watershed	Precipitation (inches)	Runoff Depth (cm)	Runoff Volume (m^3)	Suspended Solids (kg)	Dissolved Solids (kg)	BOD (kg)	COD (kg)	Phosphorus (kg)	Dissolved Phosphorus (kg)	Nitrogen (kg)	Kjeldahl Nitrogen (kg)	Nitrate Nitrate (kgasN)	Cadmium (kg)	Chromium (kg)	Copper (kg)	Lead (kg)	Nickel (kg)	Zinc (kg)
Unnamed Inlet/Pickerel Creek	0.5	0.0	360	31	293	4.2	14.7	0.34	0.02	1.16	0.54	0.38	0.00	0.00	0.00	0.00	0.00	0.03
Unnamed Inlet/Pickerel Creek	1	0.2	17,111	1,658	18,976	78.9	64.8	20.01	0.20	68.64	26.93	24.91	0.02	0.17	0.05	0.04	0.01	0.35
Unnamed Inlet/Pickerel Creek	2	1.3	110,456	9,361	111,148	423.2	216.5	113.39	0.90	398.29	154.32	147.01	0.11	1.04	0.39	0.27	0.03	1.85
Unnamed Inlet/Pickerel Creek	3	2.9	246,019	19,880	239,055	892.1	397.1	240.94	1.83	854.10	329.76	317.08	0.25	2.29	0.93	0.62	0.06	3.90
Unnamed Inlet/Pickerel Creek	4	4.8	403,219	31,748	384,421	1,421.4	590.9	384.89	2.88	1,371.33	528.49	510.67	0.40	3.74	1.59	1.04	0.09	6.23
Unnamed Inlet/Pickerel Creek	5	6.8	573,059	44,367	539,643	1,984.6	791.9	537.95	3.98	1,923.13	740.28	717.60	0.57	5.29	2.31	1.50	0.12	8.71
Unnamed Inlet/Pickerel Creek	6	8.9	750,946	57,446	700,981	2,568.7	997.3	696.60	5.12	2,496.33	960.14	932.81	0.75	6.91	3.08	1.98	0.15	11.29
Unnamed Inlet/Pickerel Creek	8	13.2	1,121,478	84,421	1,034,608	3,774.2	1,415.9	1,023.82	7.48	3,680.99	1,414.26	1,378.12	1.12	10.30	4.71	2.99	0.21	16.62
Unnamed Inlet/Pickerel Creek	10	17.7	1,503,704	112,022	1,376,722	5,008.6	1,840.4	1,358.63	9.89	4,895.22	1,879.49	1,834.99	1.50	13.78	6.40	4.05	0.28	22.09
Unnamed Inlet/Pickerel Creek	annual	8.8	748,121	64,617	761,051	3,020.7	2,040.1	781.16	7.00	2,733.95	1,063.65	1,005.47	0.75	7.06	2.57	1.82	0.27	13.46

Watershed	Precipitation (inches)	Runoff Depth (cm)	Runoff Volume (m^3)	Suspended Solids (kg)	Dissolved Solids (kg)	BOD (kg)	COD (kg)	Phosphorus (kg)	Dissolved Phosphorus (kg)	Nitrogen (kg)	Kjeldahl Nitrogen (kg)	Nitrate Nitrate (kgasN)	Cadmium (kg)	Chromium (kg)	Copper (kg)	Lead (kg)	Nickel (kg)	Zinc (kg)
Hog Pen Ditch	0.5	0.0	209	11	57	4.7	13.8	0.12	0.06	0.41	0.29	0.08	0.00	0.00	0.00	0.00	0.00	0.02
Hog Pen Ditch	1	0.1	4,006	253	2,397	51.9	105.5	3.09	0.77	10.73	5.48	3.27	0.00	0.03	0.03	0.02	0.02	0.20
Hog Pen Ditch	2	1.0	31,890	1,379	15,966	267.5	484.0	17.07	3.98	66.23	31.51	22.42	0.03	0.22	0.28	0.17	0.09	1.01
Hog Pen Ditch	3	2.4	76,424	2,918	36,090	562.2	985.1	36.18	8.35	146.46	68.22	51.17	0.07	0.53	0.69	0.39	0.19	2.13
Hog Pen Ditch	4	4.0	130,124	4,655	59,644	895.7	1,545.6	57.78	13.29	239.38	110.31	85.01	0.12	0.91	1.18	0.66	0.29	3.41
Hog Pen Ditch	5	5.9	189,444	6,504	85,231	1,251.3	2,139.4	80.77	18.55	339.75	155.52	121.87	0.18	1.33	1.72	0.96	0.41	4.78
Hog Pen Ditch	6	7.9	252,470	8,421	112,129	1,620.7	2,753.9	104.61	24.00	444.86	202.69	160.69	0.24	1.78	2.30	1.28	0.53	6.20
Hog Pen Ditch	8	12.0	385,538	12,379	168,353	2,384.3	4,019.9	153.84	35.26	663.83	300.60	241.98	0.37	2.72	3.52	1.95	0.77	9.16
Hog Pen Ditch	10	16.3	524,327	16,431	226,524	3,167.4	5,314.4	204.23	46.80	889.73	401.34	326.21	0.50	3.70	4.80	2.66	1.02	12.21
Hog Pen Ditch	annual	6.7	214,244	9,737	108,068	1,967.4	3,776.1	119.69	29.02	456.70	221.68	151.25	0.20	1.47	1.93	1.14	0.68	7.57

PLATE 5.B

Attachment 4:

Cedar Lake Sediment Erosion Study: Field

Activities September 2005

FINAL REPORT

Cedar Lake Sediment Erosion Study: Field Activities

for

US Army Corps
of Engineers ®
Chicago District

by

Sandia
National
Laboratories

Jesse Roberts

Dirk O'Daniel

Randy Buhalts

September 28, 2005

Table of Contents

List of Figures

List of Tables

1.0 Introduction

In this study, the erosion rates of sediments from Cedar Lake have been determined as a function of depth below the sediment water interface and shear stress by means of the Adjustable Shear Stress Erosion and Transport (ASSET) flume previously developed and tested by Sandia National Laboratories (Roberts, 2004). The device is similar to the SEDflume (McNeil et al, 1996; Jepsen et al, 1997a; Roberts et al, 1998) though it has the added capability to determine the transport modes (i.e. bedload or suspended load) of the eroded sediments. Sixteen core samples were retrieved from different locations around Cedar Lake (figure 1) for erosion analysis.

The erosion properties of the sediments in Cedar Lake are of interest because the Untied States Army Corps of Engineers (USACE), Chicago District is performing a study to evaluate the feasibility of implementing aquatic ecosystem restoration measures within Cedar Lake located in Northwestern Indiana. This glacial lake experiences periodic resuspension of bottom sediments due to the hydrodynamic bottom stresses created by wind and boat activity. An associated release of phosphorus from the resuspension of bottom sediments is thought to be the main contributor to water quality degradation in the lake (Indiana SPEA, 1984). The data presented here will be used to model sediment transport and water quality within the lake in order to address the effectiveness of potential ecosystem restoration measures.

Relatively undisturbed cores of sediments were obtained, and measurements of the erosion rates as a function of depth and applied shear stress were then determined using the ASSET flume. For all cores, the sediment bulk properties of bulk density or water content and mean particle size were determined as a function of depth below the sediment water interface. Sandia has also determined the particle size of 6 suspended load samples collected by the Army Corps during routine water quality monitoring as well as 34 ponar samples, and 8 grab samples

collected by the Army Corps during this field trip. The ponar and grab sample locations are

shown in figures 2 and 3 respectively.
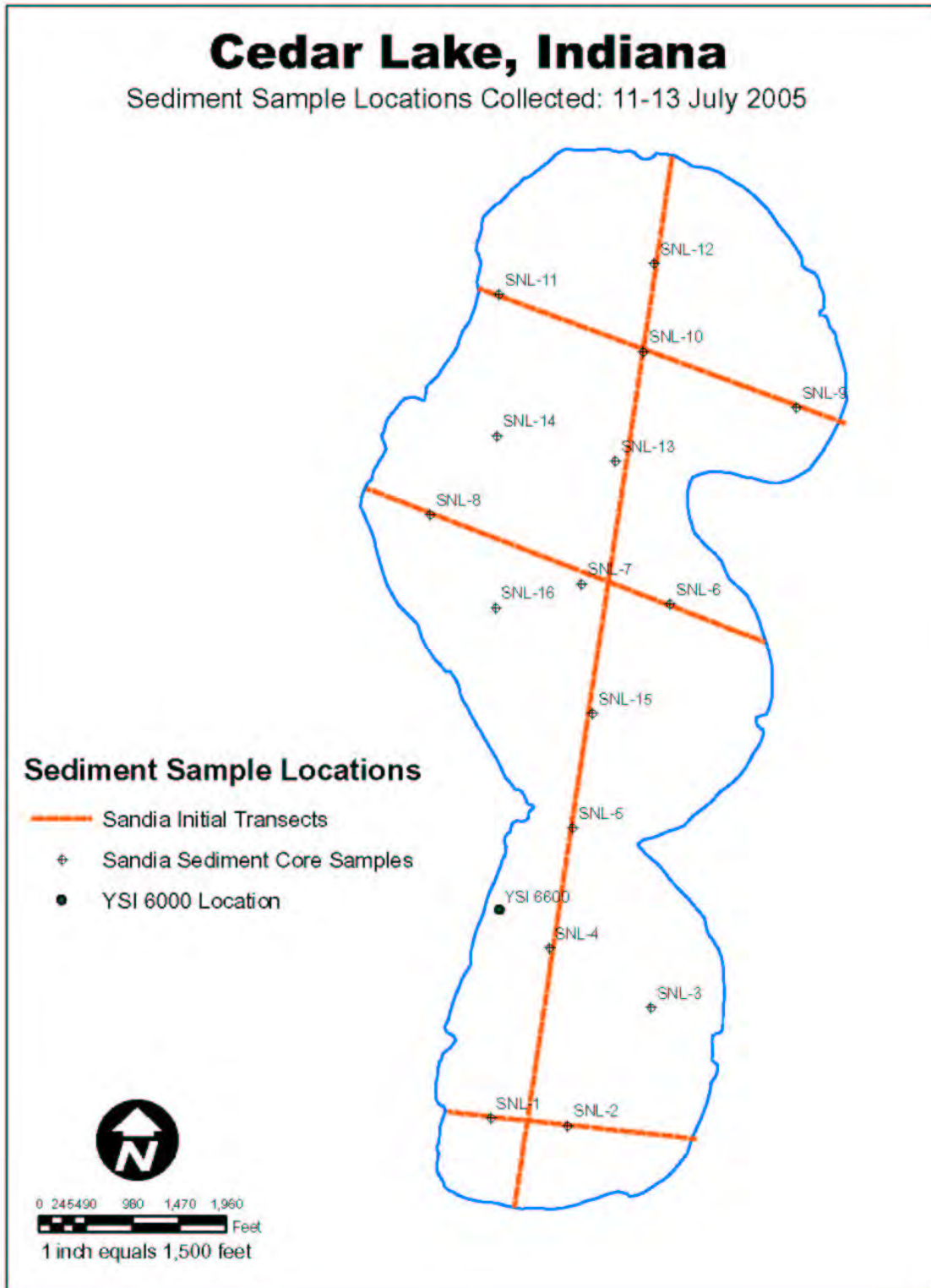
Figure 1. Sediment erosion core sampling locations around Cedar Lake.

5
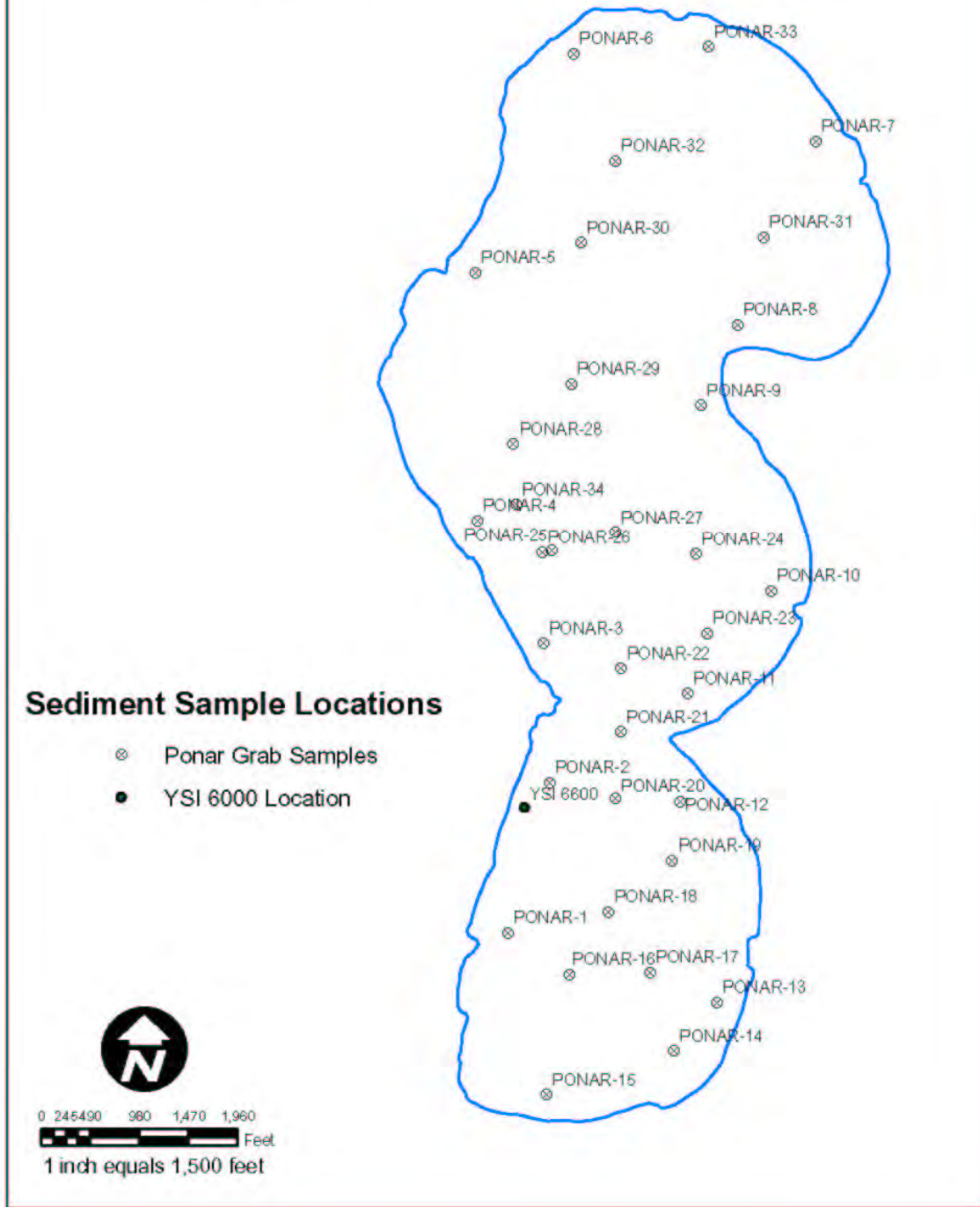
Figure 2. Ponar sampling locations a**round Cedar Lake.**
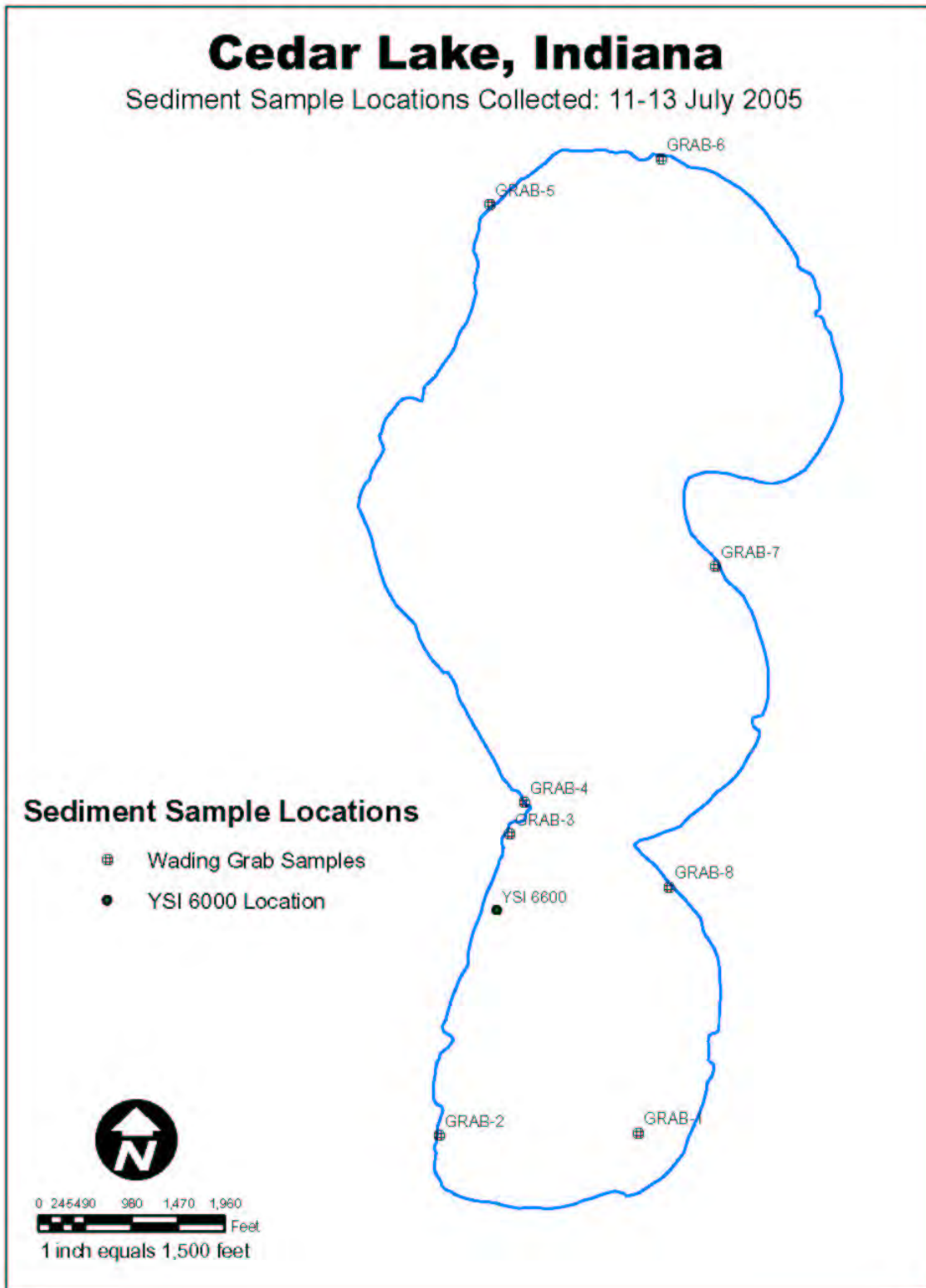
Figure 3. Wading grab sampling locations around Cedar Lake.

2.0 Experimental Procedures

2.1 Description of the ASSET Flume

The erosion test section of the ASSET Flume is identical (except for a taller channel) in design and operation to the SEDflume. The peer-reviewed literature relating to the design and operation of the SEDflume is extensive (e.g., Jepsen et al., 1997a; Roberts et al., 1998; Jepsen et al., 1999b; Roberts and Jepsen, 2001). In particular, the interested reader should review the work of McNeil et al. (1996) who introduced the SEDflume and discussed at great length its design, operation, and ability to measure sediment erosion rates with depth.

The mobile ASSET Flume consists of eight primary components. There is a 120 gallon reservoir, a 150 gpm centrifugal pump, a motor controlled screw jack, an erosion channel including erosion test section, a transport channel including bedload traps, a three way valve, a paddlewheel flow meter, and connective plumbing. Water is pumped from the reservoir through the three-way valve, which either sends water directly back to the reservoir or through the flow meter to the erosion and transport channels (and then back to the reservoir). For the experiments at Cedar Lake, the lake itself acted as an infinite reservoir by use of a sump pump placed below the lake surface. A manually controlled screw jack is used to push the sediments through the core tube to keep the sediment surface flush with the channel floor such that, as closely as possible, the sediments are exposed only to an applied shear stress and no normal stresses (this procedure will be discussed in detail later).

The ASSET Flume's enclosed (internal flow) erosion and transport channels are 4 cm tall, 10.5 cm wide (Figure 4). Several meters of inlet pipe are connected to the erosion channel with 20 cm circular to rectangular flow converter. The erosion test section is preceded by 180 cm of enclosed rectangular channel to ensure fully developed turbulent flow over the sediment core. Note that the rectangular sediment core tube is 15 cm long, but only 10 cm wide. This helps to

reduce wall effects because the channel is 10.5 cm wide. The transport channel may include

three sediment traps downstream from the sediment core. The first trap is located 1 m from the

center of the erosion test section (mobile version used for these tests has only one trap), and the

center of each successive trap (not shown in Figure 4) is 1 m from the center of the preceding

one. Based on the theoretical definition of bedload in combination with fluid velocities and

particle/aggregate settling speeds, a bedload particle/aggregate should contact the flume floor at

least once every 15 cm of downstream travel (Dyer, 1986). Consequently, the traps are 15 cm

long and span the width of the channel (10.5 cm). Capture basins that are 10 cm deep and have a

2 L volume are located below the traps, each with a baffle system that reduces recirculation and

minimizes the resuspension of trapped sediments. As the sediment core is eroded upstream, some

of the material is suspended and some is transported as bedload. All sediment that falls into the

traps is considered bedload.
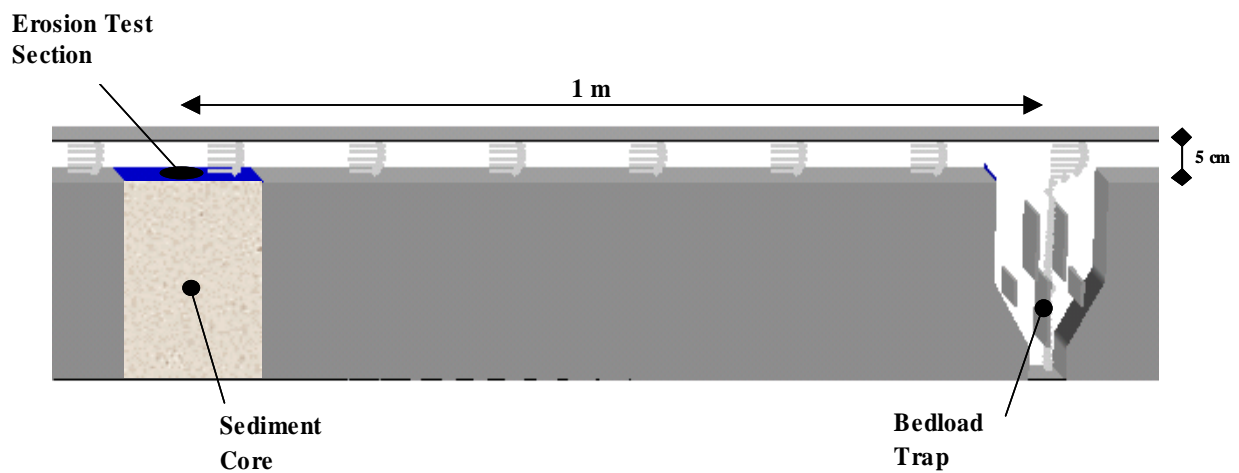
Figure 4. Schematic of the ASSET flume.

2.2 Hydrodynamics

The hydrodynamics within the flow channel of the ASSET Flume are equivalent to those of SEDflume (McNeil et al., 1996); however, the increase in duct height necessitated a change to the system inlet. To achieve fully developed turbulent flow over the sediment core, the flume inlet was lengthened to 180 cm and preceded by a 20 cm circular-to-rectangular flow converter and several meters of inlet pipe.

Turbulent flow through pipes has been studied extensively, and empirical functions have been developed that relate the mean flow rate to the boundary shear stress. In general, flow in circular cross-section pipes has been investigated. However, the relations developed for flow through circular pipes can be extended to non-circular cross-sections by means of a shape factor. An implicit formula relating the boundary shear stress to the mean flow in a pipe of arbitrary cross-section can be obtained from Prandtl's Universal Law of Friction (Schlichting, 1979). For a pipe with a smooth surface, this formula is

$$\frac{1}{\sqrt{\lambda}} = 2.0 \log\left[\frac{UD\sqrt{\lambda}}{\nu}\right] - 0.8 \qquad (2.1)$$

where U is the mean flow speed, ν is the kinematic viscosity, λ is the friction factor, and D is the hydraulic diameter. For a duct with a rectangular cross-section the hydraulic diameter is

$$D = 2hw/(h + w) \qquad (2.2)$$

where w is the duct width and h is the duct height. The friction factor is defined as

$$\lambda = \frac{8\tau}{\rho U^2} \qquad (2.3)$$

where ρ is the density of water and τ is the wall shear stress. Substituting Eqs. (2.2) and (2.3) into Eq. (2.1) yields the boundary shear stress as an implicit function of the mean flow speed. The mean flow speed and hence the boundary shear stress are controlled by the pump speed.

For flow in a circular pipe, turbulent flow theory suggests that the transition from laminar to fully turbulent flow occurs within 25 to 40 diameters from the entrance to the pipe. Because the hydraulic diameter of the duct is 6.8 cm, this indicates a necessary entry length between 170 and 270 cm, which is supplied by the inlet piping, converter, and ducting. Furthermore, for shear stresses in the range of 0.1 to 10 N/m^2, the Reynolds numbers, UD/v, are on the order of 10^4 to 10^5 implying that turbulent flow exists in all experiments performed for this study. These arguments along with direct observations indicate that the flow is fully turbulent in the test section.

2.3 Core Collection and Preparation

Sediment cores tested in the ASSET flume were relatively undisturbed cores taken from 16 locations around Cedar Lake (Figure 1). In-situ coring was done in the following manner aboard a U.S. Army Corps sampling vessel. Thin-walled polycarbonate circular core tubes ~10 cm in diameter are inserted into a PVC sleeve. Setscrews hold the polycarbonate core tube in place. Extension poles made of ~5 cm diameter PVC pipe attach to the PVC sleeve. The extension poles are approximately 150 cm long and screw together. The number of extension poles used depends on the depth of water. An inflatable rubber plug is inserted within the polycarbonate sediment core tube that is attached to an air pump with standard air hose.

The assembled coring sleeve is lowered to the sediment bed from the deck of the sampling boat. Persons collecting the core then apply pressure to the top of the extension poles, and the core sleeve, due to its weight and the applied pressure, penetrates into the sediment bed. The coring sleeve is then pushed into the sediment bed; the distance of penetration will vary due to the characteristics of the sediment (i.e., further penetration will occur in a softer sediment than in a more compact sediment). During the pushing process the inflatable plug is held at the top of

the coring tube and is deflated, allowing water to flow around it. When the core has reached

maximum penetration the rubber tube is inflated, creating a seal. The coring sleeve is then

brought back up through the water column. Prior to breaking the air/water interface a plug, later

to act as a piston, and bottom are placed in the bottom of the sediment core to prevent sediment

release from the bottom of the core. The entire assembly is then lifted onto the boat deck, the

rubber tube is deflated, and the core sleeve is removed. The outside of the sediment core is dried

and duct tape is applied to assist with the bottom seal. Throughout this process, sediment cores

are not tilted more than 30 degrees so sediment strata and density profiles are not disturbed. This

results in a sediment core that is obtained relatively undisturbed from its natural surroundings.

Sediment cores varying in length from 16 to 35 cm were obtained by this method.

2.4 Measurements of Sediment Erosion Rates

The procedure for measuring the erosion rates of the sediments as a function of shear

stress and depth was as follows. The sediment cores were obtained as described above and then

moved upward into the test section until the sediment surface was even with the bottom of the

test section. A measurement was made of the depth to the bottom of the sediment in the core.

The flume was then run at a specific flow rate corresponding to a particular shear stress.

Sediment erosion rates were calculated by measuring the core length, taking the difference

between successive measurements, and dividing by the measured time interval.

In order to measure erosion rates at several different shear stresses using only one core,

the following procedure was generally used. Starting at a low shear stress, the flume was run

sequentially at higher shear stresses with each succeeding shear stress being twice the previous

one. Generally about three shear stresses were run sequentially. Each shear stress was run until

at least 2 to 3 mm but no more than 2 cm were eroded. The time interval was recorded for each

run with a stopwatch. The flow was then increased to the next shear stress, and so on until the highest shear stress was run. This cycle was repeated until all of the sediment had eroded from the core. If after three cycles a particular shear stress showed a rate of erosion less than 10^{-4} cm/s, it was dropped from the cycle; if after many cycles the erosion rates decreased significantly, a higher shear stress was included in the cycle.

2.5 Measurements of Critical Shear Stress for Erosion

A critical shear stress can be quantitatively defined as the shear stress at which a very small, but accurately measurable, rate of erosion occurs. In the present study, this rate of erosion was chosen to be 10^{-4} cm/s; this represents 1 mm of erosion in approximately 15 minutes. Since it would be difficult to measure all critical shear stresses at exactly 10^{-4} cm/s, erosion rates are generally measured above and below 10^{-4} cm/s at shear stresses that differ by a factor of two. The critical shear stress can then be linearly interpolated to an erosion rate of 10^{-4} cm/s. This gives results with 20% accuracy for the critical shear stress.

2.6 Measurements of Sediment Bulk Properties

In an attempt to assess the parameters that affect sediment erosion, bulk properties including the bulk density or water content, mean particle size as well as particle size distribution of the sediments were determined as a function of depth for the field cores. Stratigraphy of the sediment is destroyed as the sediments are eroded in the ASSET flume, so samples were extracted between the erosion tests at intervals of approximately 3-6 cm for all sediment cores.

In order to determine the bulk density of the sediments at a particular depth, the extracted sediment samples are placed into a watertight container and then weighed (wet weight). They were then dried in the oven at approximately 75°C for 2 days and weighed again (dry weight). The water content W is then given by

$$W = \left(\frac{m_w - m_d}{m_w} \right) \qquad (2.4)$$

where m_w and m_d are the wet and dry weights respectively. A volume of sediment, V, consists of both solid particles and water, and can be written as

$$V = V_s + V_w \qquad (2.5)$$

where V_s is the volume of solid particles and V_w is the volume of water. If the sediment particles and water have densities ρ_s and ρ_w respectively, the water content of the sediment can be written as

$$W = \frac{\rho_w V_w}{\rho V} \qquad (2.6)$$

where ρ is the bulk density of the sediments. A mass balance of the volume of sediment gives

$$\rho V = \rho_s V_s + \rho_w V_w \qquad (2.7)$$

By combining Eqs. (2.5), (2.6), and (2.7), an explicit expression can be determined for the bulk density of the sediment, ρ, as a function of the water content, W, and the densities of the sediment particles and water. This equation is

$$\rho = \frac{\rho_s \rho_w}{\rho_w + (\rho_s - \rho_w)W} \qquad (2.8)$$

For the purpose of these calculations, it has been assumed that $\rho_s = 2.6$ gm/cm^3 and $\rho_w = 1.0$ gm/cm^3.

Mean particle size and particle size distributions were determined by use of a Malvern Mastersizer S particle sizing package that can measure particle diameters between 0.05 and 900 μm. All sediment samples tested had grains smaller than 900 μm. When using the Malvern particle sizer, approximately 5 to 10 grams of sediment was placed in a beaker containing about 500 mL of water and mixed by means of a magnetic stir bar/plate combination. Approximately 1 mL of this solution was then inserted into the sizers sampling system and further disaggregated

14

as it is re-circulated through the sampling system by means of a centrifugal pump. The sample was allowed to disaggregate for five minutes on the stir plate and an additional five minutes in the recirculating pump sampling system before analysis by the sizer. To ensure complete dissagregation and sample uniformity the sediment samples were analyzed multiple times and repeated in triplicate. From these measurements, the distribution of grain sizes and mean grain sizes as a function of depth were obtained.

3.0 Field Results

Sediment erosion and bulk properties were measured for sixteen sites located at throughout Cedar Lake. The sixteen sites are identified in the order they were collected as SNL-1 through SNL-16. Along with the 16 cores collected for erosion and bulk property analysis, the Army Corps collected 42 surface sediment samples using either a Ponar dropped from the boat or manual grab techniques while standing in shallow water. The sites are identified, as P1-P34 and G1-G8. The surface water samples are identified by date and location of collection as JUN-NB, JUN-MB, JUN-SB, JUL-NB, JUL-MB, JUL-SB representing collections in June and July of 2005 in the north, middle and south basins respectively.   Erosion rates (cm/s) were measured with depth for shear stresses from 0.1 to 4.0 Pa. Sediment core lengths ranged from 16 to 35 cm and were limited by the collection teams ability to push the cores into the sediment bed without greatly disturbing the sediment. All cores were eroded in the ASSET Flume within 72 hours of obtaining them. The measured bulk properties were water content or bulk density, mean particle size, and particle size distribution. Each core will be described with respect to the erosion rates and bulk properties.

3.1 Sediments samples SNL-1 through SNL-16

The erosion core sample from site SNL-1 was 20.5 cm in length and had the largest mean particle size and largest value and range of bulk density than any of the other collected cores. The surface of the sample contained organic debris and what appeared to be algae or fine-grained particles, the combination of which was more difficult to erode than the layer directly underneath. Hence, the sediment became easier to erode from the surface to a depth of ~4 cm and eroded particle-by-particle (Figures 5a). Between 4-10 cm the core became harder to erode and transitioned from particle-by-particle erosion to small aggregates that were approximately 1-2 mm in diameter, indicating an increase in fine-grained sediment content. Between 10-15 cm

16

the core became easier to erode, nearly equivalent to the layer at 4 cm, and transitioned back to particle-by-particle erosion. The critical shear stress (Figure 5b) varied throughout the depth of the core from ~0.5 Pa near the surface, ~0.25 Pa at ~3-4 cm, back to ~0.5 Pa at 5 cm, then to ~0.6 Pa until the bottom when it reduces to ~0.3 Pa.
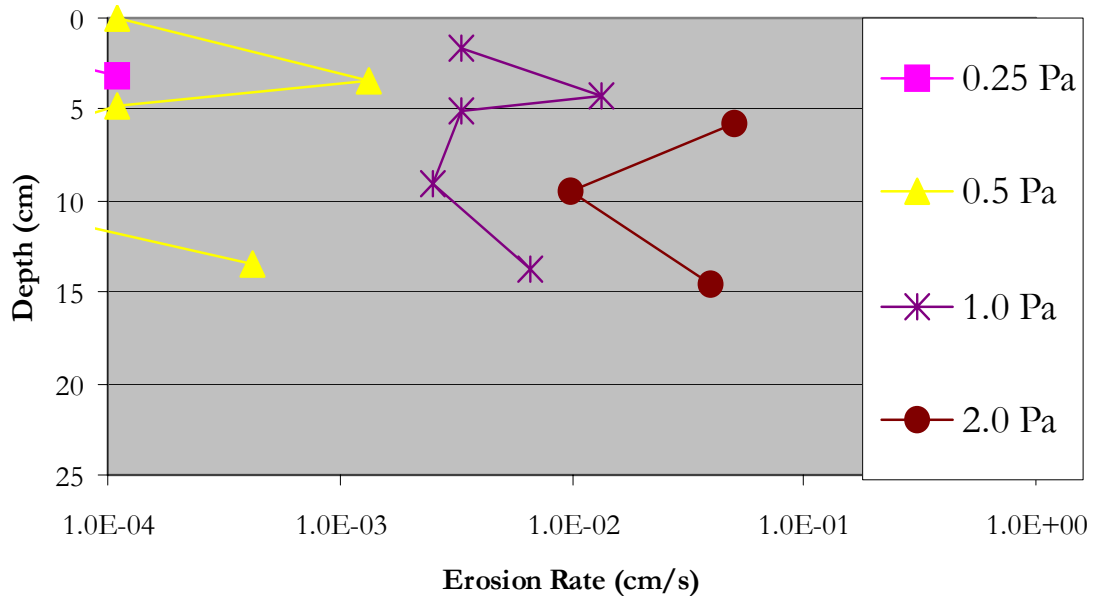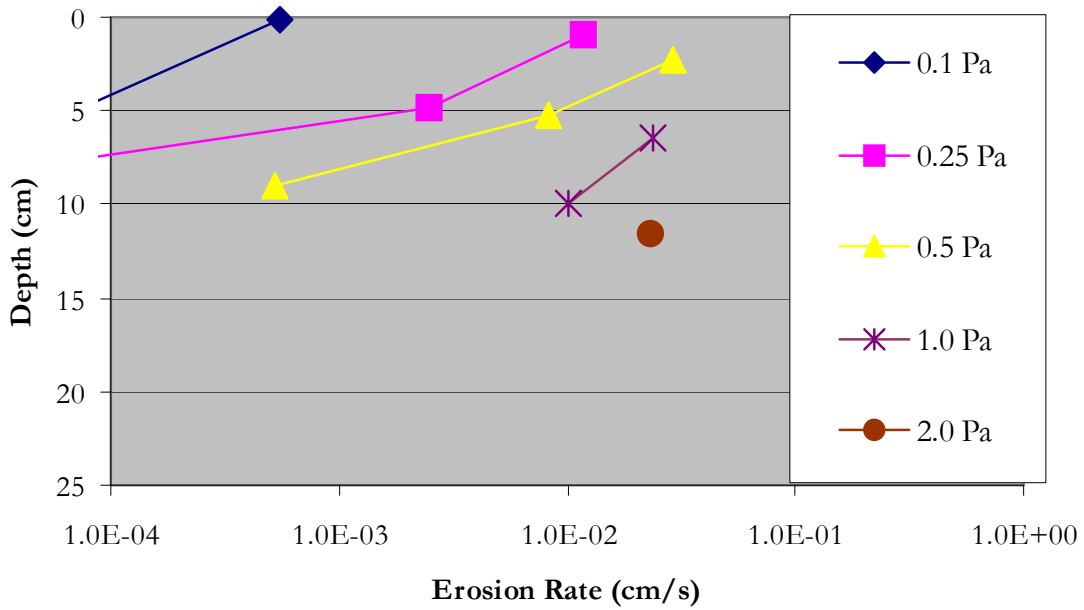

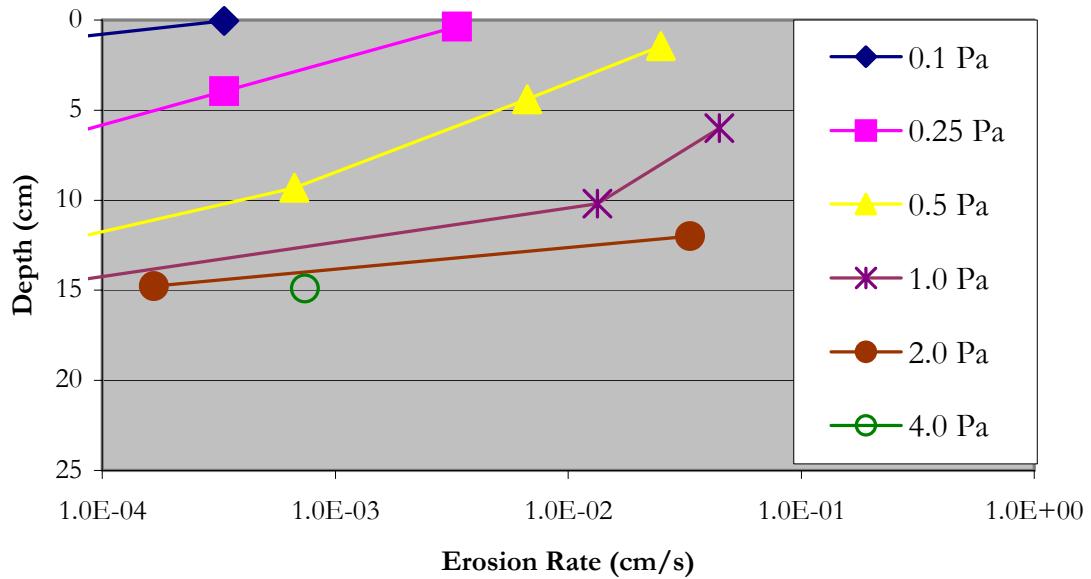**Figure 5a.** Site SNL-1. Erosion rate as a function of depth with shear stress as a parameter. Erosion rates for shear stresses of 0.25, 0.5, 1.0, and 2.0 Pa are shown. Core length of 20.5 cm.
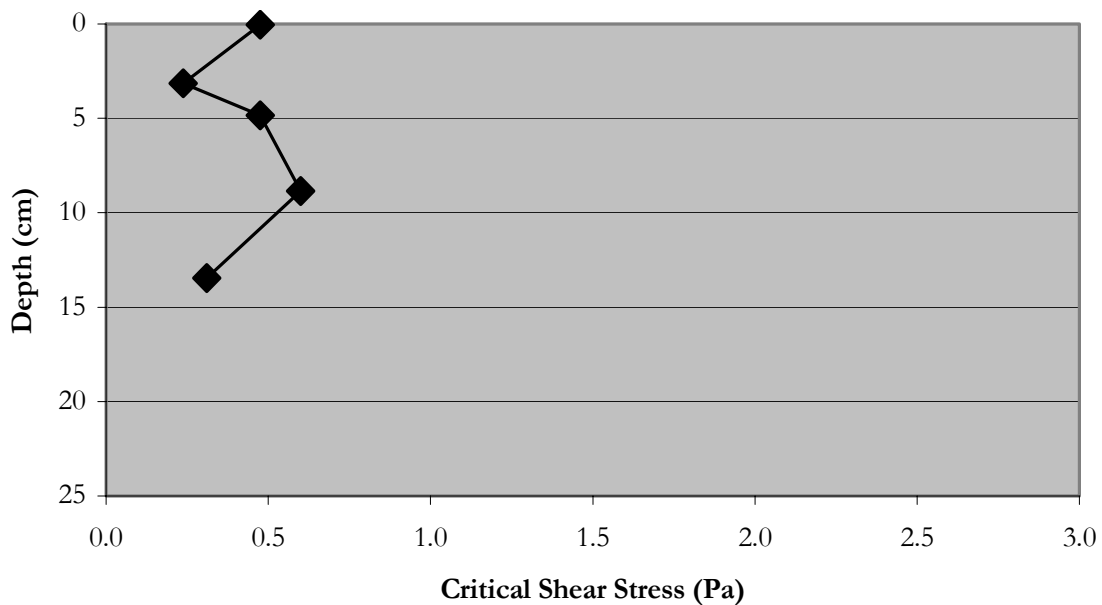
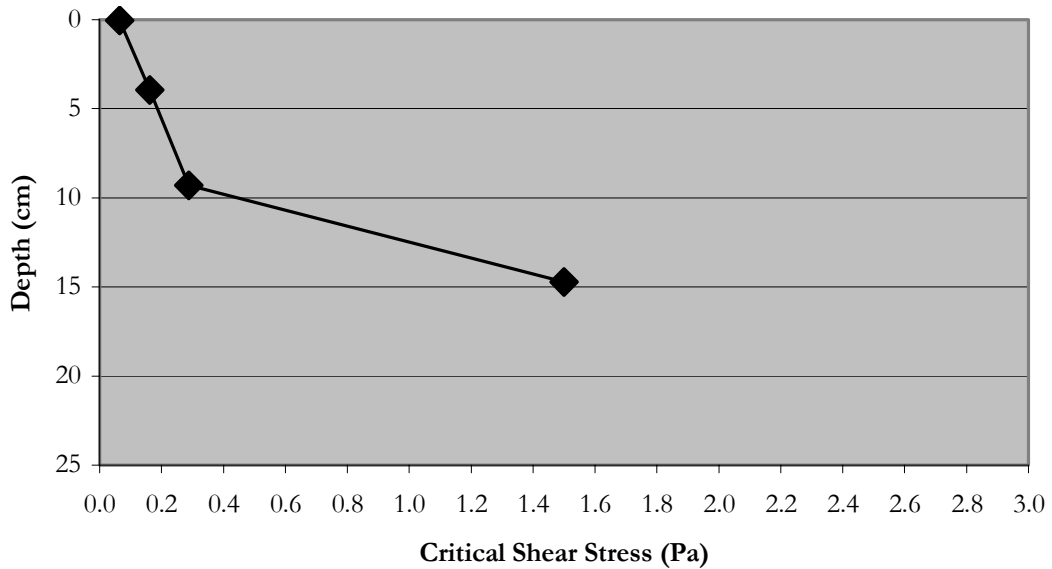**Figure 5b.** Site SNL-1. Critical shear stress as a function of depth.

17

Qualitatively the mean particle size (Figure 5c) tracked well with the erosion behavior with depth. In a relative sense the erosion transitioned from more difficult to less difficult back to more difficult and again back to less difficult with depth in the core. The particle size transitions from smaller (~200 µm), to larger (~250 µm), to smaller (~190 µm), to larger (~240 µm). This indicates that the increase in fine-grained particles is helping to bind the sediment, increasing its erosive strength. The bulk density (Figure 5d) was between 1.78-1.84 g/cm^3 for the top 7.5 cm and steadily decreased throughout the remainder of the core to 1.64 g/cm^3 at 11 cm and 1.52 g/cm^3 at the 16 cm.
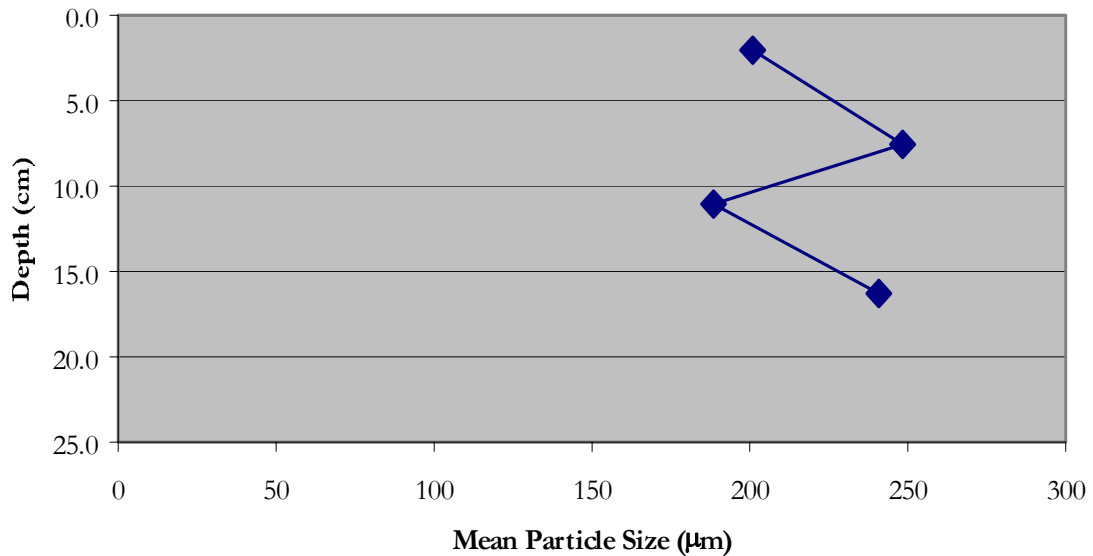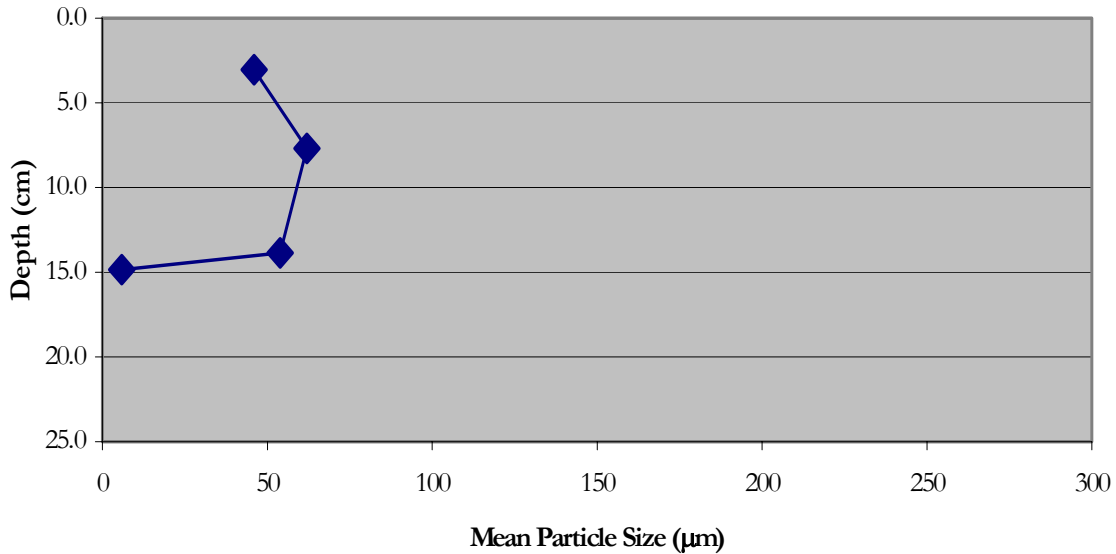

Figure 5c. Site SNL-1. Mean particle size as a function of depth.
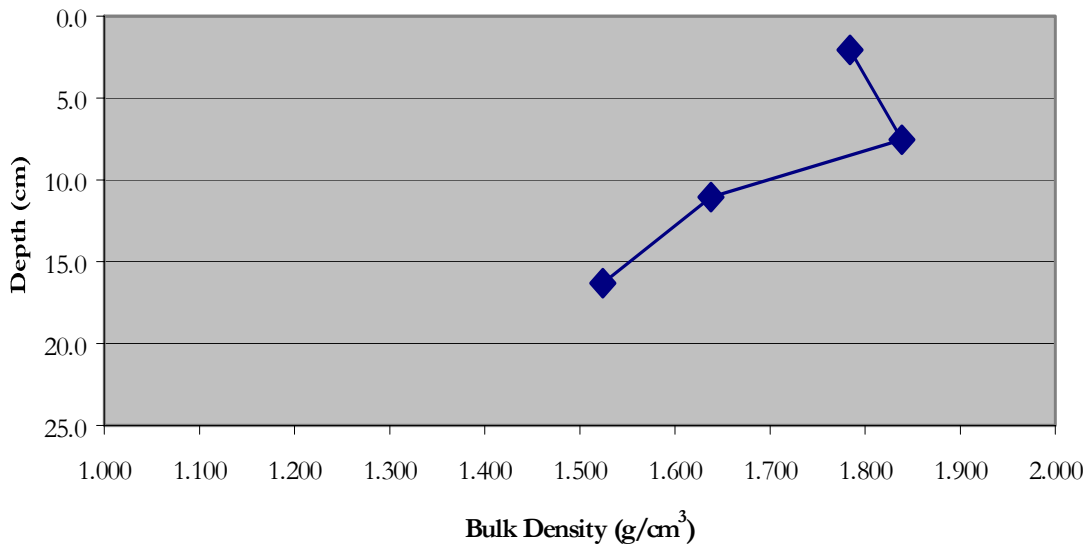
Figure 5d. Site SNL-1. Bulk density as a function of depth.

The erosion core taken at site SNL-2 was 22.5 cm long and was visually much finer-grained than SNL-1 and contained small air pockets throughout its depth. Erosion rates with depth for this core are shown in Figures 6a. The sediments at the surface were somewhat easy to erode, becoming slightly less erosive through the first 7.5 cm and eroding into 1-5 mm aggregates. Through the next few centimeters the core becomes increasingly harder to erode but when erosion did take place, it happened in larger chunks up to 1 cm in diameter, with larger chunks occurring at higher shear stresses. The last few centimeters of the core became a little easier to erode, and aggregates were ~1-3 mm in diameter. The critical shear stress (Figure 6b) was ~0.06 Pa through the first 7.5 cm, increasing to greater than 0.25 Pa near the middle of the core and decreasing near the bottom to 0.2 Pa.
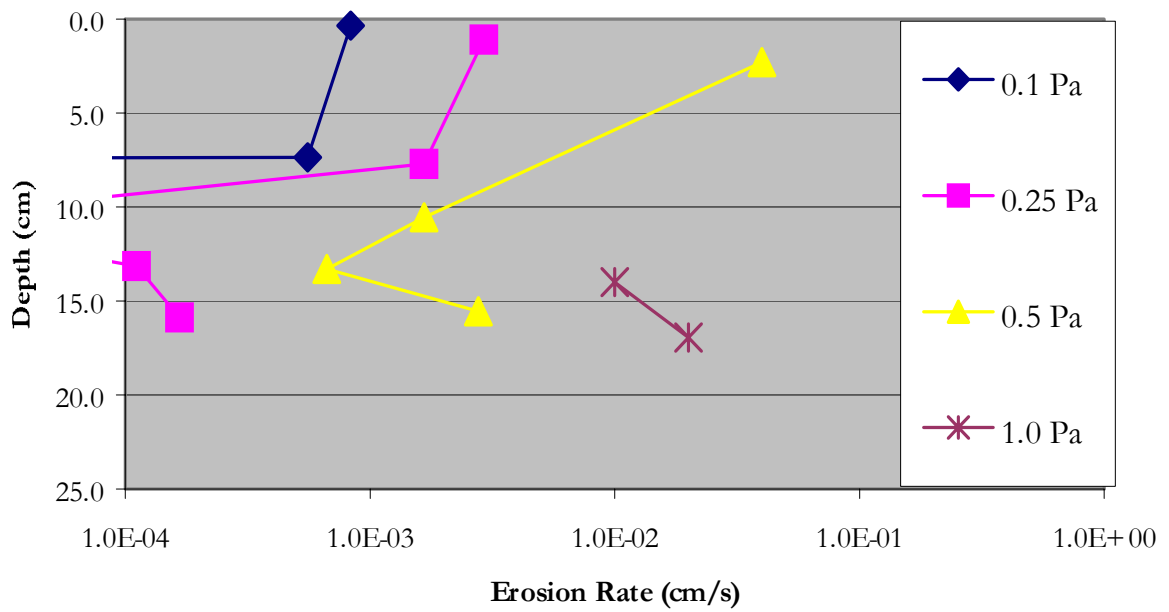
Figure 6a. Site SNL-2. **Erosion rate as a function of depth with shear stress as a parameter.** Erosion rates for shear stresses of 0.1, 0.25, 0.5, and 1.0 Pa are shown. Core length of 22.5 cm.
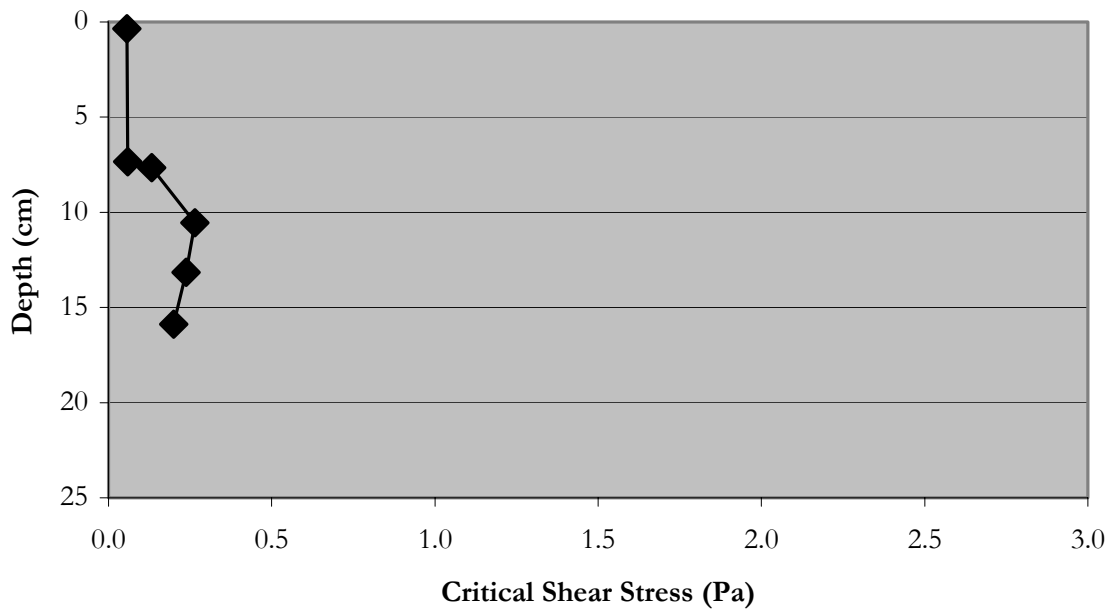
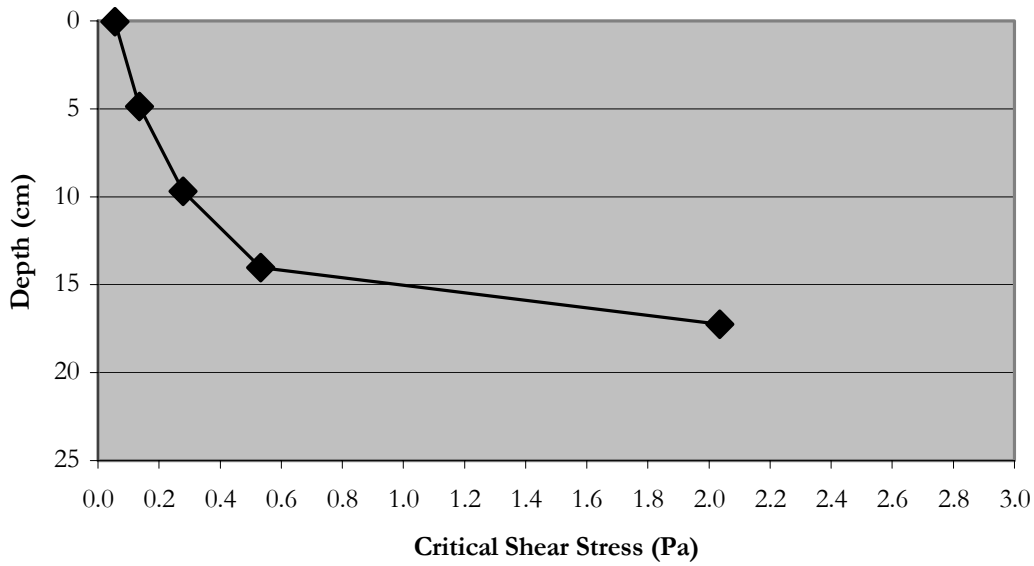**Figure 6b.** Site SNL-2. Critical shear stress as a function of depth.

The mean particle size (Figure 6c) was 67 μm near the top and bottom of the core and decreased to 38 μm in the middle. The finer particle size is consistent with the increased

cohesive strength witnessed in the middle of the core as decreased erosion rates and larger aggregate erosion. The bulk density (Figure 6d) varied between 1.16-1.17 g/cm^3 in the upper and middle sections of the core to 1.10 g/cm^3 at the bottom. A duplicate sediment core was retrieved from this site that was ~7 cm long. Particle size and bulk density at two depths within this core are also shown in figures 6c and 6d.
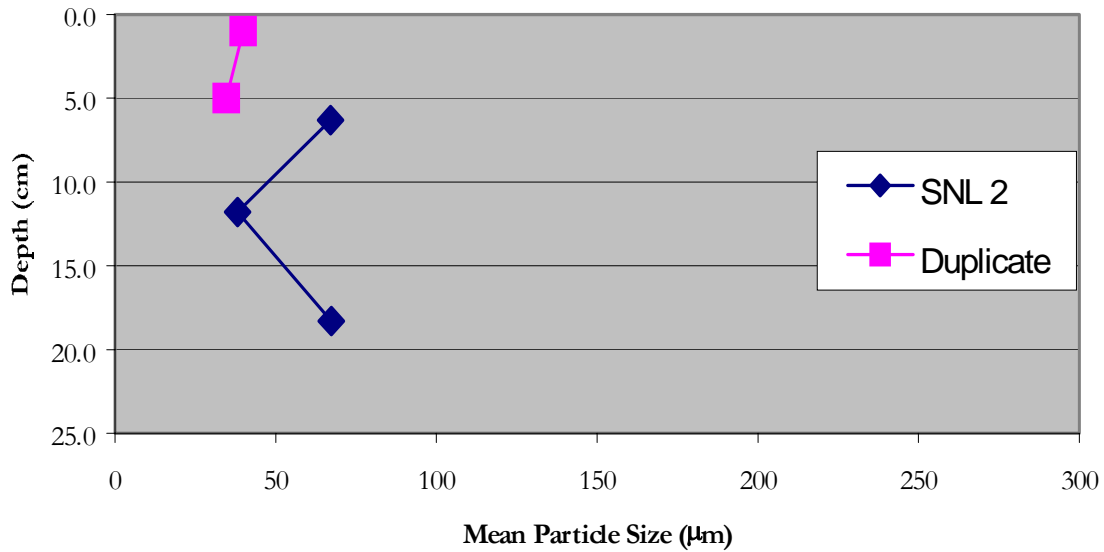
Figure 6c. Site SNL-2. Mean particle size as a function of depth. Results from a shorter duplicate core are also shown.
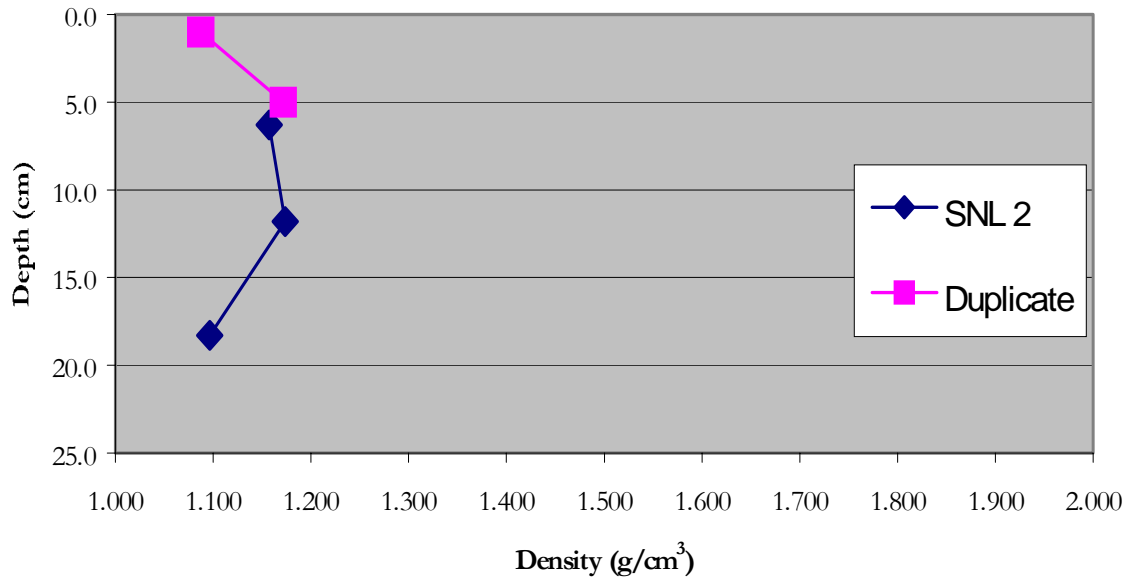
Figure 6d. Site SNL-2. Bulk Density as a function of depth. Results from a shorter duplicate core are also shown.

The erosion core from site SNL-3 was 22.8 cm in length and had a light, greenish brown floc layer on the surface, which eroded completely away at 0.03 Pa in 2 minutes. The sediment became steadily more difficult to erode with increasing depth (figure 7a). The eroded sediment was primarily in the form of aggregates ranging in size from 0.25 – 8 mm in diameter and transporting mostly in suspension. The aggregates were smallest near the surface (0.25-1.5 mm) and became larger with depth in the core and increasing shear stress. Grass-like, organic debris was observed in the core below ~10 cm in depth and increased in abundance with increasing depth. The critical shear stress increased with depth and ranged from ~0.06 Pa near the surface, increasing quickly below the floc layer, to 0.65 Pa at the bottom of the core (Figure 7b).
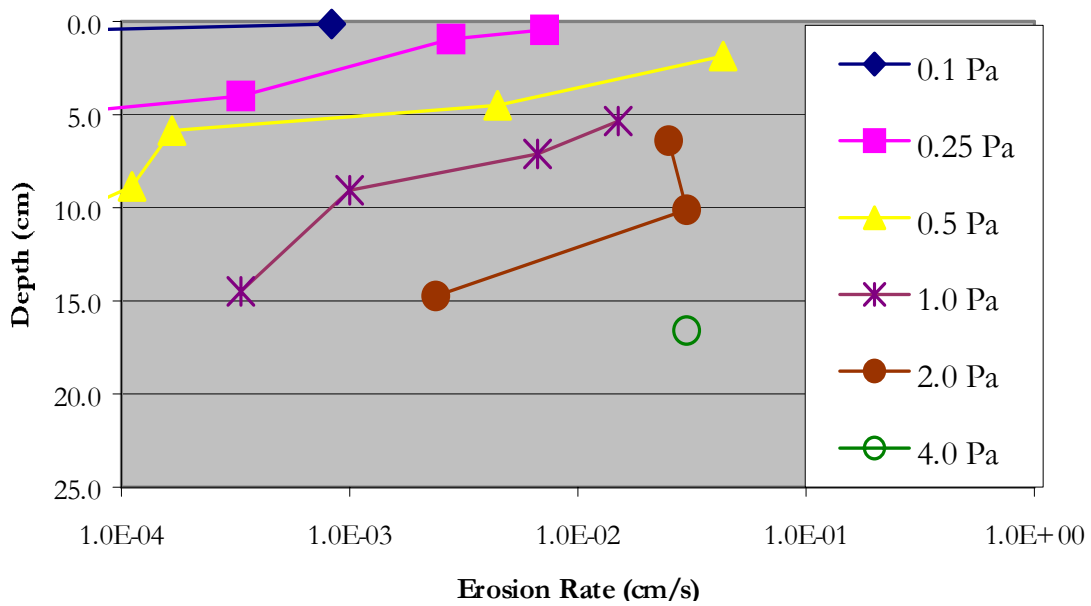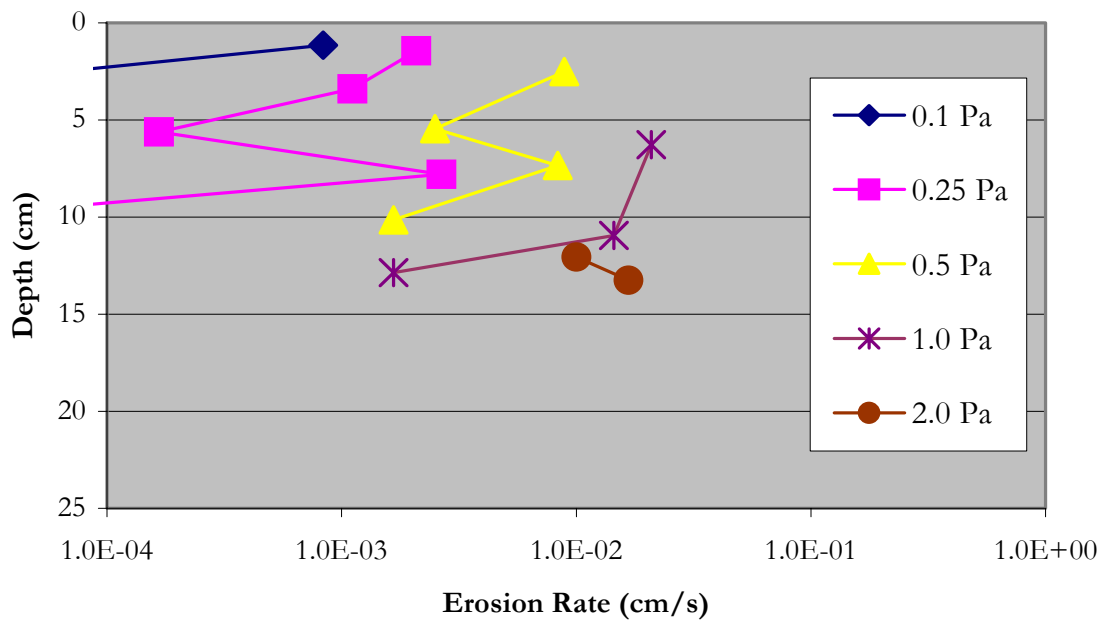
Figure 7a. Site SNL-3. Erosion rate as a function of depth with shear stress as a parameter. Erosion rates for shear stresses of 0.1, 0.25, 0.5, 1.0, 2.0 and 4.0 Pa are shown. Core length of 22.8 cm
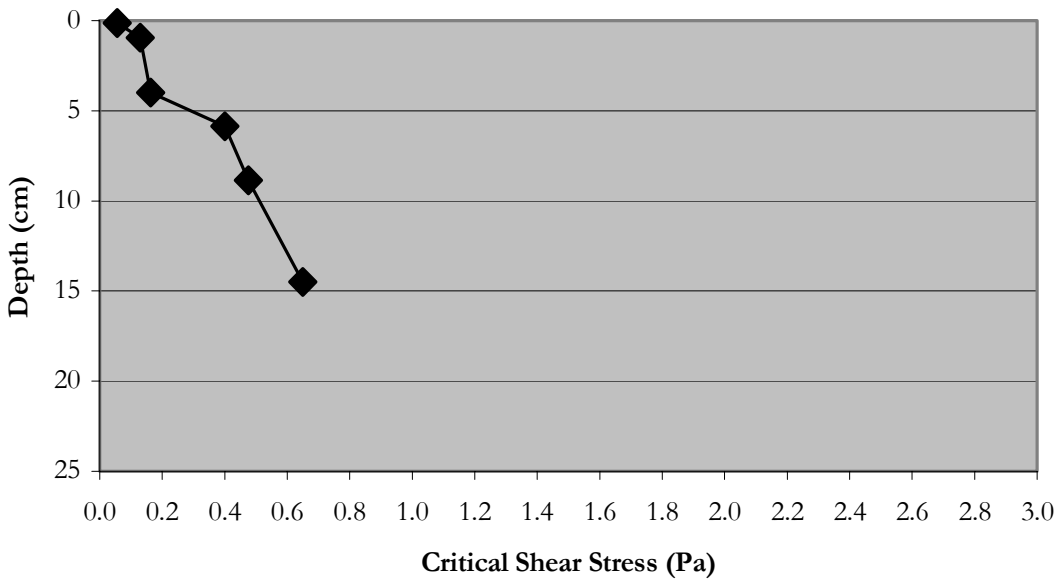
Figure 7b. Site SNL-3. Critical **shear stress as a function of depth.**

The mean particle size (Figure 7c) was 37 μm near the top of the core, decreased to 30 μm at 8 cm, and then steadily increased to 56 μm at the bottom rest of the core. The bulk density profile (Figure 7d) displayed the opposite trend as the mean particle size with similar, relatively small changes in overall magnitude. The bulk density near the surface was 1.12 g/cm^3, increased

23

to 1.16 g/cm^3 at 8 cm, and then steadily decreased to 1.09 g/cm^3 at the bottom of the core. A duplicate sediment core was retrieved from SNL-3 as well that was also ~7 cm long. Particle size and bulk density at two depths within this core are also shown in figures 7c and 7d.
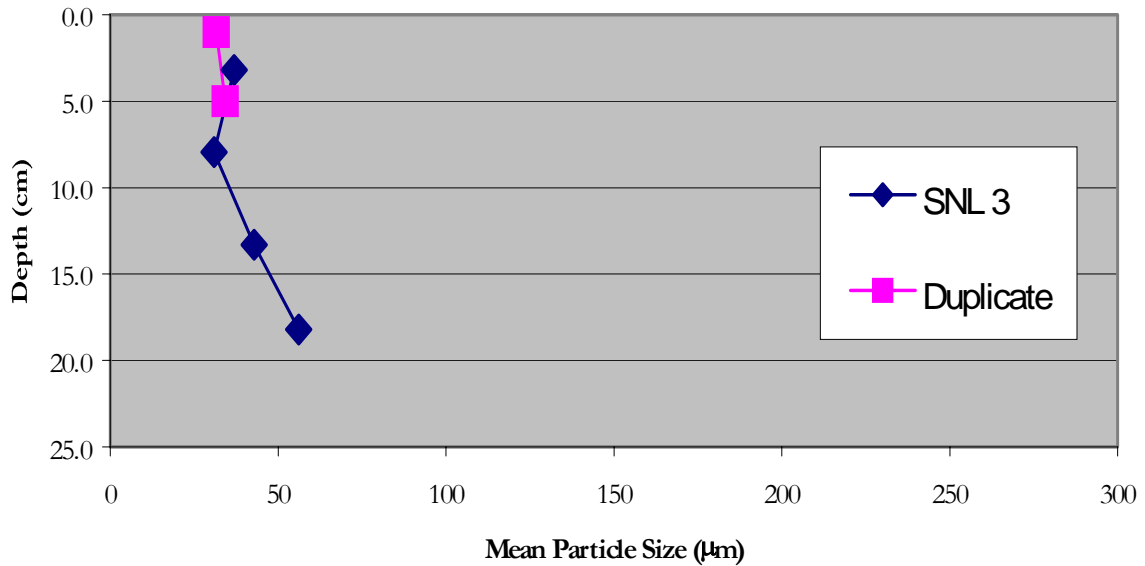
Figure 7c. Site SNL-3. Mean particle size as a function of depth. Results from a smaller duplicate core are also shown.
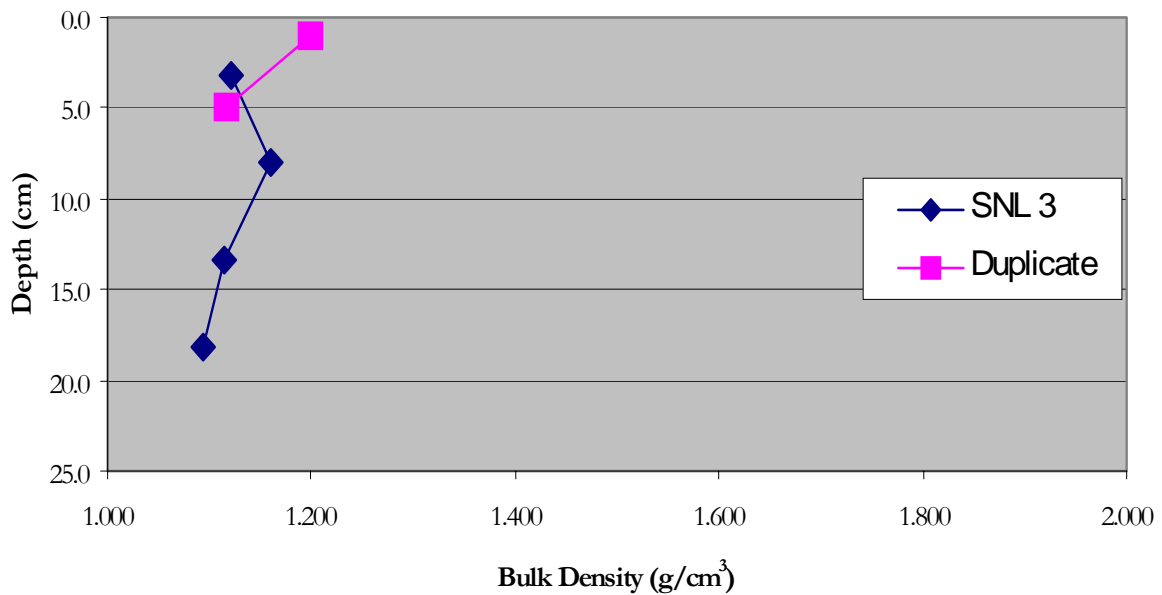
Figure 7d. Site SNL-3. Bulk Density as a function of depth. Results from a smaller duplicate core are also shown.

The erosion core from site SNL-4 was 34 cm with a 1-2 mm thick, light green/brown floc layer that easily eroded at ~0.05 Pa with darker material beneath. The core contained a relatively high concentration of air pockets throughout the first 15 cm, with reduced concentration deeper in the core. This sediment became steadily more stable (less erosive) with increasing depth in the core (figure 8a). Erosion was primarily in the form of aggregates or chunks that increased in size with increasing applied shear stress and depth in the core. The aggregates transported mostly as bed load for shear stresses less than 0.25 Pa. The critical shear stress (figure 8b) decreases with depth throughout the core, ranging from 0.053 – 0.61 Pa.
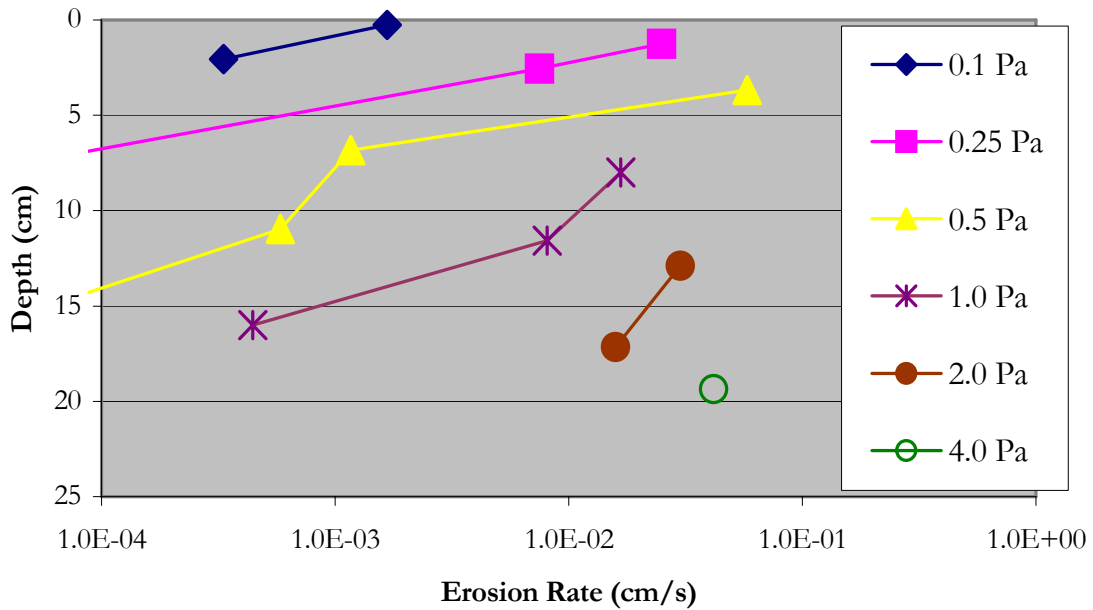
Figure 8a. Site SNL-4. Erosion rate as a function of depth with shear stress as a parameter. Erosion rates for shear stresses of 0.1, 0.25, 0.5, 1.0, 2.0 and 4.0 Pa are shown. Core length of 22.8 cm.
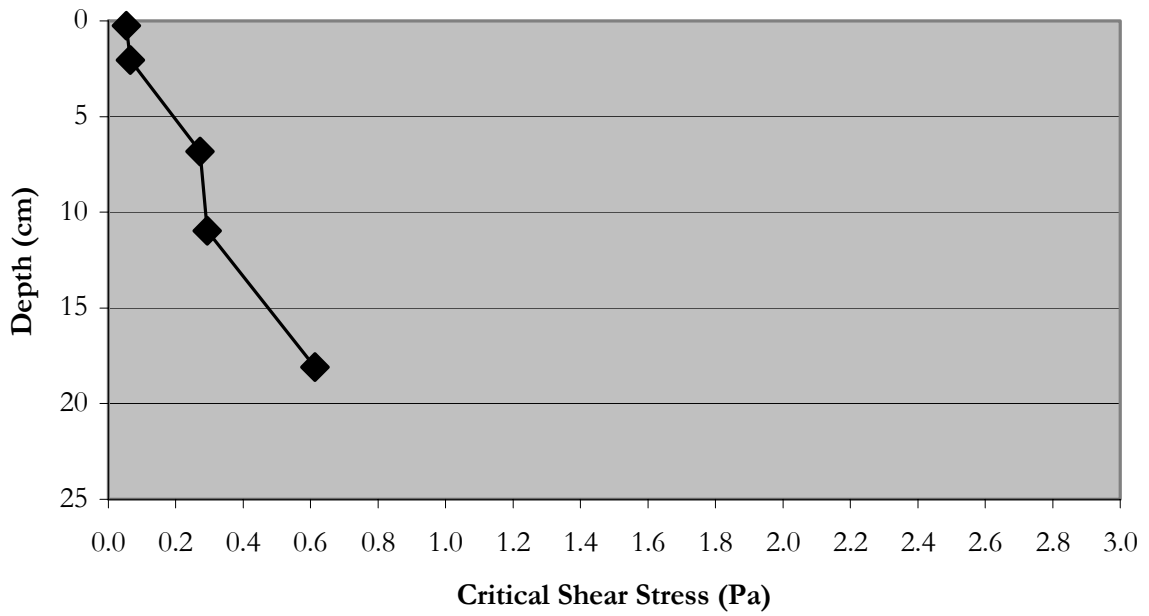
Figure 8b. Site SNL-4. Critical shear stress as a function of depth.

The mean particle size for SNL-4 remained rather consistent with depth, ranging between 18-25 μm (figure 8c). The bulk density increased progressively with depth ranging between 1.04 g/cm^3 at the surface to 1.15 g/cm^3 near the bottom (figure 8d).
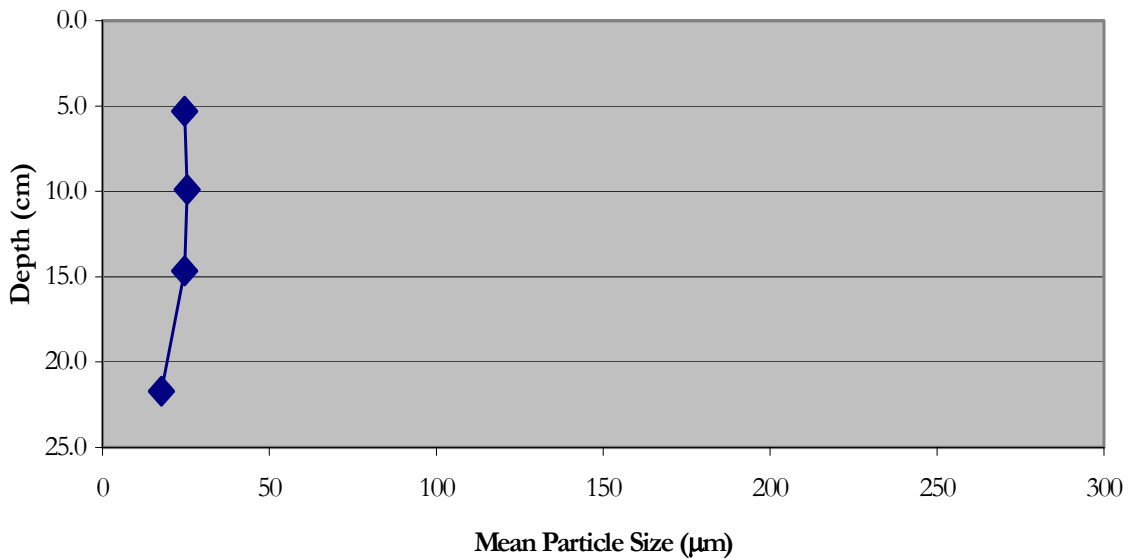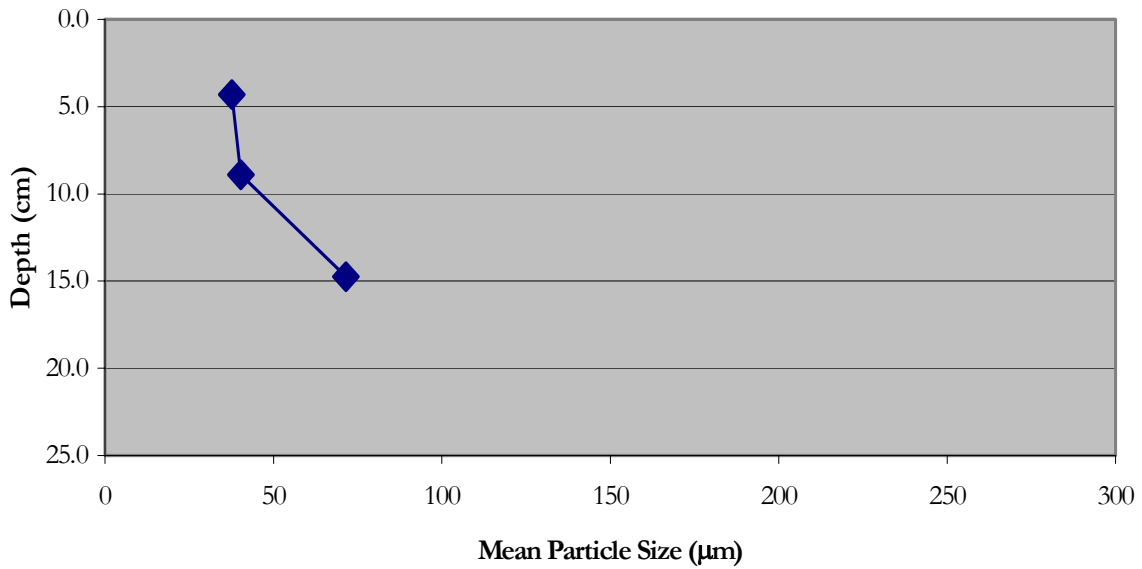

**Figure 8c.** Site SNL-4. Mean particle size as a function of depth.
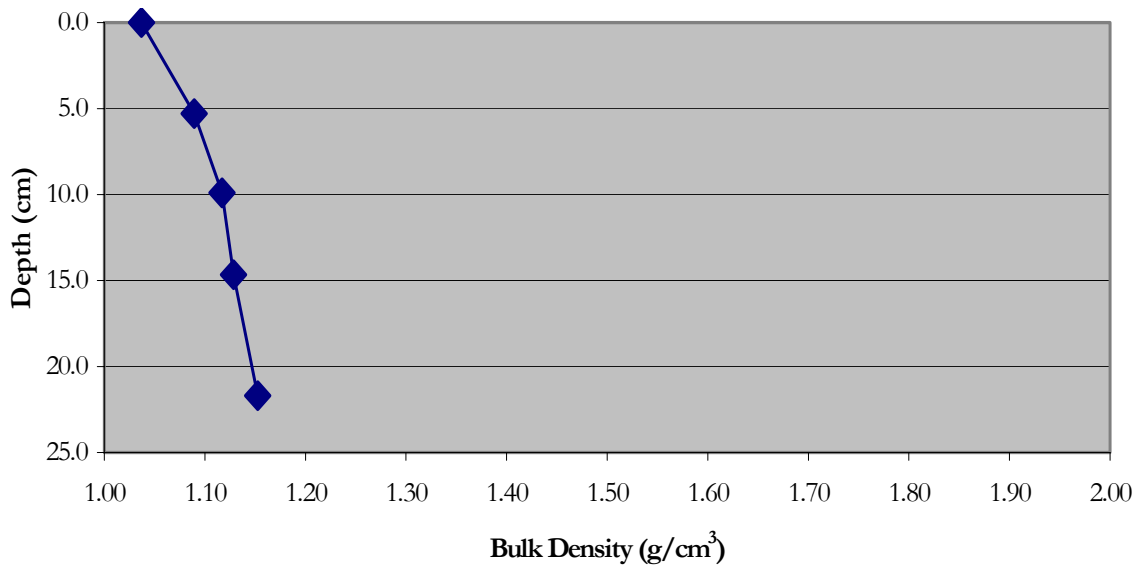
Figure 8d. Site SNL-5. Bulk density as a function of depth.

The erosion core from site SNL-5 was 20.5 cm long. Throughout the depth of core the sediments became increasingly harder to erode, behaving like a well-consolidated sediment bed (figure 9a). There was very little organic debris observed within the core at all depths. Erosion was in the form of aggregates, composed of fine-grained particles, which appeared to be ~5 mm in average diameter with some as large as 10 mm. The critical shear stress decreased with depth from 0.06 Pa at the surface to 0.3 Pa near the bottom (Figure 9b).

Figure 9a. Site SNL-5. Erosion rate as a function of depth with shear stress as a parameter. Erosion rates for shear stresses of 0.1, 0.25, 0.5, 1.0, and 2.0 Pa are shown. Core length of 20.5 cm.
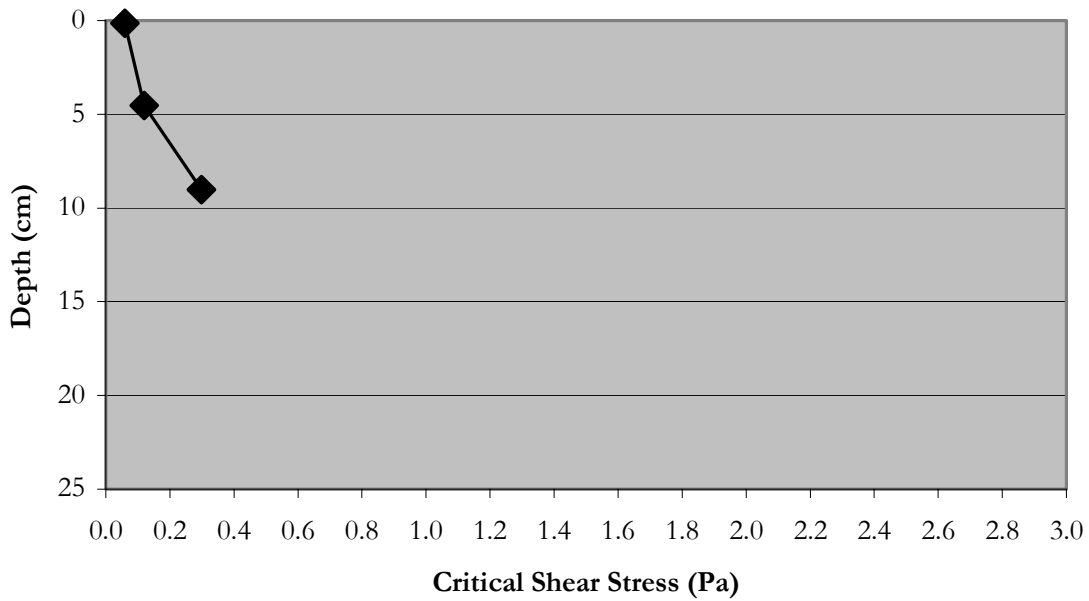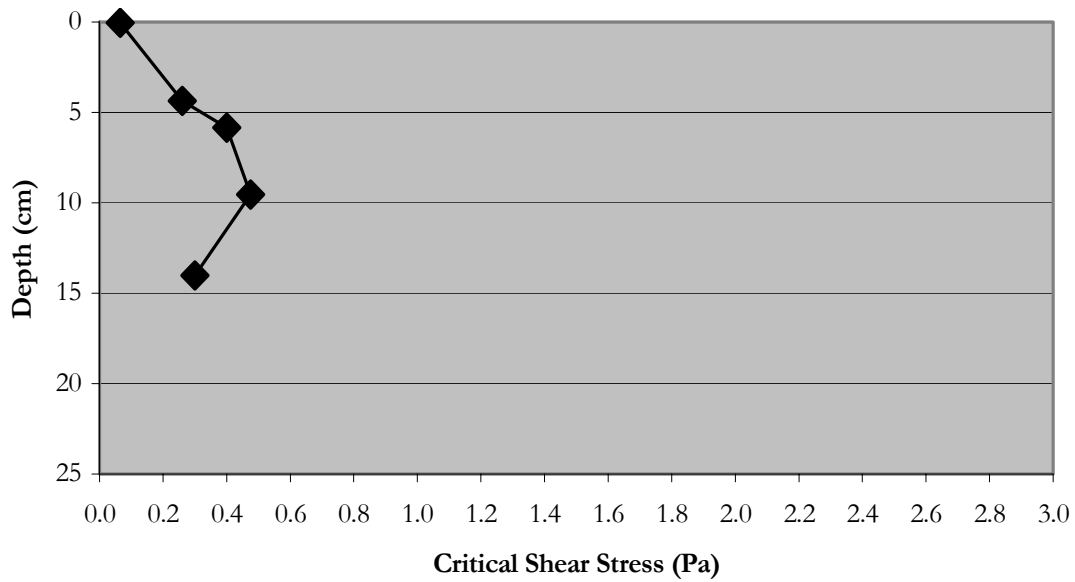

Figure 9b. Site SNL-5. Critical shear stress as a function of depth.

The mean particle size (Figure 9c) remained practically constant with depth, ranging from 29 μm at the surface to 25 μm near the bottom. The bulk density (Figure 9d) increased steadily with depth, from 1.10 g/cm^3 near the surface to 1.17 g/cm^3 near the bottom of the core.
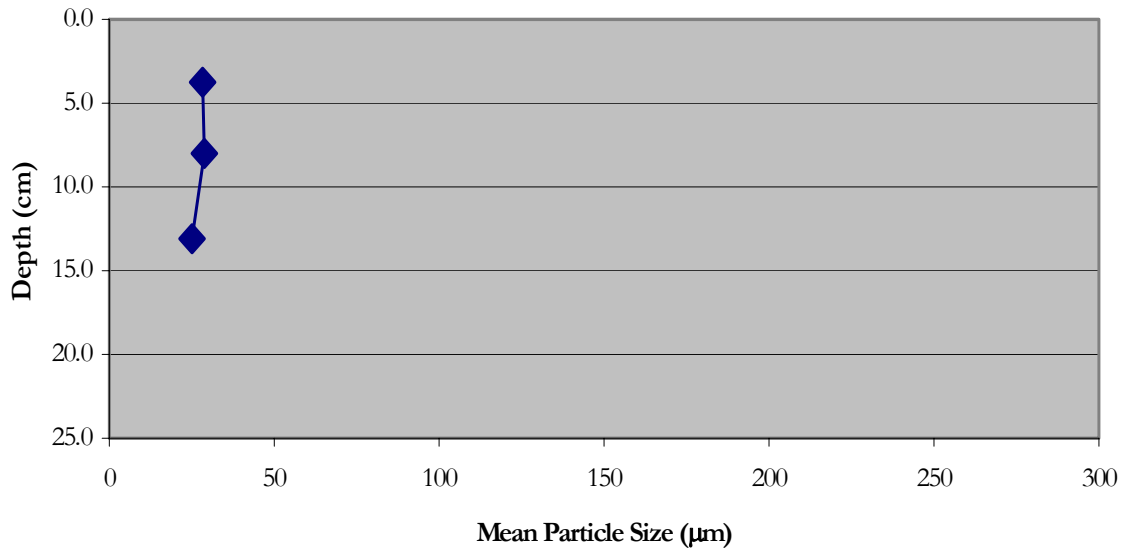
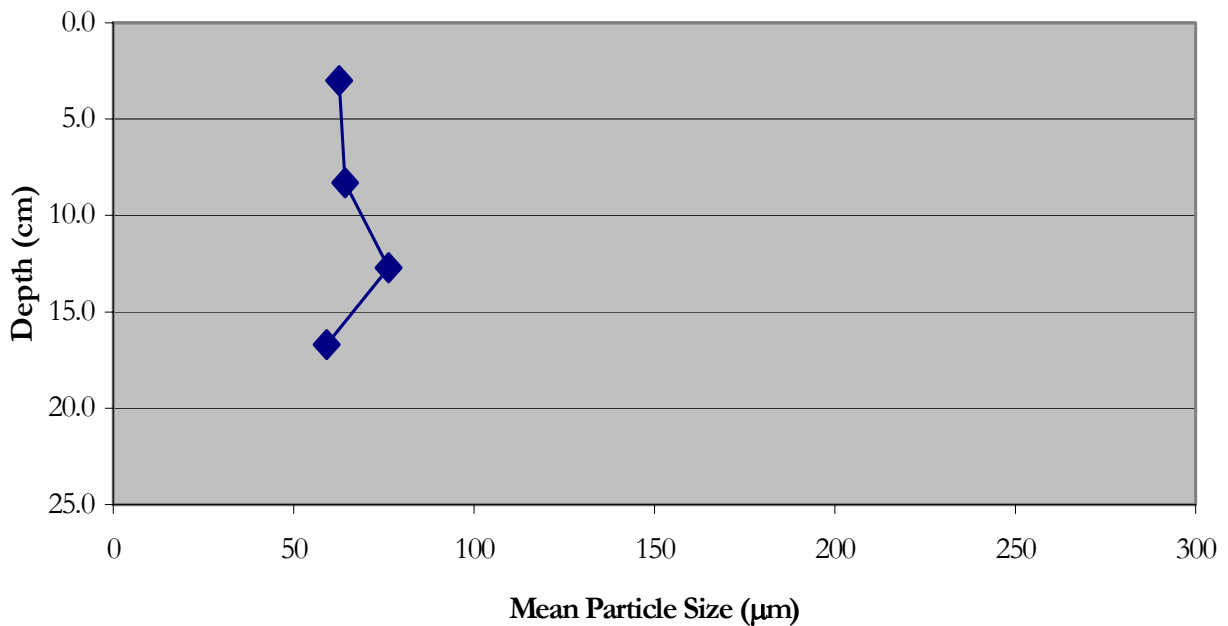**Figure 9c.** Site SNL-5. Mean particle size as a function of depth.
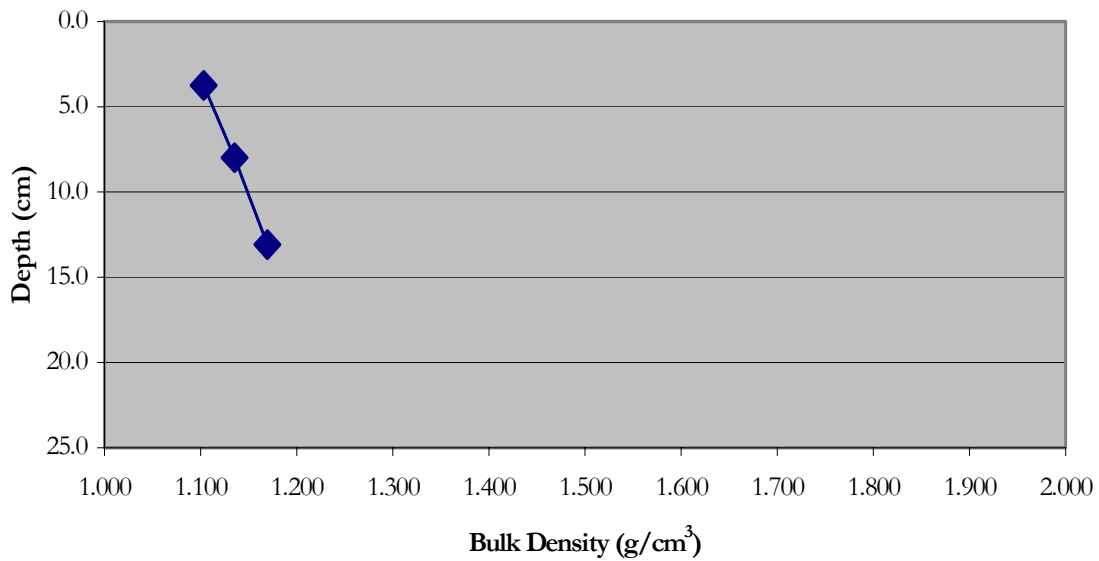
Figure 9d. Site SNL-5. Bulk Density as a function of depth.

The erosion core for the SNL-6 site was 27 cm long. The sediment contained small air pockets ranging in size from about 1-3 mm throughout the depth. Near the bottom of the core, grass-like or hair-like organic material appeared that seemed to help the stability of the sediments in that layer. The sediments eroded somewhat easily (Figure 10a) near the surface and became

significantly harder to erode deeper in the core. The critical shear stress followed the same trend (Figure 10b), becoming very large near the bottom of the core, reaching a value of 1.5 Pa.
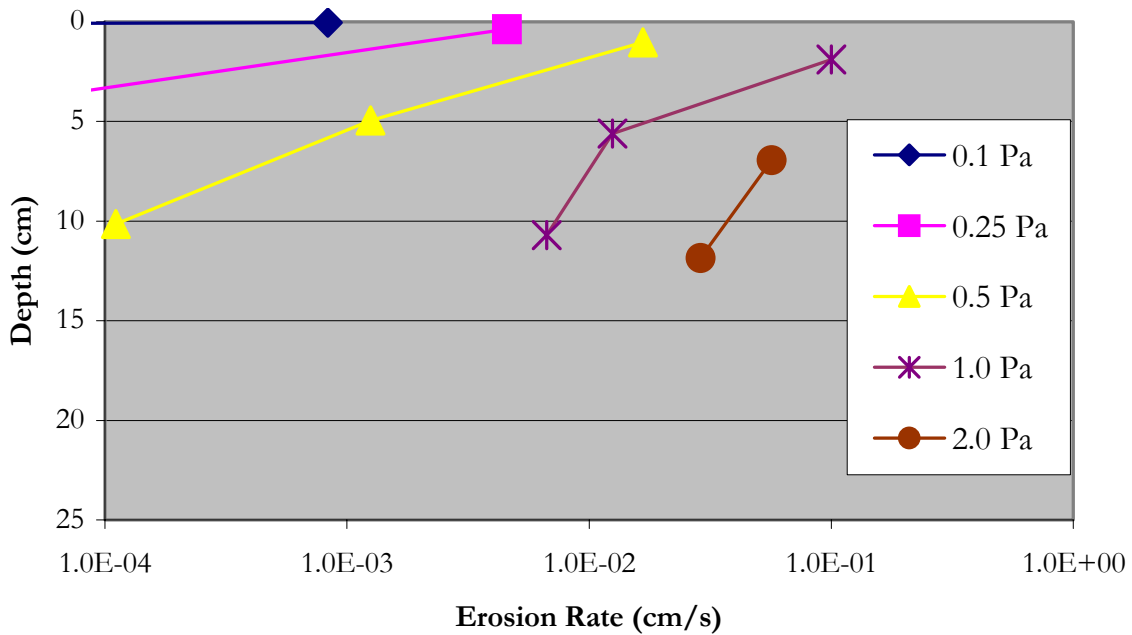

Figure 10a. Site SNL-6. Erosion rate as a function of depth with shear stress as a parameter. Erosion rates for shear stresses of 0.1, 0.25, 0.5, 1.0, 2.0 and 4.0 Pa are shown. Core length of 27 cm.
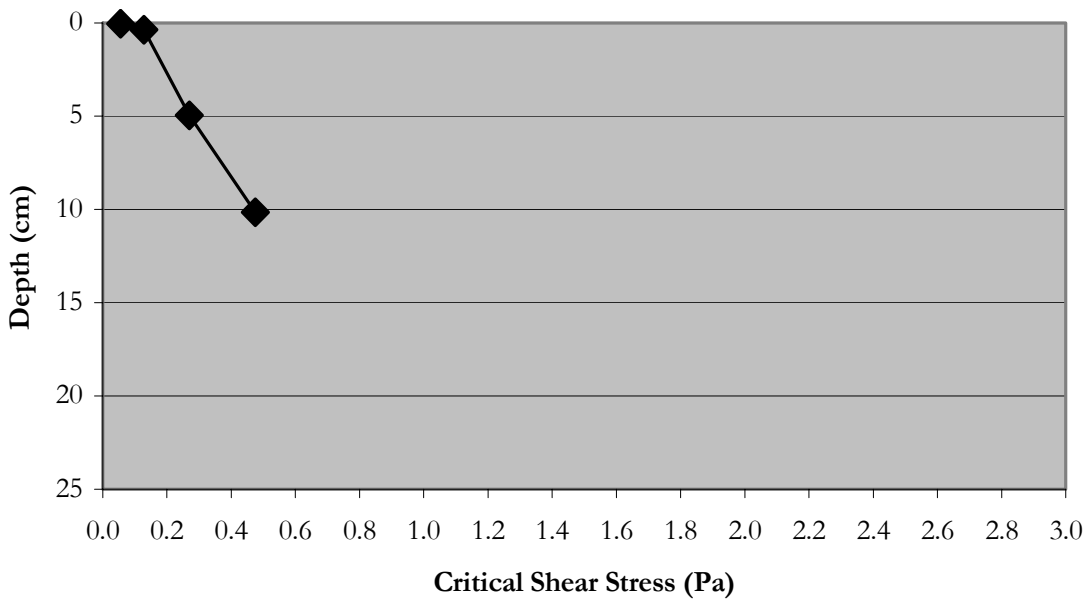

Figure 10b. Site SNL-6. Critical shear stress as a function of depth.

The mean particle size (Figure 10c) was reasonably constant with depth ranging between 46 and 62 µm for the entire core except for the bottom most layer of very fine-grained material at 15 cm deep that was ~6.0 µm. The bulk density (Figure 10d) generally decreased with depth from 1.11 g/cm^3 near the surface to 1.08 g/cm^3 at the bottom.
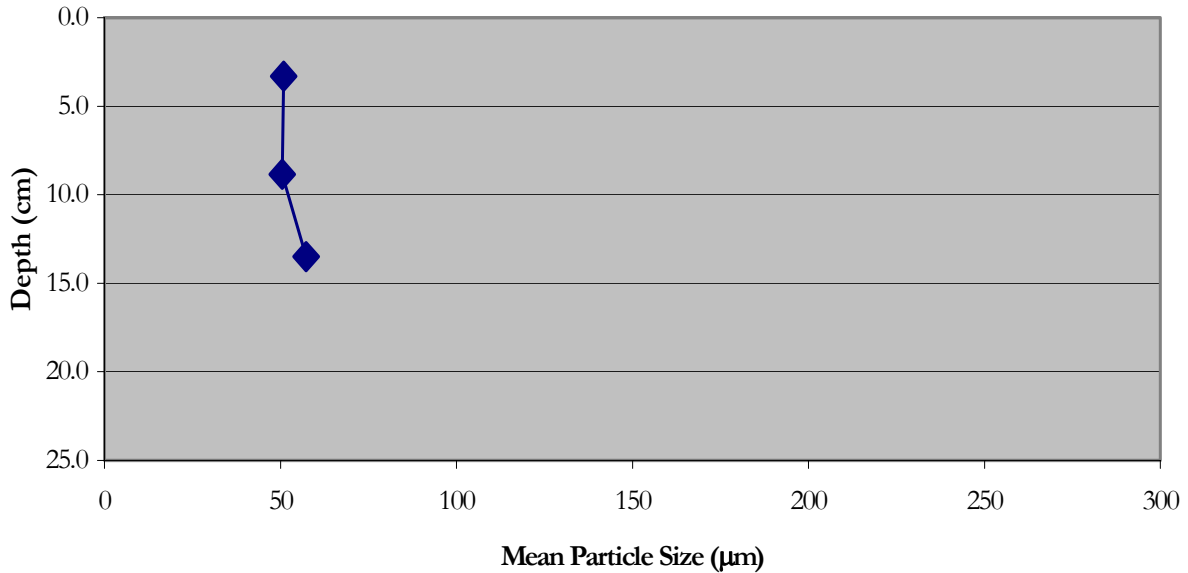

Figure 10c. Site SNL-6. Mean particle size as a function of depth.
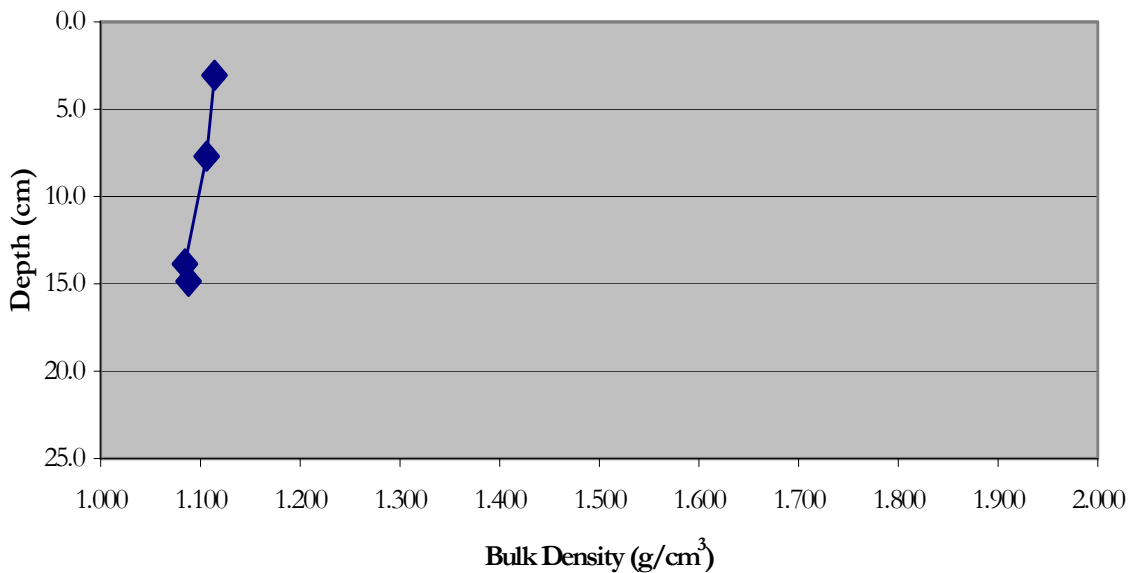
Figure 10d. Site SNL-6. Bulk den**sity as a function of depth.**

The erosion core from SNL-7 was 27.5 cm in length. There was a 1 to 2 mm floc layer on the surface that eroded immediately at ~0.05 Pa. The rest of the sediment was dark brown with

small air pockets throughout its depth. The erosion rates (Figure 11a) generally decreased with

depth throughout the entire core. For this core, as well as all other cores, the gas pockets did not

serve to appreciably alter the erosion properties of the sediments except in some instances near

the surface under low flow conditions in which localized air release served to increase erosion.

The critical shear stress progressively increased with depth from ~0.6 Pa at the surface to slightly
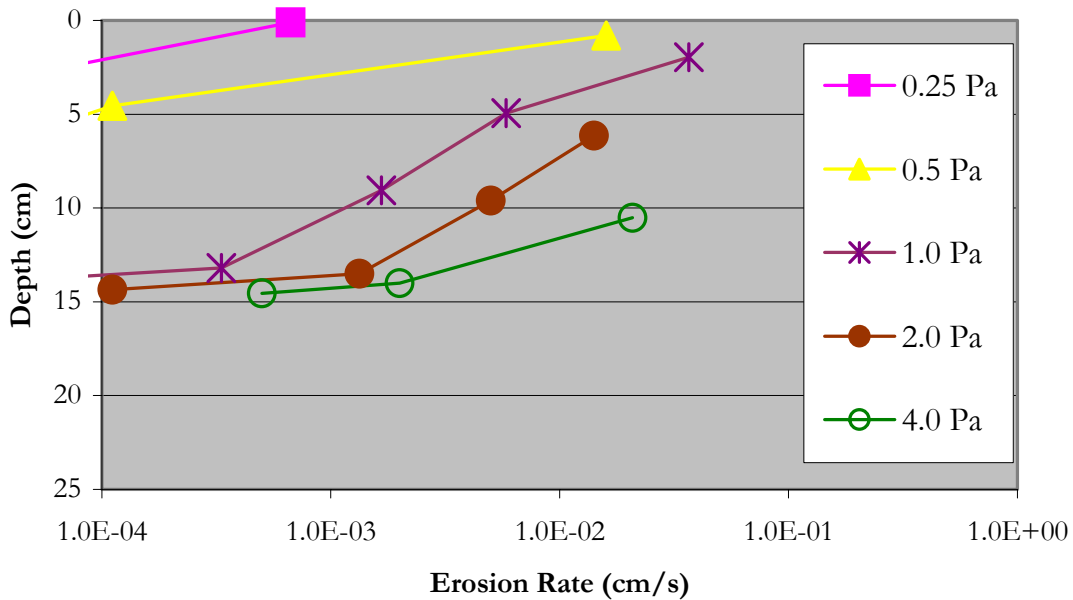
greater than 2.0 Pa (Figure 11b).
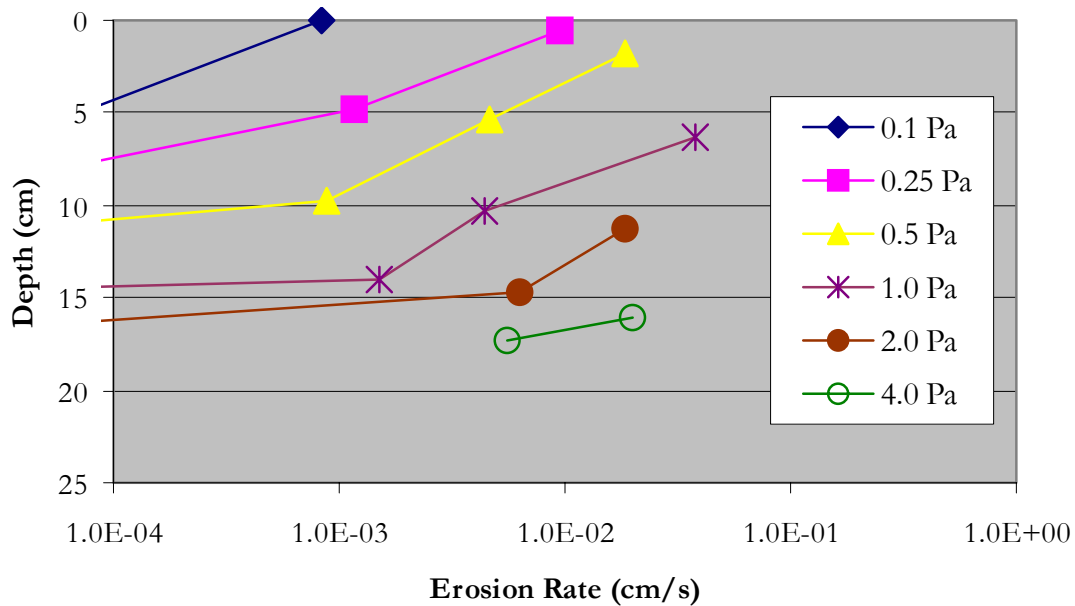
Figure 11a. Site SNL-7. Erosion rate as a function of depth with shear stress as a parameter. Erosion rates for shear stresses of 0.1, 0.25, 0.5, 1.0, 2.0 and 4.0 Pa are shown. Core length of 27.5 cm.

Figure 11b. Site SNL-7. **Critical shear stress as a function of depth.**

The mean particle size (Figure 11c) was very consistent with depth varying between 25 and 29 μm throughout the core. The bulk density generally increased from 1.05 g/cm^3 at the surface to 1.13 g/cm^3 at the bottom (Figure 11d).
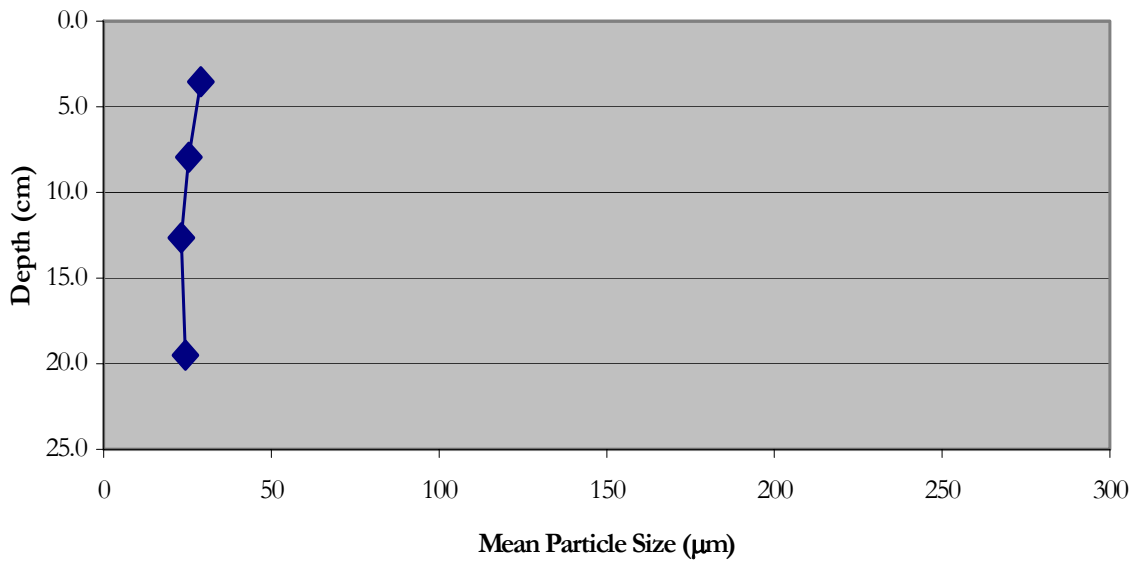
Figure 11c. Site SNL-7. Mean particle size as a function of depth.
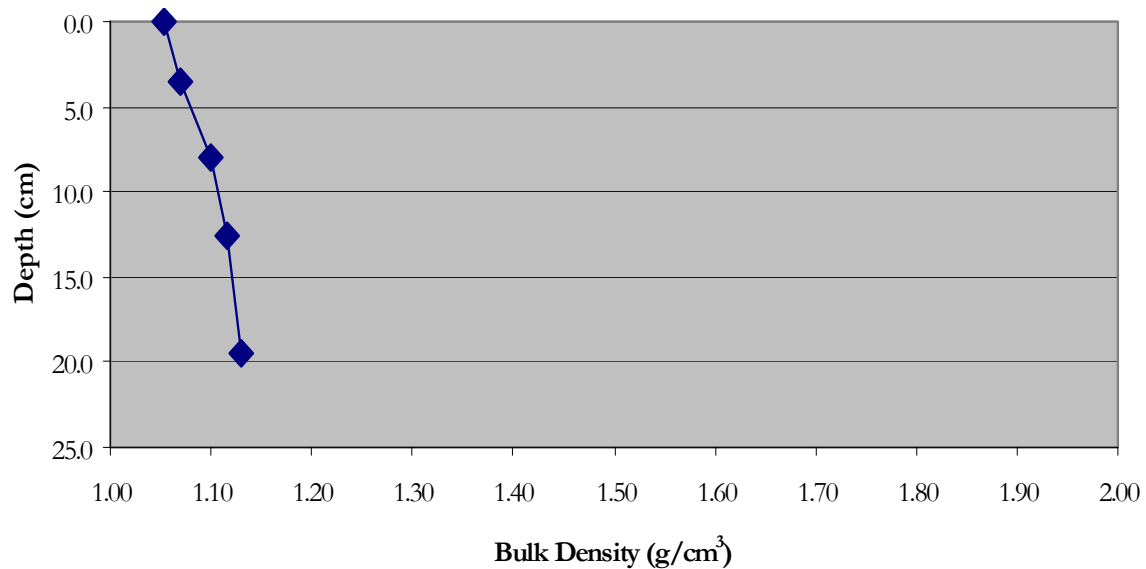
Figure 11d. Site SNL-7. Bulk density as a function of depth.

The erosion core from SNL-8 was 19 cm long. There was a 0.5-1.0 mm floc layer on the surface that eroded immediately at ~0.05 Pa. There were no visible air pockets within this core. The erosion rates (Figure 12a) generally decreased with depth for the first ~6 cm before exposing a less stable layer where erosion rates increased locally then decreased for the remainder of the core. Prior to exposing the less stable layer the sediment became very difficult to erode and then failed in large chunks, leaving a relatively rough surface for the immediately ensuing erosion measurements. The critical shear stress generally increased with depth except within the less stable layer between 6-8 cm depth (Figure 12b).

Figure 12a. Site SNL-8. Erosion rate as a function of depth with shear stress as a parameter. Erosion rates for shear stresses of 0.1, 0.25, 0.5, 1.0, and 2.0 Pa are shown. Core length of 19.0 cm.
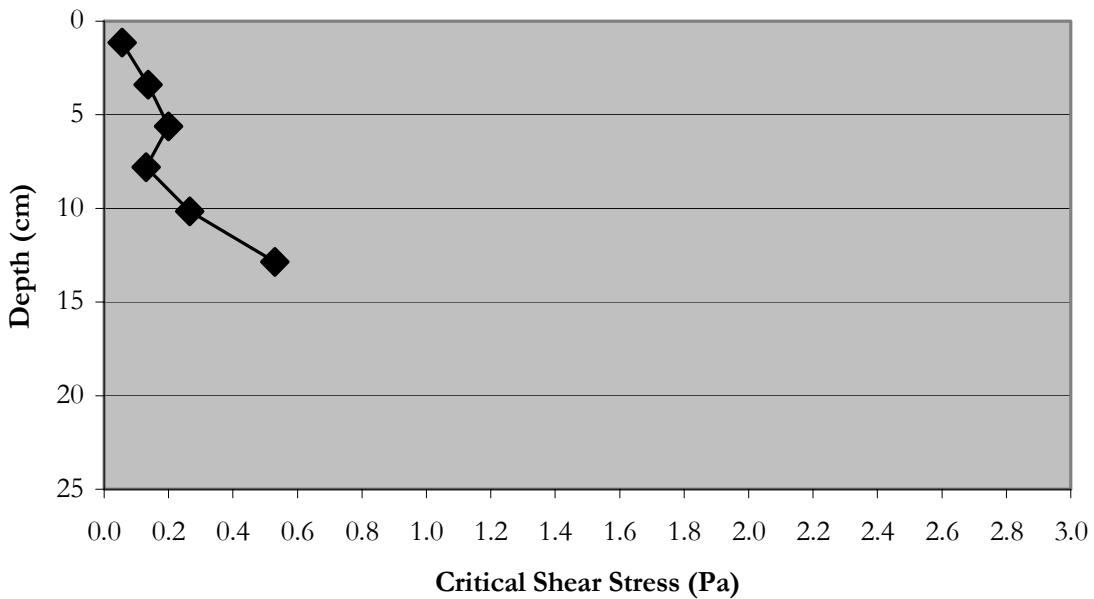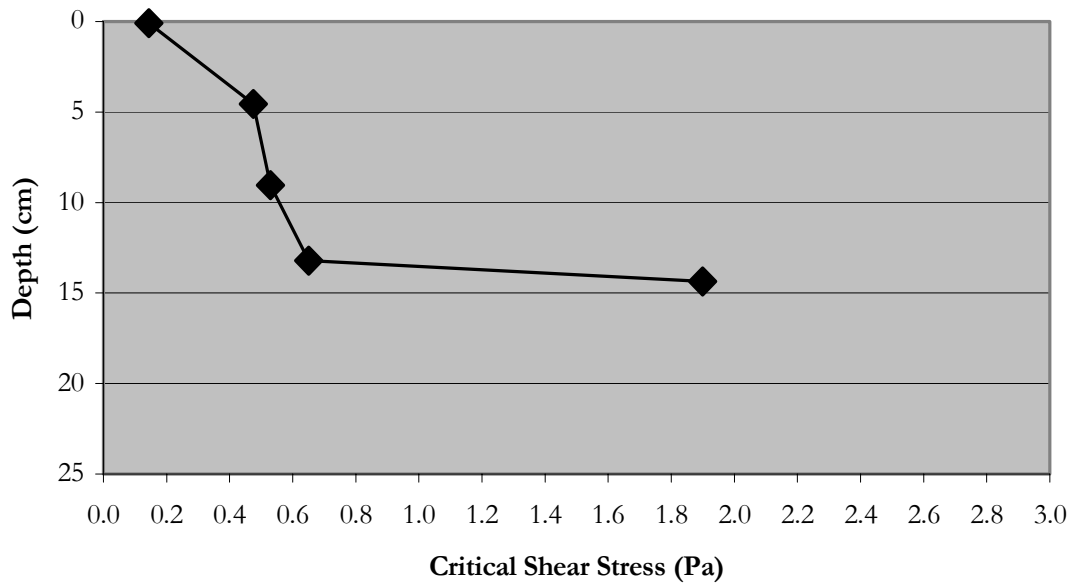

Figure 12b. Site SNL-8. Critical shear stress as a function of depth.

The mean particle size remained fairly constant for the first ~9 cm, ranging between 37-40 μm, then it increased significantly near the bottom to 72 μm (Figure 12c). The bulk density

did not vary much throughout the core, increasing from the surface to the bottom of the sample and ranging between 1.10-1.16 g/cm³ (Figure 12d).
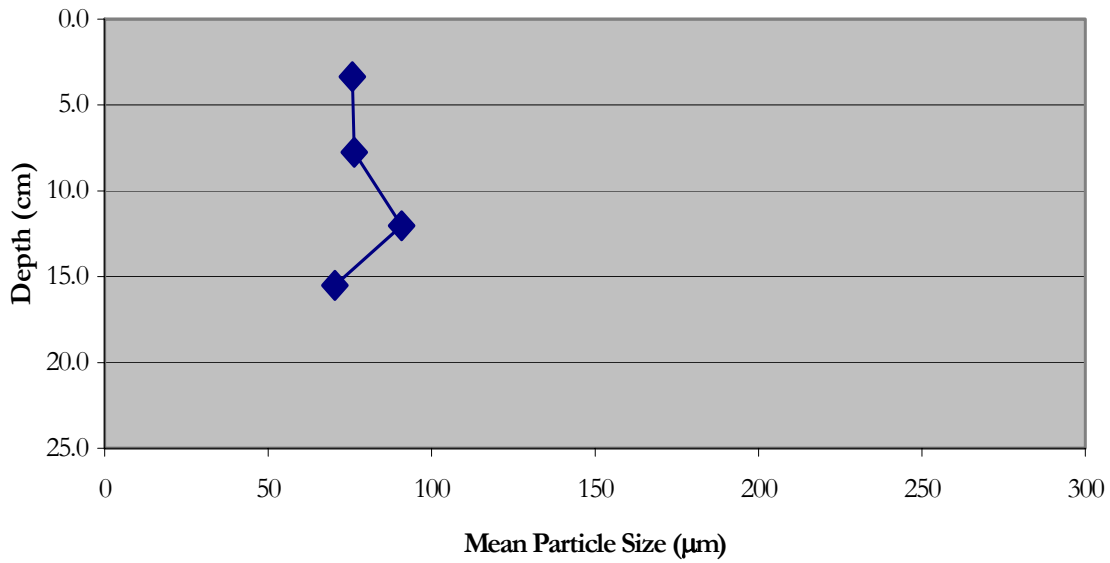

Figure 12c. Site SNL-8. Mean particle size as a function o**f depth.**
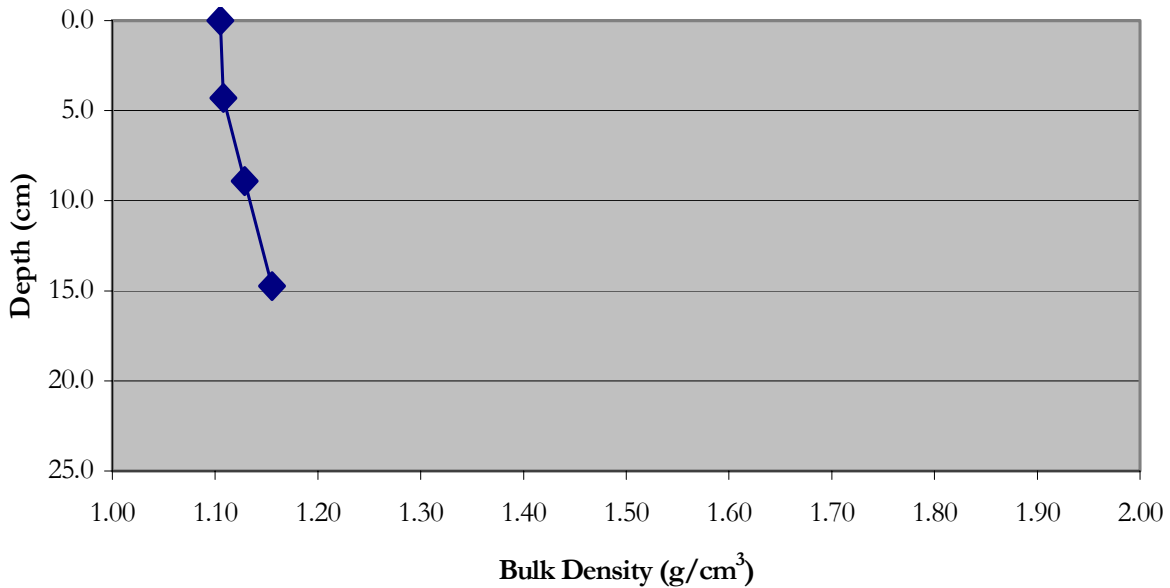
Figure 12d. Site SNL-8. Bulk Density as a function of depth.

The Erosion Core from SNL-9 was 22 cm in length and contained small air pockets, ~1 mm in diameter, throughout the core. As with most cores the initial floc/fluff layer was ~1 mm and eroded away completely at ~0.05 Pa. At all shear stresses the erosion rates decreased with

36

depth for the majority of the core and then became less stable near the bottom (figure 13a). Throughout the depth of the core the sediments eroded and transported in aggregates/chunks. At about the 12 cm depth mark the eroding sediment exposed an abundance of leaves and sticks which served to increased the size of the eroding aggregates from 0.5-2 mm in the layers above to 5-10 mm within this layer, also increasing the rate at which the sediments eroded.
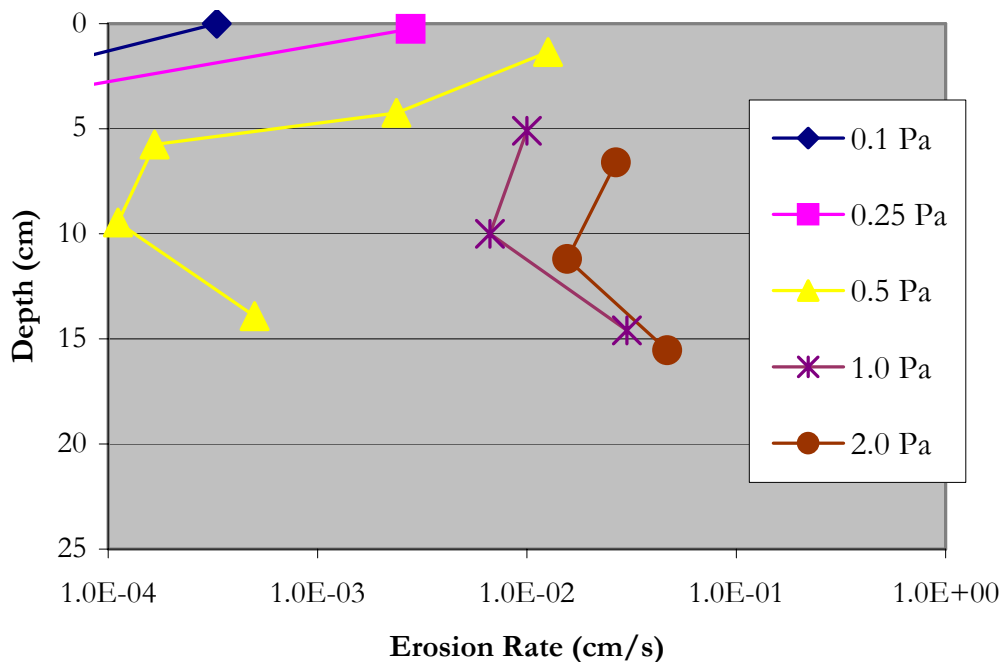
Figure 13a. Site SNL-9. Erosion rate as a function of depth with shear stress as a parameter. Erosion rates for shear stresses of 0.1, 0.25, 0.5, 1.0, and 2.0 Pa are shown. Core length of 22.0 cm.
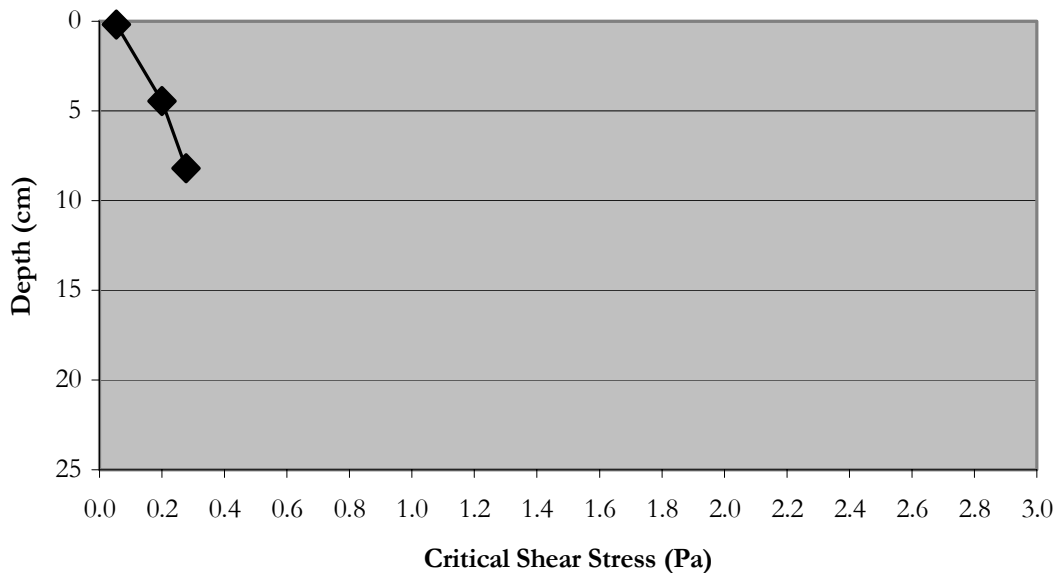
Figure 13b. Site SNL-9. Critical shear stress as a function of depth.

The mean particle size was fairly consistent with depth at ~60 µm except for a small increase at 13 cm to 76 µm (Figure 13c). The bulk density increased from the surface to the bottom of the core, although the magnitude of the density increases decreased with depth in the core, and ranged from 1.05 – 1.21 g/cm^3 (Figure 13d).

Figure 13c. Site SNL-9. Mean particle size as a function of depth.
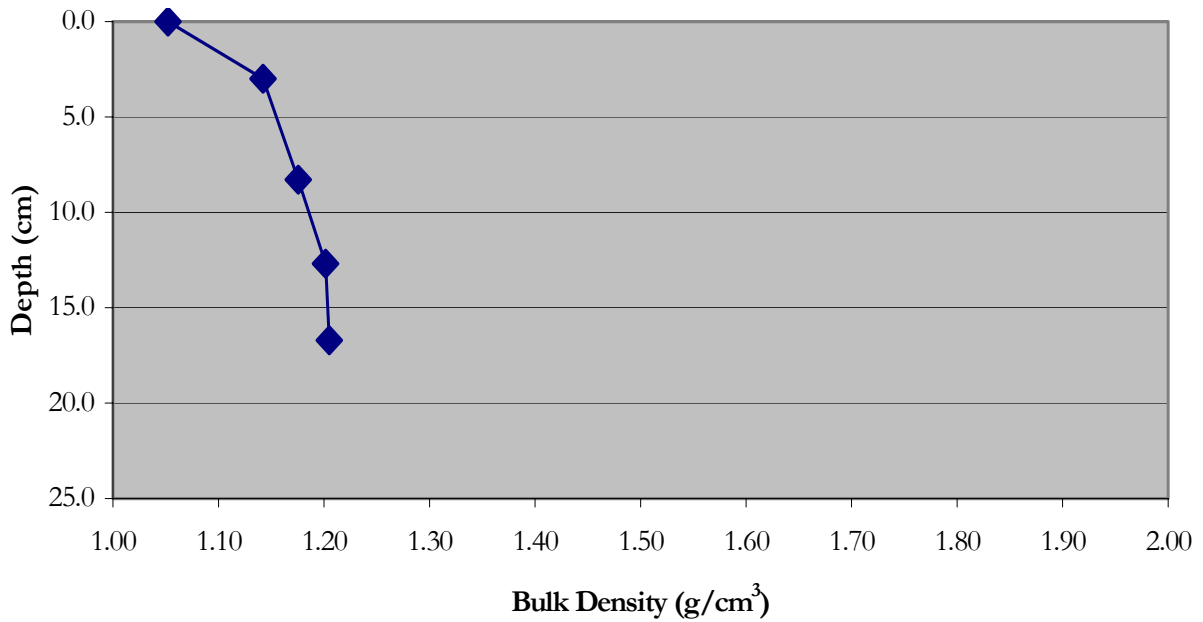
Figure 13d. Site SNL-9. Bulk Density as a function of depth.

The erosion core, SNL-10 was 19.5 cm long, with relatively large air pockets visible through the side of the sediment core (3-10 mm). The surface of this core was slightly harder than some of the previous cores in that the floc/fluff layer just began to move at 0.05 Pa, but completely eroded at 0.1 Pa in two minutes. The critical shear stress then rapidly increased to greater than 0.1 Pa and the erosion rates for all shear stresses decreased with depth (figure 14a, b). The maximum critical shear stress at the bottom of the core was just shy of 0.5 Pa.
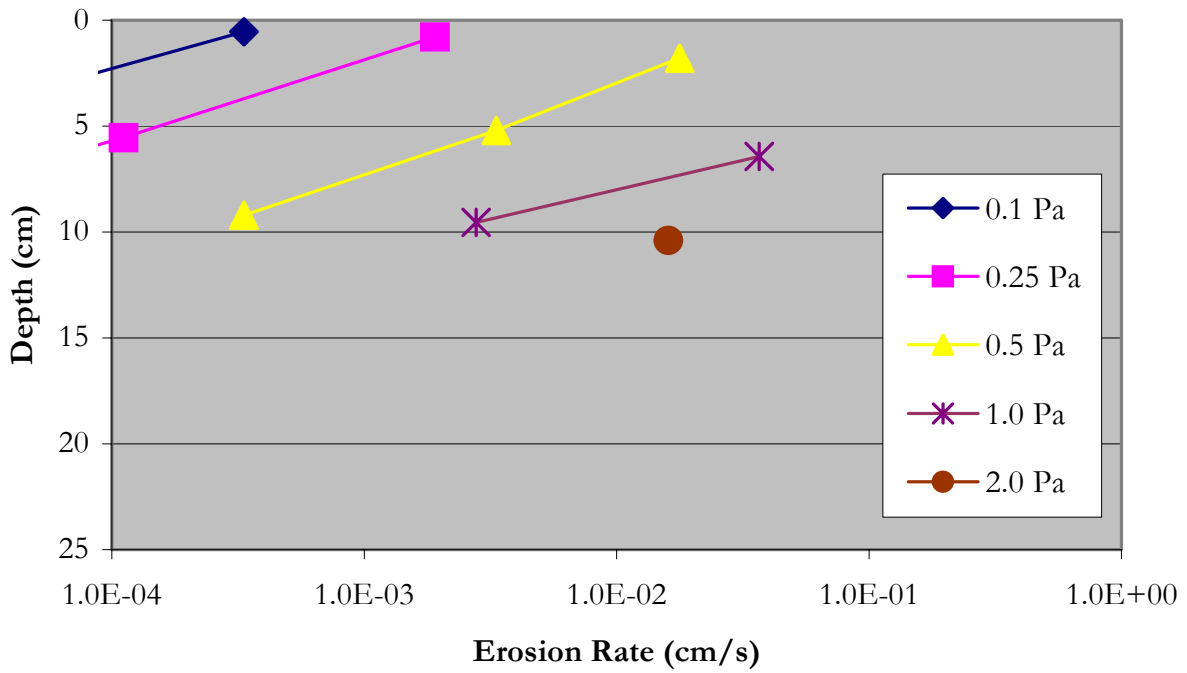
Figure 14a. Site SNL-10. Erosion rate as a function of depth with shear stress as a parameter. Erosion rates for shear stresses of 0.1, 0.25, 0.5, 1.0, and 2.0 Pa are shown. Core length of 19.5 cm.
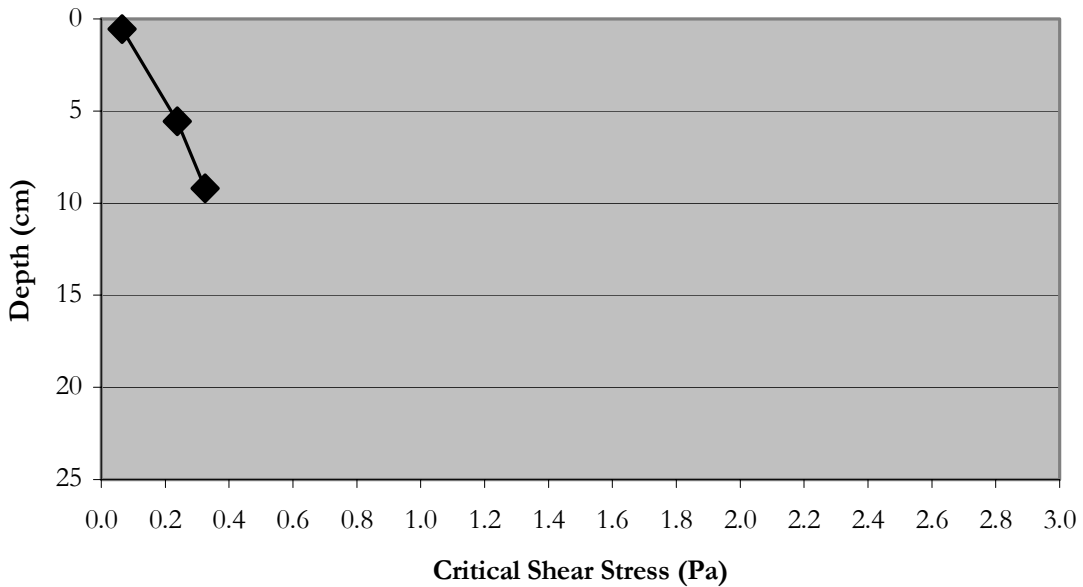

Figure 14b. Site SNL-10. Critical shear stress as a function of depth.

The mean particle size remained nearly constant with depth between 50-57 μm (Figure 14c). The bulk density increased with depth significantly between the surface and the layer

beneath and then showed a slight increase with depth for the remainder of the core (Figure 14d).

The bulk density ranged from 1.06-1.13 g/cm^3.

Figure 14c. Site SNL-10. Mean particle size as a function of depth.
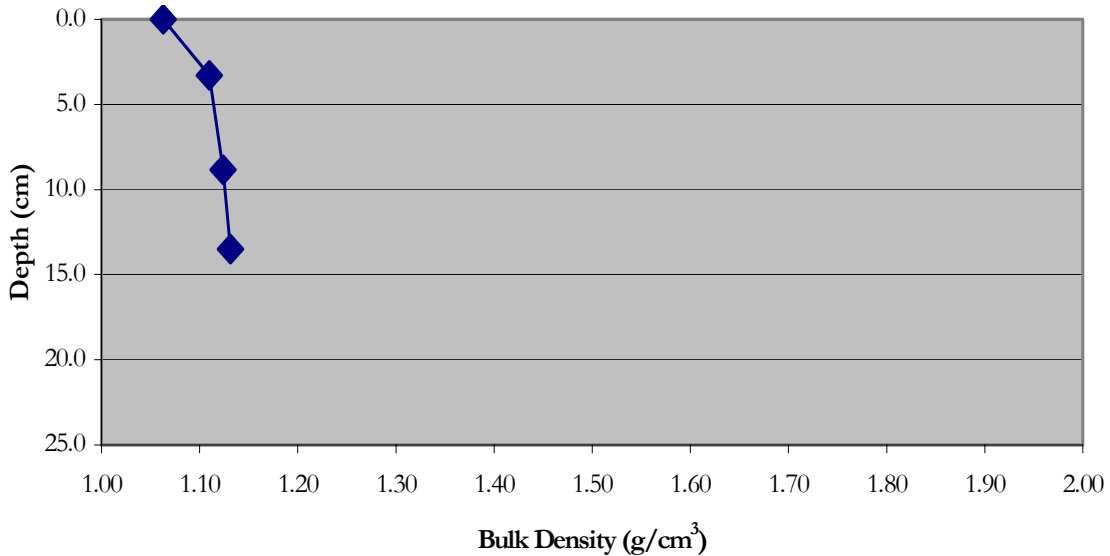
Figure 14d. Site SNL-10. Bulk Density as a function of depth.

The erosion core from site SNL-11 was 27 cm long that contained some air pockets visible from the side of the sediment core. This core displayed a different trend then most other cores in that the erosion occurred as aggregates that were largest near the surface and decreased with depth. In general, erosion rates decreased with depth for all shear stresses (figure 15a).

Near the bottom of the sediment core a rapid decrease in erosion rate is attributed to the presence of an abundance of long thin "hair-like" or "grass-like" organic material. The critical shear stress increased rapidly with depth initially, then the increased slowed through successive layers until the bottom of the core where the organic material stabilized the bed and an extremely rapid increase in critical shear was measured (Figure 15b). Critical shear was ~0.15 at the surface and increased to 1.9 Pa at the bottom of the sediment core.
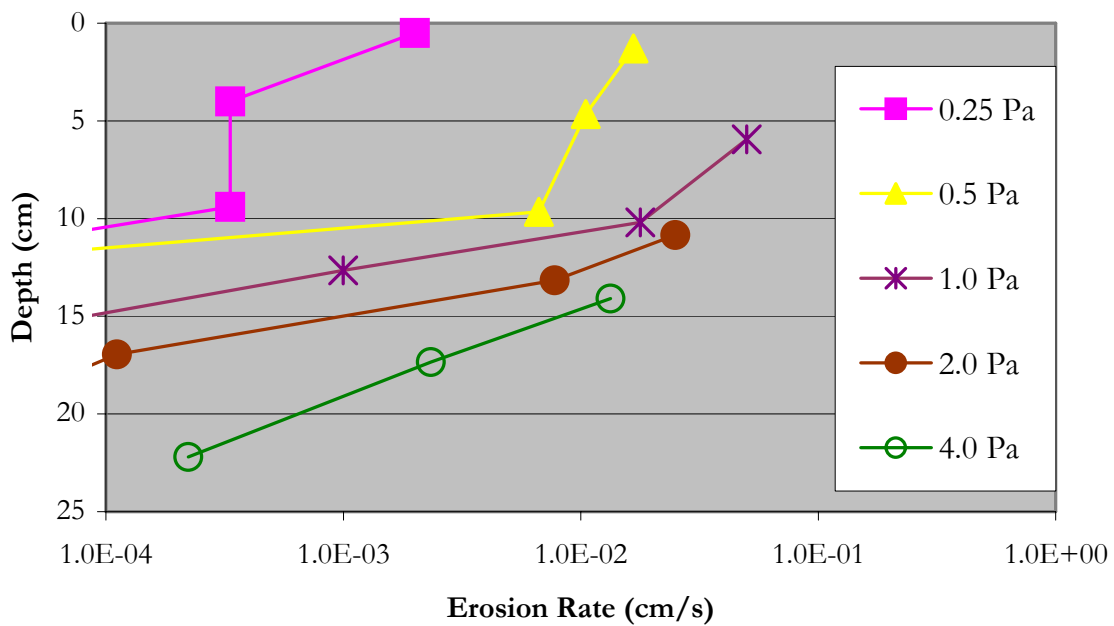

Figure 15a. Site SNL-11. Erosion rate as a function of depth with shear stress as a parameter. Erosion rates for shear stresses of 0.25, 0.5, 1.0, 2.0 and 4.0 Pa are shown. Core length of 27 cm.
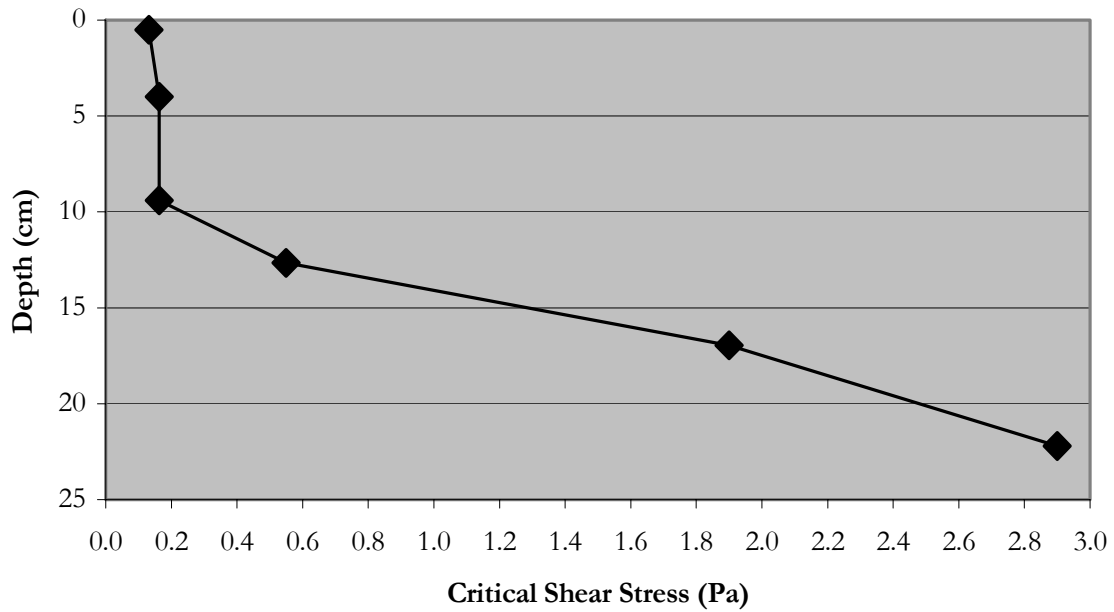
Figure 14b. Site SNL-10. Critical shear stress as a function of depth.

The mean particle size remained relatively constant with depth between 70-75 µm except for a small increase at 12 cm to 90 µm (Figure 15c). The bulk density increased significantly with depth for the first 8 cm, remained nearly constant to 12 cm and then decreased rapidly to the bottom of the core (Figure 15d). The decrease in bulk density near the bottom of the core is most likely a result of the presence high concentration of organic material observed at the bottom of the core. The bulk density magnitude and range was greater than that for most cores investigated, between 1.17-1.54 g/cm^3.
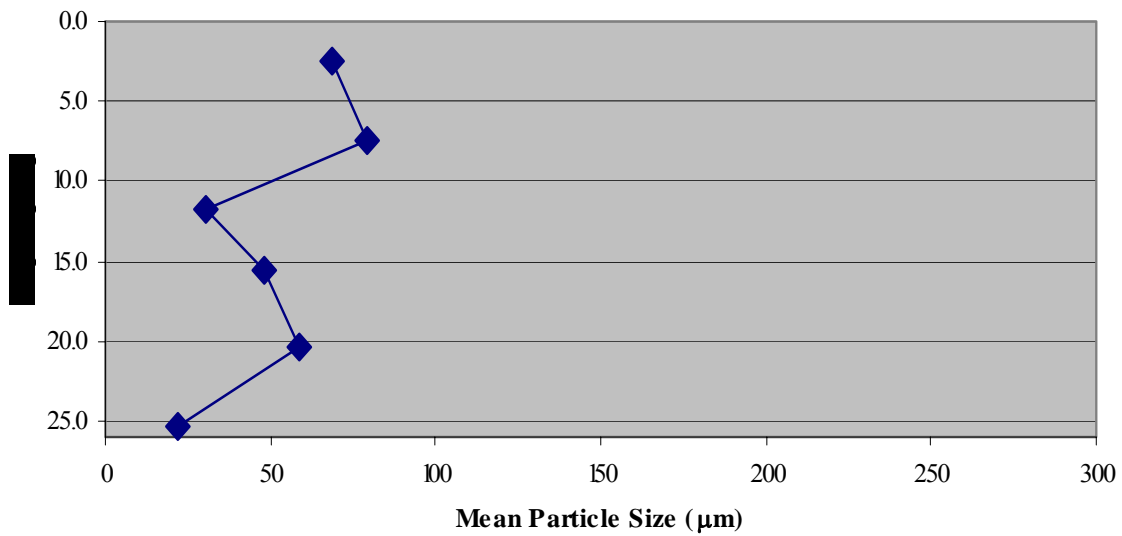
Figure 15c. Site SNL-11. Mean particle size as a function of depth.
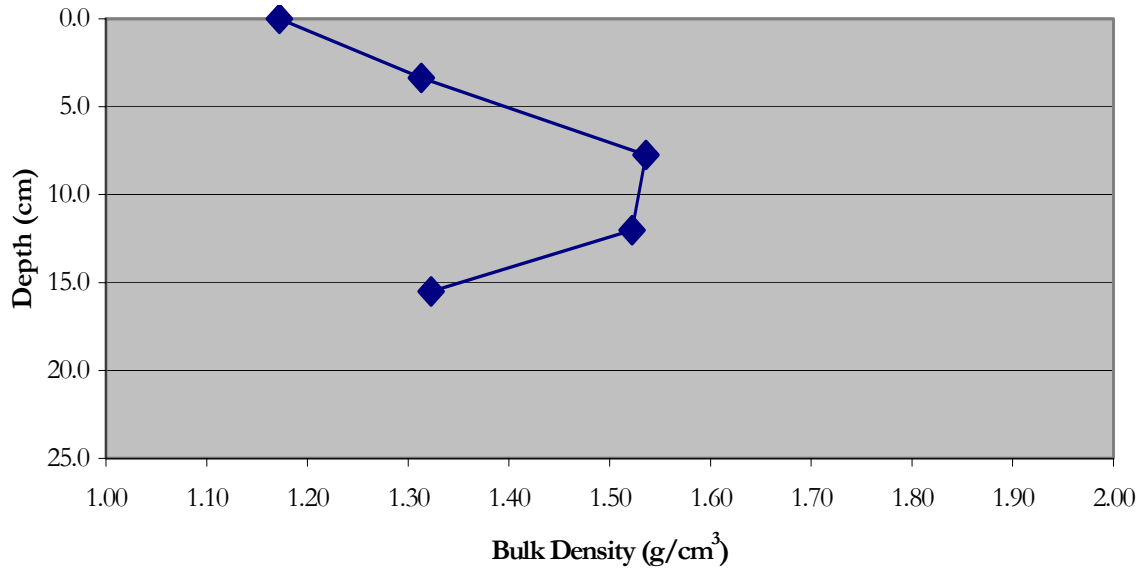
Figure 15d. Site SNL-11. Bulk density as a function of depth.

The site SNL-12 erosion core was just 16 cm long and contained only one visible air pocket that was ~5 mm in diameter. A 1-2 mm floc layer was completely eroded at 0.05 Pa. The remainder of the core became more erosion resistant with depth (figure 16a,b).
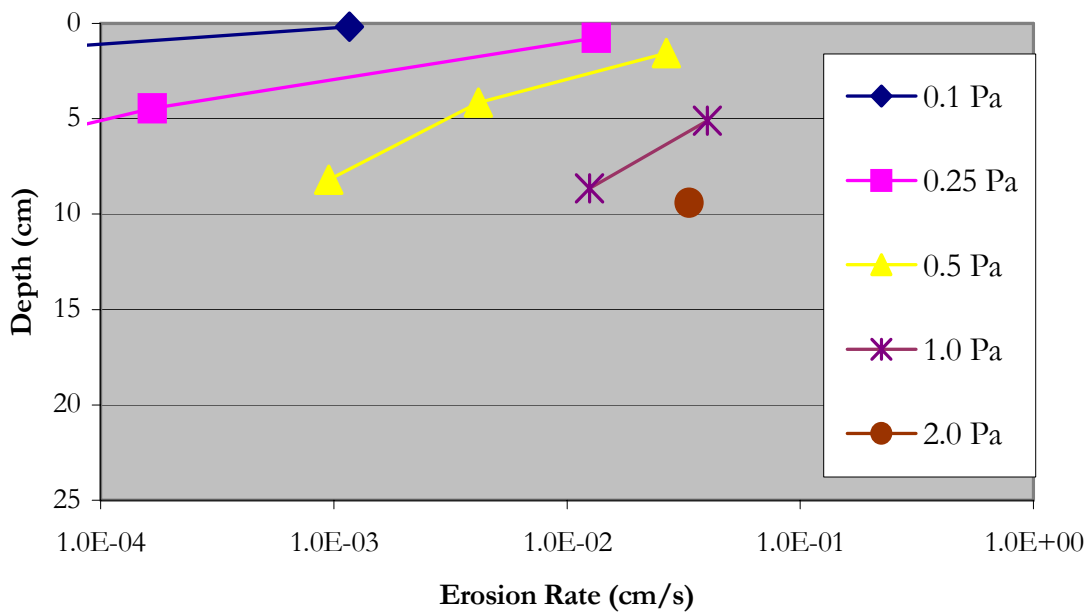
Figure 16a. Site SNL-12. Erosion rate as a function of depth with shear stress as a parameter. Erosion rates for shear stresses of 0.1, 0.25, 0.5, 1.0, and 2.0 Pa are shown. Core length of 16 cm.

Figure 16b. Site SNL-12. Critical shear stress as a function of depth.

The mean particle size decreased slightly with depth from 74 – 67 μm (Figure 16c). The bulk density increased with depth throughout the entire core (Figure 16d) to between 1.05-1.17 g/cm³.
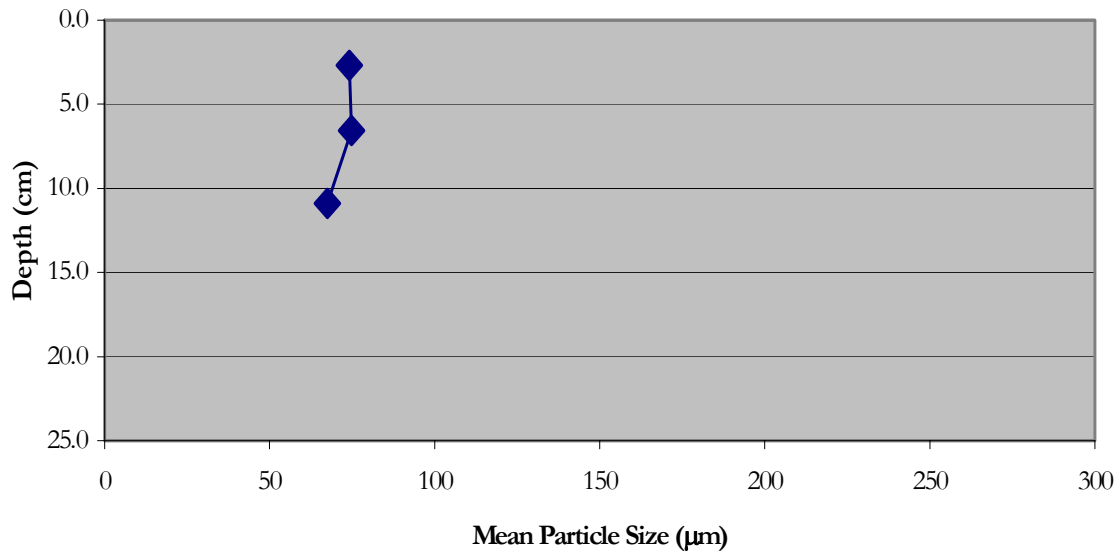
Figure 16c. Site SNL-12. Mean particle size as a function of depth.
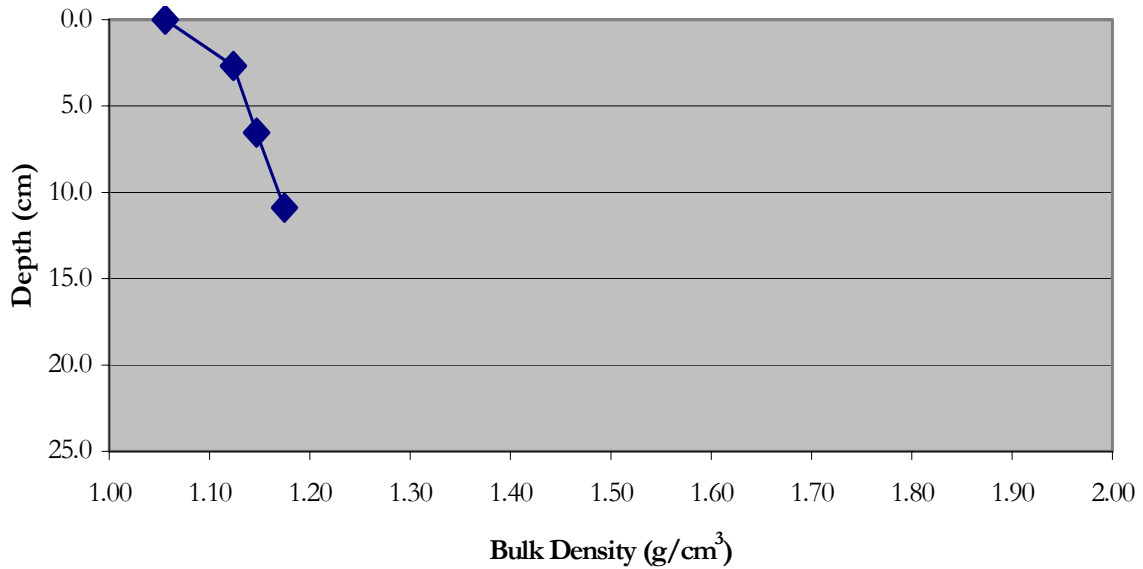
Figure 16d. Site SNL-12. Bulk density as **a function of depth.**

The erosion core from site SNL-13 was 17.5 cm long with small, ~1 mm diameter, air pockets visible from the side of the core. A 0.5-1 mm floc layer eroded away at 0.05 Pa. For all shear stresses tested the sediment erosion rates steadily decreased with depth (figure 17a) and the critical shear stress increased with depth (Figure 17b).
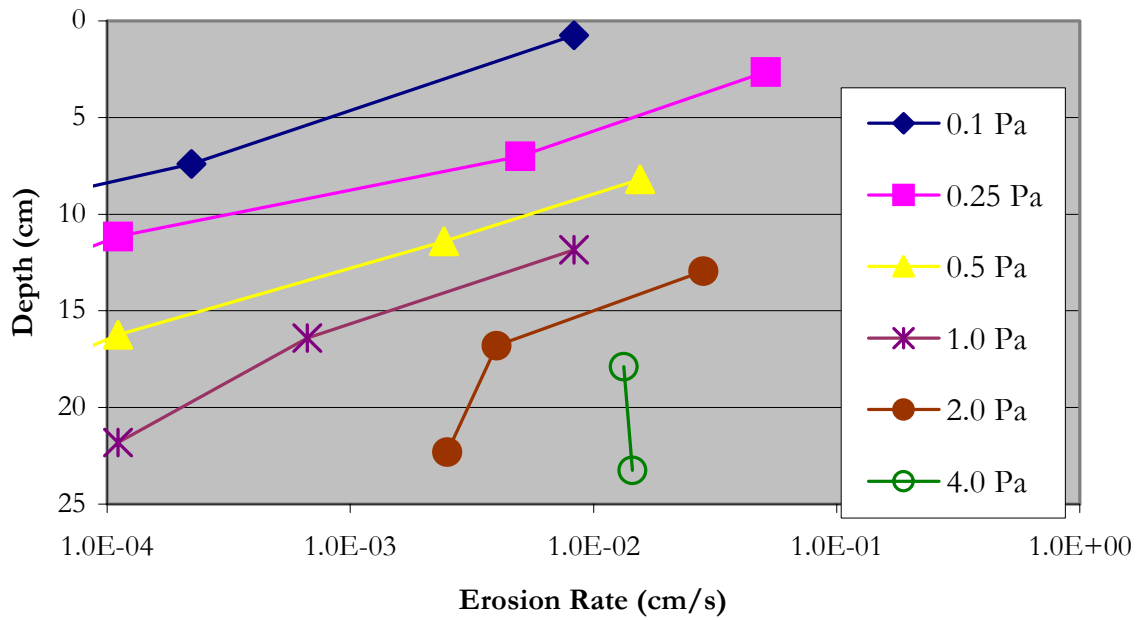
46

Figure 17a. Site SNL-13. Erosion rate as a function of depth with shear stress as a parameter. Erosion rates for sh**ear stresses of 0.1, 0.25, 0.5, 1.0, and 2.0 Pa are shown. Core length of 16 cm.**
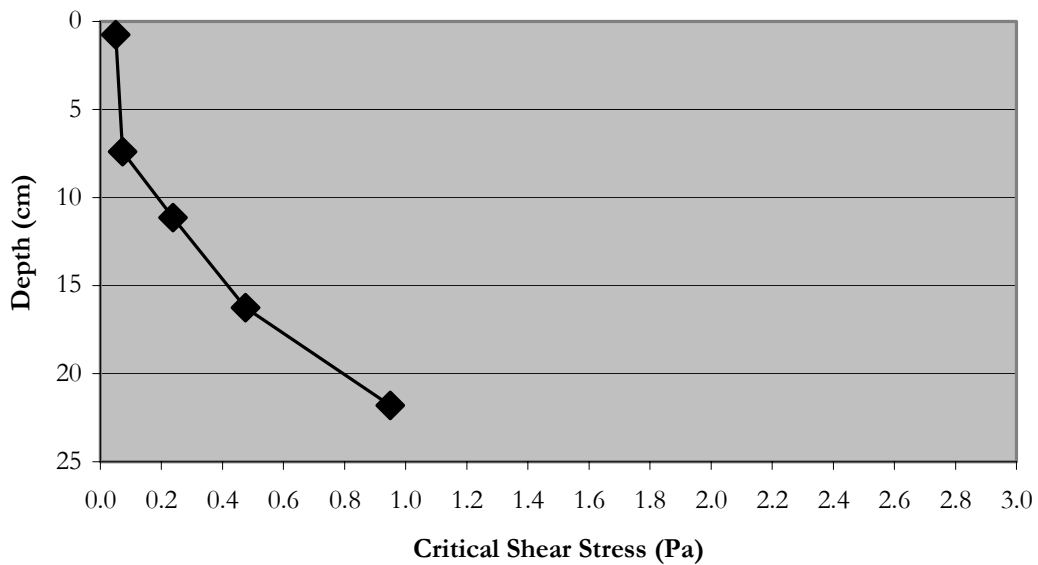

Figure 17b. Site SNL-13. Critical shear stress as a function of depth.

The mean particle size decreased with increasing depth in the core, from 65 μm near the surface to 35 μm near the bottom (figure 17b). The bulk density increased with depth, with larger increases measured deeper in the core (figure 17c) and ranging from 1.09-1.17 g/cm³.
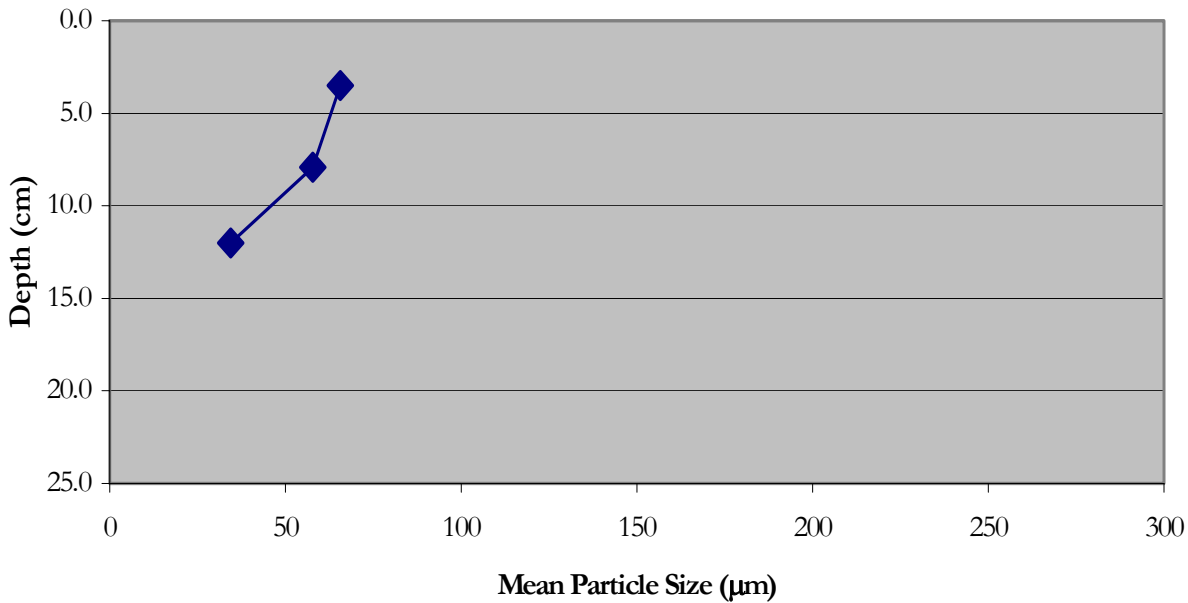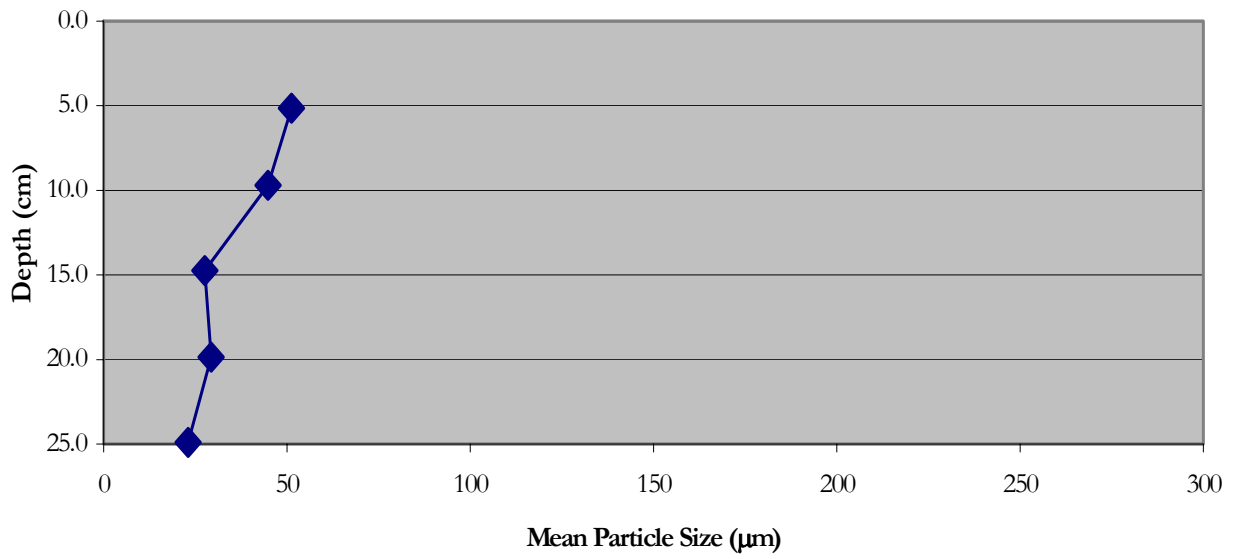

Figure 17b. Site SNL-13. Mean particle size as a function of depth.
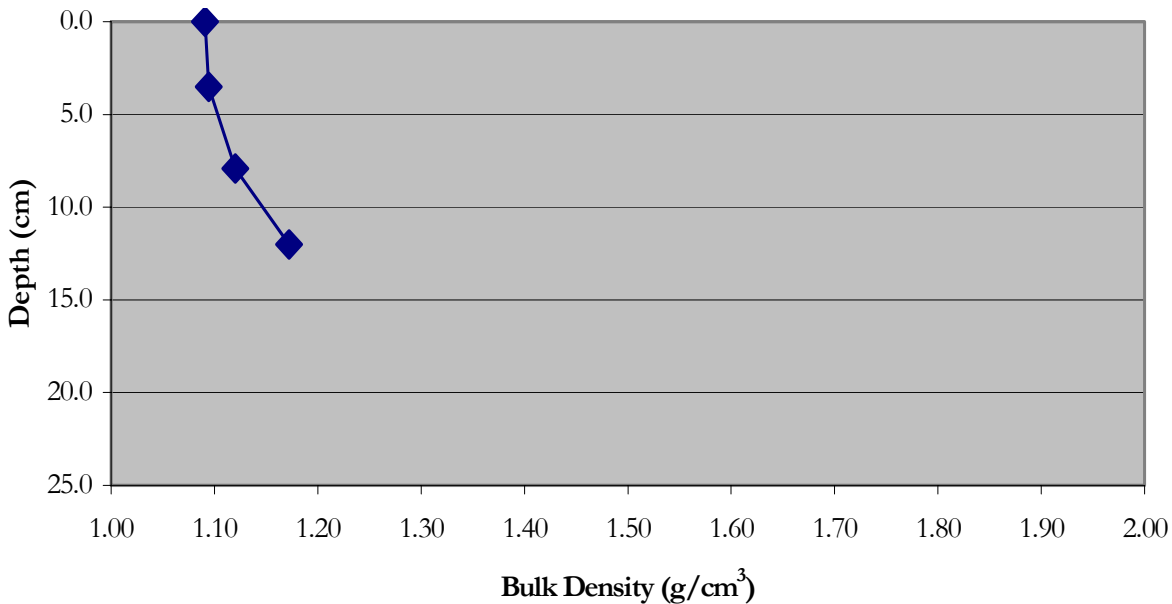
Figure 17c. Site SNL-13. Bulk Density as a function of depth.

The core from site SNL-14 was 35 cm long and contained two distinct layers. The upper layer was dark brown/black, extending 10-15 cm below the surface, and the lower layer was

lighter gray and contained some small air pockets. A 0.5 mm floc layer eroded instantly at 0.1 Pa and the erosion rate was zero at 0.1 Pa below this surficial layer. In general the erosion rates decreased and critical shear increased with increasing depth in the core (figure 18a,b). Around 12 cm deep the core became significantly more erosion resistant (decreased erosion rates) and a layer of grass or crop residue was first observed. Below this layer the erosion rates steadily decrease for all applied shear stresses and the concentration of organic material in the form of crop residue or grass increases.
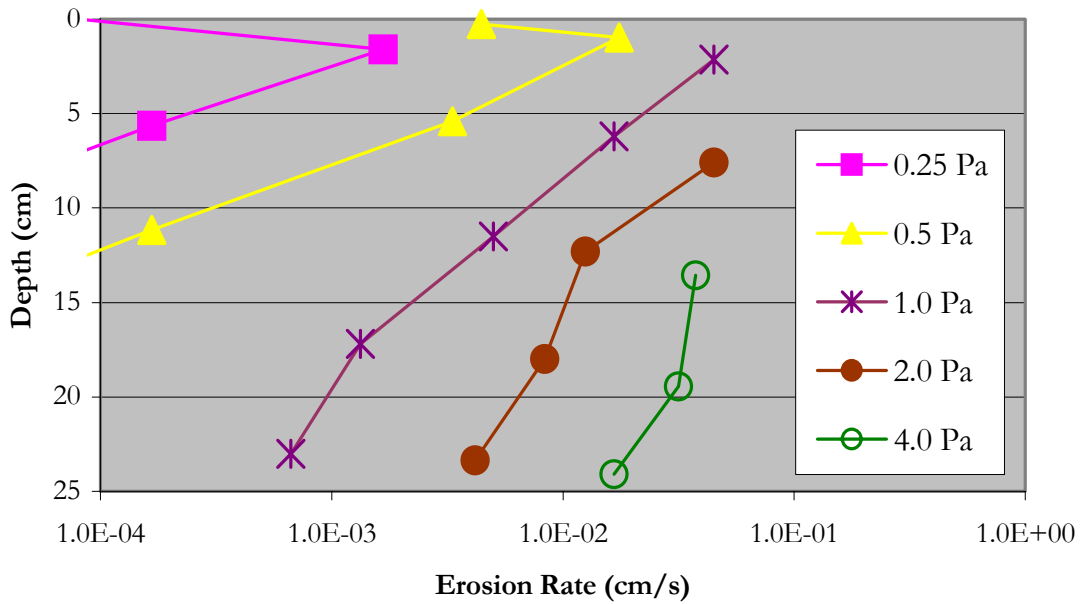

Figure 18a. Site SNL-14. Erosion rate as a function of depth with **shear stress as a parameter. Erosion rates for shear stresses of 0.25, 0.5, 1.0, 2.0 and 4.0 Pa are shown. Core length of 16 cm.**
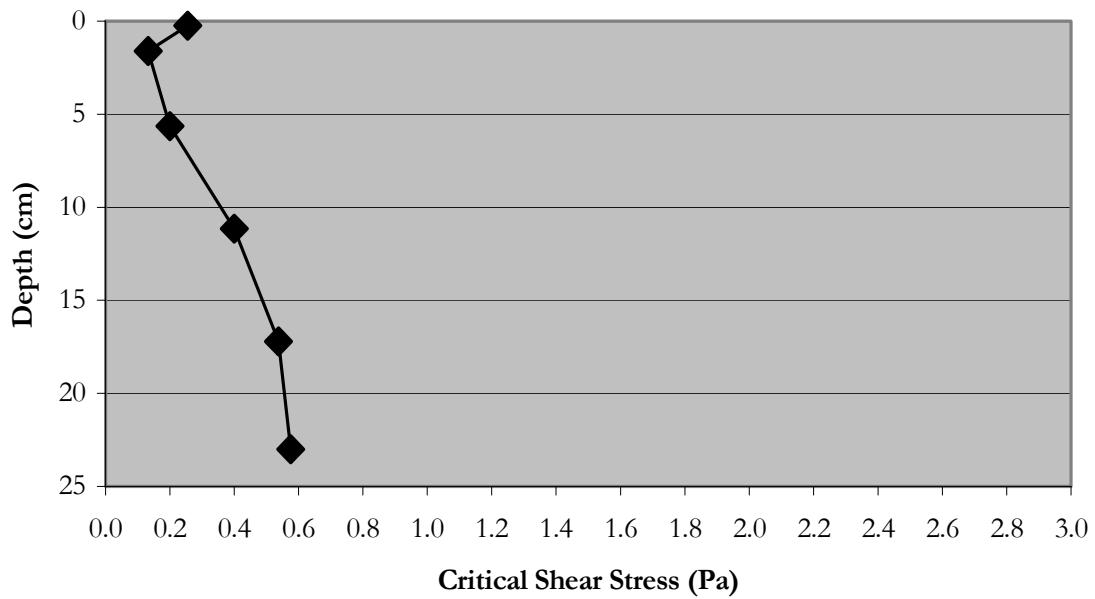
Figure 18b. Site SNL-14. Critical shear stress as a function of depth.

In general, the mean particle size decreased with depth in the core (Figure 18c), but much more staggered than in most other cores investigated. In the first two layers the particle size ranged from 68 –79 μm, then it dramatically decreased to 30 μm, increasing through the next two layers to 48 and 58 μm respectively before decreasing to 22 μm at the bottom of the core. The bulk density showed a general increase with depth in the core (Figure 18d) with a localized decrease in density between 15-20 cm, where the organic material was observed in its highest concentrations. Bulk density ranged from 1.04 at the surface to 1.19 at the bottom.
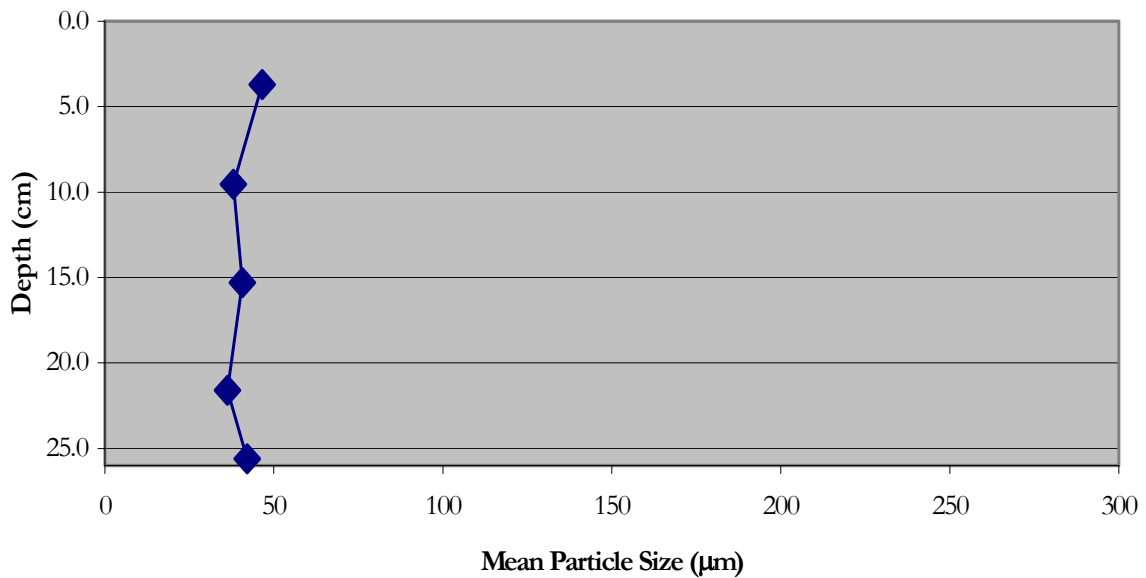
Figure 18c. Site SNL-14. Mean particle **size as a function of depth.**
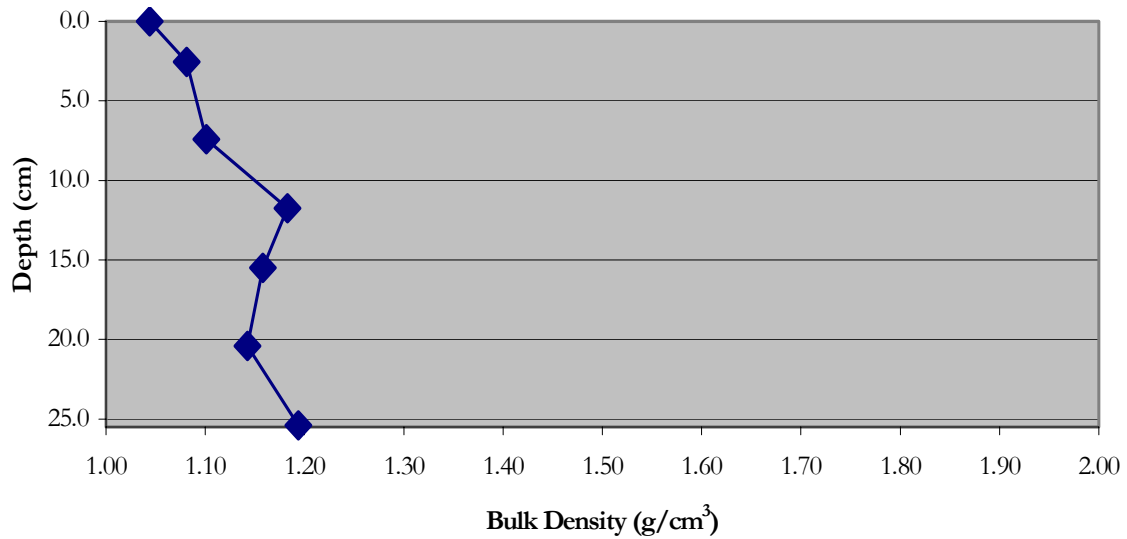
Figure 18d. Site SNL-14. Bulk density as a function of depth.

The erosion core from site SNL-15 was 30.5 cm long and had a thick floc layer that seemed to blend in with the remainder of the core at about 1.5 cm deep. Large air pockets were visible in the side of the core (~1 cm). The erosion rates steadily decreased throughout most of the core with an exception near the bottom (figure 19a), where at both 2.0 and 4.0 Pa the sediment began to breakup and erode in very large aggregates on the order of 2 cm.

Figure 19a. Site SNL-15. Erosion rate as a function of depth with shear stress as a parameter. Erosion rates for shear stresses of 0.1, 0.25, 0.5, 1.0, 2.0 and 4.0 Pa are shown. Core length of 16 cm.

Figure 19b. Site SNL-15. Critical shear stress as a function of depth.

The mean particle size gradually decreased with depth in the core, between 58 µm near the surface and 23 µm at the bottom (Figure 19c). The bulk density gradually increased with depth, between 1.04 g/cm³ at the surface to 1.14 g/cm³ at the bottom (Figure 19d).

Figure 19c. Site SNL-15. Mean particle size as a function of depth.
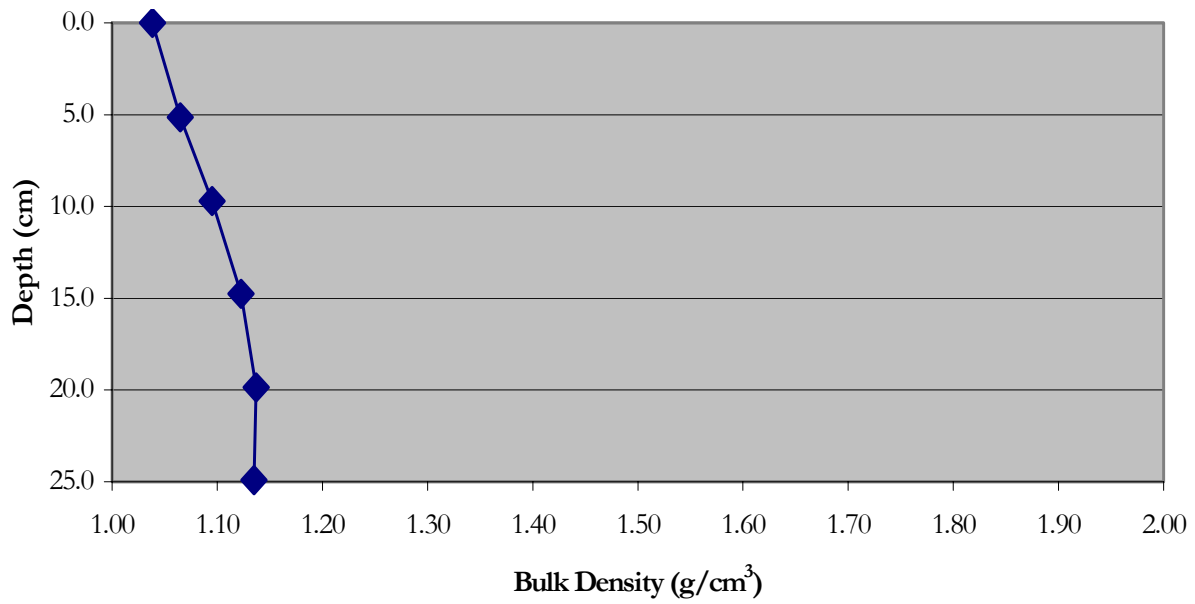
Figure 19d. Site SNL-15. Bulk density as a function of depth.

The erosion core from site SNL-16 was 33 cm long and had a hard surface layer with a critical shear between 0.25 and 0.5 Pa. Once this layer was eroded away erosion rates at all shear stresses decreased with depth in the sediment core (Figure 20a) and the critical shear stress increased (Figure 20b). Erosion was in the form of small aggregates (0.5-2 mm) through the first half of the core and increased deeper in the core to over 1 cm in diameter.

Figure 20a. Site SNL-16. Erosion rate as a function of depth with shear stress as a parameter. Erosion rates for shear stresses of 0.25, 0.5, 1.0, 2.0 and 4.0 Pa are shown. Core length of 33 cm.

Figure 20b. Site SNL-16. Critical shear stress as a function of depth.

The mean particle size remained fairly constant with depth, ranging between 36 and 46 μm (Figure 20c). The bulk density gradually increased with depth, ranging between 1.04 and 1.17 g/cm³ (Figure 20d).

Figure 20c. Site SNL-16. Mean particle size as a function of depth.

55
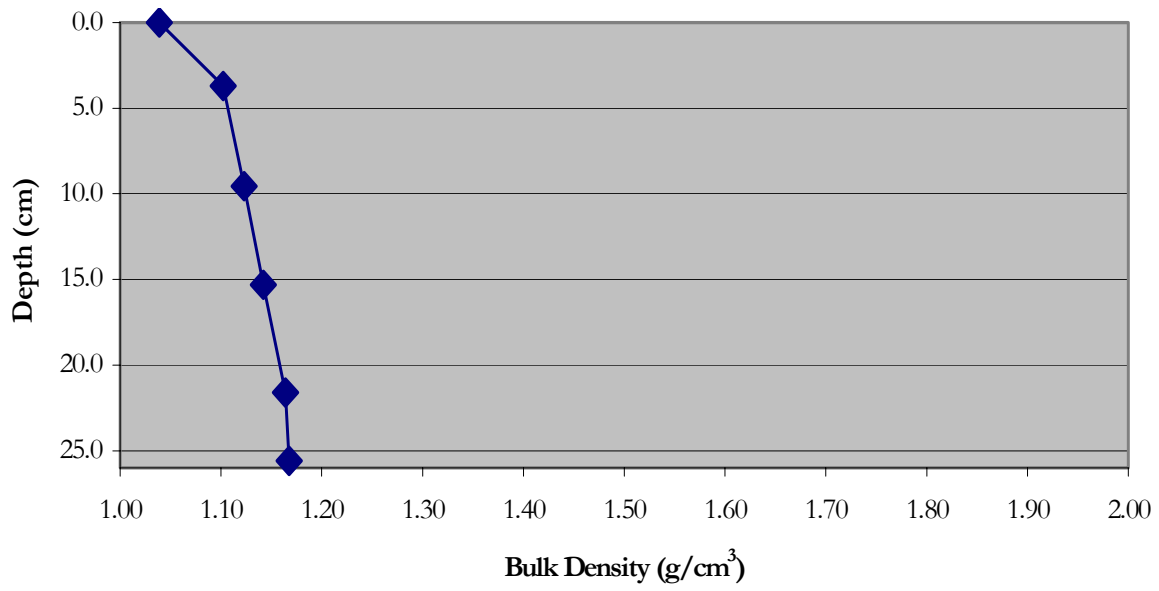
Figure 20d. Site SNL-16. Bulk density as a function of depth.

3.2 Ponar and grab samples

Surface sediment samples were collected at various locations around Cedar Lake using both a ponar device and manually grabbed while wading in shallow water near the lakes edge (figures 2 and 3). The mean particle size of each sample is tabulated below.

Table 1: Mean Particle Size of the Ponar Sediment Samples

Sample ID	Mean Particle Size (µm)
P1	333.22
P2	76.37
P3	226.14
P4	145.97
P5	168.51
P6	15.89
P7	111.76
P8	111.62
P9	267.5
P10	152.98
P11	328.48
P12	192.07
P13	218.67
P14	182.02
P15	154.04
P16	45.82
P17	89.62
P18	50.11
P19	60.61
P20	58.18
P21	69.29
P22	103.07
P23	120.75
P24	94.7
P25	(>1 mm)*
P26	89.09
P27	62.00
P28	98.48
P29	66.81
P30	96.02
P31	121.03
P32	107.02
P33	129.91
P34	63.87

* All particles in this sample were greater than 1 mm and could not be analyzed with the laser particle sizer.

Table 2: Mean Particle Size of the Grab Sediment Samples

Sample ID	Mean Particle Size (μm)
G1	47.65
G2	336.47
G3	240.91
G4	341.57
G5	21.02
G6	254.00
G7	304.81
G8	302.46

3.3 Surface water samples

Water samples were collected within the northern, middle and southern basins of Cedar Lake in June and July of 2005. The mean particle size of each sample is tabulated below.

Table 3: Mean Particle Size of the Water Samples

Sample ID	Mean Particle Size (μm)
JUN-NB	44.94
JUN-MB	34.54
JUN-SB	33.60
JUL-NB	25.56
JUL-MB	47.65
JUL-SB	30.49

4.0 Discussion and Concluding Remarks

In general, the erosion characteristics and bulk properties for sediment erosion cores SNL-2 through SNL-16 were reasonably consistent while SNL-1, located in the southeast corner of Cedar Lake and fairly close to the marina, contained a much higher fraction of coarse-grained sediment, significantly increasing the bulk density. SNL-1 also varied in that it eroded in a particle-by-particle manner where as the rest of the cores, being much finer grained, eroded as aggregates/chunks consisting of much finer particles. For cores SNL-2 through SNL-16 aggregate sizes tended to increase at higher shear stresses and deeper in the core. This phenomenon was enhanced in the presence of larger organic matter such as leaves and sticks and was retarded or the reverse trend was observed when finer organic matter, such as grass or crop residue, helped to bind the sediments deeper in the core (SNL-11). In general, visual observation deemed that the aggregates transported mostly as bedload at shear stresses less than 0.5 Pa and mostly in suspension at shear stresses greater than 0.5 Pa. Although, this was a sliding scale and depended on the size of the eroded aggregates and their density. As the aggregate size and/or density increased so too did the fraction of eroded sediment that transported as bedload. Although air pockets were present in most of the erosion cores, they did not have an appreciable/noticeable effect on sediment erosion rates or critical shear stresses.

For many of the sediment cores, it is easy to see that a decrease in erosion was directly tied to an increase in bulk density. This has been well documented (Jepsen et al, 1997a; Roberts et al, 1998) and is simply the result of sediments becoming more stable at greater states of consolidation. An exception to this rule was observed when an increased amount of organic matter helped to stabilize the sediment bed (decrease erosion) but also served to decrease the bulk density of the sediment.

Table 4: Summary of Bulk Properties for the Erosion Cores

Sample ID	Critical Shear Stress (Pa)		Mean Particle Size (μm)		Bulk Density (g/cm^3)	
	Low	High	Low	High	Low	High
SNL-1	0.24	0.6	190	250	1.52	1.84
SNL-2	0.06	0.27	38	67	1.10	1.17
SNL-3	0.06	0.65	30	56	1.09	1.16
SNL-4	0.05	0.61	18	25	1.04	1.15
SNL-5	0.06	0.30	25	29	1.10	1.17
SNL-6	0.07	1.5	6	62	1.08	1.11
SNL-7	0.06	2.0	25	29	1.05	1.13
SNL-8	0.06	0.53	37	72	1.10	1.16
SNL-9	0.07	0.48	60	76	1.05	1.21
SNL-10	0.06	0.48	50	57	1.06	1.13
SNL-11	0.14	1.9	70	95	1.17	1.54
SNL-12	0.05	0.28	67	76	1.05	1.17
SNL-13	0.07	0.33	35	65	1.09	1.17
SNL-14	0.13	2.9	22	79	1.04	1.19
SNL-15	0.05	0.95	23	58	1.04	1.17
SNL-16	0.13	0.56	36	46	1.07	1.17

In the present study, the erosion rates of relatively undisturbed sediments from 16 locations around Cedar Lake have been determined as a function of depth and shear stress. The bulk properties of particle size, size distribution, and bulk density were also determined with depth for each erosion core. The erosion cores displayed similar characteristics in their erosion and bulk properties with the exception of SNL-1.

In addition, particle size and size distribution for 42 surface sediment samples (34 collected with a ponar device and 8 sediment samples collected by hand while wading in shallow water) were measured. Finally, particle size and size distribution was determined for 6 water samples collected at three different locations for two separate sampling trips. All of

this information will be used in the development of a numerical model to predict the effect of sediment erosion and re-suspension on the water quality in Cedar Lake.

5.0 References

Jepsen, R., J. Roberts, and W. Lick, 1997a. Effects of Bulk Density on Sediment Erosion Rates, *Water, Air, and Soil Pollution*. Vol. 99, pp. 21-31.

Jepsen, R., J. Roberts, and W. Lick, 1997b. Long Beach Harbor Sediment Study, Report Submitted to U.S. Army Corps of Engineers, DACW09-97-M-0068

Jepsen, R., J. Roberts, J. Gailani, 2003. Effects of bedload and suspended load on the separation of sands and fines in mixed sediment, Journal of Waterway, Port, Coastal, and Ocean Engineering, submitted.

McNeil, J., C. Taylor, and W. Lick, 1996. Measurements of the Erosion of Undisturbed Bottom Sediments with Depth, *Journal of Hydraulic Engineering*. Vol. 122, No. 6, pp. 316-324.

Roberts, J., Jepsen, R., and Lick, W, 2000. Effects of Particle Size and Bulk Density on the Erosion of Quartz Particles, *Journal of Hydraulic Engineering*, Vol 124, No. 12: 1261-1267.

Roberts, J., Jepsen, R., Bryan, C., and Chapin, M. 2000. Boston Harbor Sediment Study, SAND 2001-2226, Sandia National Labs, Albuquerque, New Mexico, 87185. Report to the U.S. Army Corps of Engineers, New England District.

Roberts, J., and Jepsen, R. 2000. Development for the Optional Use of Circular Core Tubes with the High Shear Stress Flume. SNL report to the US Army Corps of Engineers, Waterways Experiment Station.

Roberts, J., R. Jepsen, S. James, 2003. Measurements of Sediment Erosion and Transport with the ASSET Flume, *Journal of Hydraulic Engineering*, Vol. 129, No. 11: 862-871, 2003.

Schlichting, H., 1979. *Boundary-Layer Theory*. Seventh Edition, McGraw-Hill.

SPEA, 1984. Cedar Lake Restoration Feasibility Study: Final Report. Prepared for Clean Lakes Coordinator, State of Indiana. Bloomington, Indiana. January.

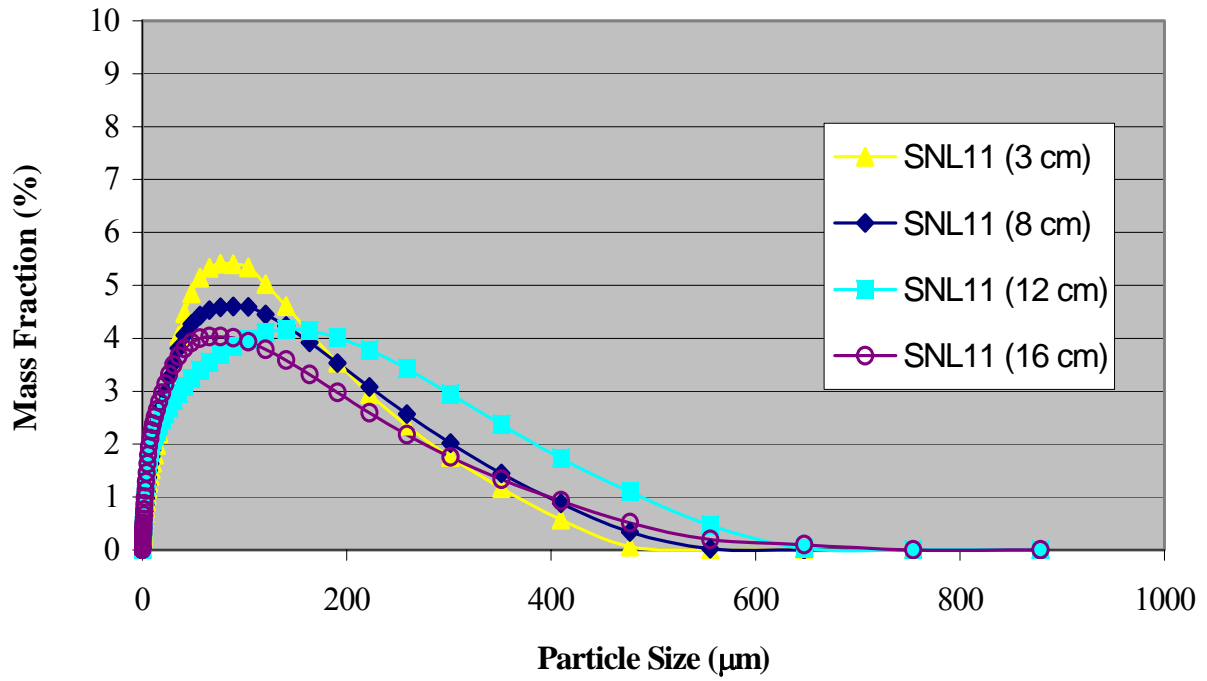# Appendix A: Particle Size Distributions for SNL-1 - SNL-16
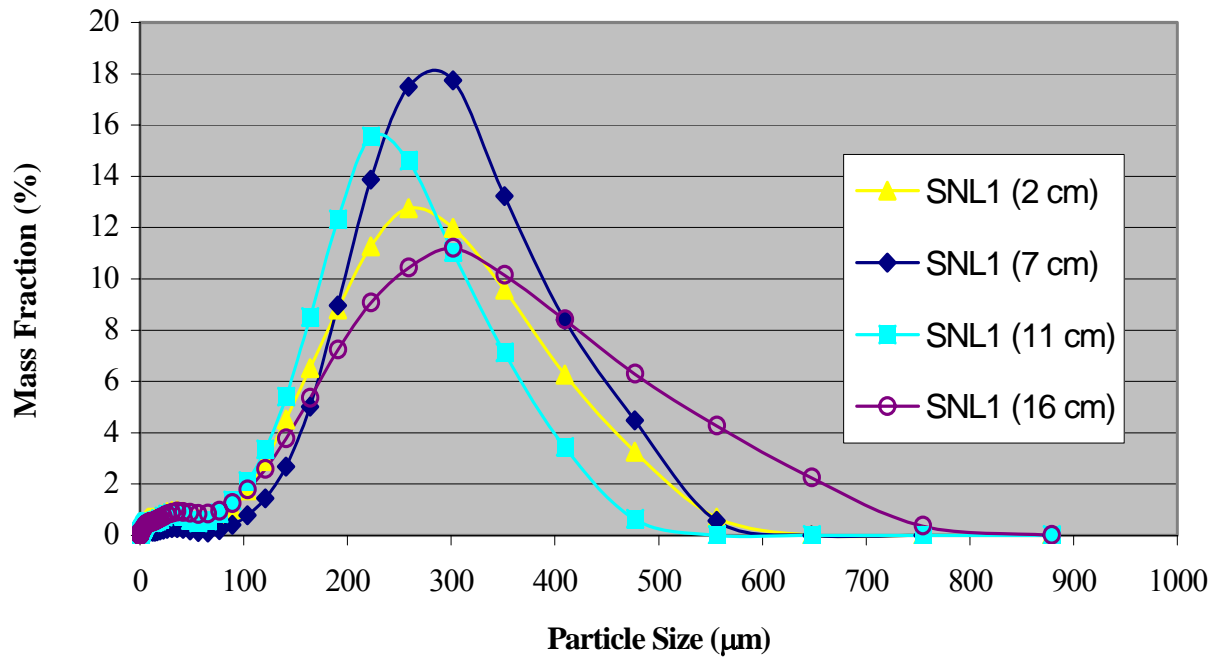
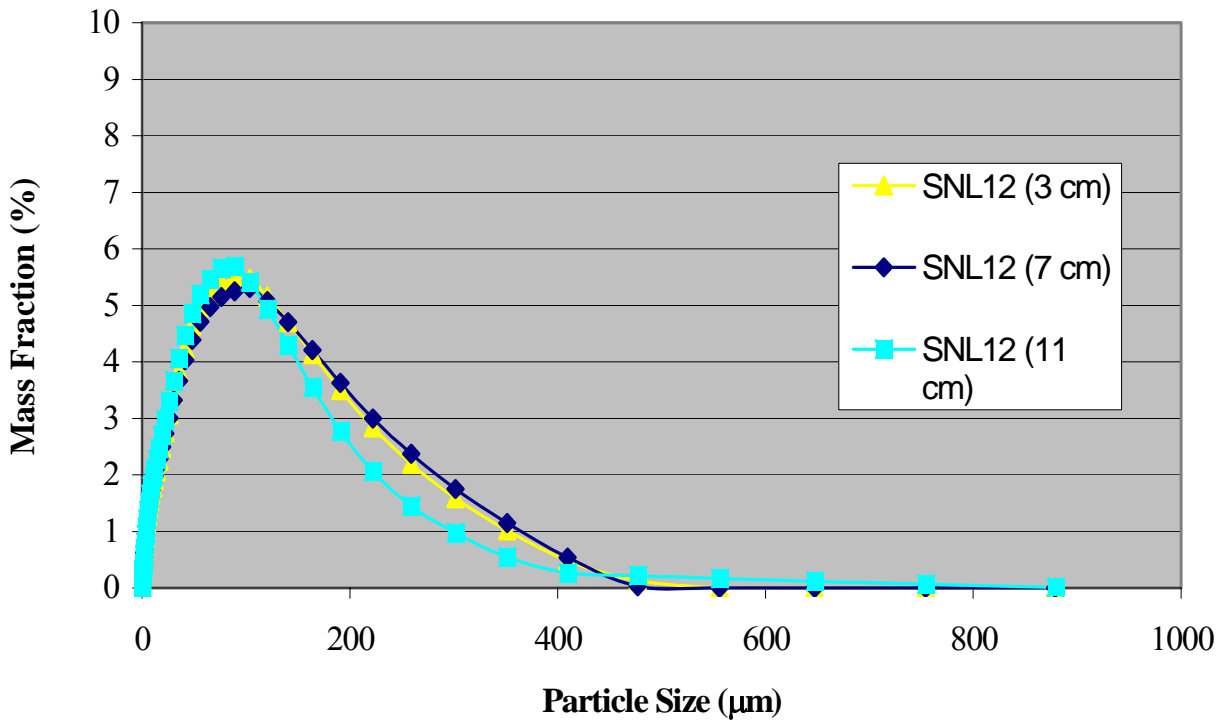**Figure 21.** Particle size distributions for SNL-1.
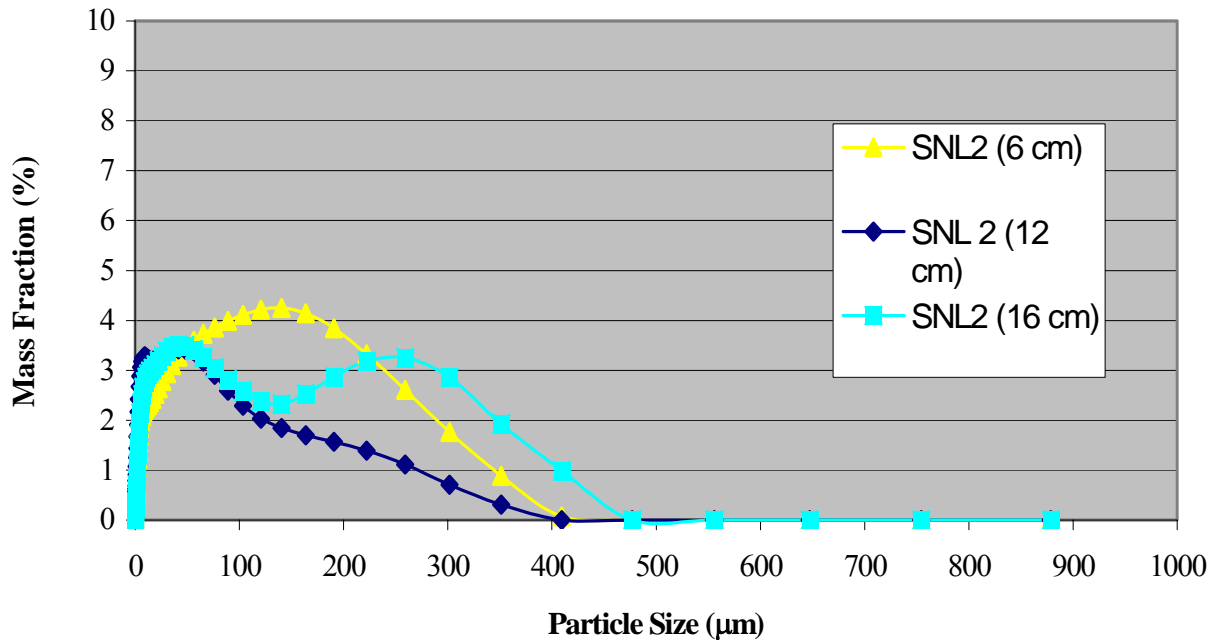
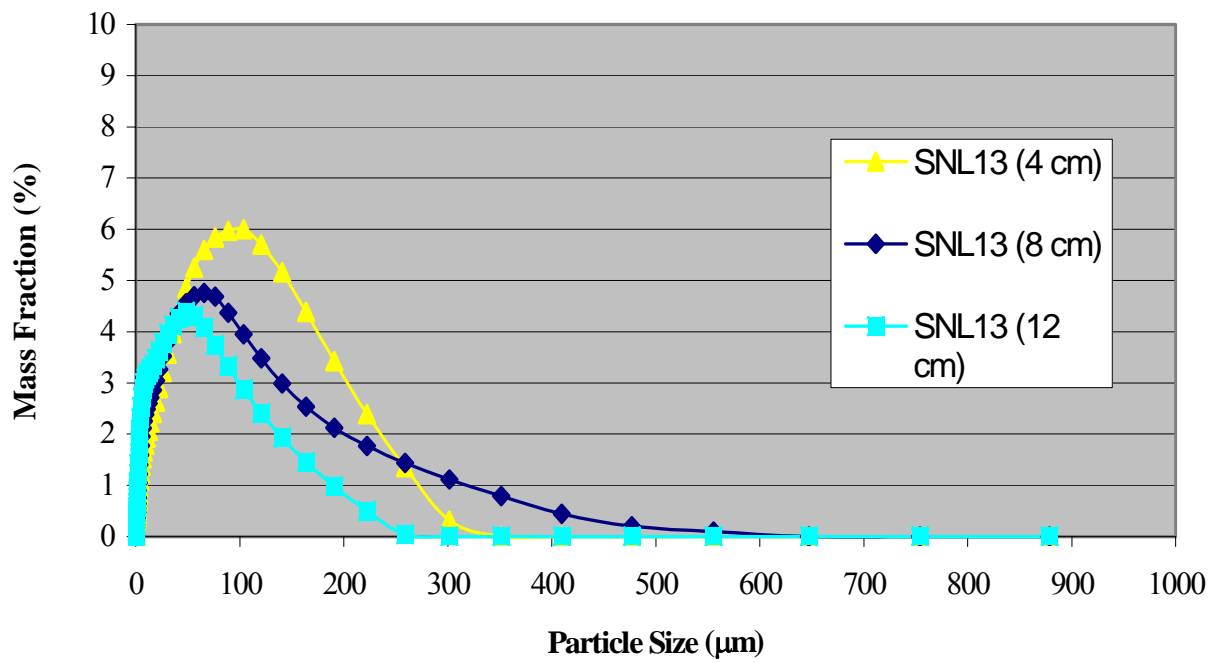**Figure 22.** Particle size distributions for SNL-2.
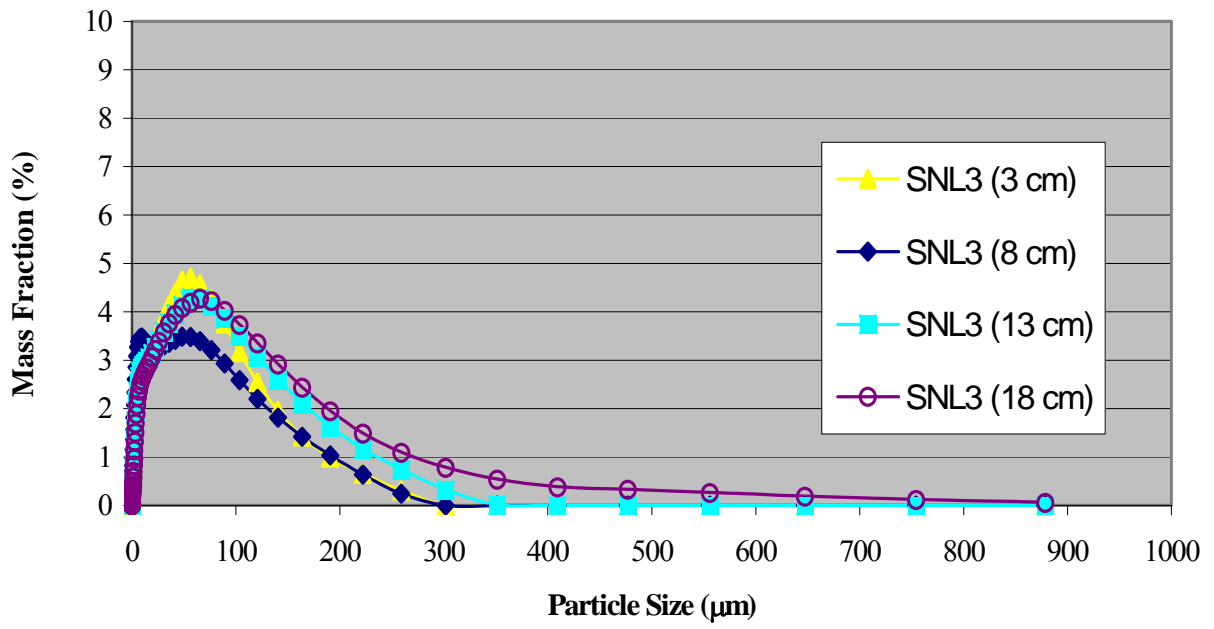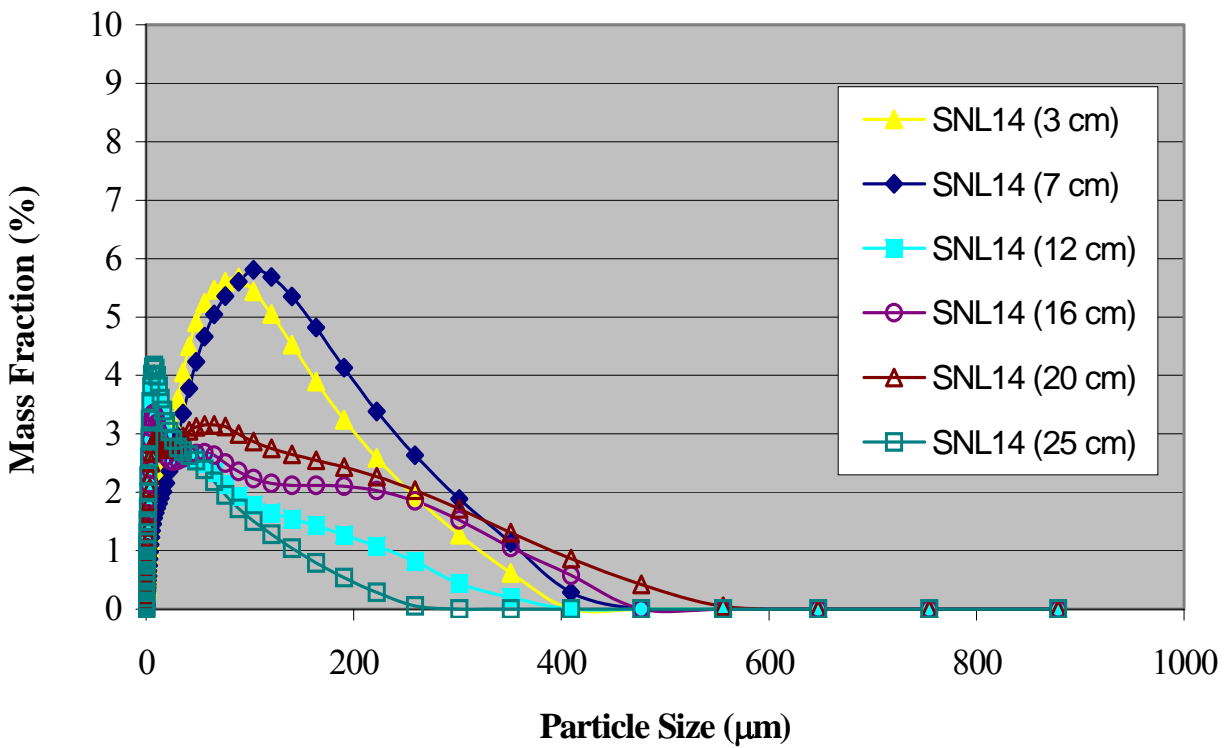
Figure 23. Particle size distributions for SNL-3.
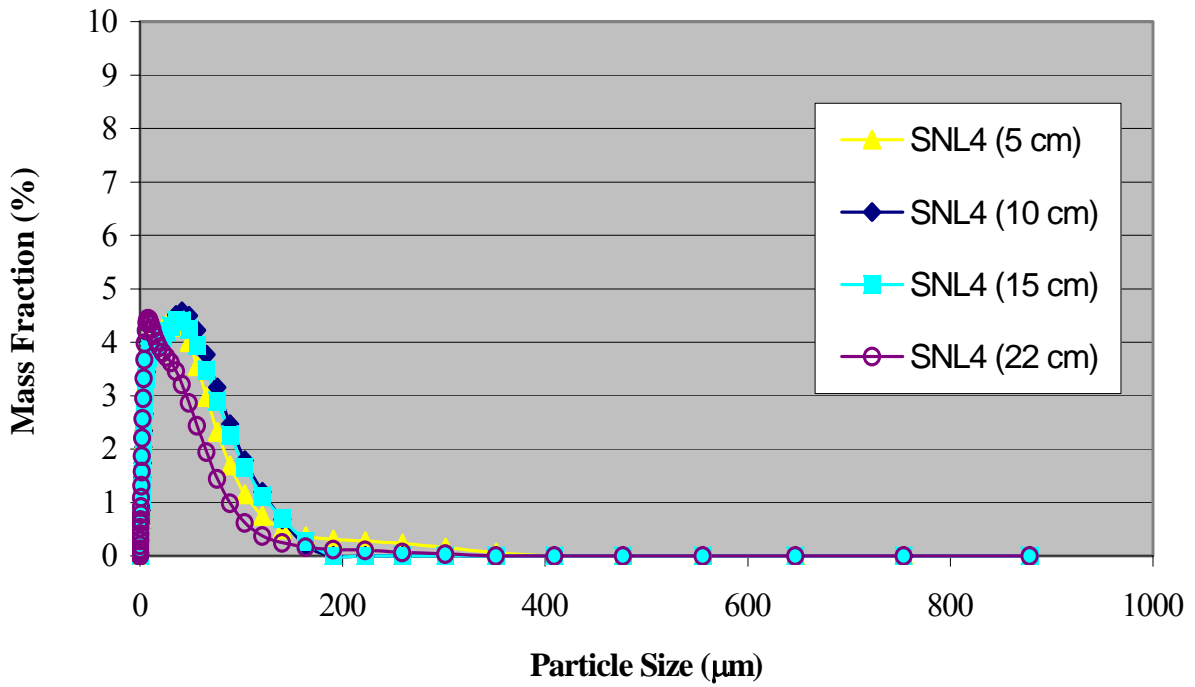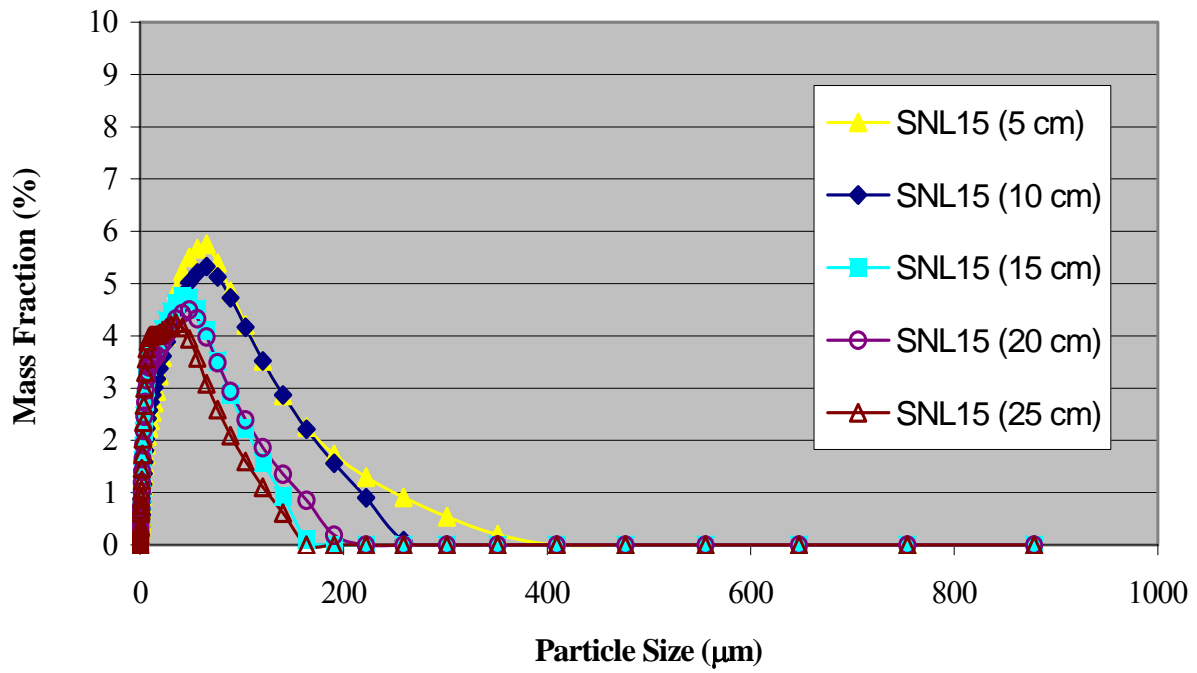

Figure 24. Particle size distributions for SNL-4.
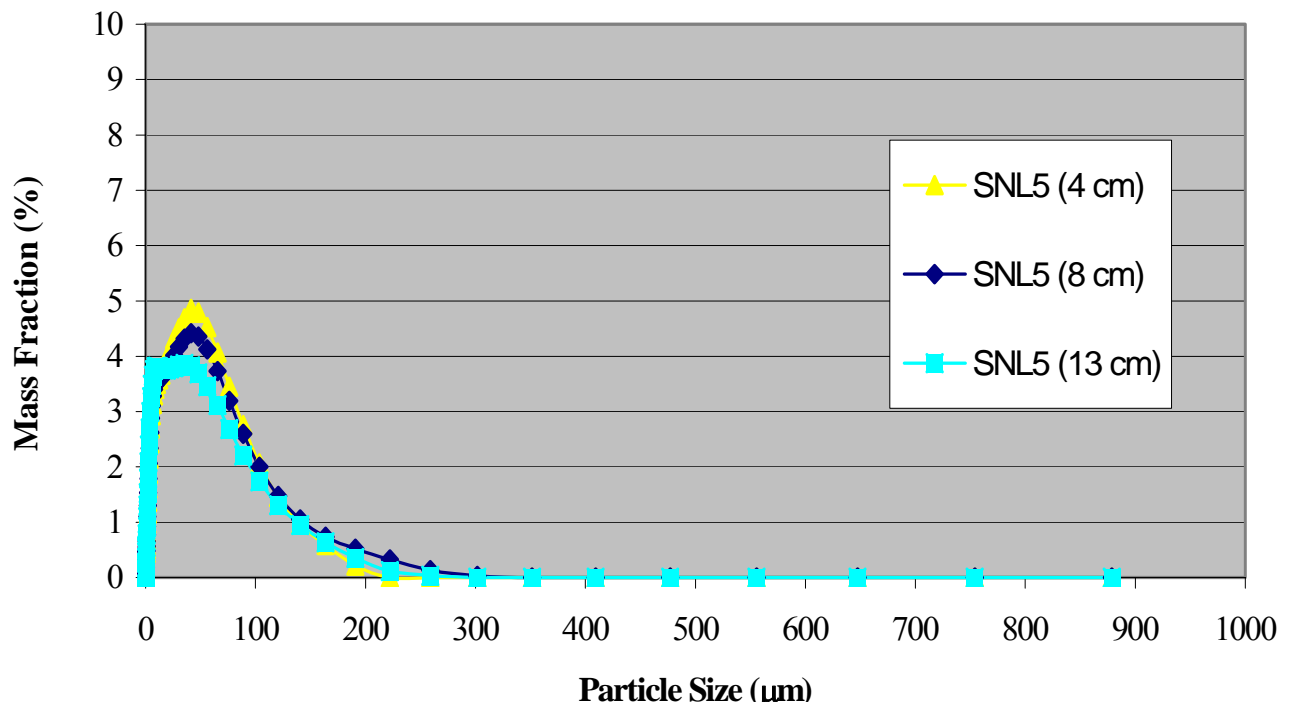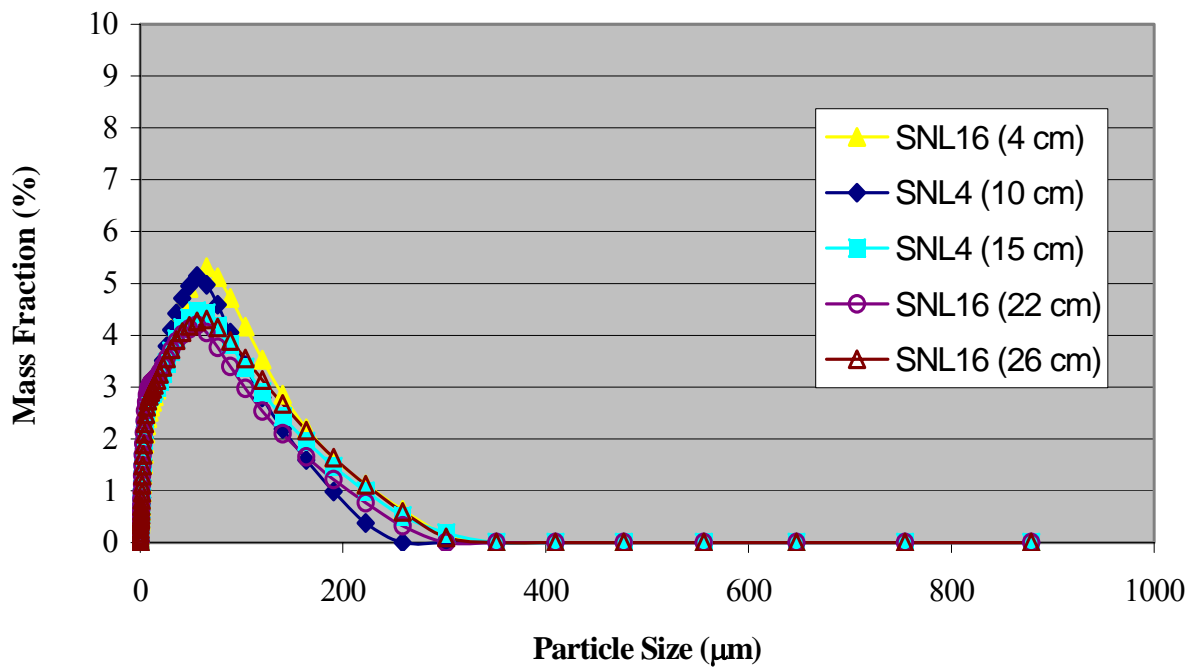
Figure 25. Particle size distributions for SNL-5.
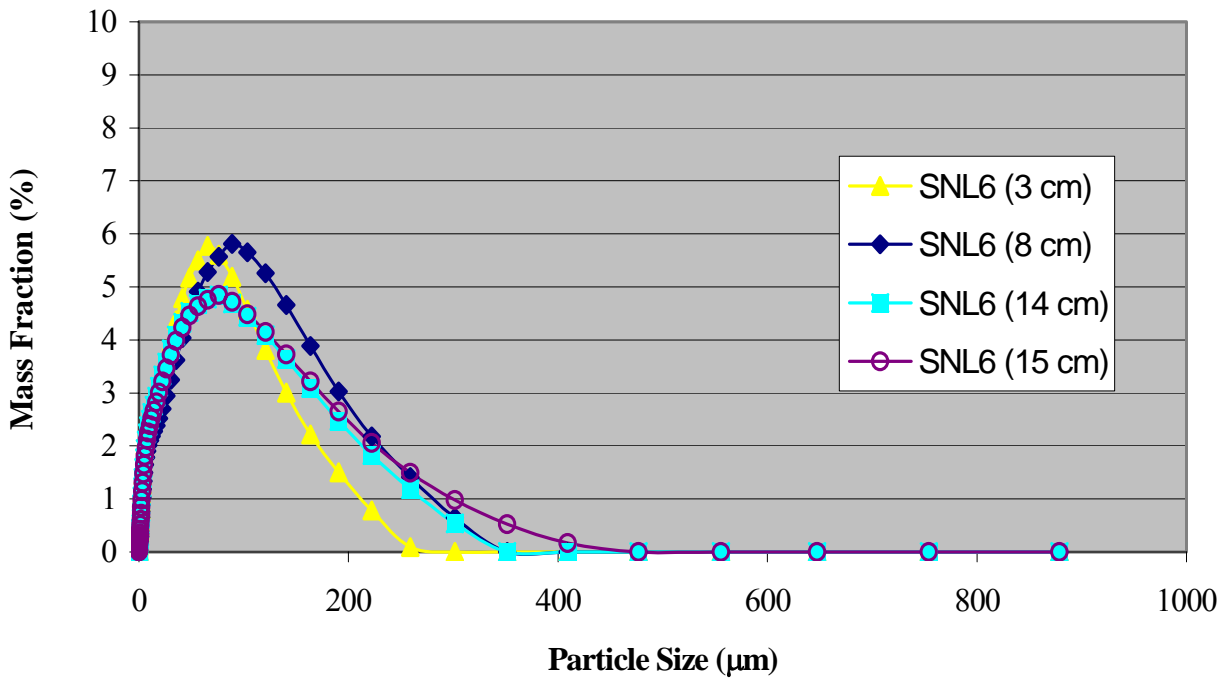
Figure 26. Particle size distributions for SNL-6.
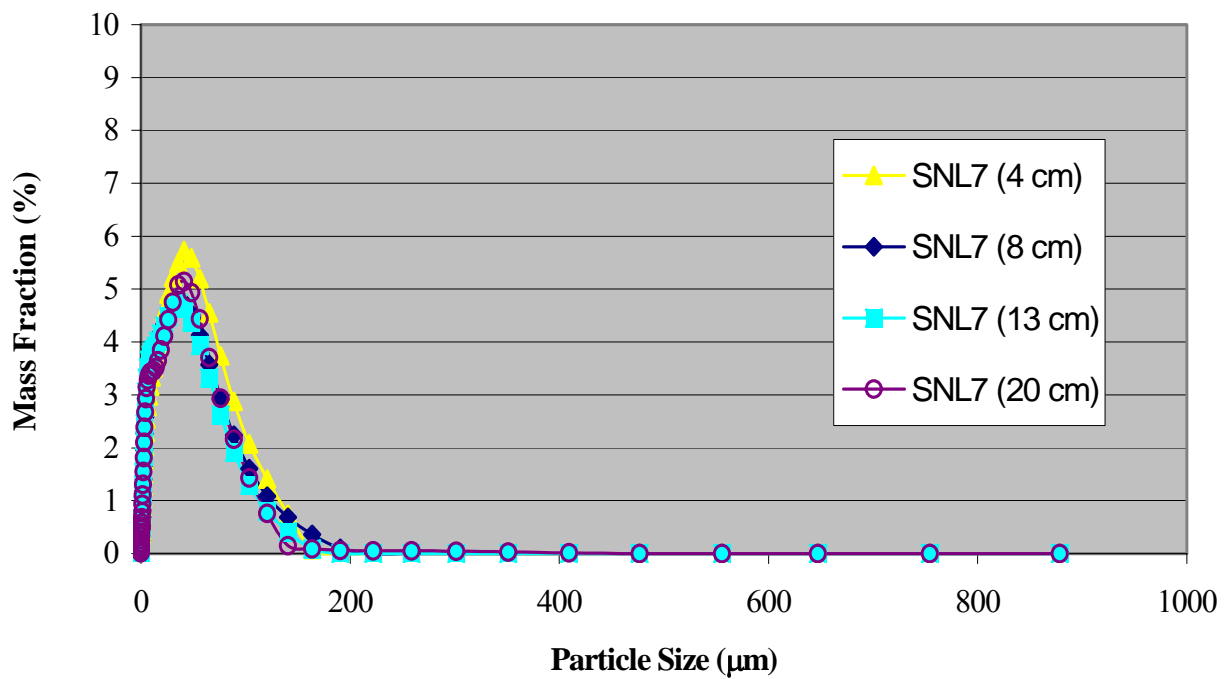
Figure 27. Particle size distributions for SNL-7.
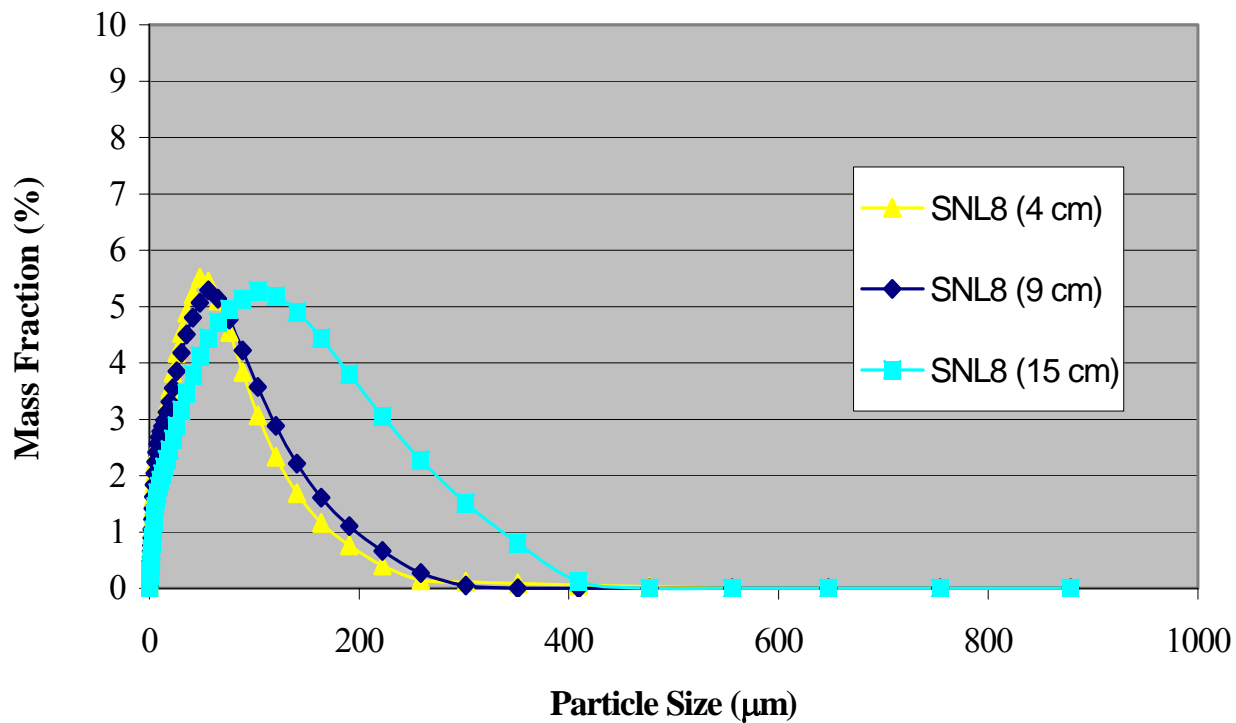
Figure 28. Particle size distributions for SNL-8.
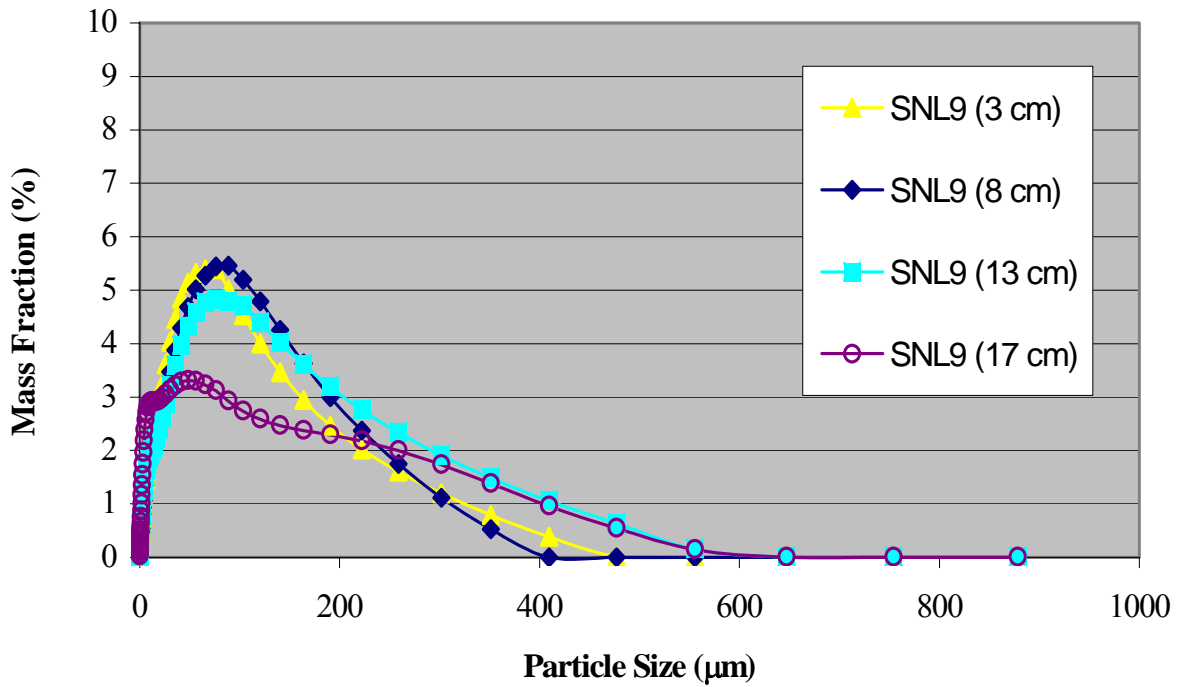
Figure 29. Particle size distributions for SNL-9.
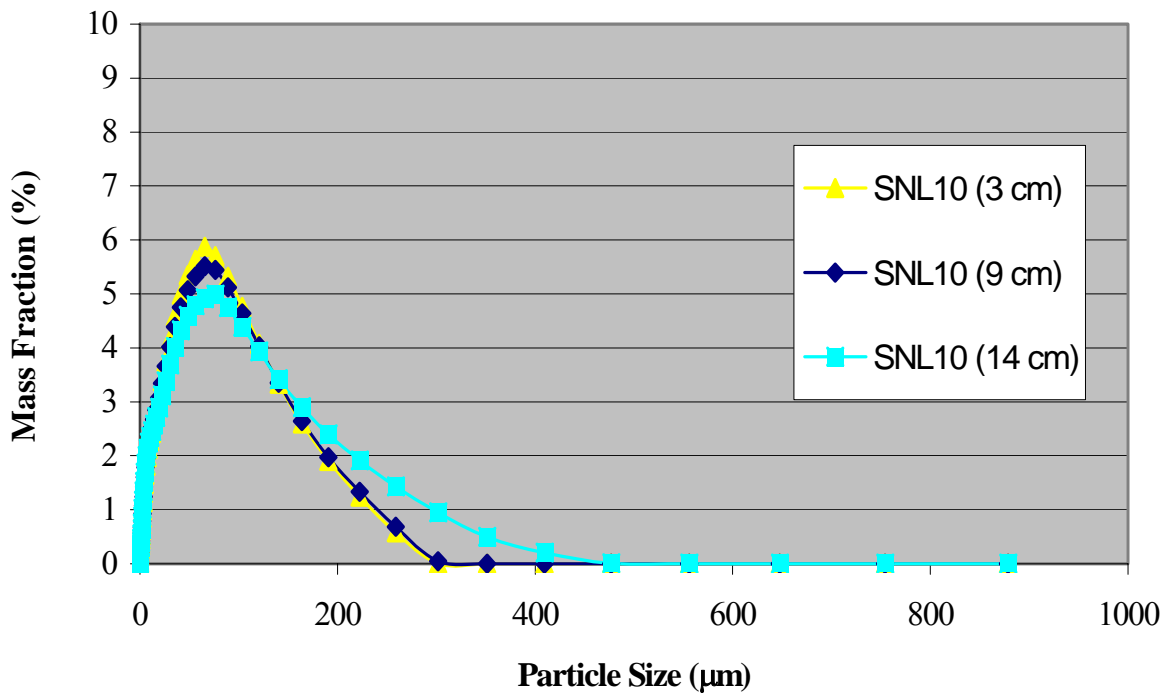
Figure 30. Particle size distributions for SNL-10.

Figure 31. Particle size distributions for SNL-11.

Figure 32. Particle size distributions for SNL-12.

Figure 33. Particle size distributions for SNL-13.

Figure 34. Particle size distributions for SNL-14.

69

Figure 35. Particle size distributions for SNL-15.

Figure 36. Particle size distributions for SNL-16.

Appendix B: Particle Size Distributions for the Water Samples
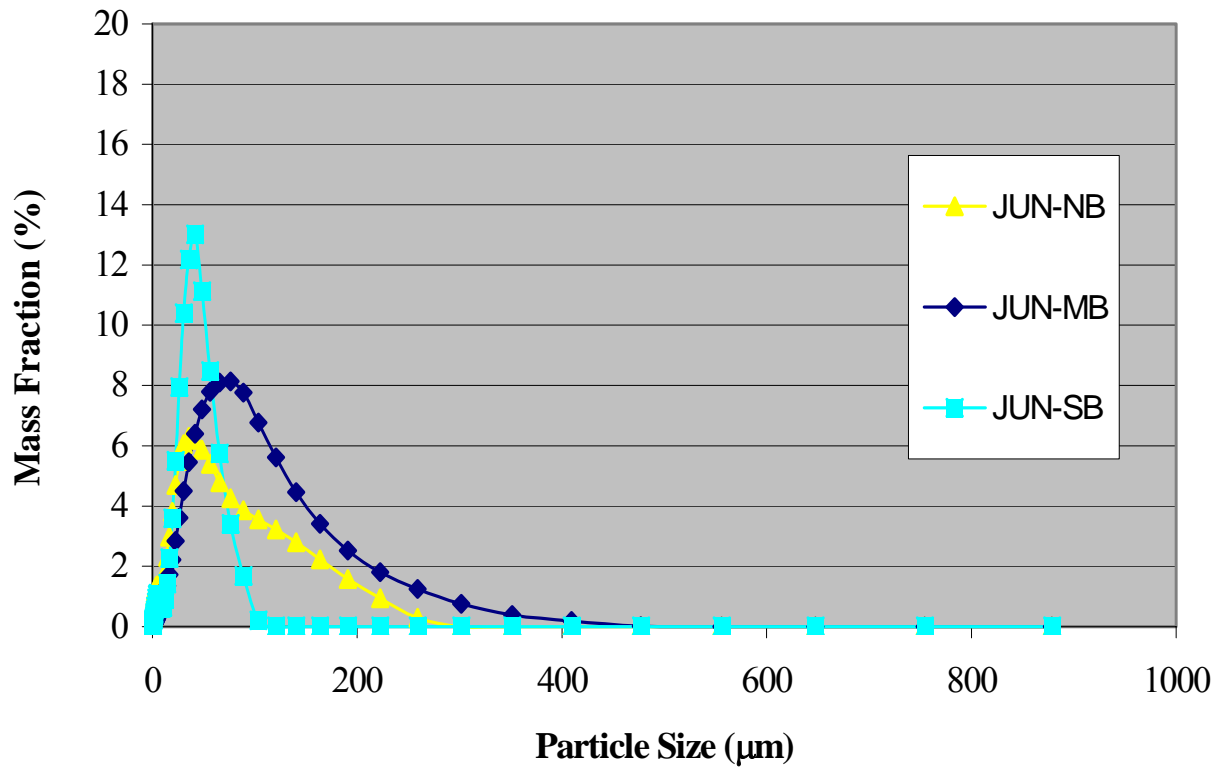
Figure 37. Particle size distributions for June water samples
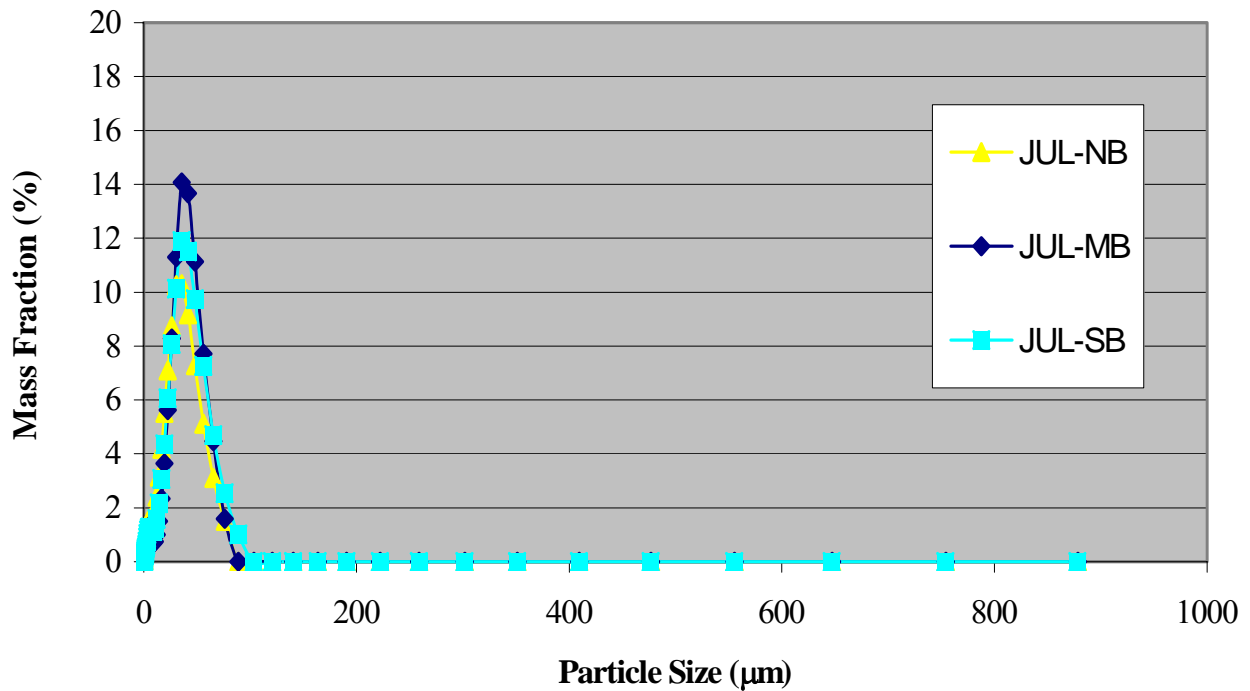
Figure 38. Particle size distributions for the July water samples

Appendix C: Particle Size Distributions for the Grab Samples
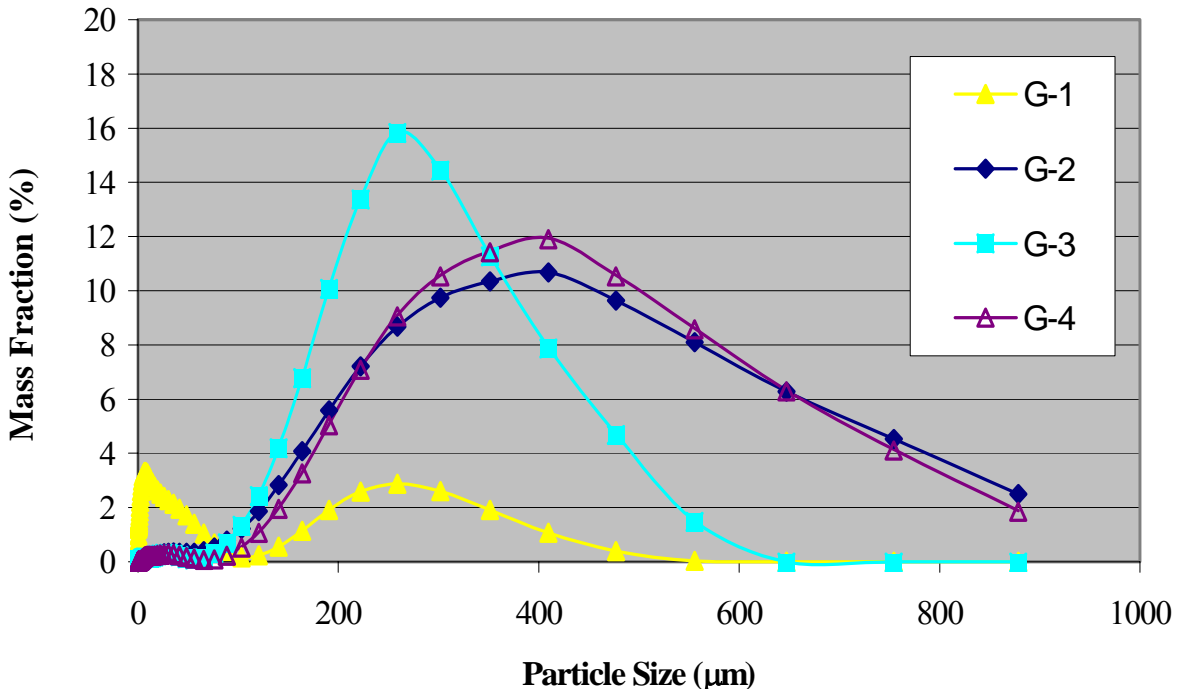
Figure 39. Particle size distributions for the Grab samples; G1-G4.
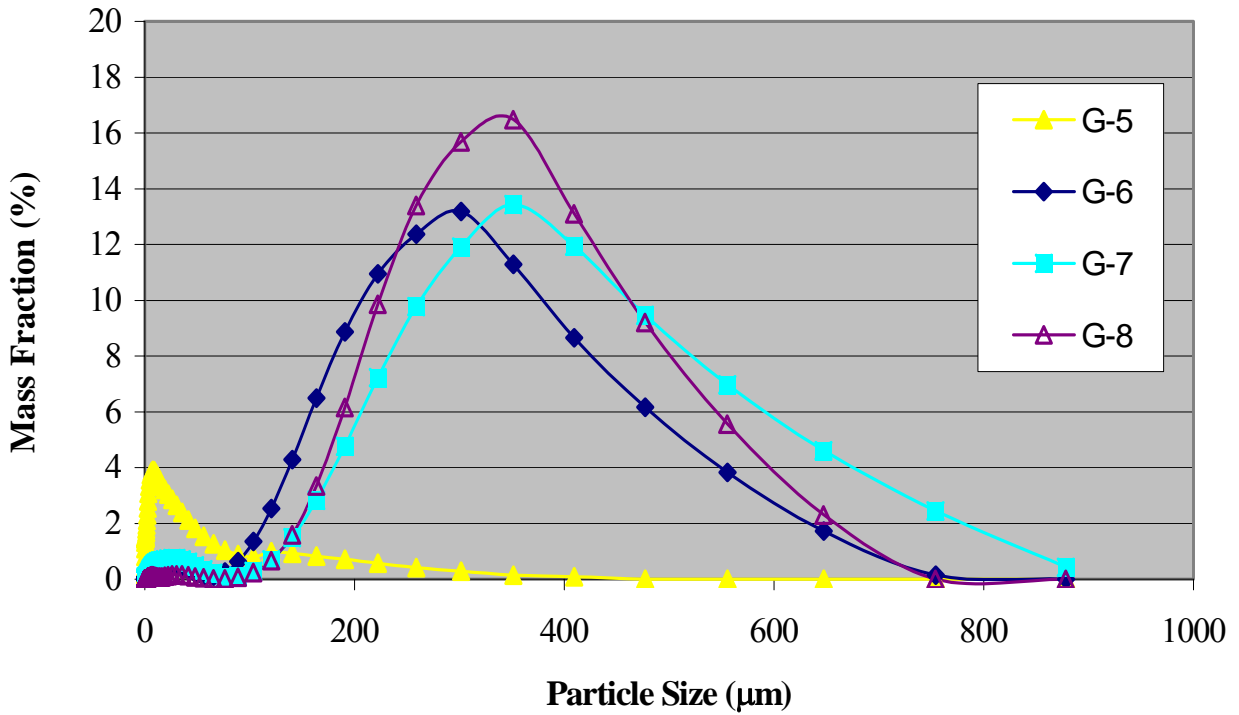
Figure 40. Particle size distributions for the Grab samples; G5-G8.

Appendix D: Particle Size Distributions for the Ponar Samples
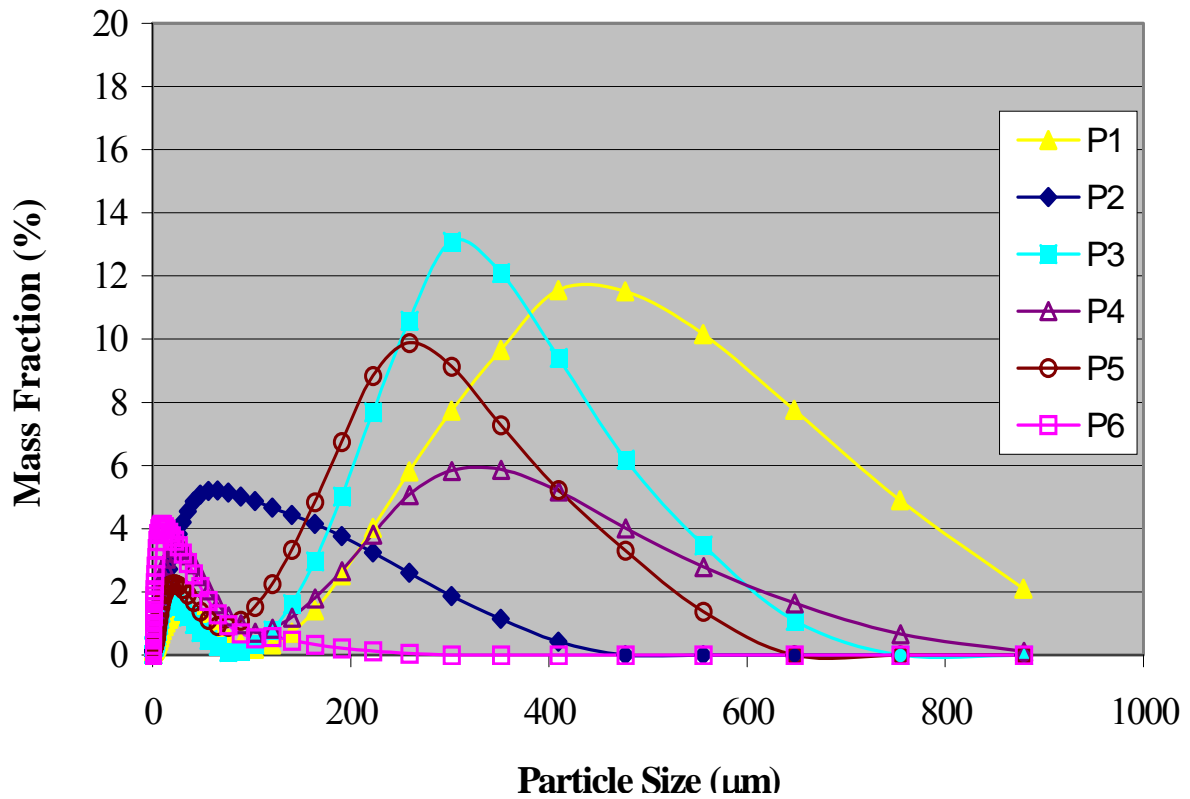
Figure 41. Particle size distributions for Ponar samples, P1-P6.
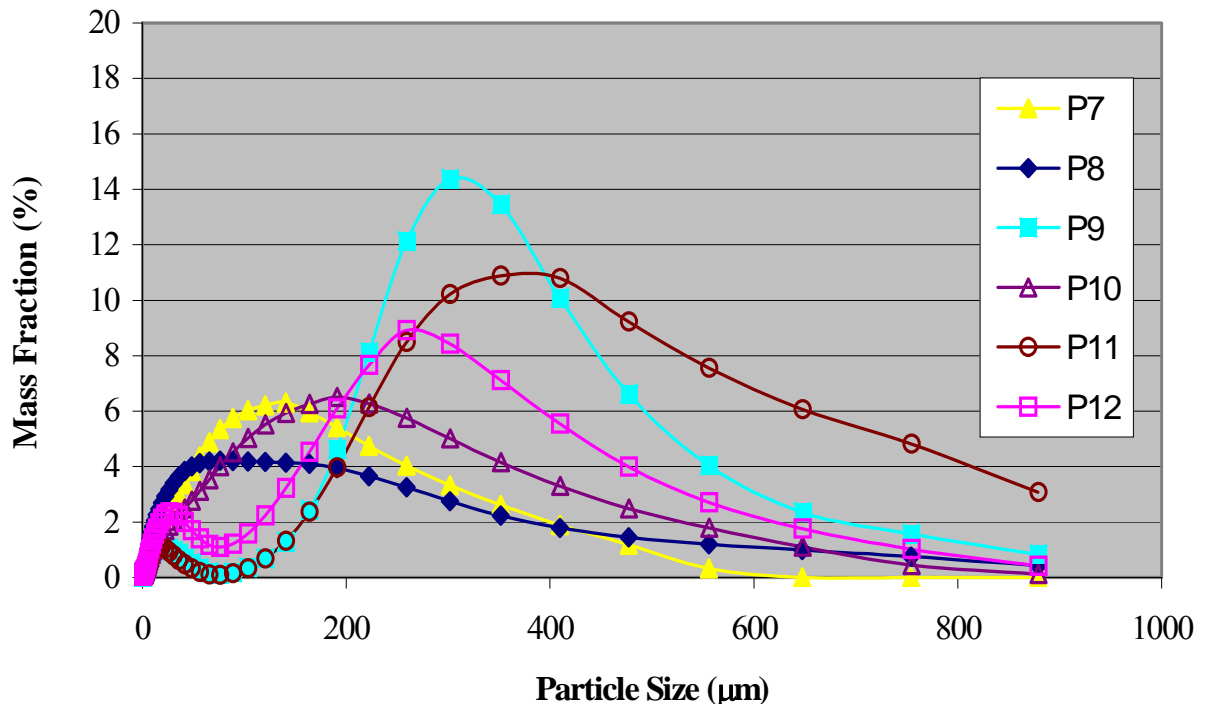
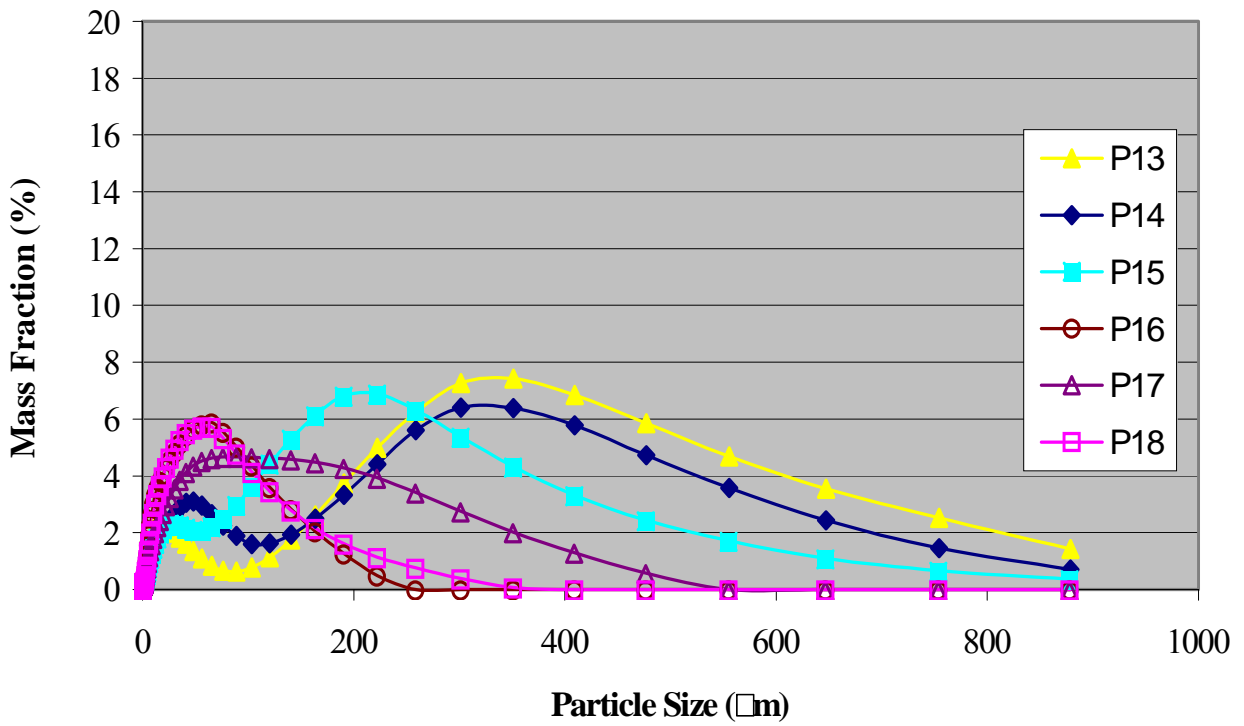**Figure 42.** Particle size distributions for Ponar samples, P7-P12.

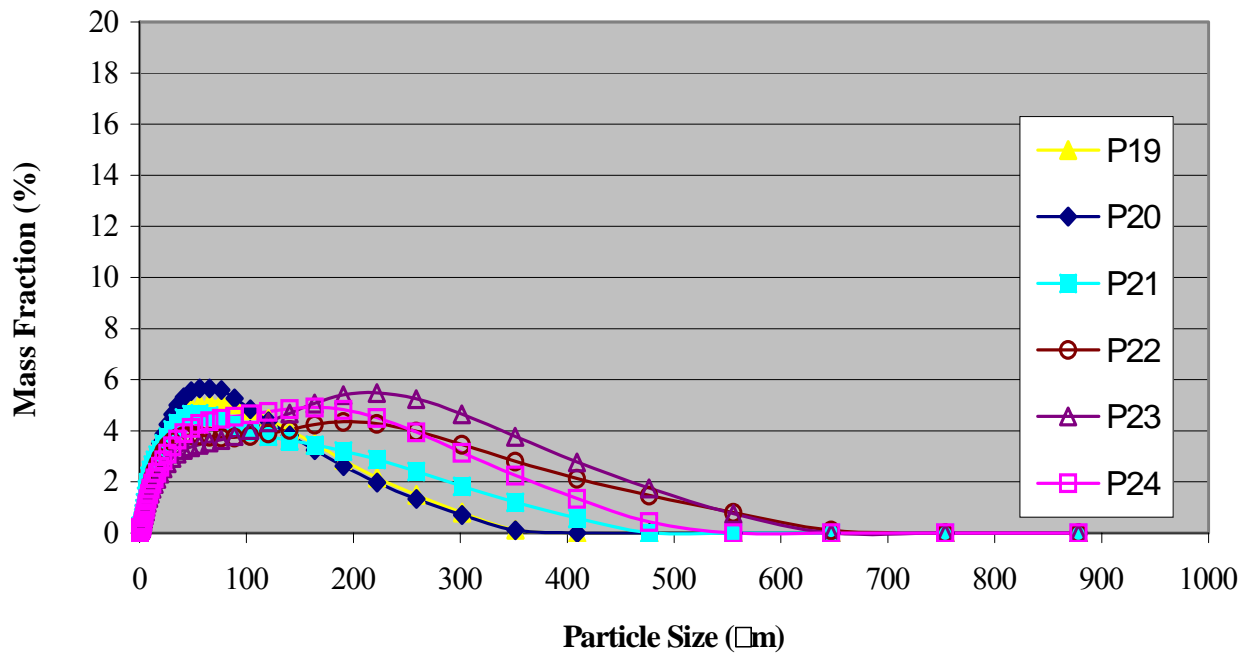**Figure 43.** Particle size distributions for Ponar samples, P13-P18.

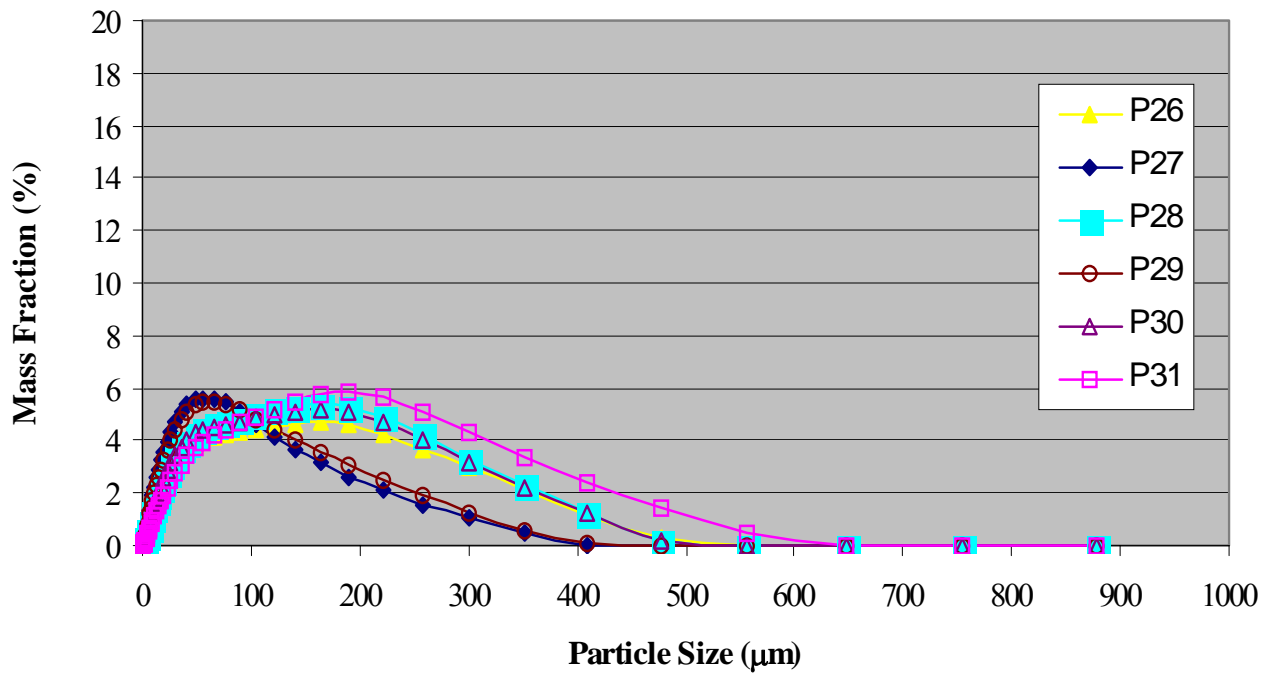**Figure 44.** Particle size distributions for Ponar samples, P19-P24.

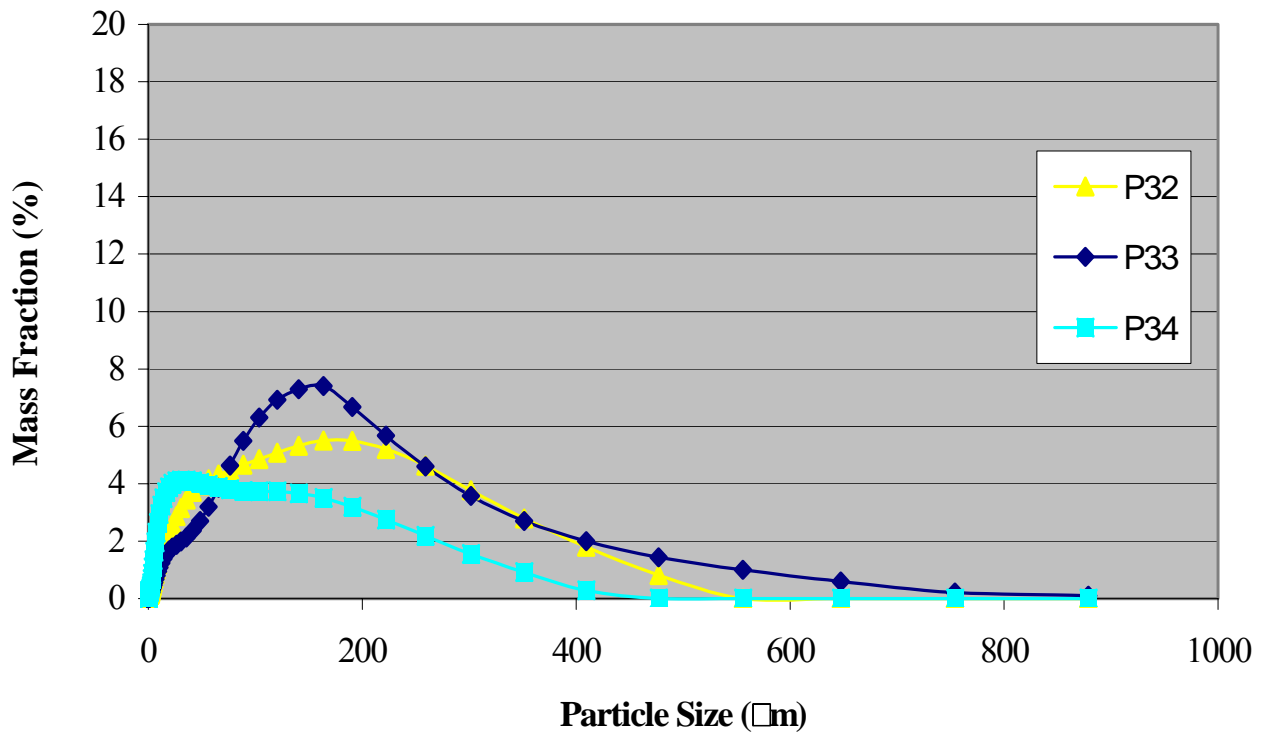**Figure 45.** Particle size distributions for Ponar samples, P26-P31.

Figure 46. Particle size distributions for Ponar samples, P32-P34.

75